Universidade do Minho
I3Bs - Instituto de Investigação em Biomateriais, Biodegradáveis e Biomiméticos

Isabel Maria Lopes de Matos Oliveira

Smart delivery biomaterials for targeting hyperplasic synovium and treatment of rheumatoid arthritis

Março de 2021

Smart delivery biomaterials for targeting hyperplasic synovium and treatment of rheumatoid arthritis
Isabel Maria Lopes de Matos Oliveira
UMinho | 2021

Universidade do Minho

I3Bs - Instituto de Investigação em Biomateriais, Biodegradáveis e Biomiméticos

Isabel Maria Lopes de Matos Oliveira

Smart delivery biomaterials for targeting hyperplasic synovium and treatment of rheumatoid arthritis

Tese de Doutoramento

Doutoramento em Engenharia de Tecidos, Medicina Regenerativa e Células Estaminais

Trabalho efetuado sob a orientação do

Doutor Joaquim Miguel Antunes Correia de Oliveira

Professor Doutor Rui Luís Gonçalves dos Reis

Março de 2021

ACKNOWLEDGMENTS

The journey and preparation of this thesis would not be possible without the help and support of important people.

First, I would like to start by expressing my thankfulness to my supervisor and director of the 3B`s Research Group, Professor Rui L. Reis. He gave me the opportunity to join his group and to develop my PhD thesis, under his supervision and leadership. A special acknowledgment to my supervisor, Doctor Joaquim Miguel Oliveira. To him, I want to thank his support, availability, and trust on me, even in less good times, with words of encouragement. This thesis would not be possible without all your knowledge and his helpful supervision.

I want to thank Professor Gilson Khang for giving me the opportunity to work in the Department of Polymer Nano Science & Technology, at Chonbuk National University. This experience enriched me both personally and professionally, allowed me to overcome some fears, become a more independent researcher, and believe more in myself. I would also like to acknowledge the co-authors in this thesis, especially Doctor Cristiana Gonçalves for help in the initial phase of work and with the correction of papers. Her inputs were very important. To Doctor Mariana Carvalho and Diogo Fernandes for their precious help and extreme support in the late phase of my PhD. I am extremely grateful to my friends in 3B`s Research Group, especially Joana Gomes, Gabriela Diogo, Teresa Oliveira, Ana Luísa Graça, Catarina Oliveira, Cláudia Lima, Cristiana Carvalho and João Costa, with whom I shared good and bad moments and they were important support during this journey.

I would like to acknowledge the Horizonte Norte2020 for my scholarship (NORTE-08-5369-FSE-000044) and REMIX project (G.A. 778078 — REMIX — H2020-MSCA-RISE-2017) for the financial support for the international experience.

I would like to thank to my friends from Coimbra especially Andreia Fonseca for all the emotional support and motivational words.

Finally, I would like to thank all my family, especially the pillars of my life: mother, sister, and boyfriend. I am so deeply grateful for unconditional love, patience, advices, motivation words, and support in bad moments. They were undoubtedly my strength to be able to continue every day. I Love you so much!

STATEMENT OF INTEGRITY

I hereby declare having conducted this academic work with integrity. I confirm that I have not used plagiarism or any form of undue use of information or falsification of results along the process leading to its elaboration.

I further declare that I have fully acknowledged the Code of Ethical Conduct of the University of Minho.

ABSTRACT

Smart delivery biomaterials for targeting hyperplasic synovium and treatment of rheumatoid arthritis

Rheumatoid Arthritis (RA) is an autoimmune and inflammatory disease that affects approximately 1 % of people worldwide. The pathogenesis of RA is characterized by joint synovial inflammation and cartilage and bone tissue destruction. Several treatments are available to control the inflammation, however, traditional drugs administration are not fully effective and present severe undesired side effects. Novel treatment routes are considering the advantages of personalized therapies that can make use of smart nanobiomaterials as drug delivery systems. These topics are the focus of Section 1, in **Chapters I**, **II**, and **III**. In this thesis, we developed PAMAM dendrimers functionalized with chondroitin sulfate (CS) as nanocarriers, covalently linked to anti-TNF α Abs to provide anti-inflammatory properties. This targeted delivery is aimed at treating the inflammation on RA **(Chapter V)**. Besides nanoparticles, the use of different biomaterials as 3D drug delivery systems is attracting a great deal of attention due to their tunable mechanical properties. We innovatively proposed enzymatically crosslinked Tyramine-Gellan gum (Ty-GG) hydrogels as a drug delivery vehicle to provide a sustained release and improve the treatment safety in patients with RA **(Chapter VI)**. To further increase mechanical properties, biocompatibility, and therapeutic efficacy in controlling inflammation processes in RA, Ty-GG with Silk Fibroin hydrogels were produced **(Chapter VII)**. To potentiate the nanoparticles and hydrogels performances, a combined system using these two platforms was developed and evaluated *in vitro* under static and dynamic conditions, aiming to achieve controlled drug release kinetics **(Chapter VIII)**. In **Chapter IX**, an *in vitro* human 3D inflammatory cartilage model on-a-chip was developed to be used as a drug screening platform. In this sense, an inflammatory environment was established by exposing chondrogenic cells to inflamed macrophages to support with more efficiency the therapeutic effect of anti-TNF α Ab-CS/PAMAM dendrimer NPs loaded-Ty-GG in the treatment of inflammation (proof-of-concept). The major conclusions and future trends for the type of drug delivery that were developed, and screening platform used in this thesis are discussed in **Chapter X**. This work goes beyond the current state of the art in the development of nanobiomaterials and drug delivery systems scope with the potential to improve and overcome the current limitations associated to the conservative treatment of RA.

Keywords: Biomaterials, Bioreactor, Microfluidics, Nanoparticles and Rheumatoid Arthritis.

RESUMO

Biomateriais de entrega inteligente para o direcionamento do sinóvio hiperplásico e tratamento da artrite reumatoide

A Artrite Reumatóide (AR) é uma doença autoimune a inflamatória caracterizada por inflamação das articulações, destruição da cartilagem e do tecido ósseo. Vários tratamentos estão disponíveis para controlar a inflamação, contudo a administração de medicamentos tradicionais não é totalmente eficaz e apresenta efeitos secundários indesejáveis. Novas possibilidades de tratamento têm vindo a considerar as vantagens das terapias personalizadas, as quais recorrem a nanobiomateriais inteligentes como sistemas de libertação de fármacos. Estes temas são abordados e revistos no **Capítulo I**, **II** e **III**. Nesta tese, foram desenvolvidas nanopartículas a partir de dendrímeros PAMAM funcionalizados com sulfato de condroítina e covalentemente ligados ao anti-TNF α como uma estratégia de dotar estes nanosistemas com propriedades anti-inflamatórias. Este sistema de libertação controlada e direcionado visa tratar a inflamação na AR **(Capítulo V)**. Além das nanopartículas, o uso de diferentes biomateriais como sistema de libertação de fármacos (3D) estão a atrair bastante atenção. Propusemos de forma inovadora o uso de hidrogéis de goma gelana funcionalizados com tiramina (Ty-GG) e a sua aplicação como sistemas de libertação de fármacos por forma a assegurar uma melhoria no tratamento em doentes com AR **(Capítulo VI)**. Para melhorar as propriedades mecânicas, biocompatibilidade, e eficácia terapêutica no tratamento da inflamação, foram produzidos hidrogéis de Ty-GG e fibroína de seda **(Capítulo VII)**. Com o objetivo de obtermos uma cinética de libertação controlada de fármaco e potenciar uma melhoria do desempenho das nanopartículas e dos hidrogéis, um sistema dual combinando dendrímeros PAMAM funcionalizados e encapsulados em hidrogéis de tiramina-goma gelana e fibroína de seda foi desenvolvido e avaliado *in vitro* em condições estáticas e dinâmicas **(Capítulo VIII)**. No **Capítulo IX**, um modelo de cartilagem inflamatória humana 3D *in vitro* foi desenvolvido num chip para ser usado como uma plataforma de avaliação de fármacos. Nesse sentido, um ambiente inflamatório foi estabelecido para avaliar com mais eficiência, o efeito terapêutico da abordagem desenvolvida no tratamento da inflamação (prova de conceito). As principais conclusões e tendências futuras para o tipo de sistemas de libertação controlada que foram desenvolvidos nesta tese são discutidas no **Capítulo X**. Este trabalho vai além do estado da arte atual no que respeita ao desenvolvimento de nanobiomateriais e no âmbito de sistemas de libertação de fármacos, com o potencial para melhorar e superar as limitações atuais associadas aos tratamentos tradicionais da AR.

Palavras-chave: Artrite Reumatoide, Biomateriais, Biorreator, Microfluídica, Nanopartículas.

TABLE OF CONTENTS

LIST OF ABBREVIATIONS

A

α – Alpha

AA – Adjuvant-induced Arthritis

ABP – azabisphosphonate

Abs – Antibody

Abs – Absorbance

AbIA- anti-type II collagen antibody induced arthritis

Ac – Acylated Superoxide Dismutase

AC – Acrylate

AFM – Atomic force microscopy

AIA – Antigen-induced arthritis model

ANOVA – Analysis of variance

ASOs – Antisense oligodeoxynucleotides

ASTM – American Society for Testing and Materials

ATR – Attenuated Total Reflectance

Au-GAL1 – Galectin-1-nanogold

AuNPs – Gold nanoparticles

B

β – Beta

BMSCs – Bone marrow derived mesenchymal stromal cells

BPD- MA – benzoporphyrin derivate-monoacid ring A

BP – betamethasone disodium 21-phosphate

C

Calcein-AM – Calcein-Acetoxymethy

CDP – Cyclodextrin polymer

CE – chemical enhancer

CFA – Complete Freund's adjuvants

CIA – Collagen-induced arthritis

CLA – Carrageen/lipopolysaccharide-induced Arthritis

cm – centimeter

cm^{-1} – Reciprocal wavelength centimeters

COX – Ciclo-oxigenase

Coll II – Collagen Type II

CPT – Camptothecin

CS – Chondroitin sulfate

CSi – Carbosilane

CS/PAMAM – Chondroitin Sulfate poly(amidoamine) dendrimer

CSPGs – Chondroitin sulfate proteoglycans

CTR– Control

D

DAPI – 4',6-diamidino-2-phenylindole

DAPT – γ-secretase inhibitor

DDS – drug delivery systems

DEXP – dexamethasone phosphate

DGAV – Direcção Geral de Alimentação e Veterinária

DLS – Dynamic light scattering

DLTH – Dexamethasone-encapsulated thermosensitive hydrogel

DMARDs – Disease-modifying anti-rheumatic drugs

DMEM- F12 – Dulbecco's Modified Eagle's Medium: Nutrient Mixture F-12

DMSO – Dimethyl sulfoxide

DNA – Deoxyribonucleic acid

DNPs– DAPT-loaded NPs

DS – diclofenac sodium

DS – degree of substitution

dsDNA – Double-stranded DNA

DXM – dexamethasone phosphate

2D – 2-Dimensions

3D – 3-Dimensions

°C – Degree Celsius

E

ECM – Extracellular matrix

EDA – Ethylenediamine

EDC – 1-Ethyl-(3-dimethylaminopropyl) carbodiimide hydrochloride

EDC – N-(3-Dimethylaminopropyl)-N′-ethylcarbodiimide hydrochloride

EDTA – Ethylenediaminetetraacetic acid

EDS – Energy-dispersive X-ray spectroscopy

e.g. – For example, from latin exempli gratia

EHS – Engelbreth-Holm-Swarm

ELISA – Enzyme-linked immunosorbent Assay

ELS – Electrophoretic light scattering

Eq – Equation

et al. – And others

EthD-1 – Ethidium homodimer

ETX- Etoricoxib

Ex/Em – Exitation/Emission

F

FA – Fluoresceinamine/ Folic acid

FBS – Fetal bovine serum

FCA – Freund´s complete adjuvant

FDA – Food and drug administration

FITC – Fluorescein isothiocyanate

FLS –Fibroblast-like synoviocytes

FR – Folate receptor

FTIR – Fourier transform infrared spectroscopy

G

g – gram

G – Generation

G' – Storage modulus

G'' – Loss modulus

GAGs – Glycosaminoglycans

GCs – Glucocorticoids

GG – Gellan gum

GM-CSF– Granulocyte monocyte-colony stimulating factor

H

H – Hours

HA – Hyaluronic acid

HA-GG – High acyl gellan gum

HCLB – high dose-gel

hCH – Human chondrogenic primary cells

HGC – hydrophobically modified gycol chitosan

hIF – liposome-entrapped lactoferrin

H^1 NMR – Proton nuclear magnetic resonance

H_2O_2 – Hydrogen peroxide

HPMA – N-(2-hydroxypropyl) methacrylamide

HRP – Horseradish peroxidase

HSA – human serum albumin

HPMA – *N*-(2-hydroxypropyl) methacrylamide

Hz – Hertz

I

I – Integration

i.e. – "In other words", from latin *id est*

IL – Interleukin

IMC – Indomethacin

IntgP – Integral

K

k– consistency coefficient

kg – Kilogram

kHz – Kilohertz

kV – Kilovolt

L

L – Liters

LA-GG – Low acyl gellan gum

LCLB – Low dose-gel

LiBr – Lithium bromide

LN – lymph node

LPS – lipopolysaccharide

LVER – Linear viscoelastic region

M

M – Molar

mA – Milliampere

mAb – monoclonal antibody

MES – (2-(N-morpholino)ethanesulfonic acid)

MHz – megahertz

mg – milligram

min – Minute

mL – Milliliter

mm – Millimeter

mM – Millimolar

MMP – Matrix Metalloproteinase

MNP – multimodal nanoparticles

MP – Methylprednisolone

MRI – Magnetic resonance image

MSCs – Mesenchymal stem cells

MTX – methotrexate

MTT – 3-(4,5-dimethylthiazol-2-yl)-2,5-diphenyltetrazolium bromide

MTS – 3-(4,5-dimethylthiazol-2-yl)-5-(3-carboxymethoxyphenyl)-2-(4-sulfofenyl)-2H-tetrazolium

mV – Millivolts

mw – Wet weight

MWCO – Molecular weight cut off

µg – microgram

µm – micrometer

µL – microliter

N

N – Newton

n – Number of protons

n – flow behavior index

NanoIGUR – Nanoiguratimod

N/A – Not applicable, Not available

NC – Nanocomposite hydrogels

ND – Not detected

NFκB – nuclear factor kappa B

ng – Nanogram

NHS – N-Hydroxysulfosuccinimide sodium salt

NIH – National Institutes of Health

NIRF – near-infrared fluorescence

NK – Natural killer

NLCs – Nanostructured lipid carriers

NLM – National Library of Medicine

nm – Nanometer

NPs – Nanoparticles

NSAIDs – Nonsteroidal anti-inflammatory drugs

O

OVA – Ovalbumin-Induced Arthritis

P

p – Statistical level of significance

Pa – Pascal

PAMAM – Poly(amidoamine)

PAT – photoacoustic tomography

PBS – Phosphate buffer saline

PCL – poly(ε-caprolactone)

PCLA – poly(ε-caprolactone-co-lactide)

PDMS – poly(dimethylsulfoxide)

PEG – Poly (ethylene glycol)

PEO – poly (ethylene oxide)

PGs – Prostaglandins

pg – Picogram

pH – Potential hydrogenionic

PLA – Polylactic acid

PLGA – Polylactic-co-glycolic

PLP – Prednisolone phosphate

PMA – phorbol 12-myristate-13-acetate

PPI – Poly(propylene imine)

ppm – Part-per-million

PRRs – Pattern Recognition Receptors

PSI – Self-polymerization

PVA – Polyvinyl alcohol

δ – Phase angle

% – Percentage

R

RA – Rheumatoid Arthritis

Ref. – Reference

RFU – Relative fluorescence units

RGD – Tripeptide Arg-Gly-Asp

RT – Room temperature

S

Scv – Scavenging

SEM – Scanning Electron Microscopy

SF – Silk fibroin

SiMAG – ScreenMag

SLCs – Phagocytic synovial lining cells

SLNs – solid lipid nanoparticle

SOD – Superoxide dismutase

SPIONs – Superparamagnetic iron oxide nanoparticles

SSM – Sterically stabilized micelles

STEM– Scanning Transmission Electron Microscope

SUVs – Small unilamellar vesicles

s– seconds

τ – shear stress

γ – shear rate

T

T – Transmittance

TA – triamcinolone acetonide

TCPs – Tissue culture polystyrene

TCZ – Tocilizumab

TE – Tissue engineering

TFs – Transfersomes

TG – triglycerol monostearate

TGC – Thiolated gycol chitosan

TGF – Transforming growth factor

THP-1 – Human monocytic cell line

TNF – Tumor necrosis factor

TNX – Tenoxicam

TP – triptolide

TRAIL – apoptosis inducing ligand

TRX-20 – 3,5-dipentadecyloxybenzamidine hydrochloride

TWHF – Tripterygium

Ty – Tyramine

Ty-GG – Tyramine Gellan Gum

Ty-GG/SF – Tyramine Gellan Gum/ Silk fibroin

U

U – Units

UV – Ultraviolet

V

v – Volume

(v/v) – Percentage of volume/volume

VEGF – Vascular endothelial growth factor

VECs – vascular endothelial cells

VPI – vasoactive intestinal peptide

W

w_f – Final weight

w_i – Initial weight

w_w – Wet weight

(w/v) – Percentage of weight/volume

λ – Wavelength

LIST OF EQUATIONS

LIST OF FIGURES

LIST OF TABLES

LIST OF SUPPLEMENTARY TABLES

SHORT *CURRICULUM VITAE*

Isabel Oliveira was born in 1990 in Guimarães, Portugal. She is currently a PhD student at 3B's Research Group - I3Bs, Research Institute on Biomaterials, Biodegradables and Biomimetics, at University of Minho, Headquarters of the European Institute of Excellence on Tissue Engineering and Regenerative Medicine at Avepark, Caldas das Taipas, Guimarães, Portugal, under the supervision of Doctor Joaquim Miguel Oliveira and Professor Rui Luis Reis.

She graduated in Biology (2008-2011) and received her MSc degree in 2013 in Human Evolution and Biology at Laboratory of Biochemistry Center for Neuroscience and Cell Biology, University of Coimbra, Portugal with a final grade of 16 (0-20). During that period, she was enrolled in the project entitled "Mitochondrial genome analysis in frontotemporal lobar degeneration: tRNA contribution".

In February 2015, she started doing an internship at 3B's Research Group, at University of Minho, Portugal and integrated on ERC funded project - ComplexiTE actively participating in the work about synthesis and functionalization of the dendronized polymers. In September 2016, she started pursuing her PhD at 3B's Research Group with an awarded Horizonte Norte2020 PhD scholarship (Norte-08-5369-FSE-000044) in the PhD program in Tissue Engineering, Regenerative Medicine and Stem Cells (TERM&SC) in the University of Minho, being the main focus of her research smart delivery biomaterials to treat rheumatoid arthritis. In September 2018, she had the great opportunity to spend 6 months at Department of Polymer Nanoscience and Polymer BIN Research Centre, Chonbuk National University, Jeonju, Republic of Korea.

As a result of her research work, she is author or co-author of 8 peer-reviewed papers in international journals as first-author (5 published, 3 submitted), 1 in co-authorship, 6 book chapters and 11 poster presentations. She attended several important conferences in the field of tissue engineering and regenerative medicine.

LIST OF PUBLICATIONS

The work performed during the PhD period resulted in the publications listed below.

Papers in international scientific journals with referees (as first author)

1. **Oliveira I. M**., Gonçalves C., Reis R. L., Oliveira J. M. "Engineering Nanoparticles for Targeting Rheumatoid Arthritis: Past, Present and Future Trends" Nano Research, 2018, 11(9):1-18. doi: 10.1007/s12274-018-2071-3.
2. **Oliveira I. M.**, Gonçalves C., Oliveira E. P., Simón-Vasquez R., Silva-Morais A., González-Fernandez A., Reis R. L., Oliveira J. M. "PAMAM Dendrimers Functionalized with an Anti-TNF α Antibody and Chondroitin Sulfate for Treatment of Rheumatoid Arthritis" Materials Science and Engineering: C, 2021, 121. doi.org/10.1016/j.msec.2020.111845.
3. **Oliveira I. M.**, Gonçalves C., Shin, M. E., Lee S., Reis R. L., Oliveira J. M. Khang, G. "Enzymatically crosslinked tyramine-gellan gum hydrogels as drug delivery system for rheumatoid arthritis treatment". Drug Delivery and Translational Research 2020. doi: 10.1007/s13346-020-00855-9.
4. **Oliveira, I. M.**, Gonçalves C., Shin, M. E., Lee S., Reis R. L., Oliveira J. M. Khang, G. "Anti-inflammatory Properties of Injectable Betamethasone-loaded Tyramine-modified Gellan Gum/Silk Fibroin Hydrogels" Biomolecules 2020, 10(10), 1456. doi: 10.3390/biom10101456.
5. **Oliveira, I. M.**, Fernandes, D.C., Cengiz, I. F. Reis R. L., Oliveira J. M. "Hydrogels in the treatment of Rheumatoid Arthritis: Drug delivery systems and artificial matrices for dynamic *in vitro* models". (Submitted)
6. **Oliveira, I.M**., Fernandes, Maia F. R., Canadas, R.F., Reis, R.L., Oliveira, J.M. "Bioengineered nanoparticles loaded-hydrogels to target TNF alpha in inflammatory diseases". (Submitted)
7. **Oliveira, I.M.**, Carvalho, M.R., Fernandes, D.C., Abreu, C.M., Maia, F. R., Pereira, H., Caballero, D., Kundu, S.C., Reis, R.L., Oliveira, J.M. "Modulation of inflammation by anti-TNF α mAb-dendrimer nanoparticles loaded in tyramine-modified Gellan gum hydrogels in a cartilage-on-a-chip model". (Submitted)

Papers in international scientific journals with referees (as co-author)

1. Goncalves C., Silva S. S., Gomes J. M., **Oliveira I. M.**, Canadas, R. F., Maia F. R., Radhouani H., Reis R. L., Oliveira, J. M. "Ionic liquid-mediated processing of SAIB-Chitin scaffolds". ACS Sustainable Chemistry & Engineering, 2020, 8(9): 3986-3994. doi: 10.1021/acssuschemeng.0c00385.

Book Chapters

1. **Oliveira I. M.**, Gonçalves C., Reis R. L., Oliveira J. M. "Synovial Knee Joint". Regenerative Strategies for the Treatment of Knee Joint Disabilities. Oliveira J. M., Reis R. L. (Eds.), Springer, 2016, 21:21-28. doi:10.1007/978-3-319-44785-8_2.
2. **Oliveira I. M.**, Carvalho A. L., Radhouani H., Gonçalves C., Oliveira J. M., Reis R. L. "Promising Biomolecules". Osteochondral Tissue Engineering. Oliveira J. M., Pina S., Reis R. L., SanRoman J. (Eds.), Springer, 2018, 1059:189-205. doi:10.1007/978-3-319-76735-2_8.
3. **Oliveira I. M.**, Vieira S, Oliveira J. M., Pina S., Reis R. L. "Nanoparticles-Based Systems for Osteochondral Tissue Engineering". Nanoparticles-Based Systems for Osteochondral Tissue Engineering. Oliveira, J., Pina, S., Reis, R.L., San Roman, J. (Eds.), Springer, 2018, 209-217, doi:10.1007/978-3-319-76735-2.
4. Gonçalves C., **Oliveira I. M.**, Reis R. L., Oliveira J. M., Sattler K. D. "Nanoparticles for Bone Tissue Engineering". 21st Century Nanoscience Â– A Handbook: Bioinspired Systems and Methods. Sattler K. D. (Eds.), CRC Press, 2020, 7:1-14.
5. Gonçalves C., López-Cebral, R., Radhouani H., **Oliveira I. M.**, Silva-Correia J., Reis R. L., Oliveira J. M. "Natural polysaccharides" Biomaterials Handbook. Granja, P. L.; Engqvist, H.; Mantovani, D. (Eds.), Willey, 2020 (In press).
6. **Oliveira I. M.**, Carvalho, M.R. Reis R. L., Oliveira J. M. "Dendrimers in Tissue Engineering". Dendrimer as Nanotherapeutics. Kesharwani, P. (Eds.), Elsevier, 2021 (In press).

Conference posters

1. **Oliveira I. M.**, Gonçalves C., Reis R. L., Oliveira J. M. "Functionalized dendronized nanoparticles for targeting hyperplastic synovium and treatment of rheumatoid arthritis." TERM STEM and GENE2SKIN, Guimarães, October, 2016.

2. **Oliveira I. M.**, Gonçalves C., Reis R. L., Oliveira J. M. "Functionalized dendronized nanoparticles for targeting hyperplastic synovium and treatment of rheumatoid arthritis." Chem2Nature summer school, Porto, June, 2017.

3. Gonçalves C., Radhouani H., **Oliveira I. M.**, Gonçalves C., Reis R. L., Oliveira J. M. "Characterization methods of intra-articular injection products". Chem2Nature Summer School, Porto, June, 2017.

4. **Oliveira I. M.**, Gonçalves C., Reis R. L., Oliveira J. M. "Tyramine modified Gellan Gum for targeting hyperplasic synovium and treatment of rheumatoid arthritis." GENE2SKIN Winter School, TERM STEM and FORECAST, Porto, November 2017.

5. Gonçalves C., Silva S., **Oliveira I. M.**, Maia R., Radhouani H., Reis R. L., Oliveira J. M. "Green Processing of SAIB-based scaffolds for Tissue engineering applications", TERM STEM and FORECAST, Porto, November 2017.

6. **Oliveira I. M.**, Gonçalves C., Reis R. L., Oliveira J. M. "Tyramine modified Gellan Gum for targeting hyperplasic synovium and treatment of rheumatoid arthritis." Chem2Nature Summer school, Porto, June, 2018.

7. Gonçalves C., Silva S., **Oliveira I. M.**, Maia R., Radhouani H., Reis R. L., Oliveira J. M. "SAIB-Based Scaffolds For Tissue Engineering" Chem2Nature Summer school, Porto, June, 2018.

8. Gonçalves C., Silva S., **Oliveira I. M.**, Maia R., Radhouani H., Reis R. L., Oliveira J. M. "Development of Biomaterials Based on Sucrose Acetate Isobutyrate" Chem2Nature Final Conference, Guimarães, October, 2018.

9. **Oliveira I. M.**, Gonçalves C., Shin M.E., Lee S., Reis R. L., Khang G., Oliveira J. M. "Ty-GG and Ty-GG/Silk hydrogels for targeting hyperplasic synovium and treatment of rheumatoid arthritis". FORECAST Workshop, Porto, June, 2019.

10. **Oliveira I. M.,** Gonçalves C., Shin M.E., Lee S., Reis R. L., Khang G., Oliveira J. M. "Ty-GG and Ty-GG/Silk fibroin hydrogels for targeting hyperplasic synovium and treatment of rheumatoid arthritis". 1st Discoveries Forum on Regenerative and Precision Medicine, September, June, 2019.

11. **Oliveira I. M.,** Gonçalves C., Oliveira E. P., Simón-Vasquez R., Silva-Morais A., González-Fernandez A., Reis R. L., Oliveira J. M. "Sulphur-functionalized PAMAM towards rheumatoid arthitis treatment" TERM STEM, Braga, November, 2019.

Awarded grants

1. Horizonte Norte2020 PhD scholarship (Norte-08-5369-FSE-000044).
2. REMIX project (G.A. 778078 – REMIX – H2020-MSCA-RISE-2017).

INTRODUCTION TO THE THESIS FORMAT

To make a clear organization of the work performed under the scope of this PhD, this thesis is divided into four main sections (1 to 4) containing ten chapters (**I to X**).

A general introduction (Section 1) can be found divided in three different chapters: **Chapters I, II and III.** This section is followed by Materials and Methods description, corresponding to Section 2, that includes **Chapter IV**. Section 3, in which **Chapters V** to **IX** can be found, focuses on the experimental studies and results obtained in the context of this thesis and their discussion. This corresponds to the main body of the thesis is based on a series of publications published in international journals or already submitted for publication. Each individual chapter is presented in a manuscript form, *i.e.* abstract, introduction, experimental section, results and discussion, conclusion, and acknowledgements. A list of relevant references is also provided as a subsection within each chapter. The contents of each part and chapter are described below in more detail. Final Conclusions and Future Perspectives can be found in the last section of this thesis, Section 4 (**Chapter X**).

Section 1 – General introduction

Chapter I – Rheumatoid Arthritis: Pathogenesis and Current Therapeutic Strategies: This chapter focuses on the analysis of the pathogenesis of Rheumatoid Arthritis, discussing the role of pro-inflammatory cytokines involved in disease, and presenting the current therapeutic strategies used in the treatment of RA.

Chapter II – Engineering nanoparticles for targeting rheumatoid arthritis: Past, Present and Future Trends: This chapter presents an extensive overview of recent studies using nanoparticles in the treatment of Rheumatoid Arthritis namely, liposomes, polymeric nanoparticles, dendrimers, and metallic nanoparticles

Chapter III – Hydrogels in the treatment of Rheumatoid Arthritis: Drug delivery systems and artificial matrices for dynamic *in vitro* models: This chapter reviews and discuss the recent studies using hydrogels in the treatment of Rheumatoid Arthritis, featuring different hydrogel formulations. Besides, their use as artificial extracellular matrices in dynamic *in vitro* articular cartilage and Rheumatoid Arthritis disease models are reviewed in depth.

Section 2 – Detailed description of experimental materials and methodologies

Chapter IV – Materials and Methods: A list of the materials used, and methods performed to obtain the results described further on is provided, being the basis for the all work described in this thesis.

Section 3 – Experimental work regarding the nanoparticles and biomaterials approach to the treatment of inflammation on Rheumatoid Arthritis

Chapter V – PAMAM dendrimers functionalized with an anti-TNF α antibody and chondroitin sulphate for treatment of rheumatoid arthritis: This chapter focuses on the development and evaluation of PAMAM dendrimers functionalized with chondroitin sulfate and linked to an anti-TNF α antibody, based on targeted delivery to the treatment of inflammation on Rheumatoid Arthritis. The PAMAM dendrimer was functionalized with chondroitin sulfate and synthesized as nanocarriers, to help receptor-ligand interaction and low toxicity, while the covalently linked anti-TNF α Abs provides anti-inflammatory properties.

Chapter VI – Enzymatically crosslinked tyramine-gellan gum hydrogels as drug delivery system for rheumatoid arthritis treatment: In this chapter, we developed tyramine-modified gellan gum hydrogels (crosslinked by both physical and chemical mechanisms) in the presence of horseradish peroxidase and hydrogen peroxide. The Ty-GG hydrogels were loaded with betamethasone in order to provide it sustain release and improve the treatment safety in patients with Rheumatoid Arthritis.

Chapter VII – Anti-Inflammatory Properties of Injectable Betamethasone-Loaded Tyramine-Modified Gellan Gum/Silk Fibroin Hydrogels: In this chapter, we aimed to produce hydrogels of Tyramine-modified Gellan gum with silk fibroin via horseradish peroxidase, with encapsulated betamethasone, to improve the biocompatibility and mechanical properties, and further increase therapeutic efficacy to treat rheumatoid arthritis.

Chapter VIII – Bioengineered nanoparticles loaded-hydrogels to target TNF alpha in inflammatory diseases: In this chapter, monoclonal anti-TNF α antibody linked to chondroitin sulfate modified poly(amidoamine) dendrimer nanoparticles and loaded into Tyramine-Gellan gum hydrogels and Tyramine-Gellan gum/Silk Fibroin hydrogels were developed. The therapeutic efficacy was evaluated using cells-based inflammation *in vitro* model under standard static conditions and dynamic conditions using a bioreactor.

Chapter IX – Modulation of inflammation by anti-TNF α mAb-dendrimer nanoparticles loaded in tyramine-modified Gellan gum hydrogels in a cartilage-on-a-chip model:

This chapter describes focuses on the development of a new *in vitro* human 3D inflammatory cartilage-on-a-chip model aiming to be used as a drug screening platform. An inflammatory environment was established by means of culturing human primary chondrocytes exposed to active pro-inflammatory macrophages to support with more efficiency the therapeutic effect of anti-TNF α mAb-CS/PAMAM dendrimer NPs loaded-Ty-GG in the treatment of inflammation

Section 4 – Concluding remarks

Chapter X – General Conclusions and Future Perspectives: The final Section of the thesis presents the main conclusions of each chapter, current limitations and potential of the advanced strategies for application in the treatment of Rheumatoid Arthritis. The future perspectives of the advanced strategies developed in this thesis were also provided.

No great discovery was ever made without a bold guess”

—Isaac Newton

SECTION 1

GENERAL INTRODUCTION

Chapter I

Rheumatoid Arthritis: Pathogenesis and Current Therapeutic Strategies

Chapter I

Rheumatoid Arthritis: Pathogenesis and Current Therapeutic Strategies[1]

ABSTRACT

Rheumatoid Arthritis (RA) is an autoimmune and inflammatory disease that affects approximately 1% of people worldwide. The exact cause of RA remains unknown, however, seems to result from interaction among genetic and environmental factors. The pathogenesis of RA is characterized by the infiltration of several inflammatory cells into the synovial membrane and by subsequent cartilage and bone tissue destruction. The synovial membrane is the central area of pathology. The specialized connective tissue becomes thickened and hyperplastic containing an infiltration of inflammatory cells. These cells form a complex network that promotes the production of pro-inflammatory cytokines that play important roles in the pathophysiology of RA. Although there is no cure for RA, treatments can help reduce inflammation in the joints, relieve pain, and prevent or slow down joint damage. This chapter focuses on the analysis of the pathogenesis of RA, discussing the role of pro-inflammatory cytokines involved in disease, and presenting the current therapeutic strategies used in the treatment of RA.

Keywords: Rheumatoid arthritis, Pathogenesis, Cytokines, Current treatments.

[1]This chapter is based on the following publication:

Oliveira I. M., Gonçalves C., Reis R. L., Oliveira J. M. "Synovial Knee Joint". Regenerative Strategies for the Treatment of Knee Joint Disabilities. Oliveira J. M., Reis R. L. (Eds.), Springer, 2016, 21:21-28. doi:10.1007/978-3-319-44785-8_2.

I-1. INTRODUCTION

I-1.1. Pathogenesis of Rheumatoid Arthritis

Rheumatoid Arthritis (RA) is a chronic, progressive, inflammatory autoimmune disease that arises more frequently in females than males, affecting approximately 1% of people worldwide. This arthritic disease is associated with progressive disability, premature death, and socioeconomic burdens [1]. The exact cause of RA remains unknown, however, initiation of the disease seems to result from interaction among genetic susceptibility and environment triggers (smoking, obesity) [2]. The pathology of RA is characterized by the infiltration of several inflammatory cells into the synovial membrane and by subsequent cartilage and bone tissue destruction **(Figure I-1).**

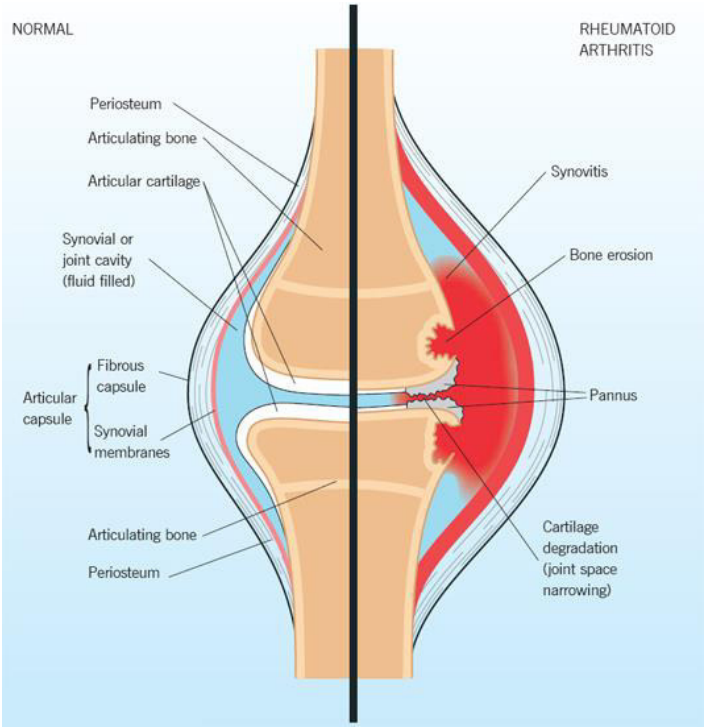

Figure I-1 - Pathophysiology of Rheumatoid Arthritis and comparation with normal joint. Reprinted with permission [3].

The synovial membrane (synovium) is the central area of pathology in several inflammatory joint diseases, including RA. This membrane is a thin highly organized structure that is present between the joint cavity and the fibrous joint capsule [4]. The synovial membrane has two layers, the inner layer, constituted by macrophages or synoviocytes, and the outer layer, composed of two to three layers of synoviocytes over connective tissue with fibroblasts, secreting collagen, and other extracellular matrix proteins. The outer layer has few macrophages and lymphocytes, blood vessels containing nutrients to

the synovial membrane, and the adjacent avascular cartilage and fat cells [5]. The synovial membrane is surrounding the cavity of joints, taking the space with synovial fluid [6]. The synovial fluid, secreted by the synovial membrane, is responsible for (i) joint lubrication (which reduces friction and lessen shock between the surfaces of cartilage) and (ii) has an important role in the nutrition of the articular cartilage [7].

The joint synovial structure changes substantially in RA patients. RA is initially characterized by a pre-vascular inflammatory phase, followed by a vascular phase with an increase in vessel growth. The normal synovial membrane becomes hyperplastic, containing a superficial lining layer of synovial fibroblast and macrophages, overlying an interstitial zone that comprises a marked cellular infiltrate, which includes synovial fibroblasts, macrophages, mast cells, CD4+ T-cells, CD8+ T-cells, natural killer (NK) cells, NKT cells, B-cells and plasma cells [8]. The inflammation of the synovium invades adjacent cartilage and subsequently, it can promote articular destruction. Articular damage is featured by an environment hypoxic and angiogenesis (growth of new blood vessels), characteristic of RA joints. The increased number of blood vessels is associated with synovial cell hyperplasia and mononuclear cell infiltration. The angiogenesis allows cells to migrate from the blood into the inflamed synovium, where pro-inflammatory cytokines and chemokines have an important role in the pathogenesis of RA [9],[10],[11].

I-1.2. Pro-inflammatory cytokines involved in the pathogenesis of rheumatoid arthritis

Various immune modulators (cytokines and effector cells) and signaling pathways are involved in the pathophysiology of RA [12]. The RA pathogenesis begins with the activation of immune cells (including dendritic cells, T cells, B cells, plasma cells, macrophages, and mast cells) and by angiogenesis. Macrophages, T cells, B cells, and other immune cells form a complex network that promotes the production of pro-inflammatory cytokines that play important roles in the pathophysiology of RA [13]. Cytokines support cell-to-cell communication in immune response and stimulate the movement of cells towards sites of inflammation, infection, and trauma. In rheumatic joints, the upregulation of pro-inflammatory cytokines and downregulation of anti-inflammatory cytokines favors the induction of autoimmunity, chronic inflammation, and thus joint damage [14].

The pro-inflammatory cytokines most directly implicated in the RA disease process are tumor necrosis factor-α (TNF-α), interleukin (IL-1), and IL-6. These cytokines produce an overlapping spectrum

of biological actions, they act in concert with each other and other cytokines to produce many of their pathophysiological effects [15]. The main role of pro-inflammatory cytokines in the pathogenesis of RA disease is summarized in **(Table I-1)** [16].

TNF-α is expressed as a type II transmembrane protein consisting of 233 amino acid residues (26 kDa). After processing by the TNF-α-converting enzyme, the soluble form of TNF-α is cleaved from transmembrane TNF-α (17 kDa). The soluble TNF-α and its precursor form, transmembrane TNF-α, are involved in the inflammatory response. Soluble TNF-α acts at sites remote from the TNF-α-producing cells and transmembrane TNF-α exerts its biological function in a cell-to-cell contact (binding to TNF-α receptors). Therefore, transmembrane TNF-α plays a critical role in local inflammation [17]. The main supply of TNF-α are macrophages, T-cells, B-cells, mast cells, synovial fibroblasts, chondrocytes, and osteoblasts. It is one of the key cytokine molecules that cause inflammation in RA. TNF-α stimulates the production of other inflammatory cytokines, IL-1, IL-6, IL-8, granulocyte monocyte-colony stimulating factor (GM-CSF), MMP (Matrix Metalloproteinases), attracting and activating immune and inflammatory cells into the joint (leukocytes, endothelial cells and fibroblast-like synoviocytes (FLS) [18]. This process is enabled by the upregulation of key integrins and adhesion molecules. The destruction of the underlying articular cartilage and subchondral bone is initiated by the proteolytic and MMPs which provoke the destruction of the underlying cartilage, and the initiation of osteoclast resorptive activity, which brings about the destruction of the subchondral bone [19]. In cultures of synovial cells from RA patients, blocking TNF-α with antibodies significantly reduces the production of IL-1, IL-6, IL-8, and GM-CSF. Thus, the inhibition of TNF-α may have a wider effect on inflammation than the inhibition of other cytokines present in high concentrations in synovial fluid [20].

The IL-1 family comprises a total of 11 members. Several members of the IL-1 superfamily have been implicated in the pathogenesis of RA. IL-1α and IL-1β are expressed in abundance in the synovial membrane and produce the biological effects attributed to IL-1 cytokine [21],[22]. This pro-inflammatory cytokine is expressed by macrophages, B cells, T cells, synovial fibroblasts, and chondrocytes. IL-1α and IL-1β increase cytokine production by synovial monocellular cells, chemokine, prostaglandins (PGs), and MMP released by fibroblasts. Furthermore increases catabolism and cytokine production by chondrocytes, and bone erosion by osteoclasts [23]. Due to the role of this cytokine in the RA pathology, the IL-1 blockade has an important therapeutic effect in disease [24].

The IL-6 is a pro-inflammatory cytokine that also plays an important role in the pathophysiology of RA. This cytokine is found in abundance in the synovial fluid and serum of patients of RA and the level associates with the disease activity and joint destruction [25]. It is mainly produced in the inflamed joints by macrophages, FLS, B cells, and T cells. IL-6 can induce synovitis and joint destruction by stimulating neutrophil migration, osteoclast maturation, and vascular endothelial growth factor (VEGF)-stimulated pannus proliferation [26]. IL-6 may also contribute to the induction and maintenance of the autoimmune process through B-cell maturation and TH-17 differentiation. So, the inhibition of IL-6 is a desirable therapeutic option in the treatment of RA [27].

Table I-1 - Main pro-inflammatory cytokines involved in the pathogenesis of Rheumatoid Arthritis.

Cytokine	Cell source	Role in the disease process
TNF-α	Macrophages, T-cells and B-cells Mast cells Synovial fibroblasts Chondrocytes Osteoblasts	Activates immune and inflammatory cells (leukocytes, endothelial cells, and synovial fibroblasts); Increase the monocyte activation, cytokine, chemokine, adhesion molecules, and MMP release; Actives the destruction of the underlying articular cartilage and subchondral bone;
IL-1	Macrophages T-cells and B-cells Synovial fibroblasts Chondrocytes	Increase the synovial fibroblast cytokine, chemokine, MMP, and PG release; Osteoclast activation; Endothelial cell adhesion molecule expression;
IL-6	Macrophages T-cells and B-cells Synovial fibroblasts	Neutrophil recruitment; Osteoclast activation; Pannus formation via promotion of VEGF production; B-cell proliferation and antibody production; T-cell proliferation and differentiation;

I-2. CURRENT THERAPEUTIC STRATEGIES FOR RA

Treatments for RA can help reduce inflammation in the joints, relieve pain, and prevent or slow down joint damage. Although there is no cure for rheumatoid arthritis, suitable treatment early during RA can reduce the risk of joint damage and limit the impact of the condition [28].

The current treatment principles for established RA involve symptomatic management and disease modification. There are five main classes of drugs frequently used in the treatment of RA, analgesics, NSAIDs, GCs, DMARDs, and biological agents. The most usually used therapeutic strategies comprise analgesics, NSAIDs, GCs. However, DMARDs and biological agents are the first line of treatment in RA in order to relieve joint damage and control the disease progression [29],[30].

Despite recent advances in medical therapeutics, the treatments still raise major efficiency concerns. The therapeutic strategies are associated with poor pharmacokinetic distribution to the specific site of disease, short half-life, and several side effects. The current strategies used in RA treatment are summarized in **(Table I-2)** [31],[32].

Analgesics provide pain relief from slight to moderate arthritis. In these groups are included acetaminophen, tramadol, capsaicin, and narcotics. Since these drugs do not exhibit any anti-inflammatory properties, they are usually combined with GCs, NSAIDs, DMARDs, and biological therapies [31],[33].

NSAIDs have both analgesic and anti-inflammatory properties but do not change the course of the disease of RA or prevent joint destruction. NSAIDs are useful for treating the symptoms of RA but are incapable to avoid the development of the progressive disease. The drugs in this class include ibuprofen, aspirin, naproxen, and indomethacin. This class of drugs inhibits ciclo-oxigenase (COX)-1 and COX-2, blocking PGs synthesis that are mediators of inflammation and pain [34],[35]. Although NSAIDs are essential to the treatment of RA, they can cause severe gastrointestinal adverse events and ulcers [36]. Recent studies have verified that their analgesic and anti-inflammatory effects are mediated mainly through inhibition of the COX-2 iso-enzyme. Three selective COX-2 inhibitors are celecoxib, rofecoxib, and valdecoxib [37]. Compared with traditional NSAIDs, they have been shown to have comparable efficacy and a better overall safety profile. As NSAID gastropathy is one of the most significant side effects associated with NSAIDs, and because this toxicity seems to associate closely with inhibition of COX-1, one of the greatest potential advantages for COX-2 selective inhibition was anticipated to be their lower incidence of gastropathy. However, if the patient has a medical story of cardiovascular disease,

COX-2 inhibitors can increase ischemic cardiovascular events [38],[39]. Although COX-2 inhibitors can lower the rate of gastrointestinal adverse events, they do not completely protect high-risk patients from recurrent ulcer complications [40],[41].

Glucocorticoids have both anti-inflammatory and immunoregulatory activity. GCs have profound effects on the distribution and function of circulating leukocytes. They inhibit neutrophil migration to sites of inflammation reducing their adherence to vascular endothelium and interfere with cytokine stimulation. This class of drugs includes prednisone, methylprednisolone, betamethasone, dexamethasone, among others [42],[43]. They can be administered orally, intravenously, or by intra-articular injection. The actions of these drugs on joint pain are much greater than NSAIDs and analgesics but they have more side effects including osteoporosis, weight gain, muscle weakness, diabetes, hypertension, and glaucoma. Due to their multiple side effects, they are now used mainly as a therapeutic adjunct in low doses or as a bridge therapy aimed at controlling symptoms during periods when disease activity is high [43].

DMARDs include a large group of drugs that reduce the progression of joint erosion. Although both NSAIDs and DMARDs agents improve symptoms of active RA, only DMARDs agents have shown to alter the disease course [44],[45]. DMARDs have slow onsets and no analgesic activity. In most cases, when the diagnosis RA is confirmed, the therapy with DMARDs agents should be started [46]. The currently available drugs include gold compounds, penicillamine, hydroxychloroquine, cyclophosphamide, and methotrexate. The actions of these drugs are possibly related to the decrease of phagocytosis and immune responses. Due to powerful action, DMARDs can cause several side effects, normally, stomachache, liver problems, blood problems, among others [47],[48].

Biological agents have recently been developed to treat RA. This class of drugs acts by decreasing the inflammatory response in affected joints. Biological agents target specific components of the immune system that play an important role in the sustenance of the disease process and tend to work more quickly than conventional DMARDs [49],[12]. There is substantial evidence that the pro-inflammatory cytokines TNF-α, IL-1, and IL-6 are upregulated in RA [18]. Recent clinical trials targeting these cytokines have shown a significant clinical improvement and slowing of disease progression. Examples of these drugs include anti-TNF-α agents, IL-1 and IL-6 receptor antagonists [50],[51]. However, these agents may induce side effects, tuberculosis, respiratory infection, skin infection, and urinary tract infection. These drugs are newer treatments and in the future supplementary biological therapies will possibly become available [52].

Table I-2 - Main pro-inflammatory cytokines involved in the pathogenesis of rheumatoid arthritis.

Therapy	Drug	Mechanism of action	Side effects
Analgesics	Acetaminophen Tramadol Capsaicin Narcotics	Analgesia	Gastrointestinal problems
NSAIDs	Ibuprofen Aspirin Naproxen Indomethacin Celecoxib Rofecoxib Valdecoxib	COXs inhibitors Immunomodulation	Gastrointestinal problems Cardiac disfunction Ulcers
GCs	Prednisone Methylprednisolone Betamethasone Dexamethasone	Immunosuppression	Osteoporosis Weight gain Muscle weakness Diabetes Hypertension Glaucoma
DMARDs	Gold compounds Penicillamine Hydroxychloroquine Cyclophosphamide Methotrexate	Immunosuppression Disease-modifying activity	Gastrointestinal problems Liver and kidney problems Blood problems
Biological agents	Etanercept Infliximab Adalimumab Anakinra Tocilizumab Sarilumab	TNF-α inhibitor IL-1 receptor inhibitor IL-6 receptor inhibitor	Tuberculosis Respiratory infections Urinary tract infection Skin infection

I-3. CONCLUSION AND FUTURE PERSPECTIVES

RA is a frequent and chronic painful disease that affects synovial joints. Recently acquired knowledge regarding the pathogenesis of RA has significantly improved the therapy of the disease. Current treatments focus on suppression inflammation preventing the progression of joint damage but

rarely provide complete pain relief. Pain is not the only important consequence for RA patients but also exacerbates disability and psychological suffering. RA pain can be mediated by inflammation mechanisms and structural damage. A better understanding of the different contributions of these mechanisms should lead to more effective treatment targeting, as well as the development of new approaches with fewer side effects.

I-4. REFERENCES

1. Guo, Q., et al., *Rheumatoid arthritis: pathological mechanisms and modern pharmacologic therapies.* Bone research, 2018. **6**: p. 15-15.
2. Deane, K.D., et al., *Genetic and environmental risk factors for rheumatoid arthritis.* Best practice & research. Clinical rheumatology, 2017. **31**(1): p. 3-18.
3. Clancy, J. and H. Hasthorpe, *Pathophysiology of rheumatoid arthritis: nature or nurture?* Primary Health Care, 2011. **21**(9).
4. Kiener, H.P. and T. Karonitsch, *The synovium as a privileged site in rheumatoid arthritis: cadherin-11 as a dominant player in synovial pathology.* Best Pract Res Clin Rheumatol, 2011. **25**(6): p. 767-77.
5. de Sousa, E.B., et al., *Synovial fluid and synovial membrane mesenchymal stem cells: latest discoveries and therapeutic perspectives.* Stem cell research & therapy, 2014. **5**(5): p. 112-112.
6. Korochina, K., V. Polyakova, and I. Korochina, *Morphology of synovial membrane and articular cartilage in the knee joint in experimental chronic heart failure.* Bulletin of experimental biology and medicine, 2016. **160**(3): p. 376-380.
7. Revell, P., *Synovial lining cells.* Rheumatology International, 1989. **9**(2): p. 49-51.
8. McInnes, I.B. and G. Schett, *Cytokines in the pathogenesis of rheumatoid arthritis.* Nature Reviews Immunology, 2007. **7**(6): p. 429-442.
9. Marrelli, A., et al., *Angiogenesis in rheumatoid arthritis: a disease specific process or a common response to chronic inflammation?* Autoimmunity reviews, 2011. **10**(10): p. 595-598.
10. Pham, C.T., *Nanotherapeutic approaches for the treatment of rheumatoid arthritis.* Wiley Interdisciplinary Reviews: Nanomedicine and Nanobiotechnology, 2011. **3**(6): p. 607-619.
11. Oda, K. and M. Minata, *Drug free remission after steroid-dependent disappearance of lymphoproliferative disorder in rheumatoid arthritis patient treated with TNF-alpha blockade: case study.* SpringerPlus, 2015. **4**(1): p. 41.
12. Yap, H.-Y., et al., *Pathogenic Role of Immune Cells in Rheumatoid Arthritis: Implications in Clinical Treatment and Biomarker Development.* Cells, 2018. **7**(10): p. 161.
13. Choy, E., *Understanding the dynamics: pathways involved in the pathogenesis of rheumatoid arthritis.* Rheumatology, 2012. **51**(suppl_5): p. v3-v11.
14. Wojdasiewicz, P., Ł.A. Poniatowski, and D. Szukiewicz, *The role of inflammatory and anti-inflammatory cytokines in the pathogenesis of osteoarthritis.* Mediators of inflammation, 2014. **2014**: p. 561459-561459.
15. Zhang, J.-M. and J. An, *Cytokines, inflammation, and pain.* International anesthesiology clinics, 2007. **45**(2): p. 27-37.

16. Lubberts, E. and W.B. van den Berg, *Cytokines in the pathogenesis of rheumatoid arthritis and collagen-induced arthritis*, in *Madame Curie Bioscience Database [Internet]*. 2013, Landes Bioscience.
17. Horiuchi, T., et al., *Transmembrane TNF-alpha: structure, function and interaction with anti-TNF agents.* Rheumatology (Oxford, England), 2010. **49**(7): p. 1215-1228.
18. Kany, S., J.T. Vollrath, and B. Relja, *Cytokines in Inflammatory Disease.* International journal of molecular sciences, 2019. **20**(23): p. 6008.
19. Brennan, F.M. and I.B. McInnes, *Evidence that cytokines play a role in rheumatoid arthritis.* The Journal of clinical investigation, 2008. **118**(11): p. 3537-3545.
20. Vasanthi, P., G. Nalini, and G. Rajasekhar, *Role of tumor necrosis factor - alpha in rheumatoid arthritis: a review.* APLAR Journal of Rheumatology, 2007. **10**(4): p. 270-274.
21. Dinarello, C.A., *Overview of the IL-1 family in innate inflammation and acquired immunity.* Immunological reviews, 2018. **281**(1): p. 8-27.
22. Kay, J. and L. Calabrese, *The role of interleukin-1 in the pathogenesis of rheumatoid arthritis.* Rheumatology (Oxford), 2004. **43 Suppl 3**: p. iii2-iii9.
23. Chow, Y.Y. and K.-Y. Chin, *The Role of Inflammation in the Pathogenesis of Osteoarthritis.* Mediators of inflammation, 2020. **2020**: p. 8293921-8293921.
24. Kaneko, N., et al., *The role of interleukin-1 in general pathology.* Inflammation and regeneration, 2019. **39**: p. 12-12.
25. Le Goff, B., E. Romas, and N.C. Walsh, *IL-6 is a critical cytokine for inflammatory bone loss in rheumatoid arthritis.* International Journal of Clinical Rheumatology, 2010. **5**(6): p. 609.
26. Yoshitomi, H., *Regulation of Immune Responses and Chronic Inflammation by Fibroblast-Like Synoviocytes.* Frontiers in immunology, 2019. **10**: p. 1395-1395.
27. Srirangan, S. and E.H. Choy, *The role of interleukin 6 in the pathophysiology of rheumatoid arthritis.* Therapeutic advances in musculoskeletal disease, 2010. **2**(5): p. 247-256.
28. Scott, D.L., F. Wolfe, and T.W. Huizinga, *Rheumatoid arthritis.* Lancet, 2010. **376**(9746): p. 1094-108.
29. Köhler, B.M., et al., *Current Therapeutic Options in the Treatment of Rheumatoid Arthritis.* Journal of clinical medicine, 2019. **8**(7): p. 938.
30. Quan, L.-D., et al., *The Development of Novel Therapies for Rheumatoid Arthritis.* Expert opinion on therapeutic patents, 2008. **18**(7): p. 723-738.
31. van Laar, M., et al., *Pain treatment in arthritis-related pain: beyond NSAIDs.* The open rheumatology journal, 2012. **6**: p. 320-330.
32. Cunnane, G., M. Doran, and B. Bresnihan, *Infections and biological therapy in rheumatoid arthritis.* Best Practice & Research Clinical Rheumatology, 2003. **17**(2): p. 345-363.
33. Ong, C.K.S., et al., *An evidence-based update on nonsteroidal anti-inflammatory drugs.* Clinical medicine & research, 2007. **5**(1): p. 19-34.
34. Crofford, L.J., *Use of NSAIDs in treating patients with arthritis.* Arthritis research & therapy, 2013. **15 Suppl 3**(Suppl 3): p. S2-S2.
35. Scarpignato, C., et al., *Safe prescribing of non-steroidal anti-inflammatory drugs in patients with osteoarthritis – an expert consensus addressing benefits as well as gastrointestinal and cardiovascular risks.* BMC Medicine, 2015. **13**(1): p. 55.
36. Hawkey, C.J. and M.J.S. Langman, *Non-steroidal anti-inflammatory drugs: overall risks and management. Complementary roles for COX-2 inhibitors and proton pump inhibitors.* Gut, 2003. **52**(4): p. 600-608.
37. Zarghi, A. and S. Arfaei, *Selective COX-2 Inhibitors: A Review of Their Structure-Activity Relationships.* Iranian journal of pharmaceutical research : IJPR, 2011. **10**(4): p. 655-683.

38. Al-Saeed, A., *Gastrointestinal and Cardiovascular Risk of Nonsteroidal Anti-inflammatory Drugs.* Oman medical journal, 2011. **26**(6): p. 385-391.
39. Varrassi, G., et al., *Ibuprofen Safety at the Golden Anniversary: Are all NSAIDs the Same? A Narrative Review.* Advances in Therapy, 2020. **37**(1): p. 61-82.
40. Becker, J.C., W. Domschke, and T. Pohle, *Current approaches to prevent NSAID-induced gastropathy–COX selectivity and beyond.* British journal of clinical pharmacology, 2004. **58**(6): p. 587-600.
41. Fokunang, C., et al., *Overview of non-steroidal anti-inflammatory drugs (NSAIDs) in resource limited countries.* MOJ Toxicol, 2018. **4**(1): p. 5-13.
42. Ronchetti, S., et al., *How Glucocorticoids Affect the Neutrophil Life.* International journal of molecular sciences, 2018. **19**(12): p. 4090.
43. Liberman, A.C., et al., *Regulatory and Mechanistic Actions of Glucocorticoids on T and Inflammatory Cells.* Frontiers in endocrinology, 2018. **9**: p. 235-235.
44. Lacaille, D., *Rheumatology: 8. Advanced therapy.* CMAJ : Canadian Medical Association journal = journal de l'Association medicale canadienne, 2000. **163**(6): p. 721-728.
45. Cannella, A.C. and J.R. O'Dell, *Chapter 61 - Traditional DMARDs: Methotrexate, Leflunomide, Sulfasalazine, Hydroxychloroquine, and Combination Therapies*, in *Kelley and Firestein's Textbook of Rheumatology (Tenth Edition)*, G.S. Firestein, et al., Editors. 2017, Elsevier. p. 958-982.e7.
46. *Guidelines for the management of rheumatoid arthritis: 2002 Update.* Arthritis Rheum, 2002. **46**(2): p. 328-46.
47. Drosos, A.A., *Methotrexate intolerance in elderly patients with rheumatoid arthritis.* Drugs & aging, 2003. **20**(10): p. 723-736.
48. Rainsford, K.D., et al., *Therapy and pharmacological properties of hydroxychloroquine and chloroquine in treatment of systemic lupus erythematosus, rheumatoid arthritis and related diseases.* Inflammopharmacology, 2015. **23**(5): p. 231-269.
49. Takeuchi, T., *Treatment of rheumatoid arthritis with biological agents - as a typical and common immune-mediated inflammatory disease.* Proceedings of the Japan Academy. Series B, Physical and biological sciences, 2017. **93**(8): p. 600-608.
50. Curtis, J.R. and J.A. Singh, *Use of biologics in rheumatoid arthritis: current and emerging paradigms of care.* Clinical therapeutics, 2011. **33**(6): p. 679-707.
51. Lis, K., O. Kuzawińska, and E. Bałkowiec-Iskra, *Tumor necrosis factor inhibitors - state of knowledge.* Archives of medical science : AMS, 2014. **10**(6): p. 1175-1185.
52. Salvana, E.M.T. and R.A. Salata, *Infectious complications associated with monoclonal antibodies and related small molecules.* Clinical microbiology reviews, 2009. **22**(2): p. 274-290.

Chapter II

Engineering Nanoparticles for Targeting Rheumatoid Arthritis: Past, Present and Future Trends

Chapter II

Engineering nanoparticles for targeting rheumatoid arthritis: Past, Present and Future Trends[2]

ABSTRACT

Rheumatoid arthritis (RA) is a chronic inflammatory disease characterized by joint synovial inflammation and cartilage and bone tissue destruction. There are some treatment strategies for RA but they are not completely safe and effective. Therefore, it is important to develop and test new drugs for RA that specifically can target inflamed/swollen joints and simultaneously attenuate other possible damages to healthy tissues. Nanotechnology can be a good alternative to consider when envisioning precise medicines for the treatment of RA. Through the use of nanoparticles, it became possible to increase bioavailability and bioactivity of therapeutics and further selective targeting to damaged joints. Herein, it is reviewed the recent studies using nanoparticles in the treatment of RA namely, liposomes, polymeric nanoparticles, dendrimers, and metallic nanoparticles. These therapeutics strategies have been showing great promise to improve the RA treatment as compared with the use of traditional drugs. The results of these studies allow confirming that the use of nanoparticles is mainly due to their properties such as biocompatibility, low toxicity, controlled release, and selective drug delivery to inflamed tissues in animal RA models. Therefore, it is possible to claim that nanotechnology will have, in the near future, a crucial role in advanced treatments and patient-specific therapies for human diseases such as RA.

Keywords: Nanoparticles, Liposomes, Dendrimers, Rheumatoid arthritis

[2]This chapter is based on the following publications:

Oliveira I.M., Gonçalves C., Reis R.L., Oliveira J.M., "Engineering nanoparticles for targeting rheumatoid arthritis: Past, Present and Future Trends". Nano Research, 2018, 11:4489–4506. doi: 10.1007/s12274-018-2071-3.

Oliveira I.M., Carvalho, M.R. Reis R. L., Oliveira J. M. "Dendrimers in Tissue Engineering". Dendrimer as Nanotherapeutics. Kesharwani, P. (Eds.), Elsevier, 2021 (In press).

II-1. GRAPHICAL ABSTRACT

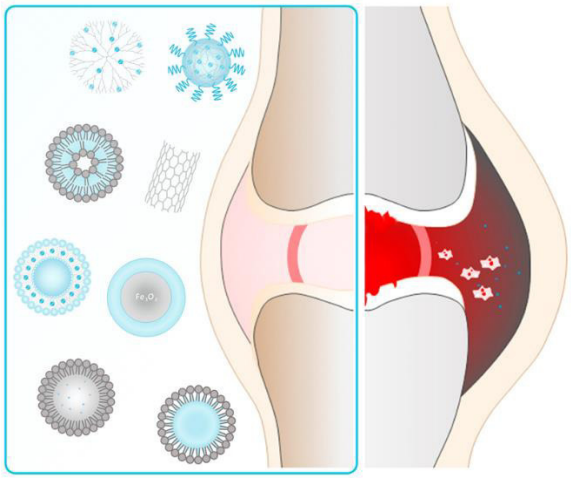

II-2. INTRODUCTION

Rheumatoid arthritis (RA) is a chronic inflammatory disease that affects approximately 1% of the general population worldwide, and it is associated with a high degree of morbidity and significant mortality [1],[2]. It is characterized by joint synovial inflammation and stiffness, and the destruction of cartilage and bone [3],[4]. Many cell types have been identified as important participants on the establishment and progression of the disease. T-cells have been implicated as primary mediators in the pathogenesis of RA, they contribute to the inflammatory response through the elaboration of cytokines and interaction with other cells that perpetuate the inflammation and joint destruction [5]. Pro-inflammatory cytokine tumor necrosis factor-α (TNF-α) has an important role in the pathogenesis of RA. It has been found to be a therapeutic target, while anti-TNF-α agents showed to induce long-term improvements in the RA symptoms and signs, by protecting affected joints from tissue degradation [6].

The treatment strategies for RA comprise the use of disease-modifying anti-rheumatic drugs (DMARDs), typically supported by non-steroidal anti-inflammatory drugs (NSAIDs) and/or glucocorticoids (GCs), in order to reduce joint inflammation and pain, maximize joint function, and prevent joint destruction and deformity. Agents that target TNF-α are the leading biological DMARDs. There are three TNF-α inhibitors well established in the RA market: (I) Infliximab, (ii) a chimeric

monoclonal antibody, and (iii) the fusion protein etanercept [7],[8]. Despite recent advances in medical therapeutics, the treatments still raise major efficiency concerns. In fact, patients fail to respond adequately or become resistant to drug therapy and long-term use of these drugs may be due to adverse events, such as tuberculosis, fungal infections, lymphomas, liver injury, myelosuppression, and heart failure. It is urgent to develop and test new drugs to specifically target inflamed joints, to attenuate damage to healthy tissues. In this sense, nanomedicine is a promising therapeutic approach to RA. Drug-loaded nanocarriers coupled with pathophysiological characteristics of inflamed joints can amplify bioavailability and bioactivity of medical therapeutic and possibly promote selective targeting to inflamed joints [9].

Encapsulating bioactive agents into nanocarriers that selective drug delivery to the intended sites of action may be reached through targeted approaches, and will be herein overviewed [5].

II-3. NANOPARTICLE SYSTEMS

Nanotechnology refers to the ability to measure, design, and manipulate materials at atomic, molecular, and supramolecular levels [10],[11]. The production of nanomaterials for drug delivery can offer new opportunities to provide a more focused and perfect treatment of the disease at molecular level, improving the potential therapeutic drugs so that they become less toxic and more effective. Most drugs have several limitations due to their poor solubility, high toxicity, high dosage, nonspecific delivery, and short circulating half-lives. Nano-size drug delivery focuses on the preparation of bioactive molecules in biocompatible nanosystems such as nanoparticles [12],[13].

Nanoparticles (NPs) have sizes ranging from 1-100 nm. The therapeutic applications of NPs are diverse. One advantage is the improvement of the poorly water-soluble solubility drugs. Nanoparticles of poorly water-soluble drugs can increase the surface area and surface interactions of NPs, which can be used to enhance the dissolution rate and allow controlling the pharmacokinetic properties of the dosage form [14]. The NPs also prolong the half-life of drug systemic circulation, releases drugs at a sustained rate, delivers drugs in a targeted manner to minimize systemic side effects, and delivers two or more drugs simultaneously for combination therapy. Drugs are used in RA treatment due to their anti-inflammatory and analgesic effect and reduction in inflammatory markers. Drugs such as clodronate, triptolide, methotrexate, indomethacin, dexamethasone, siRNA against TNF-α, among others can be loaded onto NPs by diverse methods such as being attached to the nanocarrier's surface or

encapsulated within them. They have been used as drug-delivery systems with unique architectures to work as a drug-delivery vehicle for particular disease treatment. These technologies have been studied and used for the treatment of cancer, diabetes, pain, asthma, allergy and infection [10],[11],[12],[13],[15]. There are different types of nanoparticles including polymeric NPs, liposomes, dendrimers magnetic NPs, metallic NPs, polymeric micelles, solid lipid nanoparticles, nanotubes, among others [11],[16],[17] **(Figure II-1)**. Most studied nanoparticles for RA treatment are liposomes, polymeric NPs, dendrimers and metallic nanoparticles.

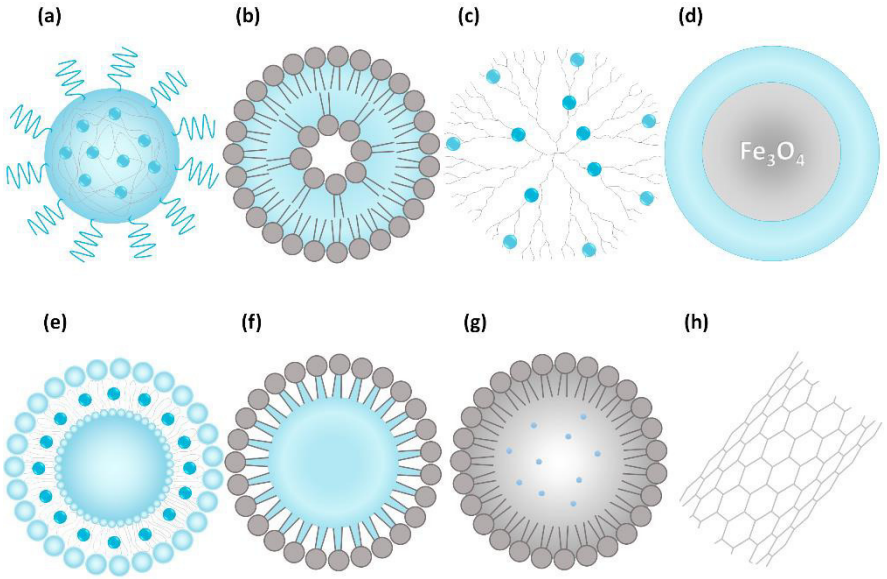

Figure II-1 - Scheme with the nanoparticles systems. a) polymeric NPs, b) liposomes, c) dendrimers, d) magnetic NPs, e) metallic NPs, f) polymeric micelles, g) solid lipid nanoparticles, and h) nanotubes.

II-3.1. Liposomes

Liposomes are spherical nanoparticles constituted of bilayer membranes with aqueous interior and can be composed of synthetic or natural phospholipids. Physical and chemical properties of a liposome include permeability, charge density, and steric hindrance. They can be used as effective drug delivery systems. Drug loading in liposomes can be in the aqueous compartment or in the lipid membrane. Generally lipid soluble drugs are incorporated in the liposomal membrane and water soluble drugs are loaded in the compartment [18],[19].

There are many studies reporting the potential applications of liposomes in RA treatment **(Table II-S1 in the Supplementary Information)**. Fong *et al.* [20] studied rabbits with and without arthritis injected with free [3H] methotrexate ([3H]MTX) or liposomes containing [3H]MTX with thioglycollate-elicited

macrophages *in vitro*. These authors found that the catchment of liposomes by the synovium was low. However, it was reported a 40-fold increase in drug retention in the joint, compared to the injection of free MTX. Liposomes can improve the efficacy and decrease the side effects of drugs into the joint cavity [21],[22].

Love and co-workers [23] have studied liposomes in the inflamed tissue of rats with induced arthritis and in rats without arthritis. Control rats and with arthritis were injected intravenously, via the tail vein, with four different sized liposome preparation. Through the study was possible to verify that there was 10 times more liposome accumulation in inflamed rats than in control rats and there were differences between the small unilamellar vesicle and multilamellar vesicle in inflamed and control paws. The small unilamellar vesicle was more accumulated in inflamed paws. Another study investigated if local removal of phagocytic synovial lining cells (SLCs) from the knee by clodronate-liposomes before the introduction of collagen-induced arthritis (CIA) influenced the development of cartilage destruction. That study showed that phagocytic SLCS depleted by a single injection of clodronate-liposomes in the knee joint accompanied of SLCs with treatment with dexamethasone decreased cartilage damage [24],[25],[26],[22]. Williams *et al*. [27] studied the liposome encapsulated with methotrexate in the inflamed knee joint to determine if conjugation would be able to modulate the severity of induced arthritis in rats. The conjugated has been shown *in vitro* to inhibit to release of two pro-inflammatory mediators, TNF-α and prostaglandin stimulated rat peritoneal macrophages. After the onset of joint inflammation, the rats were treated intravenously with liposome-methotrexate. Liposome encapsulated with methotrexate showed significant improvement in established joint inflammation and less toxicity than comparable doses of the free drug. A study made by Watson-Clark *et al*. [28] examined the use of liposomes as a boron delivery method in rats with CIA. The concentration of boron delivery by liposomes was determined after the intravenous injection of liposomes. The biodistribution of liposomes incorporated in the vesicle membrane demonstrated higher synovium/blood boron ratios, reduced boron uptake in synovial tissue, and more rapid blood clearance [26]. Another study analyzed the effect BPD-Verteporfin (liposomal benzoporphyrin derivate-monoacid ring A) in the inflamed synovium and articular and peri-articular tissues following intravenous and intra-articular administration in the rabbit model. The study showed that there was a preferred distribution of BDP-MA in the inflamed synovium and clearance from the synovium was rapid **(Figure II-2)** [29],[26],[22].

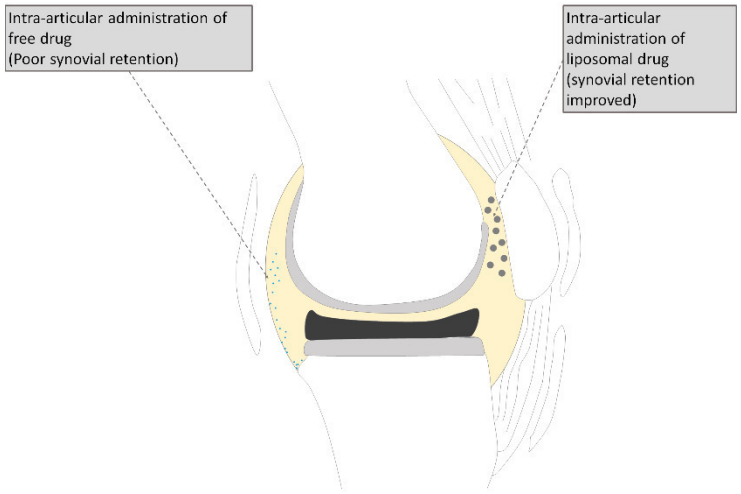

Figure II-2 - Scheme for the use of liposomes in rheumatoid arthritis. Reprinted with permission from [22] .

Highton *et al.* [30] investigated the involvement of liposomes containing clodronate as an anti-macrophage treatment for RA. They used the antigen-induced arthritis model (AIA) in sheep to evaluate the effect of clodronate liposomes. There was an uptake of liposomes into macrophages within the inflamed joint. They gave an intra-articular injection of clodronate liposome in a group of sheep (group 1), or saline liposome (group 2) and others without arthritis and no treatment (group 3). There were no differences between joint diameter and swelling in groups 1 and 2. In these groups histologic scoring was similar, and both were worse than group 3. Despite the possible pro-inflammatory effect, they were not able to show a therapeutic effect of a single dose of clodronate liposomes in this kind of animal model [26]. Another investigation explored the subcutaneous administration of superoxide dismutase (SOD) entrapped in long circulating liposomes in rats with RA. Results showed that small-sized SOD-liposomes gave a higher uptake in the inflamed foot than the large-sized SOD-liposomes. When compared the localization in the inflamed foot with the non-inflamed foot, uptake was higher for the small–sized SOD-liposomes than the large-sized SOD-liposomes. Thus, small-sized liposomes are more effective than the large-sized SOD liposomes for targeting of SOD to arthritis sites after subcutaneous administration [31],[26]. A study made by Srinath *et al.* [32] investigated the encapsulation of indomethacin in liposomes to determine anti-inflammatory potential. The study investigated the biodistribution using convention liposomes and long-circulating liposomes in a RA rat model. It was found that long-circulating liposomes have shown higher targeting efficiency in arthritis paw tissue than conventional liposomes [21],[26]. Ceponis and co-workers [33] showed that intra-articular injection of low doses of liposomal clodronate in rabbits established AIA had anti-inflammatory and antierosive effects. There were low levels of TNF-α, lining cell hyperplasia, and macrophages in the synovium of the

liposomal clodronate treatment group. Nevertheless, the effect was temporary and it did not prevent the occurrence of joint erosions over the long term [26]. A study reported by Trif *et al.*, [34] investigated the use of liposome-entrapped lactoferrin (hLf) as a delivery system to prolong hLf retention at local inflammation sites such as the rheumatoid joint. Investigators compared negatively charged liposomes, positively charged formulations, and free protein. *In vivo* studies in rats with CIA showed that the positive liposomes were more effective in prolonging the residence time of hLf in the inflamed joint when compared with other liposomes. In 2007, the same investigation group compared the capacity of free lactoferrin and lactoferrin encapsulated in liposomes to prevent established joint inflammation and to modulate the cytokine response of lymph node (LN) T lymphocytes in DBA/1 mice with CIA. The anti-inflammatory effect was higher in positive liposomes and it was inferior in the free protein. After a single injection of liposomal hLf, the arthritic score was significantly reduced. Cytokine levels produced by LN T cells showed a pro-inflammatory cytokines (TNF-α) decrease followed by an increase of the anti-inflammatory cytokines (IL-10) in encapsulated when compared with free hLf [35]. Another report has compared a dexamethasone-anti-E-selectin immunoconjugate with anti-E-selectin immunoliposomes that contain dexamethasone, analyzing *in vivo* increase in activated endothelial cells and *in vitro* binding and internalization. That study showed that dexamethasone-anti-E-selectin was internalized to a larger extent than the anti-E-selectin immunoliposomes, while the high drug-loading capacity of the liposomes may allow a larger quantity of dexamethasone to intracellular delivery. Both accumulated in activated endothelial cells in murine inflamed skin [36],[37]. Metselaar *et al.* [38] studied the intravenous treatment action of prednisolone phosphate (PLP), encapsulated in long-circulating polyethylene glycol liposomes, to target inflamed joints in rats with AIA. Liposomal PLP proved to be highly effective, with a complete reduction of the inflammatory response while the same dose of non-encapsulated PLP did not reduce inflammation [27],[28]. In 2004, the same researchers investigated the effect of treatment with encapsulated PLP in long (poly) ethylene glycol (PEG)-liposomes to target synovial lining cells in inflamed joint and cartilage destruction in mice with CIA. Mice were treated with conjugated and free PLP few days after the established disease, and liposome PLP resulted in a strong and lasting resolution of joint inflammation compared with free PLP [39],[5]. A study made by Harigai *et al.*, [40] evaluated the potential of prednisolone phosphate (PSLP) – containing 3,5-dipentadecyloxybenzamidine hydrochloride (TRX-20) liposomes to treat RA. The conjugated was added to Human Fibroblast-Like Synoviocytes (HFLS) cells. The effects of PSLP in TRX-20 liposomes, on HFLS cells were evaluated by the inhibition of the production of inflammatory cytokines and inflammatory chemokine. The symbiosis of the PSLP-containing liposomes with HFLS cells was 40 times higher than that of PSLP-containing

liposomes without TRX-20 [22]. Another study investigated if RGD peptide-exposing long circulating PEG liposomes (RGD-PEG-L). The aim of this work is to see if αvβ3 integrins expressed on angiogenic vascular endothelial cells (VECs) are efficient to connect VECs at sites of inflammation and if liposomes containing dexamethasone phosphate (DEXP) could be used as carriers to interfere with the development of experimental arthritis. In rats with AIA was evaluated DEXP-encapsulating RGD-PEG-L as compared with non-target liposomes. One intravenous injection of DEXP encapsulated in RGD-PEG-L resulted in a strong and lasting anti-arthritic effect in rat AIA [41],[25],[37],[22]. The folate-linked lipid-based nanoparticles delivery a nuclear factor kappa B (NFκB) decoy into murine macrophage RAW264.7 cells was also studied. The manifestation of the folate receptor in RAW26.7 cells activated lipopolysaccharide as confirmed by suppression of folate receptor (FR) mRNA. After transferred via NP-F, the NFκB was detected in the cytoplasm and an inhibitory effect on the translocation of NFκB in the nucleus was observed, presuming that NP-F delivered the NFκB catch into the cytoplasm. This approach is important for active macrophages in gene therapy for RA [42]. Rauchhaus *et al.*, [43] analyzed the glucocorticoid dexamethasone phosphate (DXM) encapsulated in non-PEGylated liposomes in rat AIA and rat with no drug. Injection of liposomes DXM at 6, 24, and 48 hours after arthritis induction was responsible for removing joint swelling. Liposomal DXM suppressed both chronic inflammation and joint destruction, while free DXM-P failed to prevent joint destruction. Richard *et al.*, [44] investigated the efficacy of a single dose of liposomal clodronate within small unilamellar vesicles (SUVs) to suppress joint inflammation and histological progression of AIA rats. Rats received a single injection of liposomal clodronate 7 days post-arthritis induction. The results showed that liposomal clodronate eliminates synovial macrophages, reduces inflammation, and ameliorates joint destruction in AIA. In 2001, Richard *et al.* [45], investigated the role of macrophages using liposomal clodronate in the pathogenesis of induced chronic arthritis. Ten days after arthritis induction, rats received a single intravenous injection of liposomal clodronate within SUVs. Twenty-six days after treatment, SUVs suppressed the development of arthritis. Macrophage elimination by SUVs inhibits local production of IL-1β, IL-6, TNF-α and MMP-9, and the pathogenesis of inflammatory arthritis [26]. A study made by Simões *et al.* [46] investigated a novel treatment possibility using the SOD liposome mixed lipid vesicles, Transfersomes (TFs) in the AIA rat model. Treatment of animals started on day 1 by application epicutaneous of SOD-TFs. After this application, there was the suppression of the induced rat paw edema. It was shown for the first time that SOD incorporates into TFs and applied into a skin area not necessarily close to the inflamed tissue is able to promote non-invasive treatment of induced arthritis [22]. Gaspar *et al.* [47] studied the biological behavior of Acylated Superoxide Dismutase (Ac-

SOD) enzymosomes inserted in the lipid bilayer of the liposomes, as compared to SOD that is located in the aqueous compartment of liposomes. For that study were used unmodified liposomes and long circulating liposomes coated with PEG. The results showed that liposomes coated with PEG were not influenced by the insertion of Ac-SOD in the lipid bilayers. The potential therapeutic of SOD liposome was compared with Ac-SOD enzymosomes in rats with arthritis. Ac-SOD enzymosomes presented a faster anti-inflammatory effect as observed by the volume of the inflamed paws. The results allowed conclude that Ac-SOD enzymosomes are able to exert therapeutic effect before liposome disruption and they can act as a sustained release of the enzymes. Another study determined the therapeutic effect of TNF-α siRNA administration using liposomes, in rats with rheumatoid arthritis. The therapeutic effect in rats was assessed after intravenous delivery of TNF-α siRNA by cationic liposomes. Rats showed improvements when TNF-α siRNA was administrated, combined with the liposome and with carrier DNA. There was inhibition of systemic TNF-α secretion and a decrease in the levels of IL-6. The study demonstrated the efficiency of a liposome carrier system to silence TNF-α in rats with RA [48],[26].

II-3.2. Polymeric nanoparticles

Polymeric nanoparticles (NPs) are biodegradable, good drug-delivery systems, and can be biocompatible. These nanoparticles exhibit a big potential for surface modification and functionalization with different ligands, are excellent pharmacokinetic controls, and are able to encapsulate and deliver a variety of therapeutic agents [13]. There are various studies of polymeric nanoparticles for the treatment of RA **(Table II- S2/S3 in the Supplementary Information)**. Gerlag *et al.*, [49] studied mice with CIA that were injected with RGD-containing cyclic peptide (RGD-4C) that binds selectively to the αvβ3 and αvβ5 integrins in the cells of the inflamed synovium but not in the cells of the normal synovium. αvβ3 and αvβ5 are important in angiogenesis, αvβ3 manifests on synovial blood vessels in RA and αv antagonists injected directly into the joint quell synovitis. The results showed that RGD-4C decreased rheumatoid arthritis symptoms and increased apoptosis of synovial blood vessels. A study made by Kim et al., [50] investigated the effect of single administration of Polylactic-co-glycolic (PLGA) entrapping type II collagen (II) on the development of CIA. This conjugate was studied due to the capacity of each element to be a strong candidate to suppress autoimmune disease. After a single administration of PLGA-CII in mice, the incidence and severity of arthritis on CIA was significantly reduced. Furthermore, mice showed a higher level of TGFβ (transforming growth factor β) mRNA and a

lower level of TNF-α mRNA expression compared with the other groups of mice. Another study evaluated the Fluoresceinamine bound PLGA (FA-PLGA) copolymer for intra-articular delivery system in the rat synovium after administering directly into the joint cavity. FA-PLGA nanospheres could be more adequate for delivery to inflamed synovial tissue due to their ability to pass through the synovium and can provide local-therapy action in joint disease, [50],[51]. Fienh *et al.* [52] evaluated the anti-arthritic effect human serum albumin-coupled methotrexate (MTX-HSA) as potential target cells for albumin-mediated drug delivery. The mice model of CIA was used to analyze anti-arthritis effects of MTX and MTX-HSA. Intravenously administration injection showed that MTX-HSA is superior to MTX in inhibition of the development of CIA and reduction the joint destruction as well as the number of affected paws. MTX-HSA can be one of the potential target cells to anti-arthritic treatment [21],[53]. A study by Higaki *et al.*, [54] investigated Betamethasone sodium phosphate (BSP) encapsulated in PLGA nanoparticles to target inflamed joints in rats with AIA and mice with anti-type II collagen antibody induced arthritis (AbIA). These rats were treated intravenously with PLGA-nanosteroid after the initial sign of arthritis. In AIA rats, there was a decrease in paw inflammation. A single injection of the PLGA-nanosteroid resulted in a large decrease of the inflammatory response after 1 week. Furthermore, a histological examination showed a significant decrease of the inflammatory cells in the joints [21],[58],[51]. Another study analyzed the anti-inflammatory effect of the triptolide (TP) loaded polylactic acid (PLA) nanoparticles in AIA rats. The results showed that TP-PLA-NPs significantly inhibited adjuvant arthritis and had a significant anti-inflammatory effect with the long-time administration [55],[56]. Mansouri *et al.,* [57] studied the synthesis and characterization of FA-chitosan-DNA nanoparticles and evaluated the cytotoxicity *in vitro*. Chitosan-DNA and FA-Chitosan-DNA nanoparticles were made using reductive amidation and a complex coacervation process. The transfection efficiency depends on various factors such as the chemical structure of polycations, cell type, nanoparticle size, composition, and interaction with cells. The results showed that FA-nanoparticles had decreased cytotoxicity (damaging property of a substance compared to cells), there was a good DNA condensation and particle size improved the cellular uptake (around 118 nm) [37].

A study made by Wang *et al.*, [58] investigated dexamethasone (Dex)- *N*-(2-hydroxypropyl) methacrylamide (HPMA) copolymer conjugate to target inflamed joints in rats with RA. The investigators administered dexamethasone-HPMA in the AIA rat model and it was found that dexamethasone-HPMA had more anti-inflammatory effects compared with free DEX. Moreover, bone and cartilage preservation with the dexamethasone-HPMA treatment was higher than with free Dex treatment [21],[37]. Other

study investigated nanoparticles coated with collagen II-binding-peptide (WYRGRL) to target the articular cartilage in RA disease. It was reported that peptide-functionalized nanoparticles targeted articular cartilage is much higher than nanoparticles presenting a scrambled peptide sequence following intra-articular injection in the mouse [59]. Another study made by Hwang *et al.* [8] evaluated the use α-Methylprednisolone (MP) conjugated cyclodextrin polymer-based nanoparticles (CDP) for rheumatoid arthritis therapy. The conjugate was administered intravenously in rats with CIA. A significant decrease in arthritis score was observed in rats treated with CDP-MP, after 28 days and histological evaluation showed synovitis decrease. That study showed that conjugation CDP-MP may increase the efficacy for rheumatoid arthritis treatment [5],[9]. Another group, Howard *et al.* [2] investigated chitosan/siRNA nanoparticle-mediated TNF-α reduction in macrophages for anti-inflammatory treatment in CIA mice. Histological analysis of joints showed little cartilage destruction and inflammatory cell infiltration in anti-TNF-α-treated mice. This work showed that chitosan/siRNA nanoparticle-mediated TNF-α knockdown reduces local and systemic inflammation. Ishihara *et al.* [4] studied the therapeutic activity of betamethasone disodium 21-phosphate (BP) encapsulated in nanoparticles of poly (D,L-lactic/glycolic acid) PLGA)/poly(D,L-lactic acid) (PLA) homopolymers and polyethylene glycol (PEG)-block-PLGA/PLA copolymers in rats with AIA and mice with AbIA to target inflamed joint. The conjugated was intravenously administered. In AIA rats, there was a 35% decrease in paw inflammation with a single injection [37],[5],[9]. In 2010, Ishihara *et al.* [60] investigated the degradation of poly(lactic acid) and monomethoxypolyethyleneglycol(PEG)-polylactide block copolymer along with betamethasone disodium phosphate (BP) *in vitro* during incubation. It was found that there is an accumulation of BP in the inflammatory lesion of adjuvant arthritis rat models and that the amount of BP gradually decreases. Results suggested that the BP increase in the lesion is due to the increase of the permeability and retention effect. The internalization in inflammatory macrophages is due to the loss of PEG and the release of BP in cells with PEG hydrolysis. Another study examined PEG-Dexamethasone conjugate for the treatment of RA in an AIA model. The study revealed that a single PEG-Dex conjugate improves the ankle joint inflammation of AIA rats. Histological and bone mineral density showed that there was superior anti-inflammatory and disease modifying effects with PEG-Dex conjugate [61]. A study made by Kim *et al.* [62] examined the efficiency of RA treatment through of development of nanocomplexes based on hyaluronic acid (HA) and polyethylene glycol (PEG)-derivatized TRAIL((TNF)-related apoptosis inducing ligand) (PEG-TRAIL). The nanocomplexes were prepared by mixing the positively charged PEG-TRAIL and negatively charged HA. The *in vivo* biodistribution and diffusion kinetics of Cy5.5-labeled PEG-TRAIL in mice were observed after subcutaneous injections. Results showed that there were

greater therapeutic effects in clinical scores and histology in delivery of PEG-TRAIL, with nanocomplex in 1% HA, furthermore this approach resulted in a substantial reduction of serum inflammatory cytokines and collagen-specific antibodies that are responsible for RA. A study performed by Schmitt *et al.*, [63] investigated hydrophilic nanogels based on chitosan, with hyaluronate surface, loaded with photosensitizers to target macrophages. That work showed a selective uptake by macrophages and increase retention of drugs in inflamed tissues. The injection free photosensitizers resulted in rapid liberation from the joints, while nanogel-encapsulated photosensitizers stayed in the inflamed joints for a longer period of time. The last treatment of the inflamed joints resulted in a reduction of inflammation when compared with a standard corticoid treatment [37]. Another study investigated chitosan conjugated with folate. Chitosan-DNA and folate-chitosan-DNA were intravenously injected in normal and arthritis rats. That approach showed to help transfect more efficiently folate-chitosan-DNA nanoparticles and can decrease inflammation in the arthritis rat model [64],[37]. Scheinman et al., [65] investigated the functionalization of RGD-PLGA to deliver a STAT1 siRNA in the RA model. RGD-PLGA increased paw tissue uptake and increased long delivery of nanoparticles in the arthritis mice model. RA regressed with STAT1 siRNA and STAT1 mRNA levels were lower in paws of treated animals. This conjugate showed to be effective in the treatment of arthritis, through selective inhibition of macrophage and dendritic cell activation. Another study investigated if a metalloproteinase MMP-3-specific polymeric matrix could be used for early diagnosis of arthritis in mice with CIA using a near-infrared fluorescence (NIRF) imaging system [66]. After intravenous administration of the probe, different stages of the disease through fluorescent images were obtained. A higher NIRF signal was recovered from arthritis joints compared with normal joint. The immune histochemical analysis and Western blotting confirmed that fluorescence in the *in vivo* imaging was related to MMP-3 activity in the joint tissues. A study made by Park *et al.* [67] investigated hydrophobically modified gycol chitosan nanoparticles (HGC) labeled with Cy5.5 (a dye) in mice with CIA. Activated macrophages expressing Mac-1 molecules effectively phagocyted HGC-Cy5.5 that formed spherical nanoparticles under physiologic conditions. Previous studies showed that HGC nanoparticles mainly accumulate in tumor tissue via leaky vessels, which show that the pathophysiologic properties increased permeability and retention effect. Due to a large quantity of activated macrophage and angiogenesis characterized by the permeable and disorganized structure within the synovial tissues in RA, the investigators put the hypothesis that HGC nanoparticles may preferentially within arthritis joint. The histological evaluation confirmed that the mechanism of selective accumulation of HGC-Cy5.5 within synovitis tissues included increased phagocytosis as well as permeability increase through leaky vessels. Another group, Boekhorst *et al.* [68] evaluated the anti-

inflammatory effect of poly(poly(DL-lactide-co-glycolide acid) (PLGA) nanoparticles loaded with small interfering RNA (siRNA) against TNF-α. Intra-articular treatments in joint with TNF-α siRNA-loaded NPs resulted in a disease activity reduction and no significant decrease in joint effusions was observed as compared to treatment with PLGA NPs loaded with non-specific control siRNA. The study suggested that HGC-Cy5.5 can have an important role as RA therapeutic. Rollet *et al.* [69] investigated the effect of the folic acid-human serum albumin nanocapsules (FA-HSA) to target drug delivery to chronically activated macrophages. Some studies showed that the beta folate receptor (FRβ) has a high affinity for FA and it is expressed by activated macrophages. Therefore, FA based nanoparticles can provide the possibility of delivering therapeutic agents to activated macrophages without affecting normal cells and tissues. It was reported that FRβ-expressing macrophages showed an increased binding for FA-HSA compared without FA [56]. Another study developed PLGA nanoparticles co-encapsulated of methotrexate (MTX) and Superparamagnetic iron oxide nanoparticles (SPIONS) in RA therapy and imaging applications. The NPs were functionalized with anti-CD64 antibody to specifically target rheumatoid arthritis associated macrophages, to decrease damage to the tissues. The effect of each component was compared (MTX, SPIONS, and antibody). *In vitro* studies allowed concluding on the cytotoxic profile of NPs. MTX indicated high toxicity, while MTX-free NPs were only toxic when administrated at the highest concentration holding PLGA`s biocompatibility [70]. Kim *et al.* [71] investigated the self-assembled dextran sulphate nanoparticles for targeting rheumatoid arthritis. *In vivo* results showed that these nanoparticles selectively accumulated into inflamed synovia of CIA mice, due to binding to the macrophage scavenger receptors that were overexpressed in the synovia of CIA mice thus showing the potential of dextran sulfate nanoparticles as a drug carrier for arthritis therapy. A study made by Heo *et al*. [72] investigated hyaluronam nanoparticles (HA-NPs) bearing a γ-secretase inhibitor (DAPT) for rheumatoid arthritis therapy. Results demonstrated that DNPs (DAPT-loaded HA-NPs) attenuated the severity of RA compared to DAPT alone that was evaluated from tissue damage, clinical score, and neutrophil infiltration. Furthermore, DNPs reduced the production of pro-inflammatory cytokines and collagen-specific auto-antibodies in the serum of the CIA mice. In AbIA mice, a single injection ended with the inflammatory response after one week **(Figure II-3)**.

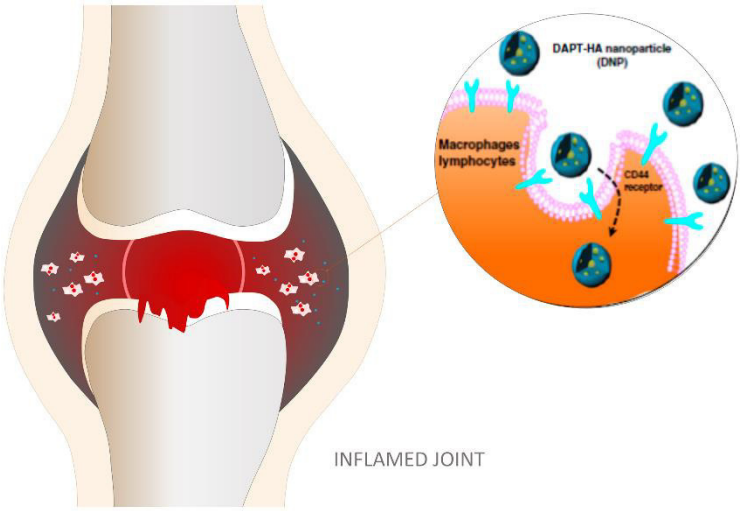

Figure II-3 - Scheme of DNPs for inflamed joint-targeted drug delivery. Reproduced and adapted with permission from [72]. Copyright Elsevier, 2016.

Lee *et al.* [73] design a nanocomplex of polymerized siRNA (poly-siRNA) targeting TNF-α with thiolated gycol chitosan (TGC) polymers for the treatment of RA. Poly-siRNA was prepared through self-polymerization that resulted in psi-TGC-NPs (nanocomplex of polymerized siRNA with thiolated gycol chitosan). These nanoparticles showed *in vitro* TNF-α gene silencing efficacy and high accumulation at the arthritic joint sites in CIA mice **(Figure II-4)**. Other study investigated folic acid-etoricoxib-bovine serum albumin nanoparticles (F-ETX-NPs) for rheumatoid arthritis treatment [74]. The etoricoxib concentration revealed targeting potential to the activated macrophage cells. The results suggested that F-ETX-NPs have the potential for activated macrophage cells targeting rheumatoid arthritis. This process could be used for early stage diagnosis of rheumatoid arthritis [74].

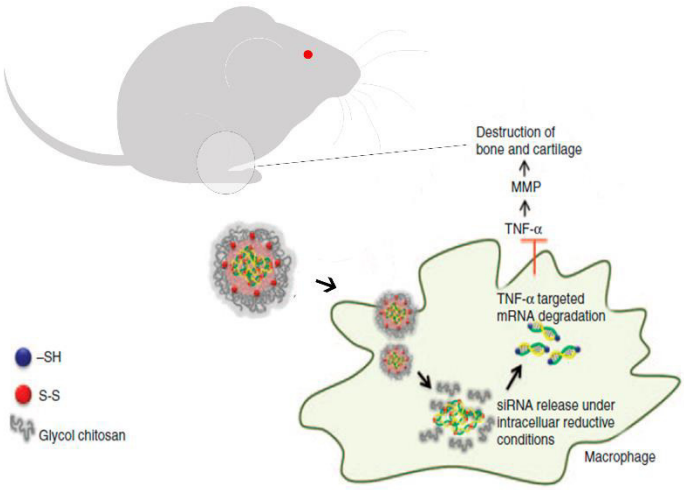

Figure II-4 - Scheme of psi-tGC–NPs into macrophage cells leading to TNF-α gene knockdown. Reproduced and adapted with permission from [73]. Copyright Nature Publishing Group, 2016.

II-3.3. Dendrimers

Dendrimers consist of three-dimensional nano-sized and branched structure, with an overall spherical geometry. The word "dendrimer" comes from the Greek word "Dendron", which means tree, as it presents a similar branching in his tree like structure [75].

The structure of the dendrimer is divided into three parts: the core, the interior, and the shell. The core affects the 3D shape of the dendrimer, the interior affects the host–guest properties of the dendrimer, namely for drug loading capacity and hydrophobic/hydrophilic interactions [76]. Finally, the dendrimer's surface can be further engineering, polymerized or modified with functional groups, allowing for a great variety of applications, from theranostic to targeting applications [76].

Regarding its synthesis, dendrimers are conventionally synthesized by two major routes: the divergent method, introduced by Tomalia *et al.* [77], and the convergent method, developed by Hawker and Fréchet [78], developed to overcome the limitation of the divergent synthesis [79]. In the first method (divergent), the final molecule grows radially from a core by the sequential addition of layers of monomers, each layer constituting a new generation (G). The number of surface groups multiplies according to the functionalities in each monomer ramification. Dendrimers benefit from straightforward, iterative syntheses that produce highly monodisperse, globular macromolecules. Their high degree of branching results in an exponential increase in end groups with each generation size [80]. In the convergent methods, the dendrimer is produced stepwise, starting from the end groups and growing

inside. When dendrons, (growing branched polymeric arms) are large enough, they are attached to a multifunctional core molecule. The convergent growth method has several advantages. They are quite easy to purify and the appearance of defects in the structure is minimal. Furthermore, it is possible to add subtle engineering into the dendritic structure through the accurate placement of functional groups at the surface of the macromolecule. However, the convergent method does not allow the formation of high generations due to steric problems that happen between reactions of the dendrons and the core molecule [81].

Dendrimers are recognized as nanosized, nonlinear, hyperbranched polymers. Whose overall 3D shape is key for their biological activity. The number and type of surface charges on each dendrimer can be controlled since different generations of dendrimers can be prepared and the termini can be modified to bear any desirable synthetic group [80].

The cytotoxicity of dendrimers depends strongly on the number and nature of functional surface groups. Anionic and neutral dendrimers present slight or no toxic effects while cationic dendrimers frequently show high toxicity. Poly(propylene imine) (PPI) and poly(amido amine) (PAMAM) dendrimers obtaining terminal primary amines are defined by concentration- and generation-dependent toxicity [82], [83], whereas grafted carbosilane – poly (ethylene oxide) (CSi – PEO) dendrimers and other dendrimers terminated with anionic or neutral groups demonstrate to be much less toxic [84]. Furthermore, modification of the surface of the cationic dendrimer with negatively charged or neutral molecules declines its cytotoxicity. Surface functionalization with pyrrolidone, polyethylene glycol (PEG), or another biocompatible compound can decrease cytotoxicity to levels better than those of currently available products [85].

Dendrimers have received great attention in biological application due to their adjustable surface functionalization, well-defined structure, high water solubility, compact globular shape, and monodispersed size. These features make them versatile carriers for drug delivery applications. Dendrimers are being considered as an additive in various routes of administration such, oral, transdermal, ocular, and intravenous administration [86],[87]. Dendrimers for drug delivery are employed using two different approaches. Drugs, enzymes, antibodies, and other bioactive agents can be physically encapsulated in a dendrimer using non-covalent interactions [88],[89] or be bounded on the surface of the dendrimers via hydrogen bonding, electrostatic interaction, van der Walls force or covalently attached [90],[91]. Small drugs are frequently encapsulated into the dendrimers while larger (bio)molecules preferably bind to the surface [92]. Drugs encapsulation depends on the structure of

both the dendrimer and the drug. It is crucial to understand the chemistry behind dendrimer structure. Selecting a suitable dendrimer is the principal step for drug encapsulation [93]. The internal structure of a dendrimer is normally hydrophobic due to hydrophobic interactions and hydrogen bond formations and it is appropriate for encapsulating hydrophobic drugs/bio-actives [94]. The drug molecules sterically encapsulated in the interior are protected from the external environment. Furthermore, this characteristic offers promising advantages of extending the residence time of the drug in the blood circulation and enhancing the stability of active and tissue targeting [95]. The physical interaction between specific groups within dendrimer and the drug is a simple process, just mixing dendrimers and drugs in either aqueous solutions or a mixture of solvents [96]. The chemical structure of the drugs to be loaded remains unchanged after the connection with dendrimer, which assures the therapeutic efficacy of the drug [97]. The effectiveness of encapsulation is highly dependent on surface functional groups of dendrimers, chemical structure, and molecular weight. It is often complicated to control the encapsulation capacity and the rate of drug release from the dendrimer because the entrapment of the drug is based on physical interactions [98].

Despite several drugs are encapsulated in dendrimers, it is usually difficult to control the retention a consequent release of drug in the dendrimer so sometimes it is necessary different conditions [99]. The reason is that the stability of drug-encapsulated dendrimers are powerfully affected by the strength of their interaction and the water solubility of the drug [100]. Therefore, attaching the drugs to surface functionalities is an attractive approach. This is a great approach for precise drug delivery because a single dendrimer molecule can stably transport many drug molecules using many functional groups (amine and carboxyl groups) on the surface and release drug molecules precisely on the target [99],[95]. The drug molecules can be linked to the dendrimer through electrostatic interaction, non-covalently or covalently. When the molecular groups present on the surface of the dendrimer are charged, the surface can electrostatically attract oppositely charged. It is possible to attach a variety of ionizable drugs or molecules electrostatically to dendrimers duo to numerous ionizable groups present on the dendrimer surface allowing this complex show adequate solubility in water [101],[102]. The covalent conjugation of the drug onto the dendrimer surface offers different advantages due to hydrolysable or biodegradable bound between dendrimer and drug allow better control over drug release when compare to drug-encapsulated dendrimer [98]. Dendrimer/drug conjugation is frequently stable *in vivo* due to the covalently bond between dendrimer and drug and release kinetics is controlled by the type of the linker systems. Each linkage system has its mechanism of cleavage modality that

splits the drug molecule from dendrimer. To improve the effectiveness of drug delivery, it is crucial to control the drug release from the dendrimer transporter in the target site with minimal contact with normal tissues [98].

There are some studies of dendrimers for rheumatoid arthritis treatment **(Table II-S4 in the Supplementary Information)**. The first study used folate targeted poly(ethylene glycol) (PEG) conjugates of G 3.5 PAMAM dendrimer as targeted drug delivery systems to inflammation and to investigate its distribution standard in arthritis rats. Folate-PEG-PAMAM was loaded with indomethacin. Folate-PEG conjugation has 10-20-fold increases in drug loading efficiency, and it was found release profile controlled delivery of indomethacin to the joints. The drug targeting efficiency was highest for folate-PEG conjugate when compare to dendrimer without PEG [103]. Another study investigated the poly(amidoamine) dendrimer (generation 5) nanoparticle conjugated with folic acid (FA) and Methotrexate (MTX) (G5-FA-MTX) into macrophages as therapeutic for the inflammatory disease of arthritis. *In vitro* and *in vivo* studies were performed in a rat model with CIA in order to evaluate the therapeutic potential G5-FA-MTX. G5-FA-MTX operated as a strong anti-inflammatory agent and reduced arthritis-induced parameters of inflammation as paw volume, cartilage damage, bone resorption [104] **(Figure II-5)**.

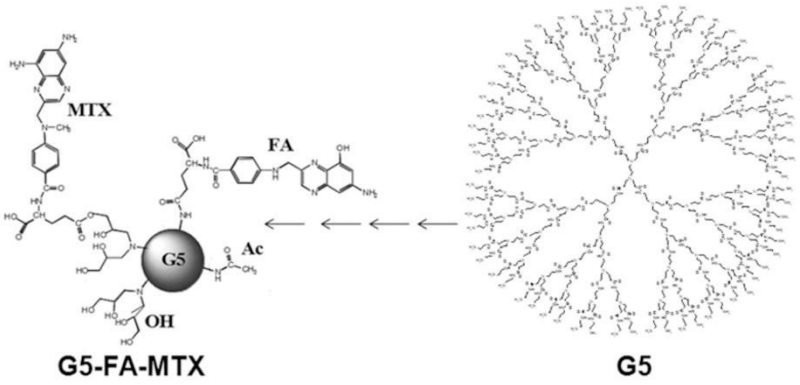

Figure II-5 - Schematic structure of G5-FA-MTX nanoparticle. Reproduced with permission from [104]. Copyright John Wiley and Sons, 2016.

Hayder *et al.* [105] explored the therapeutic potential of azabisphosphonate (ABP) dendrimer as target monocytes in the treatment of rheumatoid arthritis. In two animal models, IL-1ra(-/-)mice and mice undergoing K/BxN serum, intravenous injections of dendrimer ABP prevented the development of inflammatory arthritis. That study demonstrated that intravenous injection of dendrimer diminished levels of inflammatory cytokines, normal synovial membrane, and the default of cartilage destruction and bone erosion [106] **(Figure II-6)**.

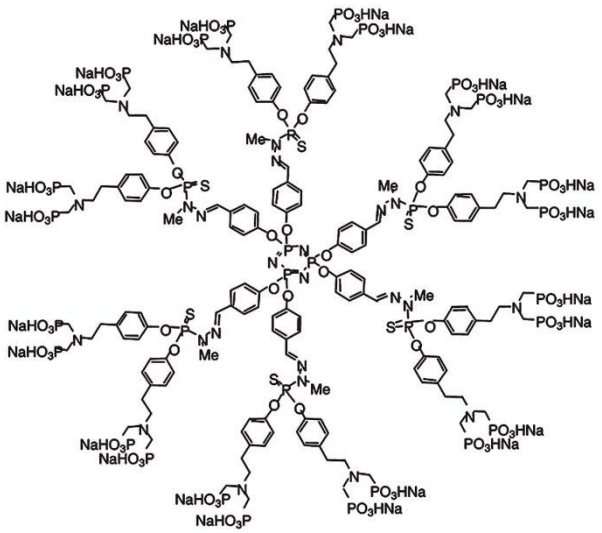

Figure II-6 - Structure of dendrimer azabisphosphonate (ABP). Reproduced with permission from [105]. Copyright. The American Association for the Advancement of Science, 2016.

II-3.4. Metallic Nanoparticles

Metallic nanoparticles are a class of materials with very useful properties. These nanoparticles can be synthesized and modified with several functional groups that allow them to be conjugated with antibodies, ligands, magnetic separation, target drug delivery, vehicles for gene and drug delivery, and diagnostic imaging [107],[108].

There are some studies about the use of metallic nanoparticles such as gold nanoparticles, iron oxide nanoparticles, and silver nanoparticles for treatment of the rheumatoid arthritis (RA) **(Table II-S5 in the Supplementary Information)**. Tsai *et al.* [109] investigated the effect of intra-articular delivery of nanogold to target VEGF (vascular endothelial growth factor) CIA in rats. Angiogenesis has an important role in RA and nanogold inhibits the activity of an angiogenic factor, VEGF. It was evaluated the microvessel density, extent infiltration of macrophages, levels of TNF-α and interleukin-1β (IL-1 β) in the ankle joint. Nanogold was administered intra-articularly to rat with CIA before the onset of arthritis. Nanogold bound to VEGF in RA resulted in inhibition of RA synovial fluid, cell proliferation, and migration. There was a diminution in ankle circumference, articular index score, and radiographic scores were observed in the nanogold rats treated with CIA when compared with the nanogold untreated animals. Histologic analyses of cartilage erosion, leukocyte infiltration, synovial hyperplasia, macrophage infiltration, and levels of TNF-α and IL-1β were very low in the ankle joints of treated rats

with nanogold, which resulted in arthritis attenuation. A study made by Chamberland *et al.* [110] investigated the potential of photoacoustic tomography in noninvasive monitoring of anti-TNF-α drug delivery helped by Etanercept-conjugated gold nanoparticles that were intra-articularly injected in the model rat. Results showed the viability of conjugation TNF antagonist pharmaceutical preparations with gold nanoparticles preserve of the mechanism of action of TNF-α antagonist with an evaluation of PAT (photoacoustic tomography) technology with anti-rheumatic drugs. Another study analyzed hyaluronic acid (HA) onto the surface of gold nanoparticles (AuNPs) in animal models of RA. In these animals of RA, local arthritis inflammation was clearly identified upon the systematic injection of gold nanoparticles. Results suggest that these nanoparticles can be used as *in vivo* optical imaging agents for the detection of local HA degrading diseases such as RA [111]. Huang *et al.* [112] investigated Galectin-1- nanogold (Au-GAL1) nanoparticles injected intra-articularly into rats with CIA. This conjugated promoted apoptosis of CD4+ T cells and decrease pro-inflammatory cytokine levels in the ankle joints and ameliorated clinical symptoms of arthritis. A study made by Lee *et al.* [113] developed RGD-attached gold (Au) half-shell nanoparticles containing methotrexate (MTX) to target chemo-photothermal for the treatment of RA. The RGD-attached gold (Au) half-shell nanoparticles containing methotrexate (MTX) combined with NIR radiation showed a higher increase therapeutic effect, than that of treatment only with MTX in CIA mice **(Figure II-7)**.

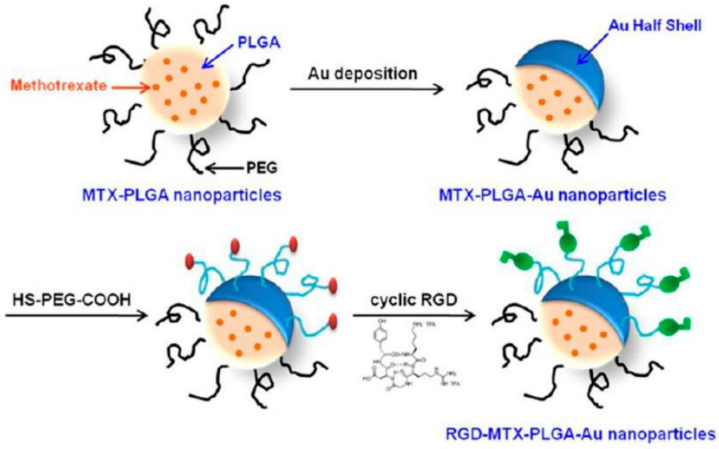

Figure II-7 - Schematic representation of the production process of RGD-MTX-PLGA Au nanoparticles. Reproduced with permission from [113]. Copyright American Chemical Society, 2016.

Lastly, Lee *et al.* [114] studied the effect of hyaluronate-gold nanoparticle/Tocilizumab (HA-AuNP/TCZ) complex for the therapeutic of RA in CIA mice model. AuNP has antiangiogenic effect and TCZ is an antibody against the interleukin-6 (IL-6) receptor and utilized as an immunosuppressive drug by interfering IL-6 in the pathogenesis of RA. HA has cartilage-protective and lubricant effect. Results *in*

vitro showed the bind HA-AuNP/TCZ to VEGF and IL-6R and therapeutic potential of HA-AuNP/TCZ **(Figure II-8)**.

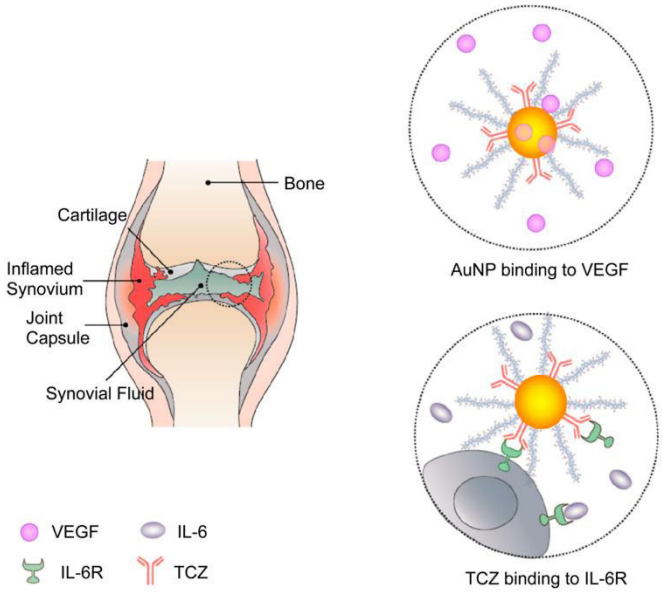

Figure II-8 - Schematic representation of HA-AuNP/TCZ complex for the treatment of RA. Reproduced with permission from [114]. Copyright American Chemical Society, 2016.

Another group, Schulze *et al.*, [115] investigated superparamagnetic iron oxide nanoparticles, coated with polyvinyl alcohol (PVA-SPIONS) that was intra-articularly applied in sheep model and evaluated their uptake by synovial membrane. The uptake was completed in 48 hrs. The nanoparticles remained within the synovial for at least five days indicating that they could extend the action of intra-articularly applied medication for treating acute or chronic joint diseases. Another study investigated SPIONS using magnetic resonance imaging (MRI) to track murine mesenchymal stem cells (MSCs) *in vivo*, labeled as ScreenMag (SiMAG), within murine model RA. After RA introduction the conjugate was implanted via-articular injection and joint swelling monitored as an indication of RA over days. A significant decrease in joint swelling was verified in groups containing SiMAG-labelled and unlabeled mMSCs, in presence of SPIONS does not affect the properties of the immunomodulating cells. This approach proved to be able to monitor the migration of stem cells population within the rheumatic joint in a non-invasive way [3].

Kim *et al.* [116] investigated multimodal nanoparticles (MNP), containing Ru(bpy)3Cl2 core surrounded by a paramagnetic coating of gadolinium chelates, as a contrast agent of inflamed synovium in a CIA model. After intravenous administration of MNP, optical and magnetic resonance (MR) images were obtained, and clinical disease was marked. MNP labeled cells monocytes/macrophages within the inflamed joints. MR demonstrated a reduction in actively inflamed joints which was evident earlier than during the course of the disease. MNP proved to be a potential modality contrast agent in inflammatory

arthritis and localize to monocytes/macrophages within inflamed synovium. A study made by Sekar [117] studied on the azathioprine-loaded silver nanoparticles for RA treatment, using a green approach. *In vitro* toxicity of this conjugate was studied by means of using a 3T3 NIH fibroblast cell line. It was found that these conjugated targets the disease site to release the drug in a controlled form and produced a combined effect to the inflammatory sites.

II-3.5. Other nanoparticle systems for treatment of RA

There are other studies made with NPs for the treatment of RA, which includes solid lipid NPs and polymeric micelles **(Table II-S6 in the Supplementary Information)**.

Ye *et al*. [118] investigated the intravenous injection formulation of solid lipid nanoparticle (SLNs) loaded with actarit for improved therapeutic efficacy and reduced side-effects associated with the oral formulation of actarit in RA pathology. The actarit-loaded SLNs exhibited a longer mean retention time *in vivo* compared with the actarit in 50% propylene glycol solution after intravenous injection in rabbits and the targeting efficiency was enhanced in the spleen while the renal distribution of actarit was reduced as compared with the actarit solution after intravenous injection in mice. Therefore, this approach can promote passive targeting of therapeutic agents for RA. Other investigation explored the anti-inflammatory effects and hepatotoxicity of Tripterygium-loaded with solid lipid nanoparticles (TWHF-SLN) in AIA rats and the effect of SLN delivery system on decreasing the hepatotoxicity induced by TWHF. After Freund´s complete adjuvant agent (FCA) injection, TWHF-SLN group and TWHF group were administered by oral gavage. The paws were evaluated for some days of FCA post-injection. Results showed that TWHF-SLN can greatly reduce rat paw volume. Histopathology data found that free TWHF caused more damage to the liver than TWHF-SLN and this last can increase the anti-inflammatory [119]. A study made by Nagai *et al*. [120] examined the effect of solid nanoparticles of indomethacin (IMC) on treatment for rheumatoid arthritis in AIA rats. These after induction of paw edema received the low doses of solid nanoparticles of indomethacin that were similar to the administration of a therapeutic dose conventional IMC. There were fewer gastrointestinal lesions in AIA rats when administered with IMC nanoparticles than with conventional IMC. These results showed that IMC nanoparticles may increase the effect of rheumatoid arthritis treatment without causing IMC-induced gastrointestinal lesions, because the bioavailability is bigger than of conventional IMC. $\alpha_v \beta_3$ –target fumagillin nanoparticles to target angiogenesis to suppress inflammatory arthritis in mice was studied by Zhou *et*

al. [121]. Arthritis was induced using K/BxN mouse model of inflammatory arthritis. After arthritis establishment, the mice received some doses of αv β3 –target fumagillin nanoparticles. Treated mice showed a lower disease activity and change in ankle thickness compared to the group that received αv β3–target fumagillin nanoparticles without drugs. There was a decrease in inflammation and angiogenesis in synovial tissues from animals treated with αv β3 –target fumagillin nanoparticles. Koo *et al.*, investigated sterically stabilized micelles (SSM) as nanocarriers for camptothecin CPT (CPT-SSM). CPT was used due *In vitro* studies show that CPT inhibits synoviocyte proliferation, matrix metalloproteinases expression in chondrocytes, and angiogenesis. The surface of CPT-SSM was modified with vasoactive intestinal peptide (VIP) for active targeting. CPT was, for the first time, reported as effective against CIA, i.e. a single subcutaneous injection of CPT-SSM-VIP administered to CIA mice alleviated joint inflammation for at least one month without systemic toxicity. However, CPT alone required a much higher dose in order to obtain the same effect.

(Table II-S7 in the Supplementary Information) shows a summary of the main characteristics of the referred drugs and bioactive agents used for the treatment of rheumatoid arthritis [122],[123]. These data were mostly obtained from online databases of drugs [122] and proteins [123], on May 2016.

II-4. CLINICAL TRIALS

Clinical trials are used to evaluate the safety and effectiveness of new treatments. ClinicalTrials.gov. is a website, maintained by the U.S. National Library of Medicine (NLM) at the National Institutes of Health (NIH), which provides access to a database with information on clinical studies, on a wide range of diseases and conditions. Information is provided and updated by the sponsor or principal investigator of the clinical study. A search on this database, using relevant keywords (such as “rheumatoid arthritis”, “nanoparticles”, “liposomes”, “polymeric nanoparticles” or “dendrimers”) returned a single registered clinical trial related to the application of nanoparticles in RA management. The trial evaluated the safety of a single intravenous administration of long-circulating liposomal prednisolone disodium phosphate and compare with pulse intramuscular methylprednisolone in patients with RA. The last method is used in the clinics as bridging therapy to assess the effect of this intervention at the synovial level. The objective is liposomal corticosteroids increase efficacy/safety ratio as compared to administration of corticosteroids. The study has been completed, however, no results were published on the database where the study was found [124].

II-5. CONCLUDING REMARKS

Several treatment alternatives that can be potentially used for the treatment of rheumatoid arthritis rather than traditional drugs are being reported. In the same way, nanotechnology making use of nanoparticles has been developed for the treatment of rheumatoid arthritis. Most of the reported approaches exhibit a great specificity in the delivery of the drug loaded-NPs to the site of action. These therapeutic strategies showed an important potential to improve the efficacy and safety, becoming less toxic and decreasing the undesired side effects in rheumatoid arthritis therapeutic as compared to the ones using the traditional drugs (such as DMARDs, NSAIDs, and corticosteroids). The NPs small size and large surface area can lead to an aggregation, which results in tough physical manipulation, limited drug loading, and burst release. Nevertheless, these limitations could be addressed by, for instance, careful development of the drug delivery systems, surface modification, drug loading strategies, and release control.

Most of the studied delivery systems in RA therapy are throughout liposomes. This type of NPs represents the most advanced carrier administration as evidenced in the animals and small clinical studies. Nevertheless, more research is needed to get better retention time and to adapt the release rate of the encapsulated drug.

The polymeric NPs also represent a large part of the studies made on the treatment of rheumatoid arthritis. Those studies showed a great positive effect when compared to free drugs. However, polymeric NPs are not as studied in comparison with the liposomes for the treatment of RA. Therefore, further studies are needed to explore the potential of these nanoparticles. Moreover, the recent studies making use of dendrimers show their great potential for the treatment of rheumatoid arthritis. Thus, further studies with these types of spherical NP's are needed in order to explore further their promising characteristics.

Metallic nanoparticles are also showing great potential, but still few studies have been exploring the accurate potential of these nanoparticles.

Other studies reporting the application of nanoparticles for the treatment of rheumatoid arthritis showed positive results. Although much research is needed to better understand the underlying mechanisms of these therapeutic approaches. The results of recent studies allow confirming that the use of nanoparticles, in general, is very promising; due to their physicochemical and biological

properties (such as biocompatibility, low toxicity, controlled release, and selective drug delivery to inflamed tissues) in animal models with RA.

Despite most studies are encouraging, it is needed some adjustments in these approaches namely in respect to efficacy and safety of the developed nanosystems, before being applied in humans. Yet, it is possible to state that advanced nanomaterials, in the future, will certainly play a crucial role when envisioning the development of nanopharmaceutics, and in particular in patient-specific approaches for the treatment of human diseases such as RA.

II-6. ACKNOWLEDGMENTS

The authors thank the financial support under the ARTICULATE project (ref. QREN-13/SI/2011-23189). This study was also funded by the Portuguese Foundation for Science and Technology (FCT) project OsteoCart (PTDC/CTM-BPC/115977/2009), as well as the European Union's FP7 Programme under grant agreement no REGPOT-CT2012-316331-POLARIS. The FCT distinction attributed to J.M. Oliveira under the Investigator FCT program (IF/00423/2012) is also greatly acknowledged. C. Gonçalves also wish to acknowledge FCT for supporting her research (SFRH/BPD/94277/2013).

II-7. REFERENCES

1. Barnes, T. and R. Moots, *Targeting nanomedicines in the treatment of rheumatoid arthritis: focus on certolizumab pegol.* International Journal of Nanomedicine, 2007. **2**(1): p. 3-7.
2. Howard, K.A., et al., *Chitosan/siRNA nanoparticle-mediated TNF-α knockdown in peritoneal macrophages for anti-inflammatory treatment in a murine arthritis model.* Molecular therapy, 2009. **17**(1): p. 162-168.
3. Markides, H., et al., *Whole body tracking of superparamagnetic iron oxide nanoparticle-labelled cells–a rheumatoid arthritis mouse model.* Stem Cell Research & Therapy, 2013. **4**(5): p. 1-14.
4. Ishihara, T., et al., *Treatment of experimental arthritis with stealth-type polymeric nanoparticles encapsulating betamethasone phosphate.* Journal of Pharmacology and Experimental Therapeutics, 2009. **329**(2): p. 412-417.
5. Pham, C.T., *Nanotherapeutic approaches for the treatment of rheumatoid arthritis.* Wiley Interdisciplinary Reviews: Nanomedicine and Nanobiotechnology, 2011. **3**(6): p. 607-619.
6. Oda, K. and M. Minata, *Drug free remission after steroid-dependent disappearance of lymphoproliferative disorder in rheumatoid arthritis patient treated with TNF-alpha blockade: case study.* SpringerPlus, 2015. **4**(1): p. 41.
7. Stoll, J.G. and U. Yasothan, *Rheumatoid arthritis market.* Nature Reviews Drug Discovery, 2009. **8**(9): p. 693-694.

8. Hwang, J., et al., *α-Methylprednisolone conjugated cyclodextrin polymer-based nanoparticles for rheumatoid arthritis therapy.* International journal of nanomedicine, 2008. **3**(3): p. 359.
9. Rubinstein, I. and G.L. Weinberg, *Nanomedicines for chronic non-infectious arthritis: The clinician's perspective.* Maturitas, 2012. **73**(1): p. 68-73.
10. Boulaiz, H., et al., *Nanomedicine: application areas and development prospects.* International journal of molecular sciences, 2011. **12**(5): p. 3303-3321.
11. Zhang, L., et al., *Nanoparticles in medicine: therapeutic applications and developments.* Clinical pharmacology & therapeutics, 2008. **83**(5): p. 761-769.
12. Mukherjee, B., *Nanosize drug delivery system.* Curr Pharm Biotechnol, 2013. **14**(15): p. 1221.
13. Parveen, S., R. Misra, and S.K. Sahoo, *Nanoparticles: a boon to drug delivery, therapeutics, diagnostics and imaging.* Nanomedicine: Nanotechnology, Biology and Medicine, 2012. **8**(2): p. 147-166.
14. Merisko-Liversidge, E.M. and G.G. Liversidge, *Drug nanoparticles: formulating poorly water-soluble compounds.* Toxicologic pathology, 2008. **36**(1): p. 43-48.
15. Kahlenberg, J.M. and D.A. Fox, *Advances in the medical treatment of rheumatoid arthritis.* Hand clinics, 2011. **27**(1): p. 11-20.
16. M, A., *Potential applications of Nanoparticles.* Int J Pharma Bio Sci,

2009. **6**(1): p. 772-784.

17. Mudshinge, S.R., et al., *Nanoparticles: emerging carriers for drug delivery.* Saudi pharmaceutical journal, 2011. **19**(3): p. 129-141.
18. Surendiran, A., et al., *Novel applications of nanotechnology in medicine.* 2009.
19. Malam, Y., M. Loizidou, and A.M. Seifalian, *Liposomes and nanoparticles: nanosized vehicles for drug delivery in cancer.* Trends in pharmacological sciences, 2009. **30**(11): p. 592-599.
20. Foong, W. and K. Green, *Association of liposome‐entrapped [3H] methotrexate with thioglycollate‐elicited macrophages in‐vitro.* Journal of pharmacy and pharmacology, 1988. **40**(3): p. 171-175.
21. Tarner, I.H. and U. Müller-Ladner, *Drug delivery systems for the treatment of rheumatoid arthritis.* Expert opinion on drug delivery, 2008. **5**(9): p. 1027-1037.
22. Kapoor, B., et al., *Application of liposomes in treatment of rheumatoid arthritis: quo vadis.* The scientific world Journal, 2014. **2014**.
23. Love, W., et al., *Specific accumulation of technetium-99m radiolabelled, negative liposomes in the inflamed paws of rats with adjuvant induced arthritis: effect of liposome size.* Annals of the rheumatic diseases, 1989. **48**(2): p. 143-148.
24. Van Lent, P., et al., *Local removal of phagocytic synovial lining cells by clodronate-liposomes decreases cartilage destruction during collagen type II arthritis.* Annals of the rheumatic diseases, 1998. **57**(7): p. 408-413.
25. Ulbrich, W. and A. Lamprecht, *Targeted drug-delivery approaches by nanoparticulate carriers in the therapy of inflammatory diseases.* Journal of The Royal Society Interface, 2009: p. rsif20090285.
26. van den Hoven, J.M., et al., *Liposomal drug formulations in the treatment of rheumatoid arthritis.* Molecular pharmaceutics, 2011. **8**(4): p. 1002-1015.
27. Williams, A., J. Camilleri, and B. Williams, *Suppression of adjuvant-induced arthritis by liposomally conjugated methotrexate in the rat.* Rheumatology, 1994. **33**(6): p. 530-533.
28. Watson-Clark, R.A., et al., *Model studies directed toward the application of boron neutron capture therapy to rheumatoid arthritis: Boron delivery by liposomes in rat collagen-induced arthritis.* Proceedings of the National Academy of Sciences, 1998. **95**(5): p. 2531-2534.

29. Chowdhary, R.K., et al., *Uptake of Verteporfin® by articular tissues following systemic and intra‐articular administration.* Biopharmaceutics & drug disposition, 1998. **19**(6): p. 395-400.
30. Highton, J., et al., *A trial of clodronate-liposomes as anti-macrophage treatment in a sheep model of arthritis.* Clinical and experimental rheumatology, 1999. **17**: p. 43-48.
31. Corvo, M.L., et al., *Subcutaneous administration of superoxide dismutase entrapped in long circulating liposomes: in vivo fate and therapeutic activity in an inflammation model.* Pharmaceutical research, 2000. **17**(5): p. 600-606.
32. Srinath, P., et al., *Long-circulating liposomes of indomethacin in arthritic rats—a biodisposition study.* Pharmaceutica Acta Helvetiae, 2000. **74**(4): p. 399-404.
33. Čeponis, A., et al., *Effects of low‐dose, noncytotoxic, intraarticular liposomal clodronate on development of erosions and proteoglycan loss in established antigen‐induced arthritis in rabbits.* Arthritis & Rheumatism, 2001. **44**(8): p. 1908-1916.
34. Trif, M., et al., *Liposomes as possible carriers for lactoferrin in the local treatment of inflammatory diseases.* Experimental Biology and Medicine, 2001. **226**(6): p. 559-564.
35. Trif, M., et al., *Designing lipid nanostructures for local delivery of biologically active macromolecules.* Journal of Liposome Research, 2007. **17**(3-4): p. 237-248.
36. Everts, M., et al., *In vitro cellular handling and in vivo targeting of E-selectin-directed immunoconjugates and immunoliposomes used for drug delivery to inflamed endothelium.* Pharmaceutical research, 2003. **20**(1): p. 64-72.
37. Mitragotri, S. and J.-W. Yoo, *Designing micro-and nano-particles for treating rheumatoid arthritis.* Archives of pharmacal research, 2011. **34**(11): p. 1887-1897.
38. Metselaar, J.M., et al., *Complete remission of experimental arthritis by joint targeting of glucocorticoids with long‐circulating liposomes.* Arthritis & Rheumatism: Official Journal of the American College of Rheumatology, 2003. **48**(7): p. 2059-2066.
39. Metselaar, J.v., et al., *Liposomal targeting of glucocorticoids to synovial lining cells strongly increases therapeutic benefit in collagen type II arthritis.* Annals of the rheumatic diseases, 2004. **63**(4): p. 348-353.
40. Harigai, T., et al., *Prednisolone phosphate‐containing TRX‐20 liposomes inhibit cytokine and chemokine production in human fibroblast‐like synovial cells: a novel approach to rheumatoid arthritis therapy.* Journal of pharmacy and pharmacology, 2007. **59**(1): p. 137-143.
41. Koning, G.A., et al., *Targeting of angiogenic endothelial cells at sites of inflammation by dexamethasone phosphate–containing RGD peptide liposomes inhibits experimental arthritis.* Arthritis & Rheumatism, 2006. **54**(4): p. 1198-1208.
42. Hattori, Y., M. Sakaguchi, and Y. Maitani, *Folate-linked lipid-based nanoparticles deliver a NF κ B decoy into activated murine macrophage-like RAW264. 7 cells.* Biological and Pharmaceutical Bulletin, 2006. **29**(7): p. 1516-1520.
43. Rauchhaus, U., et al., *Targeted delivery of liposomal dexamethasone phosphate to the spleen provides a persistent therapeutic effect in rat antigen-induced arthritis.* Annals of the rheumatic diseases, 2009. **68**(12): p. 1933-1934.
44. Richards, P.J., et al., *Liposomal clodronate eliminates synovial macrophages, reduces inflammation and ameliorates joint destruction in antigen-induced arthritis.* Rheumatology, 1999. **38**(9): p. 818-825.
45. Richards, P., B. Williams, and A. Williams, *Suppression of chronic streptococcal cell wall‐induced arthritis in Lewis rats by liposomal clodronate.* Rheumatology, 2001. **40**(9): p. 978-987.

46. Simoes, S., et al., *Developments in the rat adjuvant arthritis model and its use in therapeutic evaluation of novel non-invasive treatment by SOD in Transfersomes.* Journal of Controlled Release, 2005. **103**(2): p. 419-434.
47. Gaspar, M.M., et al., *Enzymosomes with surface-exposed superoxide dismutase: in vivo behaviour and therapeutic activity in a model of adjuvant arthritis.* Journal of Controlled Release, 2007. **117**(2): p. 186-195.
48. Khoury, M., et al., *Efficient new cationic liposome formulation for systemic delivery of small interfering RNA silencing tumor necrosis factor α in experimental arthritis.* Arthritis & Rheumatism, 2006. **54**(6): p. 1867-1877.
49. Kim, W.U., et al., *Suppression of collagen‐induced arthritis by single administration of poly (lactic‐co‐glycolic acid) nanoparticles entrapping type II collagen: a novel treatment strategy for induction of oral tolerance.* Arthritis & Rheumatism: Official Journal of the American College of Rheumatology, 2002. **46**(4): p. 1109-1120.
50. Horisawa, E., et al., *Size-dependency of DL-lactide/glycolide copolymer particulates for intra-articular delivery system on phagocytosis in rat synovium.* Pharmaceutical research, 2002. **19**(2): p. 132-139.
51. Butoescu, N., O. Jordan, and E. Doelker, *Intra-articular drug delivery systems for the treatment of rheumatic diseases: a review of the factors influencing their performance.* European Journal of Pharmaceutics and Biopharmaceutics, 2009. **73**(2): p. 205-218.
52. Fiehn, C., et al., *Albumin-coupled methotrexate (MTX-HSA) is a new anti-arthritic drug which acts synergistically to MTX.* Rheumatology, 2004. **43**(9): p. 1097-1105.
53. Ren, K., et al., *Albumin as a delivery carrier for rheumatoid arthritis.* J Nanomed Nanotechol, 2013. **4**(4): p. 176.
54. Higaki, M., et al., *Treatment of experimental arthritis with poly (D, L-lactic/glycolic acid) nanoparticles encapsulating betamethasone sodium phosphate.* Annals of the rheumatic diseases, 2005. **64**(8): p. 1132-1136.
55. Patel, J., H.S. BJigar, and D. Patel, *Novel Drug Delivery Technologies For The Treatment Of.* Internet Journal of Medical Technology, 2008. **5**(1).
56. Liu, M., et al., *Anti-inflammatory effects of triptolide loaded poly (D, L-lactic acid) nanoparticles on adjuvant-induced arthritis in rats.* Journal of ethnopharmacology, 2005. **97**(2): p. 219-225.
57. Mansouri, S., et al., *Characterization of folate-chitosan-DNA nanoparticles for gene therapy.* Biomaterials, 2006. **27**(9): p. 2060-2065.
58. Wang, D., et al., *Novel dexamethasone-HPMA copolymer conjugate and its potential application in treatment of rheumatoid arthritis.* Arthritis research & therapy, 2007. **9**(1): p. R2.
59. Rothenfluh, D.A., et al., *Biofunctional polymer nanoparticles for intra-articular targeting and retention in cartilage.* Nature materials, 2008. **7**(3): p. 248-254.
60. Ishihara, T., et al., *Preparation and characterization of a nanoparticulate formulation composed of PEG-PLA and PLA as anti-inflammatory agents.* International journal of pharmaceutics, 2010. **385**(1): p. 170-175.
61. Liu, X.-M., et al., *Syntheses of click PEG– dexamethasone conjugates for the treatment of rheumatoid arthritis.* Biomacromolecules, 2010. **11**(10): p. 2621-2628.
62. Kim, Y.-J., et al., *Ionic complex systems based on hyaluronic acid and PEGylated TNF-related apoptosis-inducing ligand for treatment of rheumatoid arthritis.* Biomaterials, 2010. **31**(34): p. 9057-9064.
63. Schmitt, F., et al., *Chitosan-based nanogels for selective delivery of photosensitizers to macrophages and improved retention in and therapy of articular joints.* Journal of Controlled Release, 2010. **144**(2): p. 242-250.

64. Shi, Q., et al., *Hydrodynamic delivery of chitosan-folate-DNA nanoparticles in rats with adjuvant-induced arthritis.* Journal of Biomedicine and Biotechnology, 2010. **2011**.
65. Scheinman, R.I., et al., *Functionalized STAT1 siRNA nanoparticles regress rheumatoid arthritis in a mouse model.* Nanomedicine, 2011. **6**(10): p. 1669-1682.
66. Ryu, J.H., et al., *Early diagnosis of arthritis in mice with collagen‐induced arthritis, using a fluorogenic matrix metalloproteinase 3–specific polymeric probe.* Arthritis & Rheumatism, 2011. **63**(12): p. 3824-3832.
67. Park, K.S., et al., *In vivo quantitative measurement of arthritis activity based on hydrophobically modified glycol chitosan in inflammatory arthritis: more active than passive accumulation.* Molecular imaging, 2012. **11**(5): p. 7290.2011. 00056.
68. Te Boekhorst, B.C., et al., *MRI-assessed therapeutic effects of locally administered PLGA nanoparticles loaded with anti-inflammatory siRNA in a murine arthritis model.* Journal of controlled release, 2012. **161**(3): p. 772-780.
69. Rollett, A., et al., *Folic acid-functionalized human serum albumin nanocapsules for targeted drug delivery to chronically activated macrophages.* International journal of pharmaceutics, 2012. **427**(2): p. 460-466.
70. Albuquerque, J., et al., *Solid lipid nanoparticles: a potential multifunctional approach towards rheumatoid arthritis theranostics.* Molecules, 2015. **20**(6): p. 11103-11118.
71. Kim, S.-H., et al., *Self-assembled dextran sulphate nanoparticles for targeting rheumatoid arthritis.* Chemical Communications, 2013. **49**(88): p. 10349-10351.
72. Heo, R., et al., *Hyaluronan nanoparticles bearing γ-secretase inhibitor: in vivo therapeutic effects on rheumatoid arthritis.* Journal of controlled release, 2014. **192**: p. 295-300.
73. Lee, S.J., et al., *TNF-α gene silencing using polymerized siRNA/thiolated glycol chitosan nanoparticles for rheumatoid arthritis.* Molecular Therapy, 2014. **22**(2): p. 397-408.
74. Bilthariya, U., et al., *Folate-conjugated albumin nanoparticles for rheumatoid arthritis-targeted delivery of etoricoxib.* Drug Development and Industrial Pharmacy, 2015. **41**(1): p. 95-104.
75. Saluja, V., et al., *Smart dendrimers: Synergizing the targeting of anticancer bioactives.* Journal of Drug Delivery Science and Technology, 2019. **52**: p. 15-26.
76. Mintzer, M.A. and M.W. Grinstaff, *Biomedical applications of dendrimers: a tutorial.* Chem Soc Rev, 2011. **40**(1): p. 173-90.
77. Tomalia, D.A., et al., *Dendritic macromolecules: synthesis of starburst dendrimers.* Macromolecules, 1986. **19**(9): p. 2466-2468.
78. Hawker, C.J. and J.M.J. Frechet, *Preparation of polymers with controlled molecular architecture. A new convergent approach to dendritic macromolecules.* Journal of the American Chemical Society, 1990. **112**(21): p. 7638-7647.
79. Ambekar, R.S., M. Choudhary, and B. Kandasubramanian, *Recent advances in dendrimer-based nanoplatform for cancer treatment: A review.* European Polymer Journal, 2020. **126**: p. 109546.
80. Abbasi, E., et al., *Dendrimers: synthesis, applications, and properties.* Nanoscale research letters, 2014. **9**(1): p. 247.
81. Klajnert, B. and M. Bryszewska, *Dendrimers: properties and applications.* Acta biochimica polonica, 2001. **48**(1): p. 199-208.
82. Jevprasesphant, R., et al., *The influence of surface modification on the cytotoxicity of PAMAM dendrimers.* International journal of pharmaceutics, 2003. **252**(1-2): p. 263-266.
83. Ciolkowski, M., et al., *Surface modification of PAMAM dendrimer improves its biocompatibility.* Nanomedicine: Nanotechnology, Biology and Medicine, 2012. **8**(6): p. 815-817.

84. Malik, N., et al., *Dendrimers:: Relationship between structure and biocompatibility in vitro, and preliminary studies on the biodistribution of 125I-labelled polyamidoamine dendrimers in vivo.* Journal of Controlled Release, 2000. **65**(1-2): p. 133-148.
85. Janaszewska, A., et al., *Cytotoxicity of dendrimers.* Biomolecules, 2019. **9**(8): p. 330.
86. Sherje, A.P., et al., *Dendrimers: a versatile nanocarrier for drug delivery and targeting.* International journal of pharmaceutics, 2018. **548**(1): p. 707-720.
87. Abbasi, E., et al., *Dendrimers: synthesis, applications, and properties.* Nanoscale Res Lett, 2014. **9**(1): p. 247.
88. Wang, Y., et al., *Targeted delivery of doxorubicin into cancer cells using a folic acid–dendrimer conjugate.* Polymer Chemistry, 2011. **2**(8): p. 1754-1760.
89. Thiagarajan, G., et al., *PAMAM-camptothecin conjugate inhibits proliferation and induces nuclear fragmentation in colorectal carcinoma cells.* Pharmaceutical research, 2010. **27**(11): p. 2307-2316.
90. Agashe, H.B., et al., *Investigations on the toxicological profile of functionalized fifth‐generation poly (propylene imine) dendrimer.* Journal of pharmacy and pharmacology, 2006. **58**(11): p. 1491-1498.
91. Jain, K., et al., *Dendrimer toxicity: Let's meet the challenge.* International journal of pharmaceutics, 2010. **394**(1-2): p. 122-142.
92. Svenson, S. and A.S. Chauhan, *Dendrimers for enhanced drug solubilization.* 2008.
93. Chauhan, A.S., *Dendrimers for Drug Delivery.* Molecules, 2018. **23**(4).
94. Medina, S.H. and M.E. El-Sayed, *Dendrimers as carriers for delivery of chemotherapeutic agents.* Chemical reviews, 2009. **109**(7): p. 3141-3157.
95. Lin, Q., G. Jiang, and K. Tong, *Dendrimers in drug-delivery applications.* Designed Monomers and Polymers, 2010. **13**(4): p. 301-324.
96. Bhadra, D., et al., *A PEGylated dendritic nanoparticulate carrier of fluorouracil.* International journal of pharmaceutics, 2003. **257**(1-2): p. 111-124.
97. Devarakonda, B., R.A. Hill, and M.M. de Villiers, *The effect of PAMAM dendrimer generation size and surface functional group on the aqueous solubility of nifedipine.* International journal of pharmaceutics, 2004. **284**(1-2): p. 133-140.
98. Zhu, J. and X. Shi, *Dendrimer-based nanodevices for targeted drug delivery applications.* Journal of Materials Chemistry B, 2013. **1**(34): p. 4199-4211.
99. Kono, K., et al., *Preparation and cytotoxic activity of poly (ethylene glycol)-modified poly (amidoamine) dendrimers bearing adriamycin.* Biomaterials, 2008. **29**(11): p. 1664-1675.
100. Lee, C.C., et al., *Designing dendrimers for biological applications.* Nature biotechnology, 2005. **23**(12): p. 1517-1526.
101. Crampton, H.L. and E.E. Simanek, *Dendrimers as drug delivery vehicles: non‐covalent interactions of bioactive compounds with dendrimers.* Polymer international, 2007. **56**(4): p. 489-496.
102. Madaan, K., et al., *Dendrimers in drug delivery and targeting: Drug-dendrimer interactions and toxicity issues.* J Pharm Bioallied Sci, 2014. **6**(3): p. 139-50.
103. Chandrasekar, D., et al., *Folate coupled poly (ethyleneglycol) conjugates of anionic poly (amidoamine) dendrimer for inflammatory tissue specific drug delivery.* Journal of Biomedical Materials Research Part A, 2007. **82**(1): p. 92-103.
104. Thomas, T.P., et al., *Folate‐targeted nanoparticles show efficacy in the treatment of inflammatory arthritis.* Arthritis & Rheumatism, 2011. **63**(9): p. 2671-2680.
105. Hayder, M., et al., *A phosphorus-based dendrimer targets inflammation and osteoclastogenesis in experimental arthritis.* Science translational medicine, 2011. **3**(81): p. 81ra35-81ra35.

106. Bosch, X., *Dendrimers to treat rheumatoid arthritis.* ACS nano, 2011. **5**(9): p. 6779-6785.
107. Edmundson, M.C., M. Capeness, and L. Horsfall, *Exploring the potential of metallic nanoparticles within synthetic biology.* New biotechnology, 2014. **31**(6): p. 572-578.
108. Mody, V.V., et al., *Introduction to metallic nanoparticles.* Journal of Pharmacy and Bioallied Sciences, 2010. **2**(4): p. 282.
109. Tsai, C.Y., et al., *Amelioration of collagen‐induced arthritis in rats by nanogold.* Arthritis & Rheumatism: Official Journal of the American College of Rheumatology, 2007. **56**(2): p. 544-554.
110. Chamberland, D.L., et al., *Photoacoustic tomography of joints aided by an Etanercept-conjugated gold nanoparticle contrast agent—an ex vivo preliminary rat study.* Nanotechnology, 2008. **19**(9): p. 095101.
111. Lee, H., et al., *Synthesis, characterization, and in vivo diagnostic applications of hyaluronic acid immobilized gold nanoprobes.* Biomaterials, 2008. **29**(35): p. 4709-4718.
112. Huang, Y.-J., et al., *Multivalent structure of galectin-1-nanogold complex serves as potential therapeutics for rheumatoid arthritis by enhancing receptor clustering.* Eur Cell Mater, 2012. **23**: p. 170-181.
113. Lee, S.-M., et al., *Targeted chemo-photothermal treatments of rheumatoid arthritis using gold half-shell multifunctional nanoparticles.* ACS nano, 2013. **7**(1): p. 50-57.
114. Lee, H., et al., *Hyaluronate–gold nanoparticle/tocilizumab complex for the treatment of rheumatoid arthritis.* Acs Nano, 2014. **8**(5): p. 4790-4798.
115. Schulze, K., et al., *Intraarticular application of superparamagnetic nanoparticles and their uptake by synovial membrane—an experimental study in sheep.* Journal of magnetism and magnetic materials, 2005. **293**(1): p. 419-432.
116. Kim, J., et al., *Multimodal optical and Gd-based nanoparticles for imaging in inflammatory arthritis.* Clin Exp Rheumatol, 2009. **27**(4): p. 580-586.
117. Prasad, S.R., et al., *Formulation and evaluation of azathioprine loaded silver nanopartilces for the treatment of rheumatoid arthritis.* Asian Journal of Biomedical and Pharmaceutical Sciences, 2013. **3**(23): p. 28-32.
118. Ye, J., et al., *Injectable actarit-loaded solid lipid nanoparticles as passive targeting therapeutic agents for rheumatoid arthritis.* International journal of pharmaceutics, 2008. **352**(1-2): p. 273-279.
119. Xue, M., et al., *Anti-inflammatory effects and hepatotoxicity of Tripterygium-loaded solid lipid nanoparticles on adjuvant-induced arthritis in rats.* Phytomedicine, 2012. **19**(11): p. 998-1006.
120. Nagai, N. and Y. Ito, *Effect of solid nanoparticle of indomethacin on therapy for rheumatoid arthritis in adjuvant-induced arthritis rat.* Biological and Pharmaceutical Bulletin, 2014. **37**(7): p. 1109-1118.
121. Zhou, H.-f., et al., *$\alpha v\beta 3$-Targeted nanotherapy suppresses inflammatory arthritis in mice.* The FASEB Journal, 2009. **23**(9): p. 2978-2985.
122. Wishart, D.S., et al., *DrugBank: a comprehensive resource for in silico drug discovery and exploration.* Nucleic acids research, 2006. **34**(suppl_1): p. D668-D672.
123. Bernstein, F.C., et al., *The Protein Data Bank: A computer‐based archival file for macromolecular structures.* European journal of biochemistry, 1977. **80**(2): p. 319-324.
124. Barrera, P., et al. *Long-circulating liposomal prednisolone versus pulse intramuscular methylprednisolone in patients with active rheumatoid arthritis*. in *Arthritis and Rheumatism*. 2008. WILEY-LISS DIV JOHN WILEY & SONS INC, 111 RIVER ST, HOBOKEN, NJ 07030 USA.

125. Čeponis, A., et al., *Effects of low‐dose, noncytotoxic, intraarticular liposomal clodronate on development of erosions and proteoglycan loss in established antigen‐induced arthritis in rabbits.* Arthritis & Rheumatology, 2001. **44**(8): p. 1908-1916.
126. Koo, O.M.Y., I. Rubinstein, and H. Önyüksel, *Actively targeted low-dose camptothecin as a safe, long-acting, disease-modifying nanomedicine for rheumatoid arthritis.* Pharmaceutical research, 2011. **28**(4): p. 776-787.

II-8. SUPPLEMENTARY TABLE

Supplementary Table II-1 - Liposomes for the delivery of Drugs/Bioactive Agent used in treatment of RA.

Drugs/Agents	Main Results	Reference(s)
Methotrexate	Increase in drug retention in the joint, compared to injection of free MTX.	[20], [27]
Clodronate	There weren`t differences between joint diameter and swelling in sheep with or without conjugate	[30]
	There were low levels of TNF-α, lining cell hyperplasia and macrophages in the synovium of the liposomal clodronate treatment group.	[33]
	Liposomal clodronate eliminated synovial macrophages, reduced inflammation and ameliorates joint destruction.	[44]
	SUVc inhibited local production of IL-1β, IL-6, TNF-α and MMP-9, and the pathogenesis	[45]
Boron	Higher synovium /blood boron ratios, reduced boron uptake in synovial tissue and more rapid blood clearance.	[28]
Verteporfin	Distribution of BDP-MA in the inflamed synovium and clearance from the synovium was rapid.	[29]
NFκB	NFκB was detected in the cytoplasm and an inhibitory effect on the translocation of NFκB in the nucleus was observed.	[42]
	presuming that NP-F delivered the NFκB catch into the cytoplasm.	
Superoxide dismutase	Small-sized liposomes are more effective than large-sized liposomes and can be used for the targeting of SOD to arthritis sites.	[31]
	SOD incorporate into Tfs and applied into a skin area not necessarily close to the inflamed tissue is able to promote non-invasive treatment of induced arthritis.	[46]
	Ac-SOD enzymosomes are able to exert therapeutic effect before liposomes disruption and they can act as a sustained release of the enzymes.	[47]
Indomethacin	Long-circulating liposomes have shown higher targeting efficiency in arthritis paw tissue than conventional liposomes.	[32]
Lactoferrin	Positives liposomes were more effective in prolonging the residence time of hLf in the inflamed joint as compared with other liposomes.	[34]
	Cytokine levels produced by LN T cells showed decreased pro-inflammatory cytokines (TNF-α) followed by increase anti-inflammatory cytokines (IL-10) in encapsulated when compared with free hLf.	[35]
Dexamethasone	Dexamethasone-anti-E-selectin was internalized to a larger extent than the anti-E-selectin immunoliposomes.	[36]
	Intravenous injection of DEXP encapsulated in RGD-PEG-L resulted in a strong and lasting anti-arthritic effect in rat AIA.	[41]
	Liposomal DXM suppressed both chronic inflammation and joint destruction, while free DXM-P failed to prevent joint destruction.	[43]
Prednisolone	Liposomal PLP proved to be highly effective in the rat AIA model with complete reduction of the	[38]

phosphate	inflammatory response	
	Liposome PLP resulted in a strong and lasting resolution of joint inflammation compared with free PLP.	[39]
	The symbiosis of the PSLP-containing liposomes with HFLS cells was 40 times bigger than that of PSLP-containing liposomes without TRX20.	[40]
siRNA against TNF-α	There was inhibition of systemic TNF-α secretion and decrease in the levels of interleukin-6.	[48]

Supplementary Table II-2 - Polymeric nanoparticles for the delivery of Drugs/Bioactive Agent used in treatment of RA.

Delivery vehicle	Drugs/Agents	Main Results	Reference(s)
PLGA NPs	II collagen (CII)	Higher level of TGFβ (transforming growth factor β) mRNA and lower level of TNF-α mRNA expression compared with the other groups of mice.	[49]
PLGA NPs	Fluoresceinamine	FA-PLGA nanospheres should be more adequate for delivery to inflamed synovial tissue due to their ability to pass through the synovium and can provide local-therapy action in joint disease.	[50]
HSA NPs	Methotrexate	MTX-HSA is superior to MTX in inhibition of the development of CIA and reduction the joint count as well as the number of affected paws.	[52]
PLGA NPs	Betamethasone sodium phosphate	Histological examination showed a significant decrease of the inflammatory cells in the joints.	[54]
PLA NPs	Triptolide	Significantly inhibited the adjuvant arthritis and more anti-inflammatory effect with the long-time administration.	[55]
Chitosan NPs	Folic acid	FA-nanoparticles decreased cytotoxicity and there was a good DNA condensation.	[57]
		Intravenous injected showed that folate-chitosan-DNA nanoparticle could decrease inflammation in arthritis rats.	[64]
HPMA NPs	Dexamethasone	More bone and cartilage preservation was observed with the dexamethasone-HPMA treatment compared with free Dex treatment.	[58]
NPs	WYRGRL	Peptide-functionalized nanoparticles targeted articular cartilage is much higher than nanoparticles presenting a scrambled peptide sequence following intra-articular injection in the mouse.	[59]
CDP NPs	Methylprednisolone	A significant decrease in score arthritis was observed in rats treated with CDP-MP after 28 days and histological evaluation showed decrease in synovitis.	[8]
Chitosan/ siRNA NPs	TNF-α	chitosan/siRNA nanoparticle-mediated TNF-α knockdown reduce local and systemic inflammation.	[2]
PLGA/PLA NPs	Betamethasone disodium 21-phosphate	There was a 35% decrease in paw inflammation with a single injection of conjugate.	[4]
PEG NPs	Dexamethasone	PEG-Dex conjugate improve of ankle joint inflammation. Histological and bone mineral density showed that there was superior anti-inflammatory and disease modifying effects with PEG-Dex conjugate.	[61]

Supplementary Table II-3 - Polymeric nanoparticles for the delivery of Drugs/ Bioactive Agent used in treatment of RA (continuation).

PEG/HA NPs	TRAIL	Substantial reduction of serum inflammatory cytokines and collagen-specific antibodies.	[62]
Chitosan/HA NPs	Photosensitizers	Inflamed joints resulted in a reduction of inflammation when compared with to a standard corticoid treatment.	[63]
Folate/Chitosan NPs	DNA	This approach can help transfect more efficiently folate-chitosan-DNA nanoparticle and can decrease inflammation in arthritis rats.	[64]
RGD-PLGA NPs	STAT1 siRNA	Rheumatoid arthritis regressed in animals treated with STAT1 siRNA and STAT1 mRNA levels were decreased in paws of treated animals.	[65]
Polymeric matrix	MMP-3	A higher NIRF signal was recovered from arthritis joints compared with normal joint.	[66]
HGC/Cy5.5 NPs	Macrophages	Histological evaluation confirmed that the mechanism of selective accumulation of HGC-Cy5.5 within synovitis tissues included increased phagocytosis as well as increase permeability through leaky vessels.	[67]
PLGA NPs	siRNA against TNF-α	Reduction in disease activity, no significant decrease joint effusions. as compared to treatment with PLGA nanoparticles loaded with non-specific control siRNA.	[68]
FA-HSA NPs	Macrophages	FRβ-expressing macrophages showed an increased binding for FA-HSA compared without FA.	[69]
PLGA NPs	Methotrexate	MTX indicated the high toxicity while MTX -free NPs were only toxic when administrated at the highest concentration it was found PLGA`s biocompatibility.	[70]
Dextran Sulphate NPs	Macrophages	Nanoparticles selectively accumulated into inflamed synovia of CIA mice,	[71]
HA NPs	γ-secretase inhibitor (DAPT)	Reduced the production of pro-inflammatory cytokines and collagen-specific auto-antibodies in the serum of the CIA mice.	[72]
psi-tGC-NPs	TNF-α	Nanoparticles showed *in vitro* TNF-α gene silencing efficacy and high accumulation at the arthritic joint sites in CIA mice.	[73]
F-ETX-NPs	Etoricoxib	F-ETX-NPs are a potential to the activated macrophages cells targeting of rheumatoid arthritis.	[74]

Supplementary Table II-4 - Dendrimers for the delivery of Drugs/Bioactive Agent used in treatment of RA.

Delivery vehicle	Drugs/Agents	Main Results	Reference(s)
FA- PEG- PAMAM dendrimer	Indomethacin	The drug targeting efficiency was highest for folate- PEG conjugate when compare to dendrimer without PEG.	[103]
FA-PAMAM dendrimer	Methotrexate	G5-FA-MTX operated as a strong anti-inflammatory agent and reduced arthritis-induced parameters of inflammation.	[104]
Dendrimer ABP	Monocytes	Intravenous injection of dendrimer diminished levels of inflammatory cytokines, normal synovial membrane, and the default of cartilage destruction and bone erosion.	[105]

Supplementary Table II-5 - Metallic nanoparticles for the delivery of Drugs/Bioactive Agent used in treatment of RA.

Delivery vehicle	Drugs/Agents	Main Results	Reference(s)
Nanogold	VEGF	There was a diminution in ankle circumference, articular index score and radiographic scores. Histologic analyses of cartilage erosion, leukocyte infiltration, synovial hyperplasia, macrophage infiltration and levels of TNF-α and IL-1β were very low in the ankle joints of treated rats with nanogold that resulted in attenuation of arthritis.	[109]
Nanogold	Etanercept	Viability of conjugation TNF-α antagonist pharmaceutical preparations with gold nanoparticles preserve of the mechanism of action of TNF-α antagonist with evaluation of PAT technology with anti-rheumatic drugs.	[110]
Nanogold	Hyaluronic Acid	Local arthritis inflammation was clearly identified upon systematic injection of gold nanoparticles.	[111]
Nanogold	Galectin-1	Conjugated promoted apoptosis of CD4+ T cells and decrease pro-inflammatory cytokine levels in the ankle joints and ameliorated clinical symptoms of arthritis.	[112]
RGD Nanogold	Methotrexate	Increased therapeutics effect than that of a treatment only with MTX in collagen-induced arthritis mice.	[113]
HA Nanogold	Tocilizumab	*In vitro* and *in vivo* showed therapeutic potential of HA-AuNP/TCZ.	[114]
SPION	PVA	The nanoparticles remained within the synovial for at least five days indicating that it could prolong the action of intra-articularly applied medication for treating.	[115]
SPIONS	Murine mesenchymal stem cells	A significant decrease in joint swelling was verified in groups containing SiMAG-labelled and unlabeled mMSCs in presence of SPIONS does not affect the immunomodulating properties of the cells.	[3]
Gadolinium MNP	Monocytes/Macrophages	After intravenous administration of MNP reduction in actively inflamed joints was evident earlier than during the course of the disease.	[116]
Silver NPs	Azathioprine	The conjugated to target the disease site to release the drug in a controlled form and produced combined effect to the inflammatory sites.	[117]

Supplementary Table II-6 - Others nanoparticle systems for the delivery of Drugs/Bioactive Agent used in treatment of RA.

Delivery vehicle	Drugs/Agents	Main Results	Reference(s)
Solid lipid nanoparticle	Actarit	The actarit-loaded SLNs exhibited a longer mean retention time *in vivo* compared with the Actarit in 50% propylene glycol solution after intravenous injection in rabbits and the targeting efficiency was enhanced in spleen while the renal distribution of actarit was reduced as compared with the actarit solution after intravenous injection in mice.	[118]
Solid lipid nanoparticle	Tripterygium	TWHF-SLN can greatly reduce rat paw volume. Histopathology date found that free TWHF caused severe damage to the liver than TWHF-SLN and this last can increase the anti-inflammatory.	[119]
Solid lipid nanoparticle	Indomethacin	IMC nanoparticles may increase the effect of rheumatoid arthritis treatment. without causing IMC-induced gastrointestinal lesions, because the bioavailability is bigger than of conventional IMC.	[120]

fumagillin NPs	αv β3	Lower disease activity, change in ankle thickness. Decrease in inflammation, angiogenesis in synovial tissues from animals treated with αv β3 –target fumagillin nanoparticles.	[121]
Silver NPs	Camptothecin	A single subcutaneous injection of CPT-SSM-VIP administered to CIA mice alleviated joint inflammation at least one month without systemic toxicity.	[126]

Supplementary Table II-7 - Characteristics of Drugs/Bioactive Agent used in treatment of RA [122], [123].

Drugs/ Agents	Molecular weight/kDa	Type of molecules	Charge	Mechanism of action
Methotrexate	0.45	DMARDs	-2	It possesses an anti-tumor activity that result of the inhibition of folic acid reductase, leading to inhibition of DNA synthesis and inhibition of cellular replication.
Clodronate	0.24	Diphosphonate	-2	It can bind strongly to hydroxyapatite; it does not inhibit protein isoprenylation but can be metabolized intracellularly to a β-γ-methylene (AppCp-type) analog of ATP (AppCCl2p), which is cytotoxic to macrophages *in vitro*; Inhibition of the ADP/ATP translocase by the metabolite AppCCl2p is a likely route by which clodronate causes osteoclast apoptosis and inhibits bone resorption; binds protein-tyrosine-phosphatase.
Verteporfin	0.72	benzoporphyrin derivative	-1	It accumulates in abnormal blood vessels; it produces highly reactive short-lived singlet oxygen and other reactive oxygen radicals, resulting in local damage to the endothelium and blockage of the vessels.
NFκB	50	Protein	-	Protein complex that controls transcription of DNA, cytokine production and cell survival and it has a key role in regulating the immune response to infection.
Superoxide dismutase	32.5	Enzyme	-1	It possesses anti-inflammatory activity; it can decrease reactive oxygen species generation and oxidative stress and, so, inhibits endothelial activation and indicate that modulation of factors that govern adhesion molecule expression and leukocyte-endothelial interactions.
Indomethacin	0.36	non-steroidal anti-inflammatory agent	-1	It is a prostaglandin G/H synthase inhibitor that acts on both prostaglandin G/H synthase 1 and 2 (COX-1 and -2).
Lactoferrin	80	Protein	+	It has antimicrobial activity and is part of the innate defense; it can interact with DNA, RNA, polysaccharides, heparin and shows some of its biological functions in complexes with these ligands.
Dexamethasone	0.39	Corticosteroids	0	It can modify the transcription, protein synthesis, in order to achieve inhibition of leukocyte infiltration at the site of inflammation, interfere in the function of mediators of inflammatory response, suppress of humoral immune responses, and it can reduce edema or scar tissue formation.
Prednisolone phosphate	0.36	Corticosteroids	0	It can inhibit leukocyte infiltration at the site of inflammation, interfere with mediators of inflammatory response and suppress humoral immune responses.
II collagen (CII)	1.5	protein	N.A	It can allow cartilage to entrap the proteoglycan aggregate and provide tensile strength to the tissue

Chapter III

Hydrogels in the treatment of Rheumatoid Arthritis: Drug delivery systems and artificial matrices for dynamic *in vitro* models

Chapter III

Hydrogels in the treatment of Rheumatoid Arthritis: Drug delivery systems and artificial matrices for dynamic *in vitro* models[3]

ABSTRACT

Rheumatoid Arthritis (RA) is an autoimmune and chronic inflammatory disorder, that mostly affects the synovial joints and can promote both cartilage and bone tissue destruction. Several conservative treatments are available to relieve pain and control the inflammation. However, traditional drugs administration are not fully effective and present severe undesired side effects. Hydrogels are a very attractive platform as a drug delivery system to guarantee these handicaps are reduced, and the therapeutic effect from the drugs is maximized. Furthermore, hydrogels can mimic the physiological microenvironment and have the mechanical behavior needed for use as cartilage in vitro model. The testing of these advanced delivery systems are still bound to animal disease models, that have shown low predictability. Alternatively, hydrogel-based human dynamic in vitro systems can be used to model diseases, bypassing some of the animal testing problems. RA dynamic disease models are still in an embryonary stage since advances regarding healthy and inflamed cartilage models, are currently giving the first steps regarding increasing complexity. Herein, recent studies using hydrogels in the treatment of RA, featuring different hydrogel formulations are discussed. Besides, their use as artificial extracellular matrices in dynamic in vitro articular cartilage and RA disease models are reviewed in depth.

Keywords: Hydrogels, Controlled Drug release, Bioreactors, Microfluidics, Rheumatoid Arthritis

[3]This chapter is based on the following publication:

Oliveira I.M., Fernandes D.C., Cengiz I.F, Reis R.L., Oliveira J.M., Hydrogels in the treatment of Rheumatoid Arthritis: Drug delivery systems and artificial matrices for dynamic in vitro models" (Submitted)

III-1. GRAPHICAL ABSTRACT

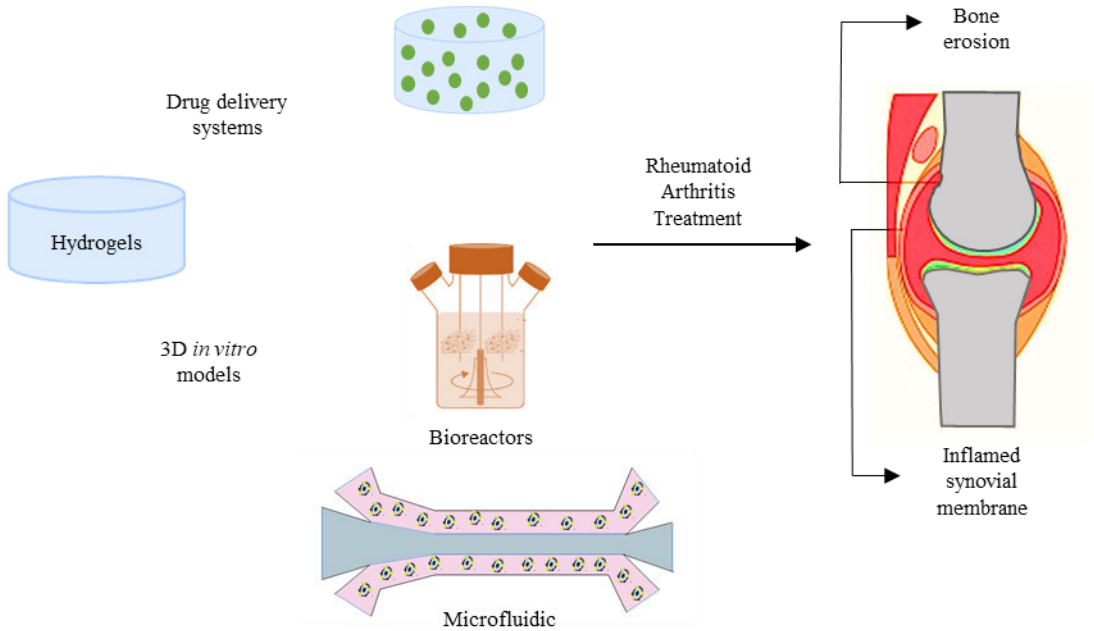

III-2. INTRODUCTION

Hydrogels are three-dimensional networks of hydrophilic polymers able to absorb vast amounts of biological fluids or water [1, 2]. Hydrogels are formed by physical and chemical crosslinking. Physically crosslinked hydrogels are produced through molecular entanglements, ionic, hydrogen bonding, or hydrophobic forces. These hydrogels are structurally weak, and their gelation is reversible. Chemical hydrogels are covalently crosslinked by redox reactions, photo-polymerization, Michael reactions, enzymatic reactions, or disulfide-forming reactions, which are strong and irreversible bonds [3, 4]. Hydrogels, according to the source, can be classified into the natural and the synthetic group [5]. Natural hydrogels include matrigel, hyaluronic acid, collagen, silk fibroin, chitosan, among others. Natural-based polymers are non-toxic materials, very similar to native tissues therefore, they can easily communicate with biological systems and improve cellular behavior such as adhesion, migration, proliferation, and differentiation. However, natural hydrogels have properties challenging to control consistently between experiences. They present low mechanical strength and batch-to-batch variation [6, 7]. Synthetic hydrogels include polyurethane, polyanhydrides, polyesters, polyphosphazenes, and poly (glycerol sebacate). This group of hydrogels has more tunable mechanic properties, higher

degradation rates, and easier processability. However, they do not mimic the extracellular matrix (ECM) composition, presenting low cell-scaffold interaction, and toxic solvents are used for their preparation. Natural and synthetic polymers present advantages and disadvantages, to increase the physicochemical and biological properties, several materials can be used together [8].

Experiments with 2D cell cultures are the usual practice in cell-based assays for various biomedical research purposes, presenting, however several limitations. This cell culture system is incapable of reproducing the anatomical and biochemical properties of tissues and organs [9]. Therefore, the development of model systems that better mimic the physiological microenvironment of the tissue and disease, such as stiffness, topography, and biochemistry, with the capacity to execute prolonged culture tests while maintaining tissue function is required [10]. *In vivo*, cells are embedded by ECM that plays an important role in several cellular processes such as regulating growth and cell-cell communication and assembling cells into various tissues and organs. So, developing an *in vitro* cell culture environment that mimics the native ECM is required [11]. Hydrogels are one of the leading biomaterials used and appropriate options due to their unique properties, high water content, porosity, and flexibility. they can mimic the native ECM. Additionally, hydrogels do not affect the metabolic processes of living organisms, and metabolites can pass easily through the hydrogels [12]. So, such an engineered native-like ECM is most likely to offer cells with rational indications for diagnostic and therapeutic investigations. Due to these appealing features, an extensive range of 3D hydrogel platforms have been developed to mimic better the natural tissue environment *in vitro* [13]. Traditional approaches include cellular encapsulation into hydrogels, cell seeding on porous and fibrous hydrogels. However, advanced hydrogel platforms have emerged to use hydrogels in functional tissue models, including hydrogel microspheres, hydrogel sandwich systems, hydrogel-based microwells, and 3D bioprinted tissue–hydrogel. Furthermore, hydrogels are usually incorporated within culture platforms such as transwell microfluidic devices **(Figure III-1)** [14]. Hydrogels have been used to develop a wide range of tissue and disease models. These three-dimensional networks of hydrophilic polymers can undergo physiological swelling and have the mechanical behavior desired for use as an articular *in vitro* model [15].

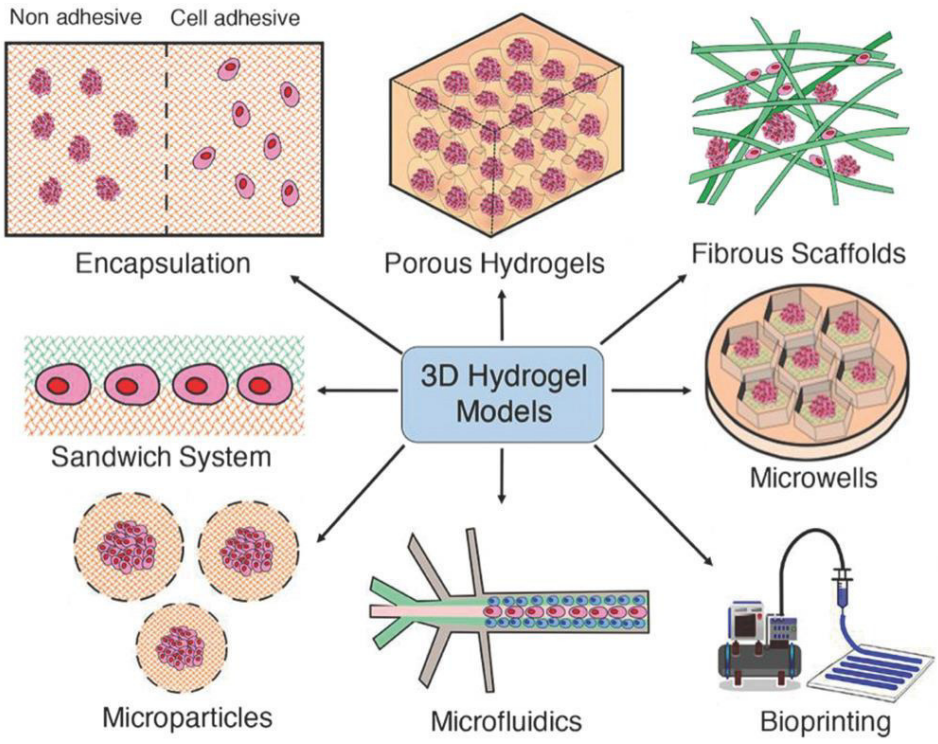

Figure III-1 - Schematic illustration of the 3D hydrogel models, including hydrogels (encapsulation), porous hydrogels, fibrous hydrogel scaffolds, hydrogel sandwich systems, microwells, hydrogel microparticles, microfluidics, and bioprinted scaffolds. Reprinted from publication [14], Copyright (2019) with permission from Jonh Wiley and Sons Inc.

The process of therapeutic approval is long from *in vitro* tests to widespread medical practice. With the increased costs of drug development, the paradigm of using animal experimentation as a predictor of results in humans has been questioned. After revising several systematic reviews and meta-analyses evaluating results, from animal experimentation, during the last two decades, several publications have emphasized the shortcomings of animal testing. [16-20]

A group of academia and industry experts recently presented an alternative for the near future to animal models: human-based microphysiological models, developed with the tissue engineering principles [21]. These systems have the advantage of having human cells, annulling the issue of between species results translation. However, it carries several engineering challenges, mostly bound to organs' complexity and systemic dynamics.

Articulations are areas of particular fluid and mechanical dynamics, considering the fact of being a flexible, load-bearing tissue requiring, for this reason, a highly lubricated environment, where synovial

fluid plays a central role. Thus, to produce a fully biomimetic model of a joint's cartilage, it is necessary to ensure that these dynamics are transposed from *in vivo* to *in vitro* [22].

The need for mechanical load and dynamic fluid circulation makes this cartilage a promising candidate for innovative, multi stimuli dynamic culture systems particularly, bioreactors. Since 1993 that exist dynamic culture systems for three-dimensional culture of cartilage models that show the production of cartilage-specific extracellular matrix by cultured chondrocytes [23],[24].

In summary, a biomimetic dynamic articular cartilage model must include a biocompatible hydrogel, with physiological values of physical and biochemical cues for chondrogenesis; multi-axial mechanical stimulation, mimicking the articulated limbs; and physiological synovial fluid shear stress, transporting nutrients and regulating the soluble oxygen levels. To improve the outcome of drug development, existing such models, with throughput and scale-up capacity in a near-future, it is necessary that innovative therapeutics systems are developed meanwhile.

The unique physical properties of hydrogels (*e.g.* high porosity, controlled drug release, biocompatibility, biodegradation, and flexibility) make this system an appealing platform for drug delivery applications [25]. The porosity of hydrogels allows the encapsulation of drugs into the gel and consequent drug release at a rate dependent on the diffusion coefficient of the molecule by the hydrogel network [26]. The advantages of hydrogels for drug delivery of the gel formulation. The hydrogels can be produced in a way in which drugs are released slowly, keeping a high local concentration of the drug in the place where they are administrated for a long time [27, 28]. Hydrogels are also biocompatible due to their high content and structural and mechanical similarity of hydrogels to the ECM. The biodegradation pattern is an essential parameter for a drug delivery system. The controlled drug release and degradation profile may be design into hydrogels via the hydrolytic, environment (pH, temperature) or enzymatic pathways **(Figure III-2)** [29-33].

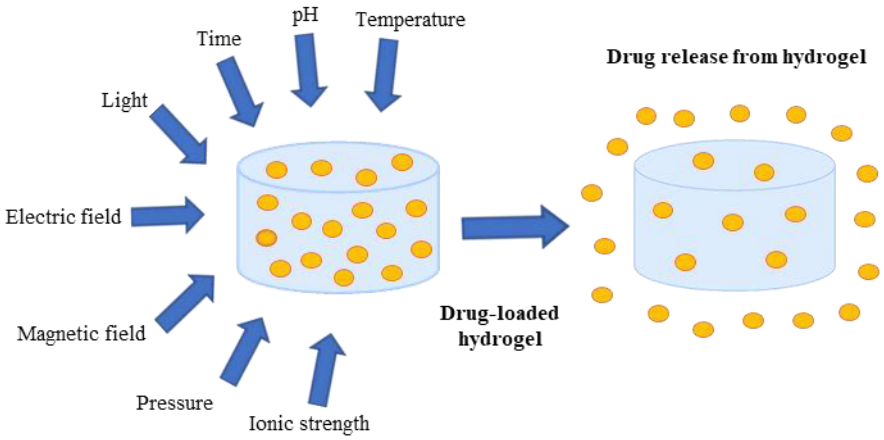

Figure III-2 - Drug delivery hydrogel in response to several physical and chemical stimuli.

The administration of hydrogels is also versatile, for example, through oral administration, implantation, or it can be injected with minimal invasive administration [34]. Injectable hydrogels demonstrate promising properties as carriers for targeted drug delivery. They are attracting more attention because they are more comfortable, less painful, have a faster recovery period, lower costs, and present fewer complications and side effects [35]. This promising approach is fundamentally a kind of *in situ*-forming hydrogels, that is, they can spontaneously gel in physiological conditions after injection. For this, the hydrogel should be made by processing, mostly by transporting the solution or pre-gel to a targeting site for gelation through an injection device [36]. *In situ*-forming hydrogels can be produced by physical or chemical crosslinking. The crosslinking procedure can change the properties of the material, including the molecular mass, mechanical strength, and resistance [37]. Either chemical or physical crosslinking produces the three-dimensional structure of hydrogels, allows the encapsulation and release of drugs or biomolecules [38]. Physically crosslinking hydrogels frequently have weak mechanical properties and faster degradability which maybe not satisfy the requirements depending on the application. However, a disadvantage of *in situ* producing chemical hydrogels is the likely dissolution of hydrogel and complete drug release instantly after injection due to slow gelation time [39]. Therefore, the combination approach of the mechanical force of a chemical hydrogel with the fast gel formability of physical hydrogels has gained special attention [40].

Although conventional hydrogels have several appealing features, one of the handicaps of hydrogels is low mechanical strength, particularly when the application request high mechanical strength with good compliance of compression and adequate elasticity at the same time, for example,

cartilage tissues [41]. Several strategies have been explored to improve the performance of hydrogels, among which is the incorporation of nanoparticles (NPs) in the hydrogels matrix to fabricate nanocomposite hydrogels (NC gels). NC hydrogels, inorganic-organic hybrid biomaterials, attract significant attention as artificial 3D materials for biomedical applications such as drug delivery [42, 43]. This approach can combine the various advantages characteristics of NPs (e.g., size, shape, electric, optical and mechanical properties) with those of soft 3D hydrogel networks (e.g., elasticity, hydrophilicity, porosity, high water absorption) [44, 45]. The incorporation of NPs within the polymer gel network produces hydrophilic polymers chain binding strongly onto the large surface area provided by the NPs. Furthermore, the large surface area improves the protein and cell-adhesiveness of NC hydrogels. Therefore, NC hydrogels show better mechanical force, cell adhesion, proliferation, migration, and differentiation than conventional hydrogels without NPs [46, 47]. Thus, the innovative combination of NPs and hydrogels represent a promising approach for medicine regenerative and tissue engineering application [48].

Rheumatoid Arthritis (RA) is an autoimmune and chronic inflammatory condition, that mainly affects the synovial joints and subsequent cartilage and bone tissue destruction. The cause of RA remains poorly known but can involve genetic and environmental factors [49, 50]. The clinical manifestations comprise redness, swelling, and limitation a range of motion. Several treatments, including analgesics, NSAIDs, GCs, DMARDs, and biological agents, are available to relieve pain and control inflammation with the final goal to achieve disease remission [51]. However, traditional drug administration often involves high dosages or frequent administration to promote a therapeutic effect, which can decrease overall efficacy and result in severe side effects (*e.g.* heart problems, kidney damage, diabetes, lung infections, among others) [52]. Drug delivery systems are emerging to address existent failures in traditional methods. The advantages of these new approaches are delivering a drug more selectively to a specific site allowing more accurate and less frequent dosing. Furthermore, decrease in variability in systemic drug concentration, the absorption is more consistent with the site and action mechanism, and it reduces the side effects of therapeutics. Hydrogels are a desirable as a drug delivery system to guarantee these handicaps are reduced, and the therapeutic effect from the drugs is maximized [28, 53].

III-3. HYDROGELS FOR THE TREATMENT OF RA

Current strategies for the treatment of RA can decrease inflammation in the joints, alleviate pain, and slow down joint damage however, the treatments are associated with poor pharmacokinetic distribution to the specific site of disease, short half-life, and several side effects [54]. The hydrogels offer suitable drug delivery vehicles to guarantee that the handicaps of traditional drugs are reduced, and the therapeutic effects from the medications are maximized.

Several studies report the potential application of hydrogels in the treatment of RA. In this section, some of the studies developed in the last years with hydrogels in the treatment of RA are summarized **(Table III-1)**.

Qi *et al*. [55] developed chitosan thermosensitive hydrogels with diclofenac sodium-loaded alginate microspheres to assess the potential of hydrogels as drug delivery systems for promoting the anti-inflammatory effect. The results showed that the anti-inflammatory efficacy of hydrogels in rabbits with RA was higher than that of diclofenac solution and chitosan hydrogels alone. The results confirmed that thermosensitive hydrogels with diclofenac sodium-loaded alginate microspheres showed promising characteristics as a drug delivery system for enhancing the therapeutic effect of diclofenac.

A study made by Dong *et al*. [56] produced transplantable platform-based cationic hydrogels to deliver antisense oligodeoxynucleotides (ASOs) targeting the mRNA of TNF-α. Different kinds of animal models were used to assesses the therapeutic benefits of ASO-Gel, including collagen-induced Arthritis (CIA), carrageen/lipopolysaccharide (LPS)-induced Arthritis (CLA), adjuvant-induced Arthritis (AA), and models. The effects of ASO-c-agarose in decreasing inflammation and tissue destruction were demonstrated in most tested animals, with reduction of main inflammatory cytokines and decrease of joint swelling and tissue destruction. The results suggested that this approach could become a useful therapeutic against rheumatoid arthritis and other disorders.

Liu *et al*. [57] transplanted fibrin gel- and poly(l-lactide-co-glycolide)-poly(ethylene glycol)-poly(l-lactide-co-glycolide) (PLGA-PEG-PLGA) hydrogel-assisted (bone marrow mesenchymal stem cells) BMMSCs referred to FGB and HGB groups, respectively, into subchondral defects of Ovalbumin-Induced Arthritis (OVA) in rabbits for the treatment of antigen-induced arthritis. The administration of BMMSCs reduced inflammatory cytokine levels and improved joint swelling in both groups. Furthermore, the preservation of adjacent cartilage and enhanced cartilage repair were detected. The HGB group

presented a better therapeutic benefit than the FGB group. Therefore, transplantation of BMMSCs in subchondral defects shows a promising approach in RA remission.

Another study reported the production of an injectable self-assembled nanofibrous hydrogel, which can encapsulate and release agents in response to matrix metalloproteinases (MMP-2 and MMP-9) that are upregulated in RA. The results showed that nanofibrous gels could persist stably after injection into healthy joints of mice, and *in vitro* studies showed that release loaded agents in response to synovial fluid from arthritic patients. This strategy represents a next-generation therapeutic approach for the targeted treatment of proteolytic diseases [58].

Goindi *et al*. [59] developed microemulsion-based topical hydrogels of Tenoxicam (TNX) to treat Arthritis. *In vivo* anti- inflammatory and anti-arthritic activity of the TNX formulations was assessed using several inflammatory models. Microemulsion formulations demonstrated to be better in controlling inflammation than traditional topical forms and presented efficacy similar to an oral formulation. Results suggested that the microemulsion formulations can be used for topical delivery of TNX to treat several inflammatory diseases, including RA.

A study made by Garg *et al*. [60] investigated the use of nanostructured lipid carriers (NLCs) produced through lipid mixture and chemical permeation increaser-based hydrogel for an effective transdermal delivery of methotrexate (MTX) to induce apoptosis of RA. The immunocytochemistry to detect IL-6 expression and immunofluorescence assay showed that promoted apoptosis occurred in an *in vitro* arthritis model treated with NLCs-MTX. It was verified decreased inflammation and activated apoptosis promoted by MTX encapsulated NLCs in rheumatoid arthritic cells. Furthermore, histopathological analysis of skin suggested the safety potential of NLCs. Posteriorly the same group [61] evaluated the effect of MTX encapsulated nanostructured lipid carriers and chemical enhancer co-incorporated hydrogel (gel-(MTX-NLCs+CE)) for competent transdermal delivery of MTX in a Complete Freund's adjuvants (CFA)-induced arthritis in rats. Results showed that the transcutaneous ability of MTX loaded NLCs and CE co-incorporated hydrogel significantly reduced the inflammation in the RA animal model. So, the presented approach has the potential to be a novel therapeutic modality for RA patients with minimum adverse effects **(Figure III- 3** a**)**.

Sallam *et al*. [62] developed a lecithin organogels (LO) transdermal delivery system for diflunisal and studied human skin penetration capability compared to optimized microemulsion-based hydrogel. The lipogels delivered a significant amount of drug through the skin than the hydrogel. The constitution

of lecithin showed to affect the skin permeability increasing the capability of the lipogel. The lecithin organogels are promising carriers that produce an excellent opportunity for transdermal delivery of diflunisal reducing the side effects relating to its oral administration.

Joshi and coworkers [63] reported the production of a triglycerol monostearate (TG-18) hydrogel encapsulated with triamcinolone acetonide (TA) releases after being in contact with enzymes or synovial fluid from patients with RA. In arthritic mice, hydrogel encapsulated with a fluorescent dye showed flare-dependent disassembly assessed as a loss of fluorescence. Furthermore, a unique dose of TA-encapsulated hydrogel decreased arthritis manifestation in the injected paw. The results propose flare-responsive hydrogel as a potential next-generation drug delivery strategy for the RA treatment.

Another study developed methotrexate aspasomes encapsulated into a hydrogel and tested in adjuvant-induced arthritis (AIA) model in Wistar rats [64]. Transdermal application of methotrexate-loaded aspasome hydrogel in model disease demonstrated a more significant decrease of rat paw diameter, tumor necrosis factor-alpha (TNF-α), interleukin (IL-1) β, cartilage damage, inflammation, pannus formation, and bone resorption when compared to arthritic control rats. Furthermore, the group treated with free methotrexate exhibited intermediate effects however, the group treated with free aspasome did not show to have an effect. The results demonstrated that drug-loaded therapeutically active carrier system presented a non-invasive controlled release transdermal formulation with good drug encapsulation, drug permeation rate, and showed a more effective therapeutic effect in treatment of RA than the drug alone. Therefore, this approach provides a more attractive therapeutic strategy for RA [64].

A study performed by Cokelaere *et al.* [65] evaluated the administration intra-articular sustained of two formulations of celecoxib (40 mg/g and 120 mg/g) in a poly(ε-caprolactone-*co*-lactide) PCLA-PEG-PCLA triblock copolymer in an equine repeated LPS synovitis model. Only one intra-articular injection of the low dose (LCLB)-gel or high dose (HCLB)-gel demonstrated a sustained and controlled intra-articular release in healthy and inflamed joints. The celecoxib formulations presented a soft effect on inflammatory and synovial fluid biomarkers, but these returned to the threshold one week after administration. High levels of celecoxib were detected in the joint after one month, but no overall anti-inflammatory effects was observed, maybe due to the moderate synovitis. Furthermore, there were no side effects during the study period. Therefore, this approach should be assessed for its impact on longer-term relief of inflammatory joint pain.

Yeo *et al*. [66] evaluated the capability of the nitric oxide (NO)-scavenging nanogel (NO-Scv gel) to treat RA. The NO-Scv gel decreased inflammation levels and showed good biocompatibility. Moreover, the therapeutic effect of the NO-Scv gel in diminishing the onset of RA is observed in a mouse RA model when compared to the effects of dexamethasone alone. Consequently, the results showed the potential of the NO-Scv gel for biomedical applications (Figure III-3 b).

Wang and coworkers [67] produced a sustained release formulation-intra-articular injectable dexamethasone-encapsulated thermosensitive hydrogel (DLTH) chitosan-glycerin-borax as the carrier for the suppression of inflammation and pain in collagen-induced arthritis rats. The data showed that paw swelling, arthritis scores, and joint inflammation destruction were reduced in the group treated with DLTH. DLTH demonstrated down-regulated serum IL-17A and mRNA levels of inflammatory factors. Furthermore, DLTH-treated rats elucidated the pain-reducing effects of DLTH. So, these results suggested that DLTH joint injection prevents synovial inflammation and can help in the regulation of RA pain.

A study made by Kuçukturkmen *et al*. [68] analyzed the effect of *in situ* gelling hydrogel formulations (Poloxamer 407 and chitosan) containing diclofenac sodium (DS) loaded Poly(lactic-co-glycolic acid) (PLGA) and poly(ε-caprolactone) (PCL) nanoparticles for lengthy local delivery. After one-month prolonged *in vitro* release of DS was reached by using polymeric nanoparticles with *in situ* hydrogels. In conclusion, the local administration of DS loaded PLGA and PCL can be a promising approach to reduce side effects associated with a decreased amount of drug in dosage form as compared to the traditional oral dose.

Another study investigated the effect of nanoiguratimod-loaded Hyaluronic Acid–Acrylate (HA-AC) hydrogel (NanoIGUR-loaded hydrogel) composites in collagen-induced arthritis (CIA) rats to improve the bioavailability of drug and to alleviate side effects through the sustained release of therapeutics [69]. The results demonstrated superior bioavailability and longer half-life time with NanoIGUR-loaded hydrogel than traditional iguratimod. Animal experiments for 21 days showed that subcutaneous injection of NanoIGUR-loaded hydrogel (10 mg/kg every 3 days) and traditional iguratimod (10 mg/kg daily) exhibited identical efficacy in diminishing arthritis index score, pathological score, and expression of inflammatory cytokines. Therefore, NanoIGUR-loaded hydrogel can be a potential drug-delivery strategy in the treatment of RA [69].

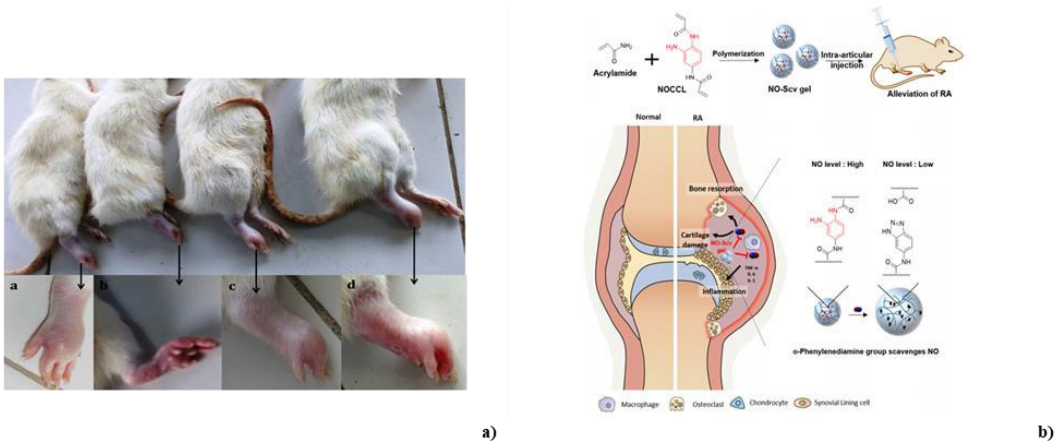

Figure III-3 - a) Evaluation of the severity of inflammation in right paw of CFA induced experimental rat. a. treatment with gel-(MTX-NLCs); b. treatment with gel-(MTX-NLCs + CE); c. treatment with gel-MTX ; d. CFA control (without treatment). The severity of inflammation was significantly decreased after the treatment of gel-(MTX-NLCs + CE) compared to gel-(MTX-NLCs) and gel-MTX. Reprinted from publication [61], Copyright (2019) with permission from Elsevier. b) Schematic Illustration of intra-articular injection of NO-Scv Gel in suppressing o RA in a mouse model. Reprinted with permission from [66]. Copyright (2019) American Chemical Society.

Table III-1 - Hydrogels for the delivery of Drugs/Bioactive Agents used in the treatment of RA.

Delivery vehicle	Drugs/Agents	Conditions	Main Results	Reference
Chitosan hydrogels combined with alginate microspheres	Diclofenac	In vivo study New Zealand rabbits (3 weeks post-treatment)	The anti-inflammation efficacy of the combined hydrogels in rabbits with RA was higher than that of drug solution and pure chitosan hydrogels.	[55]
Cationic agarose hydrogels	ASO	In vivo study AA CLA CIA	Alleviating inflammation and tissue destruction were demonstrated in more than 90% of the testing animals Reduction of central inflammatory cytokines and decrease of joint swelling and tissue damage.	[56]
Fibrin gel (FGB) and PLGA-PEG-PLGA hydrogel (HGB)	BMMSCs	In vivo study OVA rabbits (12 weeks post-treatment)	The administration of BMMSCs reduced inflammatory cytokine levels and improved joint swelling in both groups The preservation of adjacent cartilage and enhanced cartilage repair were detected.	[57]
Nanofibrous hydrogel	MMP-2 and MMP-9	In vivo study Balb/C mice (8 weeks post-treatment)	The results showed that nanofibrous gels could persist stably after injection into healthy joints of mice in vitro studies showed that release loaded agents in response to synovial fluid from arthritic patients.	[58]
microemulsion-based topical hydrogels	TNX	Ex vivo study Laca Mice Sprague-Dawley (48 hours post-treatment)	Microemulsion formulations demonstrated be superior in controlling inflammation as compared to traditional topical dosage forms and presented efficacy equivalent to the oral formulation.	[59]
NLCs	MTX	In vivo study Wistar rat (24 hours post-treatment)	The immunocytochemistry to detect IL-6 expression and immunofluorescence assay showed that promoted apoptosis occurred in an in vitro arthritis model treated with NLCs-MTX. It was verified decreased inflammation and activated apoptosis promoted by MTX encapsulated NLCs in rheumatoid arthritic cells. Histopathological analysis of skin suggested the safety potential of NLCs.	[60]

MTX-NLCs+CE hydrogel	MTX	In vivo study CFA induced arthritis rat (17 weeks post-treatment)	MTX-NLCs+CE hydrogel significantly decreases the inflammation in RA animal model.	[61]
Lipogel and hydrogel microemulsion	Diflunisal	Ex vivo study Human abdominal skin (24 hours post-treatment)	The lipogels delivered a significant amount of drug through the skin than the hydrogel. The constitution of lecithin showed to affect the skin permeability increasing the capability of the lipogel.	[62]
TG-18 hydrogel	TA	In vivo study K/BxN serum-transfer model of IA (14 days post-treatment)	In arthritic mice, hydrogel encapsulated with a fluorescent dye showed flare-dependent disassembly assessed as a loss of fluorescence. A unique dose of TA-encapsulated hydrogel decreased arthritis manifestation in the injected paw.	[63]
aspasome hydrogel	MTX	In vivo study AIA in Wistar rats (21 days post-treatment)	Transdermal application of methotrexate-loaded aspasome hydrogel in model disease demonstrated a more significant decrease of rat paw diameter, tumor necrosis factor-alpha (TNF-α), interleukin (IL-1) β, cartilage damage, inflammation, pannus formation, and bone resorption when compared to arthritic control rats. The group treated with free methotrexate exhibited intermediate effects however, the group treated with free aspasome did not show to have an effect.	[64]
propyl-capped PCLA-PEG-PCLA gel	Celecoxib (40 mg/g and 120 mg/g)	In vivo study Dutch Warmblood horses (5 weeks post-treatment)	One intra-articular injection of LCLB-gel or HCLB-gel demonstrated a sustained and controlled intra-articular release in healthy and inflamed joints. The celecoxib formulations presented a soft effect on inflammatory and synovial fluid biomarkers, but these returned to threshold one week after administration High levels of celecoxib were detected in the joint after one month, but no overall anti-inflammatory effects was observed, maybe due to the moderate synovitis There were no adverse effects during the study period.	[65]
Scv gel	NO	In vivo study collagen-induced arthritis mouse model (35 days post-treatment)	The NO-Scv gel decreased inflammation.n levels and showed good biocompatibility. Therapeutic effect of the NO-Scv gel in decreasing the onset of RA is observed in a mouse RA model when compared to the effects of dexamethasone alone.	[66]
DLTH with chitosan-glycerin-borax	Dexamethasone	In vivo study Collagen-induced arthritis wistar rats (3 weeks post-treatment)	Paw swelling, arthritis scores, and joint inflammation destruction were reduced in the group treated with DLTH DLTH demonstrated down-regulated serum IL-17A and mRNA levels of inflammatory factors. DLTH-treated rats elucidated the pain-reducing effects of DLTH.	[67]
Hydrogel formulations (Poloxamer 407 and chitosan) loaded PLGA and PCL nanoparticles	DS	In vitro study	After one-month prolonged in vitro release of DS was reached by using polymeric nanoparticles with *in situ* hydrogels.	[68]
HA-AC Hydrogels	Iguratimod	In vivo study CIA rats (21 days post-treatment)	The results demonstrated superior bioavailability and longer half-life time with NanoIGUR-loaded hydrogel than traditional iguratimod. Animal experiments for 21 days showed that subcutaneous injection of NanoIGUR-loaded hydrogel (10 mg/kg every 3 days) and traditional iguratimod (10mg/kg daily) exhibited identical efficacy in diminishing arthritis index score, pathological score, and expression of inflammatory cytokines.	[69]

The list of U.S. Food and Drugs Administration (FDA) approved drugs for RA is still limited [54, 70], and RA is still an incurable disease with a high impact on the patient's lifestyle. The drug development process has systemic problems, several of them related to the use of animal (non-human) models. This problem, alongside its alternatives, is discussed in the following section, reviewing the most recent articular cartilage healthy and RA diseased models with drug testing platform potential.

III-4. DYNAMIC SYSTEMS FOR RA: FROM HEALTHY TO DISEASED MODELS OF ARTICULAR CARTILAGES

The near-physiological dynamic systems most commonly used are bioreactors, the systems with a working volume that can range from few milliliters to several liters, and microfluidic devices, with working volume that range from nanoliters to microliters. Bioreactors, mainly in continuous operation mode, have better mixing capacity since they often allow turbulent flow, while microfluidic devices can only achieve laminar flow due to the micrometric sized features.

Recently, bioreactor-based tissue engineering for articular cartilage has explored deeper its tissue-specific particularities [64-66]. These systems allow both the increase the knowledge about the role of the tissue specificities and cell biology and as a proof-of-concept of biomimetic capacity. One particularity of cartilage is it is an avascular tissue, i.e. it is absent of vascularity, providing cells an environment with a hypoxic environment [71] when compared to the one from surrounding muscles and bones, which are highly vascularized tissues. Considering that this oxygen-deprived environment plays a central role in chondrocytes' survival [72] and is a particularity of tissue, it is an important feature to mimic in representative *in vitro* models. Using a 3% oxygen concentration, a bioreactor-based system produced cartilage samples with volumes ranging from 60 to 400 cm^3, showing increased chondrogenesis and matrix proteins when compared to 20% [73].

However, according to recent modeling efforts, the physiological oxygen concentration, or physoxia, of articular cartilage is, in fact, a gradient, with a decreasing oxygen concentration from the contact with the subchondral bone with an oxygen concentration of 5%, to the synovium, where the concentration should be slightly above 1% [71]. Thus, it is essential to uncover the impact of this gradient on cartilage properties and inner physiology. To do so, a bioreactor with feedback control of oxygen concentration allowed the assessment of the effect of 1%, 2.5%, and 5% of oxygen concentration on chondrocyte's matrix transcriptomic and metabolomic alterations. This work revealed that oxygen at 2.5% leads to a

maximum of tissue-specific collagen production, surface markers, and activation of metabolic pathways in a tumor growth factor-β (TGF-β) dependent way [74]. This work shows that the articular cartilage is a complex, spatially heterogeneous tissue where the spatial control of the oxygen control is a requirement for any model's representativity of the native tissue.

Although the importance of oxygen concentration or metabolic cues to the homeostasis of any joint's cartilage, its most relevant macroscopic characteristic is the capacity to withstand and facilitate the multiaxial movement between two rigid surfaces while bearing a load. Not only this is its most relevant characteristic, but these mechanical stimuli play a central role in cartilage health [75]. For two decades that bioreactors have been designed to impose mechanical stimuli that emulate in some form or way, the compression and stress experienced by the native articulation [76]. In recent years, the complexity of the movements robotized has increased and has been combined with medical imaging-mediated biofabrication and computational simulations to increase the mimetics of this strategy. An example of this multidisciplinary approach is a recent work where a cell-laden 3D printed knee joint, designed according to a computed tomography scan, is stimulated using a two-axis bioreactor. The pressure points and the stress distribution of flexing and extending the articulation were modeled and evaluated using a computer simulation, taking into account the shape of the sample analyzed by medical imaging. This setup allows mechanical stimulation, controlled nutrient and oxygen supply, and prediction of mechanical properties, making the example of the state-of-the-art bioreactor systems for articular cartilage [77].

Bioreactors, despite allowing real-size models, using multi-stimuli setups, have a lesser throughput than miniaturized models, namely microphysiological systems that decrease the volume of consumables, decrease sample size, and increase monitoring capacity. Organ-on-a-chip technology has been more common in recent years and has been applied to in vitro development of cartilage models in the most recent years [78],[79]. These models show that this technology already allows *in vitro* model production and maintenance [78],[80], and explant culture [79]. However, from these models, only Paggi *et al.* [81] developed an articular-specific cartilage model, showing a still found shortage of research in the field of microphysiological joint models.

The room for improvement of these healthy dynamic models lies on the extension of the biomimetic approach: the creation of the oxygen gradient, practically linear from the subchondral bone to the synovium instead of the gradient from the synovial cavity inward to the cartilage core that exists

in the bioreactors; development of a biomimetic matrix emulating native tissue cell adhesion, with spatial distribution and alignment that ensure the natural anisotropy of the native matrix [82] and the use of stem cells that allow the development of spatially differentiated tissue, accounting for the different systems that intervene in the cartilage microenvironment, namely the lymphatic and immune systems [83]. The latter point is particularly crucial for *in vitro* models and the less important one regarding a regenerative medicine approach since these different systems surrounding cartilage is tightly linked to articular pathologies.

The incorporation of other cell types, mimicking the microenvironment of the cartilage is done already in disease models, which are often dependent on exacerbated and overextended reactions of the immune system causing a pathological inflammation. The most impactful consequence of pathological inflammation effecting the joints is the formation of arthritis, as discussed in previous sections. Thus, in dynamic *in vitro* models of arthritis, the presence of immune cells or metabolites is essential to portray the pathology. Dynamic models of arthritis have also been developed using bioreactors [84] and microfluidics [85],[86].

Ossendorff *et al.* used a bioreactor with mechanical stimuli to promote ex vivo culture of an explant to investigate the mechanisms behind the 20% failure rate [87] of autologous chondrocyte transplantation due to posterior arthritic-like symptoms. To do so, the authors used fibrin-polyurethane scaffolds where bovine chondrocytes were seeded and cultured for 2 weeks, with permanent 10 to 20% compression and ±25° of strain as a biomimetic multiaxial load. To promote an arthritis-like phenotype, tumor necrosis factor α (TNF-α) was added to the medium at a concentration of 20 ng/ml since it is a cytokine known to play a role in osteoarthritis [88]. Moreover, to assess the effect of the pharmaceutical sequestration of this cytokine and as a proof-of-concept of the use of this platform for drug testing, the monoclonal antibody anti-TNF-α adalimumab was also supplemented to the medium at a concentration of 10 μg/L. It was concluded that inflammation emulating cytokine leads to a chondrocytes' dedifferentiation observed particularly by the reduction in the cell-specific production of collagen type-II and production of MMP-3. Despite inducing chondrogenesis, mechanical stimulation was insufficient to stop the inflammation-induced cartilage degradation. At the concentration used, the antibody antagonized TNF-α completely, impairing the degradation of the chondrocyte deposited matrix. These results assist in the comprehension of the effects of soluble cytokines in the degradation of cartilage,

hint towards a possible attenuation but not definitive treatment of physical therapy, and point out a possibly effective treatment [84].

Nevertheless, even though it presented extremely promising results in several points, the bioreactor-based approach rarely can be seen as a future cost-effective alternative to animal models. Thus, for that purpose, dynamic arthritic microphysiological models have surfaced in recent years, mostly in the form of microfluidic disease-on-a-chip, corroborating the results achieved in bioreactors.

An example of this corroboration is a microphysiological articular cartilage model with an in-built mechanical stimulation process developed by Barbero *et al.* [86] to better understand how joint overuse is related to the development of arthritis. The platform consisted of a two-chamber microfluidic device separated by a poly(dimethylsulfoxide) (PDMS) membrane where, in an upper chamber, encapsulated human chondrocytes were cultured, and in a lower chamber, air pressure variation is used to compress the upper one. Upon hyperphysiological values of compression, estimated by numerical simulations, and supplementation of Tumor Growth Factor β (TGF-β), 3D cultured chondrocytes expressed arthritis hallmarks. Chondrocytes expressed decreased mRNA levels of collagen type-II when compared to levels of collagen type-I mRNA and increased cytokine mRNA levels upon mechanical stimulation [86]. This model shows that biomimetics can be maintained with a size reduction like the one implied in the bioreactor-to-microfluidics transition.

Other two arthritic microphysiological models were developed recently, mostly with the objective of creating models that could allow further characterization of the *in vitro* development of disease hallmarks upon different stimuli. Rosser *et al.*, [89] using equine chondrocytes, developed a 3D arthritic model within a microfluidic platform that allows the study of the effects of nutrient gradients across the articular cartilage. Arthritis was induced by TNF-α addition to the medium, with the gene expression of arthritis hallmarks being observed 24 hours after induction. This platform has the potential to promote the physiological oxygen gradient previously mentioned as a key feature of articular cartilage, unmodelled until now [89].

Rothbauer *et al.* [85] developed a real-time monitored synovium model in which hyperplasia upon inflammation induction with soluble TNF-α could be observed and measured. This monitoring was performed using light scattering measurements since, upon 3D hyperplasia, rheumatoid arthritis patients-derived synoviocytes promote further light scattering than when cultured without stimulation. The remodeling of the synovium during the progression of the disease is observed *in vitro*, which is

demonstrative of the biomimetics of the approach [85]. Although there are other monitoring techniques that were already applied to bioreactor grown articular cartilage such as, live imaging [90] and ultrasounds-mediated imaging [91], none of these represent a clear advantage regarding microfluidic devices. Due to their minimal size, microfluidic devices are often transparent, meaning that visual observation already allows tissue integrity assessment. Thus, none of these techniques would represent an advantage for microphysiological disease models, unlike light scattering measurements that add quantification capacity. The use of quantitative parameters can assist in the unbiased evaluation of therapeutics tested using this *in vitro* platform.

All of the mentioned models are 3D cultured using biomaterials to support the growth and physiologic biomechanics of tissue cells. For this purpose, these biomaterials are processed into biocompatible hydrogels or scaffolds. Biocompatibility implies biofunctionality, meaning that these biomaterials not only must promote cell viability and growth but also promote tissue-specific phenotype and physiology. Thus, the selection of the biomaterials used is crucial for the development of a representative model.

In the dynamic models here reviewed, there is a wide diversity of biomaterials used as engineered ECM **(Table III-2)**.

Table III-2 - Characterization and application of different biomaterials used in chondrocytes' and synociocytes' dynamic culture systems. PU – Polyurethane.

Biomaterials	Biochemical Recognition Motifs	Type of Dynamic System	Application	References
Alginate	Absent	Bioreactor	Hydrogels for chondrocyte encapsulation inside perfusion systems.	[90], [73], [74]
Poly(caprolactone)		Bioreactor	3D-printed scaffold for healthy knee cartilage modeling. Ensured chondrocyte growth in a mechanically stimulated perfusion bioreactor.	[77]
Agarose		Microfluidics	Hydrogel-based cell encapsulation for pressure-driven mechanical compression in a healthy cartilage model.	[81]
Poly(lactate)		Bioreactor	3D-printed articular carltilage-like scaffold for chondrocyte culture.	[92]
Fribrin-PU	Human fibrin	Bioreactor	Cylindrical PU scaffolds for chondrocyte growth in an inflammated cartilage model.	[84]
Fibrin		Microfluidics	Microfluidically constrained hydrogel for equine chondrocytes' encapsulation.	[89]
Peptide-PEG	Factor XIII glutamine acceptor and Factor XIII lysine donor	Microfluidics	Hydrogels for chondrocyte encapsulation in microfluidic channels for hyperphysiological pressure-driven mechanical compression in a inflammated cartilage model.	[86]

Matrigel®	Collagen type-IV and laminin	Microfludics	Hydrogels for synociocytes' culture in healthy and inflammated perfused microphysiological cartilage model.	[85]

In order to form articular cartilage, chondrocytes were cultured using alginate [73],[90],[74] poly(caprolactone) [77], agarose [81], poly(lactate) [91] in the healthy models and fibrin-polyurethane [84], peptide-functionalized poly(ethyleneglycol) [86] and fibrin [89] for diseased models. Synoviocytes derived from RA patients were also cultured using Matrigel [85], ECM-derived from mouse sarcoma. From these materials, poly(caprolactone) and fibrin-polyurethane were processed as scaffolds whilst the remaining biomaterials were used as hydrogels, with the expected performance thus, showing a versatility of approaches towards successful modeling.

Most of these biomaterials share features that can look contradictory to some principles of cell culture. Something most of them have in common the absence of collagen, the main component of the cartilage's ECM, they have performed as expected, showing a capacity to promote chondrogenesis. Moreover, several of these materials do not possess any binding domains for cell-ECM adhesion proteins. In fact, the only material that has proteins with mammalian adhesion motifs is Matrigel. None of the works reviewed herein, discussed the possible mechanisms of action of these biomaterials nor measured the biomechanical properties of the resulting gels [93].

This discussion is largely important since the support biomaterial's composition can induce a determined behavior or phenotype on cartilage [94]. Jeong et al. developed the only dynamic model with concerns regarding the mechanical properties of the artificial ECM. This work follows an approach that follows the most recent thinking line in cartilage tissue engineering, extracting information from imaging techniques to develop the scaffold or hydrogel [95]. Nevertheless, the viscoelastic properties of the produced tissue are scarcely discussed and deserve closer attention considering its relevance in tissue's homeostasis [96].

According to Damerau and Gaber [97], the in vitro modeling of RA is a multidisciplinary and multifactorial effort that heavily relies on mechanical stimulation and characterization, mimicry of the immune system's response, and robust biological characterization. Thus, RA specific dynamic models are still missing. Rothbauer et al. [85] developed the microphysiologic platform that more closely resembles a dynamic RA model, to which should be added articular cartilage and pro-inflammation stimulated macrophages. Despite having an innovative real-time characterization system **(Figure III- 4**

a), his platform also needs near-physiological mechanical stimuli, such as the one developed by Paggi et al. [81] (Figure III- 4 b).

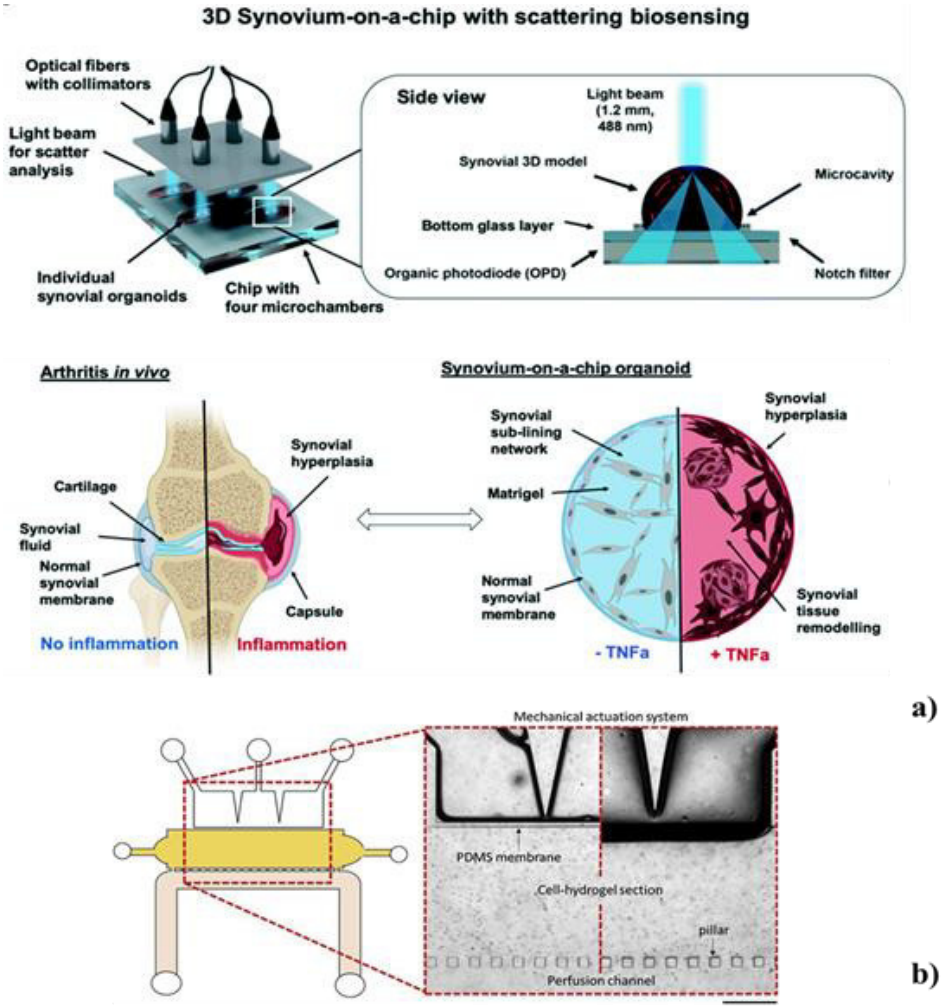

Figure III-4 - a) Characterization and mechanical stimulation methods in-built in microphysiologic healthy and diseased articular models. (a) Microfabricated system for *in vitro* development and monitoring of RA-specific synovial hyperplasia. (b) Device for mechanical compression gradient of a microfluidic hydrogel for articular cartilage mimicking. Figures adapted from (a) Rothbauer *et al.* [85] and from (b) Paggi *et al.* [81].

According to the trend of recent years, these models shall be developed in the near future, allowing to test innovative therapeutics that may improve the prognosis of this life-changing, chronic disease.

III-5. CONCLUSION AND FUTURE PERSPECTIVES

Rheumatoid arthritis is a highly debilitating chronic autoimmune disease that typically causes pain, swelling, and stiffness in the joints. Although there are several treatments that allow an improvement in

the physical condition of patients, most of them are not completely effective and have several serious side effects. Several therapeutic approaches have been developed over the past few years to improve efficacy and decrease side effects caused by drugs. Hydrogels have a unique combination of characteristics, high porosity, biocompatibility, biodegradation, and flexibility make them useful in drug delivery applications. Through the literature review where hydrogels were used to treat rheumatoid arthritis, it was possible to verify that this drug delivery platform was able to potentiate the effect of drugs when compared with traditional drugs, both in vitro and in vivo studies. Recent studies are increasingly focused on the use not only of hydrogels alone but in the combined approach of hydrogels with nanoparticles. This combinatorial approach has been shown to improve the characteristics of hydrogels as a drug delivery system in the treatment of rheumatoid arthritis. Furthermore, there has been an added concern with the method of administering hydrogels, that is, being minimally invasive. So, injectable hydrogels are emerging as a promising drug delivery platform, including for the treatment of rheumatoid arthritis. Despite the advances reached in the treatment of RA, it is important to fill some gaps namely mimic the dynamic system existing in the human body.

The drug development industry is facing a severe halt, forcing a paradigm change. One of the most blatant reasons for this hampering has been the use of animal experimentation for drug testing. Experts from academia to the industry recognize today that dynamic in vitro human models are the alternative with better prospects since it bypasses several of the problems of animal models. Only recently were developed the first articular cartilage diseased models, resulting in the absence of disease-specific dynamic in vitro models, namely for RA. The early age of articular cartilage modeling leads to the existence of several healthy cartilage models that focus on modeling one specific feature of the human joint's cartilage, like movement, mechanical load, or decreased oxygen concentration. This results in often immature models, where the remaining features often are disregarded, with particular emphasis on the nature and mechanical properties of the engineered ECM. The most complete model of articular cartilage of recent years was a bioreactor-based model, with biomimetic scaffold design, mechanical loading, and synovial fluid circulation developed by Jeong *et al.* [77] . However, is a highly sophisticated technique, where a robotized system is inserted in an incubator with coupled sensors and pumping system, reducing significantly the throughput and the potential for drug screening applications. Regarding this purpose, the systems with higher potential are microphysiological platforms that increase significantly the throughput and monitoring capacity while reduce sample volume, minimizing operation costs. Moreover, these systems were the ones showing more developed in vitro diseased

models of arthritic cartilage, showing disease hallmarks such as ECM degradation and hyperplasia of the synovial membrane.

Considering the current models, diseased articular cartilage models will evolve in the following years for a combination of intensive characterization of the biomaterials, cells, and fluid mechanics employed and biomimetic cellular diversity. Regarding specifically RA, the presence of macrophages undergone pro-inflammatory differentiation and chondrocytes, artificial synovial fluid flow, and hallmarks characterization will be paramount for the achievement of representative models for drug testing purposes.

III-6. ACKNOWLEDGMENTS

The authors thank the financial support under the Norte2020 project (NORTE-08-5369-FSE000044) and the Portuguese Foundation for Science and Technology (FCT) program (PD/BD/143081/2018). IFC thanks the TERM RES-Hub, Tissue Engineering and Regenerative Medicine Infrastructure project, funded by FCT. The FCT distinction attributed to JMO under the Investigator FCT program (number IF/01285/2015) is also greatly acknowledged.

III-7. CONFLICTS OF INTEREST

There are no conflicts to declare.

III-8. REFERENCES

1. Caló, E. and V.V. Khutoryanskiy, *Biomedical applications of hydrogels: A review of patents and commercial products.* European Polymer Journal, 2015. **65**: p. 252-267.
2. Chai, Q., Y. Jiao, and X. Yu, *Hydrogels for biomedical applications: their characteristics and the mechanisms behind them.* Gels, 2017. **3**(1): p. 6.
3. Akhtar, M.F., M. Hanif, and N.M. Ranjha, *Methods of synthesis of hydrogels ... A review.* Saudi Pharmaceutical Journal, 2016. **24**(5): p. 554-559.
4. Ghasemiyeh, P. and S. Mohammadi-Samani, *Hydrogels as Drug Delivery Systems; Pros and Cons.* Trends in Pharmaceutical Sciences, 2019. **5**(1): p. 7-24.
5. Ahmed, E.M., *Hydrogel: Preparation, characterization, and applications: A review.* Journal of Advanced Research, 2015. **6**(2): p. 105-121.

6. Silva, S.S., et al., *Natural-origin materials for tissue engineering and regenerative medicine.* 2017.
7. Mano, J.F., et al., *Natural origin biodegradable systems in tissue engineering and regenerative medicine: present status and some moving trends.* Journal of the Royal Society, Interface, 2007. **4**(17): p. 999-1030.
8. Guo, B. and P.X. Ma, *Synthetic biodegradable functional polymers for tissue engineering: a brief review.* Science China Chemistry, 2014. **57**(4): p. 490-500.
9. Edmondson, R., et al., *Three-dimensional cell culture systems and their applications in drug discovery and cell-based biosensors.* Assay and drug development technologies, 2014. **12**(4): p. 207-218.
10. Chen, F.-M. and X. Liu, *Advancing biomaterials of human origin for tissue engineering.* Progress in polymer science, 2016. **53**: p. 86-168.
11. Urbanczyk, M., S.L. Layland, and K. Schenke-Layland, *The role of extracellular matrix in biomechanics and its impact on bioengineering of cells and 3D tissues.* Matrix Biology, 2020. **85-86**: p. 1-14.
12. Geckil, H., et al., *Engineering hydrogels as extracellular matrix mimics.* Nanomedicine (London, England), 2010. **5**(3): p. 469-484.
13. Lev, R. and D. Seliktar, *Hydrogel biomaterials and their therapeutic potential for muscle injuries and muscular dystrophies.* Journal of the Royal Society, Interface, 2018. **15**(138): p. 20170380.
14. Liaw, C.Y., S. Ji, and M. Guvendiren, *Engineering 3D Hydrogels for Personalized In Vitro Human Tissue Models.* Adv Healthc Mater, 2018. **7**(4).
15. Chuang, E.-Y., et al., *Hydrogels for the application of articular cartilage tissue Engineering: A review of hydrogels.* Advances in Materials Science and Engineering, 2018. **2018**.
16. Roberts, I., *Does animal experimentation inform human healthcare? Observations from a systematic review of international animal experiments on fluid resuscitation.* BMJ, 2002. **324**(7335): p. 474-476.
17. Sandercock, P. and I. Roberts, *Systematic reviews of animal experiments.* The Lancet, 2002. **360**(9333): p. 586-586.
18. Pound, P., et al., *Where is the evidence that animal research benefits humans?* BMJ, 2004. **328**(7438): p. 514-517.
19. Akhtar, A., *The Flaws and Human Harms of Animal Experimentation.* Cambridge Quarterly of Healthcare Ethics, 2015. **24**(4): p. 407-419.
20. Bahadoran, Z., et al., *Importance of Systematic Reviews and Meta-analyses of Animal Studies: Challenges for Animal-to-Human Translation.* Journal of the American Association for Laboratory Animal Science, 2020. **59**(5): p. 469-477.
21. Marx, U., et al., *Biology-inspired microphysiological systems to advance medicines for patient benefit and animal welfare in drug development.* ALTEX, 2020.
22. McNary, S.M., K.A. Athanasiou, and A.H. Reddi, *Engineering lubrication in articular cartilage.* Tissue engineering. Part B, Reviews, 2012. **18**(2): p. 88-100.
23. Klement, B.J. and B.S. Spooner, *Utilization of microgravity bioreactors for differentiation of mammalian skeletal tissue.* Journal of Cellular Biochemistry, 1993. **51**(3): p. 252-256.
24. Freed, L.E., G. Vunjak-Novakovic, and R. Langer, *Cultivation of cell-polymer cartilage implants in bioreactors.* Journal of Cellular Biochemistry, 1993. **51**(3): p. 257-264.
25. Chai, Q., Y. Jiao, and X. Yu, *Hydrogels for Biomedical Applications: Their Characteristics and the Mechanisms behind Them.* Gels (Basel, Switzerland), 2017. **3**(1): p. 6.

26. Li, J. and D.J. Mooney, *Designing hydrogels for controlled drug delivery.* Nature reviews. Materials, 2016. **1**(12): p. 16071.
27. Hoare, T.R. and D.S. Kohane, *Hydrogels in drug delivery: Progress and challenges.* Polymer, 2008. **49**(8): p. 1993-2007.
28. Narayanaswamy, R. and V.P. Torchilin, *Hydrogels and Their Applications in Targeted Drug Delivery.* Molecules (Basel, Switzerland), 2019. **24**(3): p. 603.
29. Slaughter, B.V., et al., *Hydrogels in regenerative medicine.* Advanced materials (Deerfield Beach, Fla.), 2009. **21**(32-33): p. 3307-3329.
30. Mantha, S., et al., *Smart Hydrogels in Tissue Engineering and Regenerative Medicine.* Materials (Basel, Switzerland), 2019. **12**(20): p. 3323.
31. Mantha, S., et al., *Smart hydrogels in tissue engineering and regenerative medicine.* Materials, 2019. **12**(20): p. 3323.
32. Bacelar, A.H., et al., *Smart" hydrogels in tissue engineering and regenerative medicine applications.* Handbook of intelligent scaffolds for tissue engineering and regenerative medicine, 2017. **2**: p. 327-361.
33. Li, X. and X. Su, *Multifunctional smart hydrogels: potential in tissue engineering and cancer therapy.* Journal of Materials Chemistry B, 2018. **6**(29): p. 4714-4730.
34. Sosnik, A. and K.P. Seremeta, *Polymeric Hydrogels as Technology Platform for Drug Delivery Applications.* Gels (Basel, Switzerland), 2017. **3**(3): p. 25.
35. Lee, J.H., *Injectable hydrogels delivering therapeutic agents for disease treatment and tissue engineering.* Biomaterials research, 2018. **22**: p. 27-27.
36. Sun, Y., et al., *Recent advances of injectable hydrogels for drug delivery and tissue engineering applications.* Polymer Testing, 2020. **81**: p. 106283.
37. Moura, M.J., et al., *In situ forming chitosan hydrogels prepared via ionic/covalent co-cross-linking.* Biomacromolecules, 2011. **12**(9): p. 3275-3284.
38. Zhu, J. and R.E. Marchant, *Design properties of hydrogel tissue-engineering scaffolds.* Expert review of medical devices, 2011. **8**(5): p. 607-626.
39. Jeon, O., et al., *Mechanical properties and degradation behaviors of hyaluronic acid hydrogels cross-linked at various cross-linking densities.* Carbohydrate polymers, 2007. **70**(3): p. 251-257.
40. Huang, T., et al., *A novel hydrogel with high mechanical strength: a macromolecular microsphere composite hydrogel.* Advanced Materials, 2007. **19**(12): p. 1622-1626.
41. Song, F., et al., *Nanocomposite hydrogels and their applications in drug delivery and tissue engineering.* Journal of biomedical nanotechnology, 2015. **11**(1): p. 40-52.
42. Schexnailder, P. and G. Schmidt, *Nanocomposite polymer hydrogels.* Colloid and Polymer Science, 2009. **287**(1): p. 1-11.
43. Chen, T., et al., *Nanoparticle–polymer synergies in nanocomposite hydrogels: from design to application.* Macromolecular Rapid Communications, 2018. **39**(21): p. 1800337.
44. Wahid, F., et al., *Nanocomposite hydrogels as multifunctional systems for biomedical applications: Current state and perspectives.* Composites Part B: Engineering, 2020: p. 108208.
45. Dannert, C., B.T. Stokke, and R.S. Dias, *Nanoparticle-Hydrogel Composites: From Molecular Interactions to Macroscopic Behavior.* Polymers, 2019. **11**(2): p. 275.
46. Motealleh, A. and N.S. Kehr, *Nanocomposite hydrogels and their applications in tissue engineering.* Advanced healthcare materials, 2017. **6**(1): p. 1600938.

47. Kehr, N.S., S. Atay, and B. Ergün, *Self‐assembled monolayers and nanocomposite hydrogels of functional nanomaterials for tissue engineering applications.* Macromolecular bioscience, 2015. **15**(4): p. 445-463.
48. Merino, S., et al., *Nanocomposite hydrogels: 3D polymer–nanoparticle synergies for on-demand drug delivery.* ACS nano, 2015. **9**(5): p. 4686-4697.
49. Anaya, J.-M., et al., *Autoimmunity: from bench to bedside*. 2013: El Rosario University Press.
50. Guo, Q., et al., *Rheumatoid arthritis: pathological mechanisms and modern pharmacologic therapies.* Bone research, 2018. **6**: p. 15-15.
51. Bullock, J., et al., *Rheumatoid Arthritis: A Brief Overview of the Treatment.* Medical principles and practice : international journal of the Kuwait University, Health Science Centre, 2018. **27**(6): p. 501-507.
52. Wen, H., H. Jung, and X. Li, *Drug Delivery Approaches in Addressing Clinical Pharmacology-Related Issues: Opportunities and Challenges.* The AAPS journal, 2015. **17**(6): p. 1327-1340.
53. Sharpe, L.A., et al., *Therapeutic applications of hydrogels in oral drug delivery.* Expert opinion on drug delivery, 2014. **11**(6): p. 901-915.
54. Quan, L.-D., et al., *The Development of Novel Therapies for Rheumatoid Arthritis.* Expert opinion on therapeutic patents, 2008. **18**(7): p. 723-738.
55. Qi, X., et al., *Intra-articular Administration of Chitosan Thermosensitive In Situ Hydrogels Combined With Diclofenac Sodium-Loaded Alginate Microspheres.* J Pharm Sci, 2016. **105**(1): p. 122-30.
56. Dong, L., et al., *Spleen-specific suppression of TNF-alpha by cationic hydrogel-delivered antisense nucleotides for the prevention of arthritis in animal models.* Biomaterials, 2009. **30**(26): p. 4416-26.
57. Liu, H., et al., *Hydrogel is Superior to Fibrin Gel as Matrix of Stem Cells in Alleviating Antigen-Induced Arthritis.* Polymers (Basel), 2016. **8**(5).
58. Vemula, P.K., et al., *On-demand drug delivery from self-assembled nanofibrous gels: a new approach for treatment of proteolytic disease.* J Biomed Mater Res A, 2011. **97**(2): p. 103-10.
59. Goindi, S., M. Narula, and A. Kalra, *Microemulsion-Based Topical Hydrogels of Tenoxicam for Treatment of Arthritis.* AAPS PharmSciTech, 2016. **17**(3): p. 597-606.
60. Garg, N.K., et al., *Nanostructured lipid carrier mediates effective delivery of methotrexate to induce apoptosis of rheumatoid arthritis via NF-κB and FOXO1.* Int J Pharm, 2016. **499**(1-2): p. 301-320.
61. Garg, N.K., et al., *Effective transdermal delivery of methotrexate through nanostructured lipid carriers in an experimentally induced arthritis model.* Colloids Surf B Biointerfaces, 2016. **147**: p. 17-24.
62. Sallam, M.A., A.M. Motawaa, and S.M. Mortada, *An insight on human skin penetration of diflunisal: lipogel versus hydrogel microemulsion.* Drug Dev Ind Pharm, 2015. **41**(1): p. 141-7.
63. Joshi, N., et al., *Towards an arthritis flare-responsive drug delivery system.* Nat Commun, 2018. **9**(1): p. 1275.
64. Ghosh, S., et al., *Methotrexate Aspasomes Against Rheumatoid Arthritis: Optimized Hydrogel Loaded Liposomal Formulation with In Vivo Evaluation in Wistar Rats.* AAPS PharmSciTech, 2018. **19**(3): p. 1320-1336.
65. Cokelaere, S.M., et al., *Sustained intra-articular release of celecoxib in an equine repeated LPS synovitis model.* Eur J Pharm Biopharm, 2018. **128**: p. 327-336.
66. Yeo, J., et al., *Nitric Oxide-Scavenging Nanogel for Treating Rheumatoid Arthritis.* Nano Lett, 2019. **19**(10): p. 6716-6724.

67. Wang, Q.S., et al., *Dexamethasone-Loaded Thermosensitive Hydrogel Suppresses Inflammation and Pain in Collagen-Induced Arthritis Rats.* Drug Des Devel Ther, 2020. **14**: p. 4101-4113.
68. KÜÇÜKTÜRKMEN, B., Ö. Umut Can, and A. Bozkir, *In situ hydrogel formulation for intra-articular application of diclofenac sodium-loaded polymeric nanoparticles.* Turkish Journal of Pharmaceutical Sciences, 2017. **14**(1): p. 56.
69. Ma, Z., et al., *In Situ Forming Injectable Hydrogel For Encapsulation Of Nanoiguratimod And Sustained Release Of Therapeutics.* International journal of nanomedicine, 2019. **14**: p. 8725-8738.
70. Köhler, B.M., et al., *Current Therapeutic Options in the Treatment of Rheumatoid Arthritis.* Journal of clinical medicine, 2019. **8**(7): p. 938.
71. Zhou, S., Z. Cui, and J.P.G. Urban, *Factors influencing the oxygen concentration gradient from the synovial surface of articular cartilage to the cartilage-bone interface: A modeling study.* Arthritis & Rheumatism, 2004. **50**(12): p. 3915-3924.
72. Schipani, E., et al., *Hypoxia in cartilage: HIF-1alpha is essential for chondrocyte growth arrest and survival.* Genes & development, 2001. **15**(21): p. 2865-76.
73. Daly, A.C., B.N. Sathy, and D.J. Kelly, *Engineering large cartilage tissues using dynamic bioreactor culture at defined oxygen conditions.* Journal of Tissue Engineering, 2018. **9**: p. 204173141775371-204173141775371.
74. Jahr, H., et al., *Bioreactor-Controlled Physoxia Regulates TGF-β Signaling to Alter Extracellular Matrix Synthesis by Human Chondrocytes.* International Journal of Molecular Sciences, 2019. **20**(7): p. 1715-1715.
75. Bader, D.L., D.M. Salter, and T.T. Chowdhury, *Biomechanical Influence of Cartilage Homeostasis in Health and Disease.* Arthritis, 2011. **2011**: p. 1-16.
76. Li, K., et al., *Advances in Application of Mechanical Stimuli in Bioreactors for Cartilage Tissue Engineering.* Tissue Engineering Part B: Reviews, 2017. **23**(4): p. 399-411.
77. Jeong, H.-J., et al., *Bioreactor mimicking knee-joint movement for the regeneration of tissue-engineered cartilage.* Journal of Mechanical Science and Technology, 2019. **33**(4): p. 1841-1850.
78. Vonk, L.A., et al., *Mesenchymal Stromal/stem Cell-derived Extracellular Vesicles Promote Human Cartilage Regeneration In Vitro.* Theranostics, 2018. **8**(4): p. 906-920.
79. Zhou, G., et al., *In Vitro Regeneration of Patient-specific Ear-shaped Cartilage and Its First Clinical Application for Auricular Reconstruction.* EBioMedicine, 2018. **28**: p. 287-302.
80. Chen, Y., et al., *Efficient manufacturing of tissue engineered cartilage in vitro by a multiplexed 3D cultured method.* Journal of Materials Chemistry B, 2020. **8**(10): p. 2082-2095.
81. Paggi, C.A., et al., *Monolithic microfluidic platform for exerting gradients of compression on cell-laden hydrogels, and application to a model of the articular cartilage.* Sensors and Actuators B: Chemical, 2020. **315**: p. 127917.
82. Darling, E.M. and K.A. Athanasiou, *Articular Cartilage Bioreactors and Bioprocesses.* Tissue Engineering, 2003. **9**(1): p. 9-26.
83. Fahy, N., et al., *Immune Modulation to Improve Tissue Engineering Outcomes for Cartilage Repair in the Osteoarthritic Joint.* Tissue Engineering Part B: Reviews, 2015. **21**(1): p. 55-66.
84. Ossendorff, R., et al., *Autologous Chondrocyte Implantation in Osteoarthritic Surroundings: TNF α and Its Inhibition by Adalimumab in a Knee-Specific Bioreactor.* The American Journal of Sports Medicine, 2018. **46**(2): p. 431-440.

85. Rothbauer, M., et al., *Monitoring tissue-level remodelling during inflammatory arthritis using a three-dimensional synovium-on-a-chip with non-invasive light scattering biosensing.* Lab on a Chip, 2020. **20**(8): p. 1461-1471.
86. Occhetta, P., et al., *Hyperphysiological compression of articular cartilage induces an osteoarthritic phenotype in a cartilage-on-a-chip model.* Nature Biomedical Engineering, 2019. **3**(7): p. 545-557.
87. Pareek, A., et al., *Long-Term Outcomes after Autologous Chondrocyte Implantation.* CARTILAGE, 2016. **7**(4): p. 298-308.
88. Stannus, O., et al., *Circulating levels of IL-6 and TNF-α are associated with knee radiographic osteoarthritis and knee cartilage loss in older adults.* Osteoarthritis and Cartilage, 2010. **18**(11): p. 1441-1447.
89. Rosser, J., et al., *Microfluidic nutrient gradient–based three-dimensional chondrocyte culture-on-a-chip as an in vitro equine arthritis model.* Materials Today Bio, 2019. **4**: p. 100023-100023.
90. Bar, A., E. Ruvinov, and S. Cohen, *Live imaging flow bioreactor for the simulation of articular cartilage regeneration after treatment with bioactive hydrogel.* Biotechnology and Bioengineering, 2018. **115**(9): p. 2205-2216.
91. Melchor, J., et al., *In-bioreactor ultrasonic monitoring of 3D culture human engineered cartilage.* Sensors and Actuators B: Chemical, 2018. **266**: p. 841-852.
92. Melchor, J., et al., *In-bioreactor ultrasonic monitoring of 3D culture human engineered cartilage.* Sensors and Actuators B: Chemical, 2018. **266**: p. 841-852.
93. Kleinman, H.K. and G.R. Martin, *Matrigel: Basement membrane matrix with biological activity.* Seminars in Cancer Biology, 2005. **15**(5): p. 378-386.
94. Cheng, G., et al., *Advanced Silk Fibroin Biomaterials for Cartilage Regeneration.* ACS Biomaterials Science & Engineering, 2018. **4**(8): p. 2704-2715.
95. Armiento, A.R., et al., *Biomaterials for articular cartilage tissue engineering: Learning from biology.* Acta Biomaterialia, 2018. **65**: p. 1-20.
96. Guimarães, C.F., et al., *The stiffness of living tissues and its implications for tissue engineering.* Nature Reviews Materials, 2020. **5**(5): p. 351-370.
97. Damerau, A. and T. Gaber, *Modeling Rheumatoid Arthritis In Vitro: From Experimental Feasibility to Physiological Proximity.* International Journal of Molecular Sciences, 2020. **21**(21): p. 7916-7916.

SECTION 2

MATERIAL AND METHODS

Chapter IV

Materials and methods

Chapter IV

Materials and Methods

Overview

This chapter provides a detailed overview of the different materials and methodologies that were used for the works presented in the following sections of this thesis. A description of the main polymers used can be found in the first part of this section, followed the methods used for nanoparticles and hydrogels production and physicochemical characterization. Moreover, biological characterization, static and dynamic conditions using bioreactors and microchips will be described to better understand the proposed methodologies.

IV-1. MATERIAL AND METHODS

The several biomaterials used in this thesis are demonstrated in the following sub-sections, detailing its main properties and methods of production used.

IV-1.1.Polyamidoamine (PAMAM) dendrimers

Dendrimers are a class of polymeric compounds that have a globular and hyperbranched structure, precise molecular weight, high surface functionality, and degree of versatility. These characteristics differentiate them as optimum and unique nanocarriers in medical applications such as tumor therapy, drug delivery, diagnostics, and gene transfection [1].

Polyamidoamine (PAMAM) dendrimer was the first dendrimer that was synthetized and commercialized, and it is the most well-studied and characterized class of dendrimers [2]. The PAMAM dendrimer core can be composed of linear chain molecules containing primary amines **(Figure IV-1)**. The most common compounds are ethylenediamine (EDA, four core multiplicity), ammonia (three core multiplicity), or cystamine (four core multiplicity). There are two methods for dendrimer synthesis, such as, divergent and convergent [3]. PAMAM dendrimer is generally synthesized by the divergent approach. In the divergent method, the construction of the dendrimer occurs in a stepwise manner starting from the core and building up the molecule toward the periphery via the coupling of the monomer and de-protection or transformation of the monomer end-group to produce a new reactive surface functionality [4]. The high density of functional groups (-NH_2-COOH, OH) in PAMAM dendrimer can have potential applications in increasing the solubility of low aqueous solubility drugs and delivery systems for bioactive materials [5]. Drugs or other molecules can be encapsulated in the macromolecule interior or be attached to PAMAM end groups make them suitable for drug delivery systems [6]. Furthermore, there are studies that show the anti-inflammatory properties of dendrimers [7,8 ,9] what are beneficial characteristics for the purpose of the study.

Due to previously mentioned advantages, the PAMAM dendrimer was used as a drug delivery system, in **Chapter V**, **VIII,** and **IX**.

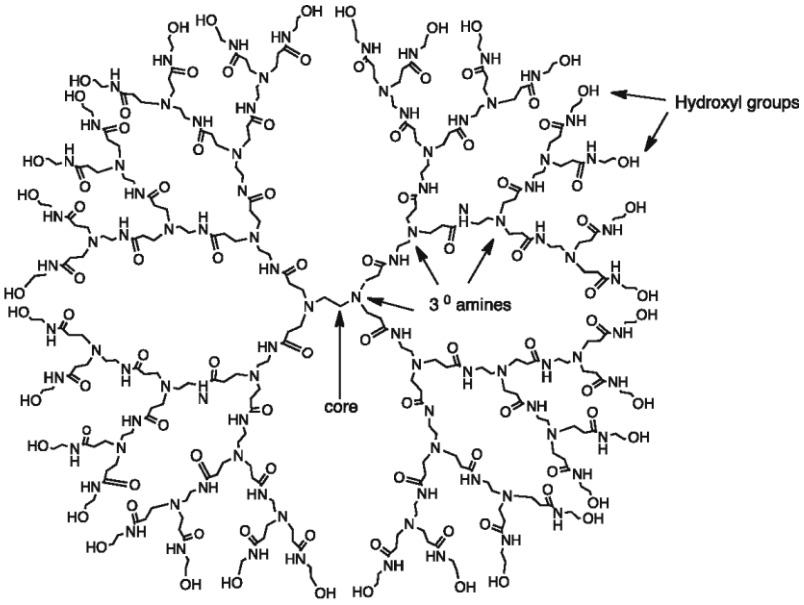

Figure IV-1 - Structure of Polyamidoamine (PAMAM) dendrimers. Reprinted with permission from [10].

IV-1.2. Chondroitin sulfate (CS)

Chondroitin sulfate is a type of sulfated glycosaminoglycan (GAG) that is a linear polysaccharide composed of repeating units of D-glucuronic (GlcA) and N-acetylgalactosamine (GalNAc) linked together through alternating β -1-3 and β -1-4 glycosidic bond. The resulting [(-4GlcA β 1-3GalNAc β 1-)$_n$] disaccharide repeating unit can be sulfated through the activity of a variety of sulfotransferases resulting in chains decorated with O-sulfo groups at various positions [11],[12]. Chondroitin sulfates are classified as CS-O,A,B,C,D,E,F,K (CS-A, chondroitin sulfate A,[GlcA β 1-3GalNAc(4 S)]; CS-C, chondroitin sulfate C, [GlcA β 1-3GalNAc(6 S)]; CS-D, chondroitin sulfate D,[GlcA(2 S) β 1-3GalNAc(6 S)]; CS-E, chondroitin sulfate E, ,[GlcA β 1-3GalNAc(4 S,6 S)]; CS-F, fucosylated chondroitin sulphate, [GlcA(α 1-3Fuc) β 1-3GalNAc(4S)]; CS-O, chondroitin,[GlcA β 1-3GalNAc]) according to their sulfation pattern, and CSs extracted from animal sources (human, pig, shark, squid) are often a combination of the different types **(Figure IV-2)** [13]. The CS repeating disaccharide unit [(-4GlcA β 1-3GalNAc β 1-)$_n$] is frequently sulfated at the C-4 and/or C-6 positions of GalNAc in CS from mammals' sources. The terms CS-A and CS-C have been used to describe CS rich in GlcA-GalNAc (4S) (A-unit) and in GlcA-GalNAc (6S) (C-unit), respectively, where 4S and 6S stand for 4- O-sulfate and 6-O-sulfate. Additionally, nonsulfated GlcA-GalNAc (O-unit) and theraredisulfated D-unit [GlcA(2S)-GalNAc(6S)] (2S stands for 2-O-sulfate) and E-unit [GlcA-GalNAc (4S, 6S)] also are often found in small proportions in mammals. Structural studies of

CS from terrestrial animals have shown great heterogeneity however this diversity is more diverse in marine species. Trisulfated (T-unit) and disulfated disaccharide units, such as D, E, and K, are found in oversulfated CS chains such as CS-D, CS-E, and CS-K, which are derived from cartilage of squid, king crab and shark fin, squid [14], [15].

Natural chondroitin sulfate has a molecular weight of 50-100kDa. It is a main component of the extracellular matrix (ECM) and cell surfaces of many connective tissues, including skin, ligaments, tendons, cartilage and bone, [16]. CS chains are covalently bound to a core protein to form CS proteoglycans (CSPGs), where at least one CS side chain is covalently attached to the panel of core proteins (xylose, galactose, GlcA). The assembly of the CS chain occurs in the endoplasmic reticulum/ Golgi compartment [17]. CSPGs present a wide range of functional events as interactions with several bioactive protein components including cell adhesion molecules, growth factors, morphogens, and cytokines [18],[19]. Furthermore, CSPGs have been implicated in diverse pathological processes such as skeletal disorders, glial scar formation after brain injury, and infections with viruses and bacteria. CS is responsible for many of the important biomechanical properties of cartilage, such as resistance and elasticity. Its high content in the aggrecan plays the main role in consenting cartilage to resist pressure stresses during several loading conditions [16],[20].

Changes in the levels or molecular nature of CS have been found in synovial fluid and cartilage of RA patients. Several *in vitro* and *in vivo* studies have shown that chondroprotective properties of CS result from an increase in the biosynthesis of connective tissue components (collagen, proteoglycans, and hyaluronan) and possess anti-inflammatory activity. Furthermore, GAG structure and sulfation pattern can influence interactions between the surface of cells and adhering microbes or other pathogenic agents, with interesting implications for the development of therapeutics [21], [22]. Therefore, in this thesis, Chondroitin sulfate A sodium salt from bovine trachea was chosen as the material to surface modify the PAMAM dendrimers, in **Chapter V**, due to the previously highlighted advantages.

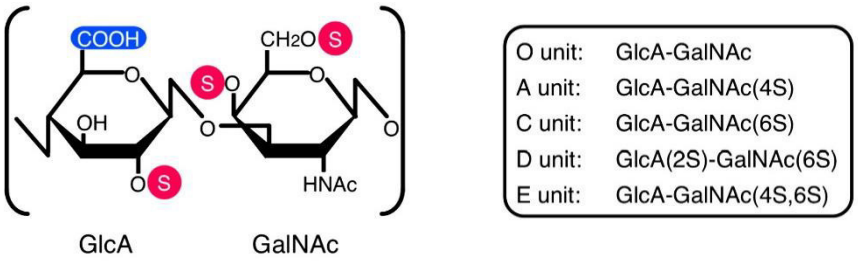

Figure IV-2 - Chemical structure and distribution of sulfation pattern of chondroitin sulfate (CS). Reprinted with permission from [17].

IV-1.3. Gellan Gum (GG)

Gellan gum is a water-soluble extracellular polysaccharide produced by the aerobic fermentation process of *Sphingomonas elodea.* It is an anionic linear polymer composed of repeating units of a tetrasaccharide [D-glucose(β1→4) D-glucuronic acid(β1→4)D-glucose(β1→4)-L-rhamnose(α1→3)]$_n$ [23],[24]. Two acyl substituents, L-glyceryl, and acetyl are present at the O-3- linked glucose at the O-2 and O-6 positions, respectively [25]. According to the degree of acyl substitution, GG can be categorized as acetylated form, high acyl (HA) GG and deacetylated form, low acyl (LA) GG **(Figure IV-3)**, being the low acyl form the most common and commercially available one [26]. Both forms of GG present heat reversible transition from a state of single random macromolecules to a more ordered state with excellent stability and high gel strength [27]. Acyl substituents in GG affect the aggregation process and the GG characteristics mostly depend on the degree of acylation and the presence of counter-ions. The HA GG form produces transparent, soft, elastic, and flexible gels that are resistant to heat and acid, while the LA GG form produces firm, non-elastic brittle gels in the presence of cations [28]. This leads to producing gels with a variety of textures, water content, and mechanical properties, and to be tuned according to the desired application [29].

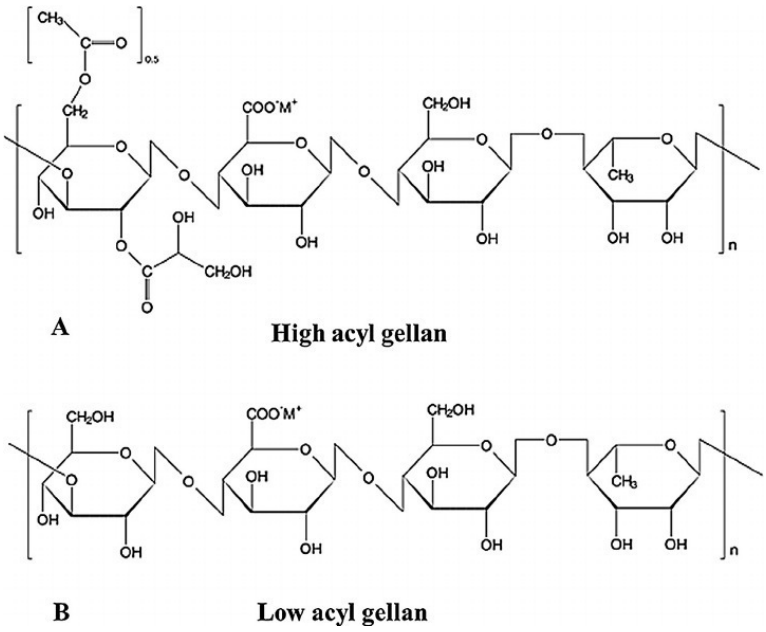

Figure IV-3 - Chemical structure of Gellan Gum (A) high acyl Gellan Gum (B) low acyl Gellan Gum. Reprinted with permission from [30].

The versatile properties of GG help in different Tissue Engineering and regenerative medicine applications. The GG is used in the pharmaceutical and biomedical fields, including for cell adhesion, gene therapy, wound healing, bone regeneration, biological signaling, as protein carriers, and delivery agents [31],[32]. The main attractive properties of GG that make it a suitable material for TE include its biocompatibility, biodegradability, structural similarities with native glycosaminoglycans, tunable mechanical properties, and ease to functionalize [33].

The GG hydrogels can be used as a sustained and controlled drug release system [34]. These hydrogels are formed by physical crosslinking methods induced by temperature variation, pH, and ionic conditions. However, in physiological conditions, GG hydrogels can become weak. The properties of GG can be improved by chemical crosslinking allowing that the hydrogels have greater mechanical strength, integrity, and swelling properties tuned by the degree of chemical crosslinking [35]. Due to previously mentioned advantages, in **Chapter VI**, **VII, VIII,** and **IX** the Gellan Gum was studied to be used as injectable hydrogel to drug delivery.

IV-1.4. Tyramine (Ty)

Tyramine (2-(4-Hydroxyphenyl)ethylamine, 4-(2-Aminoethyl)phenol, or 4-Hydroxyphenethylamine) is a primary amino compound, with molecular weight 137.18 g/mol obtained by formal decarboxylation of

the amino acid tyrosine by the action of the ubiquitous enzyme aromatic amino acid decarboxylase **(Figure IV-4)** [36]. Tyramine is a substance widely found in the body and in several foodstuffs, most particularly aged and fermented foods and beverages. Cheeses, fruits, fish, dried, and fermented meat, and wine are known to contain tyramine [37]. It is an amino acid that helps regulate blood pressure. Because of its high sensitivity to oxidation by monoamine oxidase inhibitors, tyramine's endogenous levels are very low, and tyramine is one of a group of biogenic amines which are referred to as "trace amines" [38]. Tyramine is widely used in the preparation of a variety of hydrogels for biomedical applications. In the last years, in situ gelling systems, also gelled via physical interactions or chemical reactions, have been designed [39]. Enzymatic crosslinking of polymer–phenol conjugates in the presence of horseradish peroxidase (HRP) and hydrogen peroxide (H_2O_2) has emerged as an important method to produce in situ-forming, injectable hydrogels [40]. Several groups described the *in situ* formation of hydrogels through the functionalization of polymers with tyramine [41],[42],[43]. The hydrogels are chemically crosslinked and therefore show superior characteristics in terms of stability and mechanical resistance when compared to physically crosslinked. Furthermore, this approach allows for independent tuning of gelation rate and the mechanical strength of the resulting gels, been widely used in tissue engineering, cell immobilization, and drug delivery[44]. Because of the previously mentioned advantages, tyramine was used to functionalize the Gelan Gum, in **Chapter VI**, and thus become able to undergo enzymatic crosslinking.

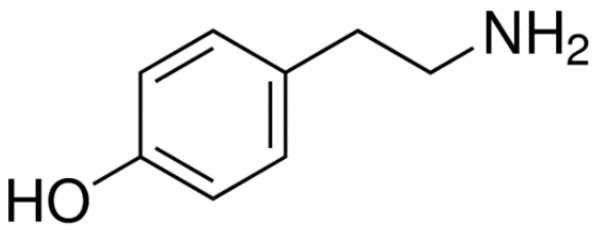

Figure IV-4 - Chemical structure of tyramine (Ty).

IV-1.5. Silk fibroin (SF)

Silk fibroin (SF) is a highly insoluble fibrous protein that can be obtained from the glands of different animals such as spiders, silkworms, scorpions, mites, and flies [45]. Bombyx mori (B. mori) domestic silkworms are the main producer of silk worldwide [46]. The SF protein obtained from

silkworm silk is a well-characterized protein employed in numerous biomedical applications due to superior biocompatibility, controllable biodegradation, suitable mechanical properties, and versatile functionalization. So, Bombyx mori silkworm cocoons were used in this thesis as a source of SF [47].

The natural silkworm is comprised of two structural proteins, fibroin (72-81%) and sericin (19-28%). Fibroin is in the inner core and provides mechanical strength, while sericin is a water-soluble glue-like protein that acts as an adhesive binder to preserve the structural integrity of the fibers [48]. Silk fibroin contains polypeptide chains with a molecular weight in the range of 200-350 kDa and its primary structure comprises of hydrophilic light chains (L-chain, M_w = 27.7 kDa) with terminal C and N groups and repetitive blocks of hydrophobic heavy chains (H-chain, Mw = 391.6 kDa) both linked by disulfate bonds [49]. The H-chain consists of 5242 amino acids while the L-chain consists of 246 amino acids. The L-chain domain comprises amino acid sequences, Alanine (Ala), Serine (Ser), Glycine (Gly), and acetylated N-terminal Ser residues. The H-chain contains Gly, Ala, Ser, Tyrosine (Tyr), and Valine (Val). The amino acid sequence of H-fibroin can be defined as $(–Gly–Ser–Gly–Ala–Gly–Ala–)_n$ **(Figure IV-5)**. Hydrophobic H-fibroin chains contain repetitive hydrophobic domains interspersed between non-repetitive hydrophilic domains [50].

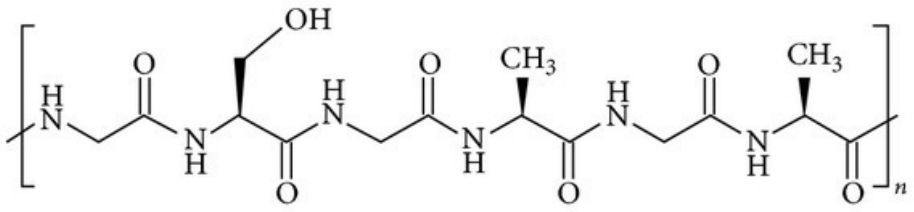

Figure IV-5 - Chemical structure of Silk fibroin (SF). Reprinted with permission from [51].

The secondary structure of silk can be classified into three crystalline forms: Silk I, Silk II, and Silk III. Silk I is the liquid, metastable form of SF and has been designated as a partial and order structure that could contain α-helix and random coil structures. Silk II is the solid SF that features β-sheet crystalline structure and silk III is a solid form of SF that presents mostly trifold helical chain conformation that is found at the air/water interface [52]. The repetitive hydrophobic amino acid domains of H-chain through hydrogen bonds, Van der Walls forces, and hydrophobic interactions allow the transition from the random coil and alpha-helix conformations to stable anti-parallel β-sheet crystallites. This conformation confers excellent mechanical strength to the silk network [50].

Silk fibroin fiber can be obtained from degummed silk, which refers to the partial or complete removal of the sericin. The removal of sericin is an important step to prevent the thrombogenic and inflammatory response of SF. The SF can be dissolved with neutral salt solutions such as lithium bromide and the mixture is dialyzed to get pure fibroin solution [53]. Through various external stimuli such as temperature, pH, ionic strength, etc., the SF can be used to prepare silk fibroin membranes, fiber, hydrogel, scaffolds, and other types of materials [54]. The processing step used to prepare the SF material can affect the chemical and molecular structure of the SF protein itself and thus modify the material's mechanical properties, biocompatibility, degradability, and reproducibility, affecting its performance as a biomaterial [55].

The SF has several unique properties which makes it a desirable biomaterial for tissue engineering and regenerative medicine [56]. Silk fibroin (SF) has been extensively used to produce injectable hydrogels as drug delivery systems due to its biocompatibility, controllable degradability, and tunable drug release properties. SF-based drug delivery systems can load and stabilize several small molecule drugs enhance their half- lives and control the release to increase their circulation time in the blood and thus the duration of action [57]. Silk fibroin hydrogels are formed in a sol-gel transition through physical or chemical procedures [58]. The enzymatically crosslinking of SF using the enzyme horseradish peroxidase to produce injectable hydrogels can offer distinctive advantages, including significantly shorter gelation time and enhanced mechanical properties of hydrogels [59]. Natural biomaterials can offer superior biocompatibility compared with synthetic degradable materials. However, natural biomaterials frequently lack the necessary control of properties and material properties needed for long-term sustained release applications [60].

So, in this thesis, SF was combined to Ty-GG, to increase the mechanical stability, biocompatibility and enhance the effect as a drug delivery system.

Silk fibroin was obtained from *Bombyx mori* silk cocoons that were purified and posteriorly dissolved in a lithium bromide solution to produce SF-based hydrogels. The cocoons were supplied by Rural Development Administration, Jeonju, Korea, and the Portuguese Association of Parents and Friends of Mentally Disabled Citizens, Castelo Branco, Portugal. SF was used in **Chapters VII** and **VIII** of the thesis.

IV-1.6. Matrigel®

Matrigel® is a soluble extract of basement membrane proteins derived from the Engelbreth-Holm-Swarm mouse (EHS) tumor **(Figure IV-6)** [61], crosslinkable into a 3D gel at 37 °C, cable to help cell morphogenesis and differentiation [62]. The basement membrane is structurally a thin layer of ECM sheets which contact with basal layer of epithelial cells, endothelial cells, and fat and smooth muscle cells [63]. Matrigel® comprises mainly of collagen type IV, perlecan (heparan sulfate proteoglycan), entactin, and laminin. It also contains other components of the basement membrane, such as growth factors and proteases. This laminin-rich mixture of Matrigel® is similar to the complex extracellular environment of the basement membrane and is used for cell-culturing model systems, mostly for evaluating cellular differentiation and angiogenesis [64].

Matrigel 3D tissue culturing systems are gaining increase approval because of their capability to offer a more physiologically relevant cell environment [65]. Approaches for culturing mammalian cells *ex vivo* are extremely needed to study cell and tissue physiology and to grow replacement tissue for regenerative medicine. Two-dimensional culture has been the standard for *in vitro* cell culture, nevertheless, it has been shown that cells behave more natively when cultured in three-dimensional environments [66]. The *in vivo* and *in vitro* extracellular matrix (ECM) plays a key role in many outcomes that direct cell fate and behavior. The key function of the ECM is to sustenance the maintenance and growth of a diversity of cells. In this sense, Matrigel® acts as a physical support or substrate for cultured cells helping to create more in vivo-like extracellular matrices that promote cell differentiation [67].

Due to previously mentioned advantages, in **Chapter IX**, Matrigel® was used to encapsulate human monocytic cell line (THP-1) and primary human chondrocyte cells in 3D culture on a microfluid chip in order to mimic an inflammatory environment *in vivo*.

Figure IV-6 - Matrigel®.

IV-2. REAGENTS

Unless addressed otherwise, all the reagents used in this thesis were purchased from Sigma-Aldrich, USA.

IV-3. METHODOLOGIES FOR PROCESSING OF BIOMATERIALS

Biomaterials processing plays a vital role in Tissue Engineering (TE) strategies. The different approaches are planned to influence the physical, chemical, and biological environment surrounding the target tissue. The processing method is the crucial factor that generally contributes to influence all the criterion that will control its behavior *in vitro* and *in vivo* [68], [69].

In this sub-section the preparation methods of different biomaterials to produce freeze-dried nanoparticles and hydrogels will be described in greater detail.

IV-3.1. Chondroitin Sulfate poly(amidoamine) dendrimer (CS/PAMAM) nanoparticles production

In this thesis, PAMAM dendrimers were functionalized with CS to increase receptor-ligand interaction since this glycosaminoglycan is an important component of the ECM and cell surface of the cartilage. Furthermore, CS has anti-inflammatory activity, which is beneficial for the goal of the approach.

For the synthesis of the CS/PAMAM dendrimer nanoparticles, Starburst® poly(amidoamine)-carboxylic terminated dendrimers, PAMAM-CT (G1.5, 20% (w/v) in methanol) with an ethylenediamine core (2934.56 g/mol) and Chondroitin sulphate A sodium salt from bovine trachea (463.363 g/mol) were purchased from Sigma-Aldrich (USA). CS/PAMAM dendrimer NPs were prepared as referred by Shaunak et al., 2004 [70], with some modifications. The PAMAM dendrimer G1.5 that has 16 carboxylic acid end groups was conjugated with CS, according to the following steps: First 20 g mol^{-1} of MES (Sigma-Aldrich, USA) was added to 50 g L^{-1} of PAMAM (diluted in MES (2-(N-morpholino)ethanesulfonic acid), then N-(3-Dimethylaminopropyl)-N′-ethylcarbodiimide hydrochloride (EDC) (Sigma-Aldrich, USA) (4 equivalents) and sulfo-NHS (N-Hydroxysulfosuccinimide sodium salt ≥98% (HPLC)) (Sigma-Aldrich, USA) (2 equivalents), in MES were mixed, stirred for 15 minutes, with the first solution of PAMAM in MES. Since the PAMAM dendrimer G1.5 has 16 end groups on the surface, an excess of chondroitin sulfate equivalent was used. That is, then, chondroitin sulfate (20 equivalents) was added with EDC (4 equivalents). Afterwards, the reactions were mixed and stirred for 15 minutes. In the end, PAMAM mixture was added to CS mixture and stirred for 24 hours. The reaction was performed to link the carboxyl group of PAMAM to the chondroitin sulfate amine group **(Figure IV-7)**. The solution was dialyzed against distilled water using a Dialysis Tubing membrane, benzoylated (Laborspirit, Loures), for 48 hours. CS/PAMAM dendrimer NPs were obtained by freezing the solution at -80°C and freeze-drying (Telstar- LyoAlfa 10/15) for approximately 7 days.

The synthesis of CS/PAMAM dendrimer was crucial in this thesis. In **Chapters V, VII,** and **IX** the effect of CS/PAMAM dendrimer on cartilage and immune system cells was analyzed.

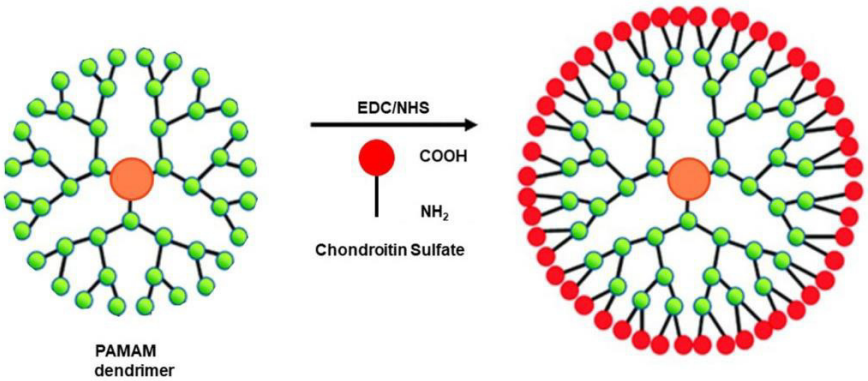

Figure IV-7 - Schematic representation of PAMAM dendrimer nanoparticles functionalized with Chondroitin Sulfate via carbodiimide chemistry.

IV-3.1.1. Labelling of CS/PAMAM dendrimer NPs with fluorescein isothiocyanate (FITC)

Labeling the dendrimer NPs with a fluorescent molecule is of vital importance as a tracking tool to evaluate their internalization by cells in real time. For this, fluorescein isothiocyanate (FITC) was chosen.

Conjugates of FITC-CS/PAMAM dendrimer NPs were prepared by covalently bonding the thiol group of CS/PAMAM dendrimer NPs and the isothyocianate group of FITC, thiourea bond (Sigma-Aldrich, USA). Firstly, 10 mg mL^{-1} of CS/PAMAM solution was prepared in a carbonate-bicarbonate coupled buffer (pH 9.2). Then 50 µL of the FITC (10 mg mL^{-1}) / DMSO (anhydrous dimethyl sulfoxide) solution was added per each mL of CS/PAMAM dendrimer NPs solution under agitation and kept in the dark at 4°C for 8 hours. Lastly, the FITC-labelled CS/PAMAM dendrimer NPs were dialyzed in ultrapure water for 48 hours. The product was achieved after dialysis and freeze-drying.

This process was applied in **Chapter V**.

IV-3.1.2. TNF α Abs linked to CS/PAMAM Dendrimer Nanoparticles

The anti-TNF α was attached to the dendrimer CS/PAMAM to provide anti-inflammatory properties. The CS/PAMAM dendrimer NPs linked to a rabbit polyclonal anti-TNF α antibody (ab7742, Abcam, United Kingdom)/mouse monoclonal anti-TNF α antibody [2C8] (ab8348, Abcam, United Kingdom) was obtained through a crosslinking reaction. A 0.2 g L^{-1} solution of CS/PAMAM in 5 mL MES was mixed with EDC (4 equivalents) and NHS (2 equivalents) for 15 minutes. Next, 20 equivalents of anti-TNF α Abs were added with EDC (4 equivalents) and were stirred for 15 minutes. Then, CS/PAMAM dendrimer NPs mixture was added to anti-TNF α Abs mixture and stirred for 24 hours. The solution was dialyzed against distilled water for 48 hours. Anti-TNF α Abs-CS/ PAMAM dendrimer NPs were obtained through dialysis and freeze-drying.

The linked of CS/PAMAM dendrimer NPs with rabbit polyclonal anti-TNF α antibody was used in **Chapter V** and in **Chapter VIII** and **IX** was used mouse monoclonal anti-TNF α antibody.

IV-3.2. Hydrogels preparation

Hydrogels are three-dimensional polymeric networks that are water-insoluble and absorb substantial amounts of aqueous solutions. Due to their high content, the hydrogels are more identical to natural living tissue than any other type of synthetic biomaterial [71]. The unique physical properties of hydrogels make them appealing for their use in TE applications. The tunable physical properties, controllable degradability, and capability to protect drugs from degradation allow being used as drug delivery platform. The drugs can be slowly released, maintaining a high local concentration of drug in the surrounding tissues over an prolonged period [72].

The gelation of hydrogels is possible by physical or chemical crosslinking methods [73]. The physical crosslinking is generally produced by intermolecular reversible interactions, such as hydrogen bonds, ionic/electrostatic interaction, hydrophilic/hydrophobic interaction, polymerized entanglements etc. However, these interactions are weak while chemical crosslinking creates strong bonds between polymer chains give them higher stability and longer gel duration [74]. Ideal gelation time should be within a few minutes, mainly for drug delivery applications. To reach a faster gelation time, the enzymatic crosslinking methods in TE has been used. The polymers containing phenol groups, aminophenol, tyramine or tyrosine can be crosslinked by the horseradish peroxidase (HRP) and hydrogen peroxide (H_2O_2) [75].

In this sense, it was proposed to modify the GG with Tyramine to be enabled to produce hydrogels via enzymatic crosslinking with HRP, on **Chapter VI**, **VIII** and **IX**. Another purpose was to produce hydrogels with modified GG an SF, which has 5% tyrosine group, to be also crosslinked via HRP and H_2O_2, on **Chapter VII** and **VIII.**

IV-3.2.1. Synthesis of Tyramine-Gellan Gum (Ty-GG)

In this thesis, Gellan Gum was modified with Tyramine to be enabled to produce Ty-GG hydrogels via enzymatic crosslinking with HRP enzyme. As previously mentioned, this process can allow to have a material with adjustable mechanical properties and with short gelation time. These are essential characteristics for the final application of the hydrogel as a drug delivery system in the treatment of RA.

The functionalization of Gellan gum with Tyramine was carried out following the method reported by Prodanović *et al.* [76], with several optimizations. Gellan gum from Gelzan™ CM (Sigma-Aldrich, USA) was dissolved in water at 90°C to a final concentration of 1% (w/v). Sodium (meta)periodate (Sigma-Aldrich, USA) was added to a final concentration of 1 mM in GG at 1% (w/v). The reaction was kept in the dark for 24 hours at 4°C. The reaction was then stopped by adding glycerol (500 mM) and incubated for 30 minutes in the dark at 4°C. The Oxidized GG was precipitated from the reaction mixture by adding NaCl at 1% (w/v) and 2 volumes of 99% (v/v) ethanol. This precipitation step was repeated two times, using the same procedure after dissolving oxidized GG at 1% (w/v) concentration in water. In the end, the precipitate was separated, dried, and dissolved in 0.1 M sodium-phosphate buffer pH 6. When dissolved at 1% (w/v) concentration, tyramine hydrochloride (Sigma-Aldrich, USA) was added by molecular equivalents (number of mol equivalents of GG to number of mol equivalents of Tyramine) and the solution was stirred for half and hour. Then, solid cyanoborohydride was added at 0.5% (w/v) final concentration, and the reaction mixture was left in the dark for 24 hours at 4°C. Modified Gellan Gum was precipitated by adding NaCl to 1 M final concentration and two volumes of 96% (v/v) ethanol. Precipitation was repeated two times using the same procedure after dissolving modified GG at 1% concentration in water. Ty-GG powder **(Figure IV-8)** was obtained by lyophilization, at 0.08 mbar and -77.7°C, during approximately 4 days.

The production of Ty-GG was performed on **Chapter VI**, **VII**, **VIII** and **IX**.

Figure IV-8 - Ty-GG.

IV-3.2.2. Preparation of Silk fibroin solution (SF)

To prepare Silk fibroin (SF), Silkworm cocoons (Rural Development Administration, Jeonju, Korea and Portuguese Association of Parents and Friends of Mentally Disabled Citizens (APPACDM, Castelo Branco, Portugal) were cut into fragments and boiled in 0.02 M Sodium carbonate (Na_2CO_3) solution

(Showa Chemical, Tokyo, Japan) for 30 min to remove sericin. Boiled silkworm cocoons were washed with distilled water three times and dried inside an oven at 70 °C. The dry silkworm cocoons are then dissolved in the oven with 9.3 M LiBr (lithium bromide) (Kanto Chemical, Tokyo, Japan) at 70 °C for 4 hours. The dissolved solution was dialyzed using a SnakeSkin Dialysis Tubing 3500 MWCO (ThermoScientific, Waltham, MA, USA), throughout 48 hours against distilled water, to remove LiBr **(Figure IV-9)**. Silk fibroin was kept at 4 °C until use. The production of SF solution was performed on **Chapter VII** and **VIII**.

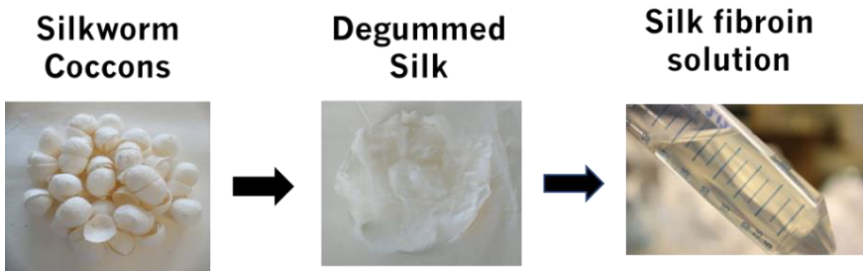

Figure IV-9- Degumming process of Silk fibroin.

IV-3.2.3. Production of Ty-GG hydrogels and Ty-GG/SF hydrogels

Horseradish peroxidase (HRP) solution (0.84 mg mL^{-1}) (Sigma-Aldrich, USA) and hydrogen peroxide solution (H_2O_2) (0.36% (v/v)) (VWR, USA) were both prepared in water. Tyramine-Gellan Gum solution of 1% (w/v) was used for the hydrogel preparation. Tyramine-Gellan gum hydrogels were prepared by mixing of Ty-GG solution with different amounts of HRP and H_2O_2 solutions **(Table IV-1).** Ty-GG hydrogels discs were prepared by adding 200 µL of the mixture solutions in a polypropylene mold at 37°C. This process was used on **Chapter VI**, **VIII** and **IX.**

Table IV-1 - Ty-GG conditions (C1, C2 and C3) with different amounts of HRP and H_2O_2 solutions.

	Ty-GG	HRP	H_2O_2
C1	167 µL	16.6 µL	10.83 µL
C2	167 µL	18.3 µL	15 µL
C3	167 µL	20 µL	13.3 µL

Tyramine-Gellan Gum/SF hydrogels **(Figure IV-10 b)** were prepared by mixing 1% (w/v) of Ty-GG and 2% (w/v) SF (1:1) solution with same amounts of HRP and H_2O_2 solutions previously mentioned **(Table IV-2)**. This method was performed on **Chapters VII** and **VIII**.

Table IV-2 - Ty-GG/SF conditions (C1, C2 and C3) with different amounts of HRP and H_2O_2 solutions.

	Ty-GG	SF	HRP	H_2O_2
C1	83.5 µL	83.5 µL	16.6 µL	10.83 µL
C2	83.5 µL	83.5 µL	18.3 µL	15 µL
C3	83.5 µL	83.5 µL	20 µL	13.3 µL

IV-3.2.4. Production of anti-TNF α Ab-CS/PAMAM dendrimer NPs loaded Ty-GG and Ty-GG/SF hydrogels

In **Chapter VIII**, to prepare the hydrogels, first a solution of horseradish peroxidase (HRP) (0.84 mg mL^{-1}) (Sigma-Aldrich, USA) in PBS, and a solution of hydrogen peroxide (H_2O_2) (0.36% (v/v)) (VWR, USA) in distilled water were prepared. Then, 1% Ty-GG solution (w/v) was prepared in distilled water and used for the preparation of Ty-GG hydrogels and Ty-GG/SF hydrogels. To obtain the Ty-GG/SF hydrogels, 1% (w/v) of Ty-GG solution was mixed with 2% (w/v) SF (1:1) solution. At this point, anti-TNF α Ab-CS/PAMAM dendrimer NPs were mixed in the Ty-GG and Ty-GG/SF solutions at a final concentration of 0.5 mg mL^{-1}. Then, two different crosslinking levels were tested by adding different amounts of HRP and H_2O_2 solutions to Ty-GG and Ty-GG/SF solutions, hereafter denominated C1, C2, C3, and C4, as described in **Table IV-3**. Each condition without anti-TNF α Ab-CS/PAMAM dendrimer NPs were used as control (hereafter designated C1 CTRL, C2 CTRL, C3 CTRL, and C4 CTRL). Then, the mixtures were transferred into polypropylene molds and incubate at 37°C until complete gelation.

Table IV-3 - Anti-TNF α Ab-CS/PAMAM loaded-Ty-GG and Ty-GG/SF hydrogels with different crosslinking levels.

Designation	Ty-GG (1% w/v)	SF (2% w/v)	Dendrimer NPs (1 mg mL^{-1})	HRP (0.84 mg mL^{-1})	H_2O_2 (0.36% v/v)
C1	167 µL	-	97 µL	16.6 µL	10.83 µL
C2	167 µL	-	100 µL	18.3 µL	15 µL
C3	83.5 µL	83.5 µL	97 µL	16.6 µL	10.83 µL

C4	83.5 µL	83.5 µL	100 µL	20 µL	13.3 µL

In **Chapter IX**, anti-TNF α mAb-CS/PAMAM dendrimer NPs loaded-Ty-GG hydrogel was produced. The hydrogel was prepared by mixing 1% (w/v) of Ty-GG solution with anti-TNF α mAb-CS/PAMAM dendrimer NPs at a final concentration of 0.5 mg mL^{-1}. Then, the enzymatic crosslinking was made by adding horseradish peroxidase (HRP) solution (0.84 mg mL^{-1}) (Sigma-Aldrich, USA) and hydrogen peroxide solution (H_2O_2) (0.36% (v/v)) (VWR, USA) prepared in PBS and water, respectively. mAb-CS/PAMAM dendrimer NPs loaded-Ty-GG hydrogel was used in the subsequent assays.

IV-3.2.5. Distribution of FITC-CS/PAMAM dendrimer NPs throughout Ty-GG and Ty-GG/SF hydrogels

To assess the distribution profile of CS/PAMAM dendrimer NPs within Ty-GG and Ty-GG/SF hydrogels, the nanoparticles were labelled with Fluorescein isothiocyanate (FITC) (Sigma-Aldrich, USA). Initially, 10 mg mL^{-1} of CS/PAMAM dendrimer NPs solution was prepared in a carbonate-bicarbonate coupled buffer (pH 9.2). Then 50 µL of 10 mg mL^{-1} of FITC in anhydrous dimethyl sulfoxide (DMSO) (VWR, USA) solution was added per each mL of CS/PAMAM dendrimer NPs solution under agitation and kept in the dark at 4°C for 8 hours. In the end, the FITC-labelled CS/PAMAM dendrimer NPs were dialyzed in ultrapure water for 48 hours and freeze-dried. Then, FITC-CS/PAMAM dendrimer NPs at a final concentration of 0.1 mg mL^{-1} were mixed with Ty-GG and Ty-GG/SF solutions, and HRP and H_2O_2 solutions as described in **(Table IV-3)**. After crosslinking, the hydrogels were immersed in PBS and kept in a water bath at 37°C for 24 hours to remove free FITC. The hydrogels were observed under a confocal microscope (Leica TCS SP8).

IV-3.2.6. Incorporation and release profile of the Betamethasone-loaded Ty-GG and Ty-GG/SF hydrogels

To assess the drug release system, Betamethasone, was incorporated in Ty-GG and Ty-GG/SF hydrogels. These hydrogels loaded with Betamethasone (Sigma-Aldrich, USA) were prepared by mixing Ty-GG or Ty-GG/SF solution, with 5 mg mL^{-1} of Betamethasone in PBS and the enzymatic crosslinking was made by adding of HRP and H_2O_2. Betamethasone release profile in Ty-GG and Ty-GG/SF hydrogels was evaluated immersing each hydrogel in PBS at 37°C. After each time point (3 hours, 6 hours, 24 hours, 72 hours, 168 hours, 336 hours and 504 hours), the supernatant was removed and kept at -

80°C until the end of the experiment. Three samples per condition were used at each time point. To formulate the calibration curve, Betamethasone dilutions were prepared (from 0 mg mL^{-1} to 5 mg mL^{-1}). The UV absorbance at 245 nm was read in a microplate reader (EMax; Molecular Devices, Sunnyvale, CA, USA) to measure the Betamethasone release.

This procedure was applied to the Ty-GG hydrogels on **Chapter VI** and with Ty-GG/SF on **Chapter VII.**

IV-3.2.7. Release profile of anti-TNF α Ab-CS/PAMAM dendrimer NPs from Ty-GG and Ty-GG/SF hydrogels

To evaluate the release profile of anti-TNF α Ab-CS/PAMAM dendrimer NPs, each release system developed, C1, C2, C3, and C4 (more details in Table IV-3) were immersed in PBS at 37 ^{O}C. After 3 hours, 24 hours, 72 hours, 168 hours, 336 hours, and 504 hours, the supernatant was removed and kept at -80 ^{O} C until further analysis. To formulate the calibration curve, anti-TNF α Ab-CS/PAMAM dendrimer NPs dilutions were prepared ranging from 0 mg mL^{-1} to 0.5 mg mL^{-1}. The UV absorbance of dendrimers NPs was read at 280 nm in a microplate reader to quantify the anti-TNF α Ab-CS/PAMAM dendrimer release (EMax; Molecular Devices, Sunnyvale, CA, USA). Three samples per condition were evaluated at each time point. The absorbance values were converted into concentrations using the calibration curve. This method was performed on **Chapter VIII**.

IV-4. PHYSICOCHEMICAL CHARACTERIZATION TECHNIQUES

IV-4.1. Morphological/morphometric evaluation

IV-4.1.1. Fourier Transform Infrared Spectroscopy (FTIR)

Fourier Transform Infrared Spectroscopy (FTIR) is a cost-effective technique that is used for the identification of organic, inorganic, and polymeric materials using infrared light for scanning the samples [77]. The FTIR is useful to identify the chemical composition of polymers and analyze polymer chemical modifications. Fourier transformation algorithm allied to IR spectroscopy gives a spectrum of IR absorption per frequency/wavelength. Similar chemical groups absorb in the IR at similar

frequencies, allowing to identify the chemical structure of a compounds, and to recognize chemical modifications [78]. FTIR was performed to verify the presence of covalently liked chondroitin sulfate in dendrimer NP in **Chapter V**, as well as the chemical modification of Gellan Gum with Tyramine in **Chapter VI** and secondary structure of the Silk fibroin in the Ty-GG/SF hydrogels in **Chapter VII**. In **Chapter V** and **VI**, the samples were mixed with potassium bromide and, using a manual press, a transparent pellet was obtained. The transmittance spectra were obtained on an IR Prestige-21 FTIR spectrometer (Shimadzu) by performing 32 scans in each spectrum over a range of 400-4400 cm^{-1} and with a resolution of 4 cm^{-1}. In **Chapter VII**, the secondary structure of the Silk fibroin was evaluated by an Attenuated Total Reflectance (ATR) model (IRPrestige-21, Shimadzu, Japan) in a FTIR equipment (Perkin-Elmer 1600 series equipment, CA, USA) equipped with a Germanium crystal as can be seen in **Figure IV-10**. The spectra were obtained between 400-4400 cm^{-1}, at a 4 cm^{-1} resolution and 32 scans.

Figure IV-10 - The Fourier transform infrared (FTIR) spectrometer is used as a standard chemical characterization technique. The samples can be analyzed as films, KBr discs, powder or liquids. The available methodologies comprise transmittance, specular reflectance, diffuse reflectance and 1attenuated total reflectance (ATR). Scale bar: 10 cm.

IV-4.1.2. Nuclear Magnetic Resonance Spectroscopy (NMR)

Nuclear Magnetic Resonance Spectroscopy (NMR) is a powerful and mature analytical tool with applications in several areas of synthetic chemistry and polymer science. This is a useful method that provides precise qualitative and quantitative information about the chemical structure of a polymeric material and provides complete information on determined aspects of chain structure which is not possible by any other method [79]. NMR is a procedure that occurs when the nuclei of determined atoms are immersed in static magnetic field and exposed to a second oscillating magnetic field. H^1NMR

is the application of nuclear magnetic resonance in NMR spectroscopy with respect to hydrogen nuclei within the molecules of a substance. This is a non-destructive technique that allows defining the structure of compounds. NMR spectra are obtained in solution, and solvent protons must not be allowed to affect [80]. In this thesis, H^1NMR analysis was performed twice, first to assess the structure and the successful modification of PAMAM dendrimers with CS in **Chapter V**, and then to evaluate the covalent link of Tyramine to Gellan Gum and degree of substitution in **Chapter VI**. For this purpose, samples were solubilized in deuterium water (D_2O) at room temperature and the samples were transferred to NMR tube. The NMR spectra were obtained on a Bruker AVANCE 400 spectrometer, at 50 °C using a resonance frequency of 400 MHz. To process and analyze the obtained spectra, MestReNova 9.0 Software was used.

The degree of substitution was determined by the relative integration of the tyramine peaks ($I_{T1,T2}$) of the modified groups to methyl protons of the internal standard (I_{CH3}), according to **Equation IV-1**. The $n_{HT1,T2}$ and n_{HCH3} correspond to the number of tyramine protons and the methyl protons of GG monomer, respectively. n_{OH} corresponds to the number of reactive -OH sites in the GG structure.

Equation IV-1- Degree of substitution.

$$DS = \left(\frac{\frac{I_{T_1T_2}}{I_{CH_3}}}{\frac{n_{H_{T_1T_2}}}{n_{CH_3}}} \Big/ n_{OH} \right) \times 100$$

IV-4.1.3. Energy-dispersive X-ray spectroscopy (EDS)

Energy-dispersive X-ray spectroscopy (EDS) is an analytical technique used for identifying and quantifying elemental composition in a sample. In an appropriately equipped scanning electron microscopy (SEM), the atoms on the surface are excited by the electron beam, emitting back specific wavelengths of X-rays that are characteristics of the atomic structure of the elements. The X-ray emissions can be evaluated using an energy dispersive detector, which is a solid-state device that

identifies among X-ray energies **(Figure IV-11)**. Adequate elements are assigned, producing the composition of the atoms on the specimen surface [81].

In **Chapter V**, CS/PAMAM dendrimer NPs were analyzed to assess the effectiveness of modifying the PAMAM dendrimer with the CS. The CS/PAMAM dendrimer NPs samples were coated with carbon (Fisons Instruments, Polaron SC 508, UK). The electric current was set at 18 mA with a coating time of 120 seconds. The sulphur, calcium, sodium, carbon and oxygen elemental analysis were achieved through an X-ray detector (Pentafet model 5526, UK) attached to the S-360 microscope, and a voltage of 10 kV was used.

Figure IV-11 - The SEM with EDS analyzer. The SEM (JSM-6010 LV, JEOL, Japan) instrument is equipped with an energy dispersive spectroscope (EDS). Scale bar: 10 cm.

IV-4.1.4. Atomic force microscopy (AFM)

Atomic force microscopy (AFM) is a surface analysis technique used to characterize micro/nanostructure coatings. This technique offers qualitative and quantitative information on many properties including morphology, size, surface texture, and roughness [82]. Comparing to the electron or optical microscopes, AFM does not form an image by focusing electron or light onto a surface. The equipment analyses the samples surface with a sharp probe or cantilever and build a map covering the height or topography of the surface of the samples [83].

In **Chapter V** the morphology of the CS/PAMAM dendrimer NPs was investigated using AFM **(Figure IV-12)**. The CS/PAMAM dendrimer NPs were dissolved in ultrapure water to achieve a final

concentration of 1 mg mL^{-1} and transferred to the surface of a 9.9 mm mica disc (Agar Scientific, England). The samples were evaluated using the Tapping model TM with a MultiMode AFM connected to a NanoScope III controller (Veeco, USA) with noncontact silicon nanoprobes (ca. 300 kHz) from Nanosensors, Switzerland. Images were plane-fitted using the third-degree-flatten procedure included in NanoScope software version 1.5. The particle morphology and size were both analysed with NanoScope 1.5 software.

Figure IV-12 - The AFM allows acquiring images of flat surfaces that can encode the surface topography, mechanical response, among other properties. Scale bar: 10 cm.

IV-4.1.5. Scanning Transmission Electron Microscope (STEM)

The Scanning Transmission Electron Microscope (STEM) is a extremely versatile instrument able of atomic-resolution imaging and nanoscale analysis. The principle of STEM is quite straightforward. A beam of electrons is focused on electron optics to produce a small illuminating probe that is raster-scanned across a sample. The sample is thinned so that most electrons are transmitted, and the dispersed electrons detected using some geometry of the detector. The intensity depending on the position of the probe produces an image [84].

In **Chapter V**, STEM (AURIGA COMPACT, ZEISS, Germany) **(Figure IV-13)** was used to measure the size and morphology of CS/PAMAM dendrimer NPs. The nanoparticles were diluted in ultrapure water

to a final concentration of 0.1 mg mL^{-1} and then 2 µL were placed on copper grids at 37°C overnight for observation.

Figure IV-13 - The AURIGA compact is a FIB-SEM instrument combining the powerful imaging and analytical performance of field emission scanning electron microscope (FE-SEM) with the superior processing ability of Focused Ion Beam (FIB). Scale bar: 10 cm.

IV-4.1.6. Dynamic light scattering (DLS) and electrophoretic light scattering (ELS)

Determination of particle size and surface charge of NPs are indispensable for the suitable characterization of NPs. The particle size can be obtained by measuring the random changes in the intensity of light scattered from a suspension or solution. This technique, commonly known as Dynamic Light Scattering (DLS), is the main common measurement technique for particle size analysis in the nanometer range. Electrophoretic Light Scattering (ELS) is a method used to measure the electrophoretic mobility of molecules in solution, or particles in the dispersion. The mobility is generally transformed to Zeta potential to allow comparison under different experimental conditions. The essential physical principle is that of electrophoresis. A dispersion is introduced into a cell including two electrodes. An electrical field is applied to the electrodes, and molecules and particles will migrate towards the oppositely charged electrode with a velocity, that is associated to their zeta potential [85],[86].

Particle size and zeta potential of CS/PAMAM dendrimer NPs were measured in a particle analyzer (Zetasizer Nano ZS, Malvern Instruments, UK) **(Figure IV-14)**, in **Chapter V**. Particle size analysis was

made by DLS technique, in an ultrapure water solution with 1 mg mL^{-1} of CS/PAMAM dendrimer NPs. Zeta potential of nanoparticles was evaluated by ELS, using the universal 'dip' cell and at pH 7.4 phosphate buffer saline (PBS) solution.

Figure IV-14 - Zetasizer Nano ZS, Malvern Instruments. Scale bar: 10cm.

IV-4.1.7. Fluorescence spectroscopy

Fluorescence spectroscopy is used for studying structural changes in conjugated system due to alterations in temperature, pH, ionic strength, solvent, and ligands. A single fluorophore can produce thousands of detectable photons that can be recurrently excited and detected, making fluorescence spectroscopy is an extremely sensitive technique [87].

The immobilization of the Abs by CS/PAMAM dendrimer NPs was evaluated by fluorescence spectrometer FP-8500 (Jasco) **(Figure IV-15)**. The rabbit polyclonal anti-TNF α / mouse monoclonal anti-TNF α antibody-CS/PAMAM dendrimer NPs and CS/PAMAM dendrimer NPs were mixed with a secondary antibody anti-rabbit/anti-mouse IgG-labelled with Alexa Fluor 488 dye (Molecular probes, USA), in PBS solution (1:1000) for 1 hour to detect the conjugation of anti-TNF α Abs to CS/PAMAM dendrimer NPs. The solutions were centrifuged, and the supernatants were visualized in the spectrometer.

This method was used in **Chapter V** using rabbit polyclonal anti-TNF α antibody and in **Chapter VIII** using mouse monoclonal anti-TNF α antibody.

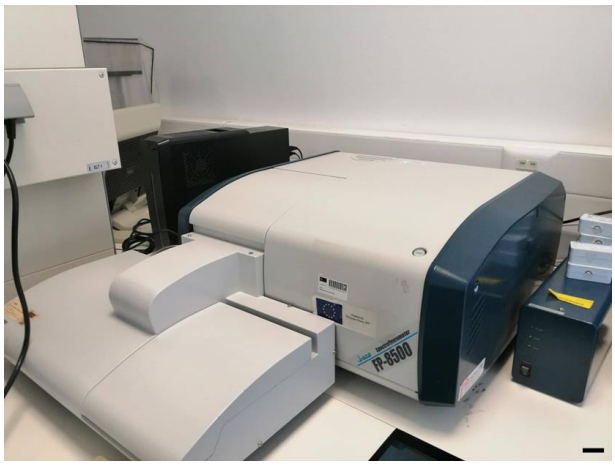

Figure IV-15 - Fluorescence spectrometer, FP-8500, Jasco. Scale bar: 10cm.

IV-4.1.8. ELISA assay

The enzyme-linked immunosorbent assay (ELISA) is used to measure target analytes such as hormones, antibodies, and protein biomarkers. In this case, ELISA analytes are antigens, the targets of antibodies. Antigens are naturally attached to a plate and specifically recognized by an antibody that has an enzyme-linked to it for detection purposes. There are many variants of ELISA, but the required principles are the same. In sandwich ELISA the antigen is bound or captured by the plated antibody and then "sandwiched" between the capture and detection antibody which is accomplished by measuring the activity of the reporter enzyme via incubation with the appropriate substrate to produce a measurable product. The main advantage of sandwich ELISA is the ability to specifically measure antigen from impure samples [88].

In **Chapter V** and **Chapter VIII**, to determinate the amount of TNF α captured by polyclonal and monoclonal anti-TNF α Abs-CS/PAMAM dendrimer NPs, theses were incubated with 1000 pg mL^{-1} of TNF α (Peprotech, United Kingdom) for 6 hours at room temperature. After centrifugation, the supernatant was put at -80°C for further analysis. Then, the free TNF-α concentration in the samples after incubation was measured using a Human TNF-alpha DuoSET ELISA kit (R&D systems, USA) and a DuoSet Ancillary Reagent Kit 2 (R&D systems, USA). Briefly, the capture antibody was plated and incubated overnight at room temperature. Then, the standard and samples were added and incubated for 2 hours and the detection antibody was added for 2 hours at room temperature. The next step was to add Streptavidin-HRP for 20 minutes at room temperature, avoiding place in direct light., then was added substrate solution for more 20 minutes and at the end the stop solution was put. The samples

were measured in the microplate reader (Synergy HT, BIO-TEK) with an optical density of 450 nm. The calibration curve was prepared using TNF-α standard solutions, with concentrations from 0 to 1000 pg mL^{-1}, which were also included in the ELISA plate.

IV-4.1.9. Rheometer

Rheology is a science which study the deformation and flow of materials under an applied force. The rheological characterization of materials allows to know the viscoelastic flow behavior of the system. This method is important to every material because the rheological properties are closely associated to the final structures of the system [89]. Polymeric and disperse systems, show mechanical properties intermediate between those liquids and solids because they are composed of viscous and elastic components. The rheology analysis provide the viscosity, elasticity, and plastic behavior of materials under changes of frequency, time, or temperature [90].

In **Chapter V,** rheological analyses were performed to CS/PAMAM dendrimer NPs using Kinexus pro+rheometer with the acquisition software rSpace (Malvern) **(Figure IV-16)**. The rotational experiments were performed using a cone-plate measuring system composed by an upper stainless-steel cone of 40 mm of diameter and a cone angle of 4°. Shear viscosity was obtained as a function of the shear rate, from 0.001 to 0.1 s^{-1} at 37°C. The oscillatory experiments were made to obtain frequency sweep curves, after Linear Viscoelastic Region (LVER) determination. In **Chapter VI** and **VII,** the mechanical properties of Ty-GG and Ty-GG/SF hydrogels were assessed through an oscillatory mode in a rheometer (Kinexus pro+rheometer, software rSpace, from Malvern). The oscillatory experiments were performed using a plate-plate measuring system compound by an upper stainless-steel plate of 8 mm of diameter, with a rough finish, so that the samples do not slip. The mechanical spectra (frequency sweep curves) were obtained from 0.1 Hz to 10 Hz of frequency, at a shear strain of 0.1 and 0.3%, respectively, for 5 minutes. The shear strain used was within the LVER of the material, previously obtained through strain sweep curves. By using a value from LVER it is ensured that the applied stress does not cause microstructure breakdowns (called yielding), and the hydrogel properties can be accurately determined. All experiments were repeated 3 times at 37°C.

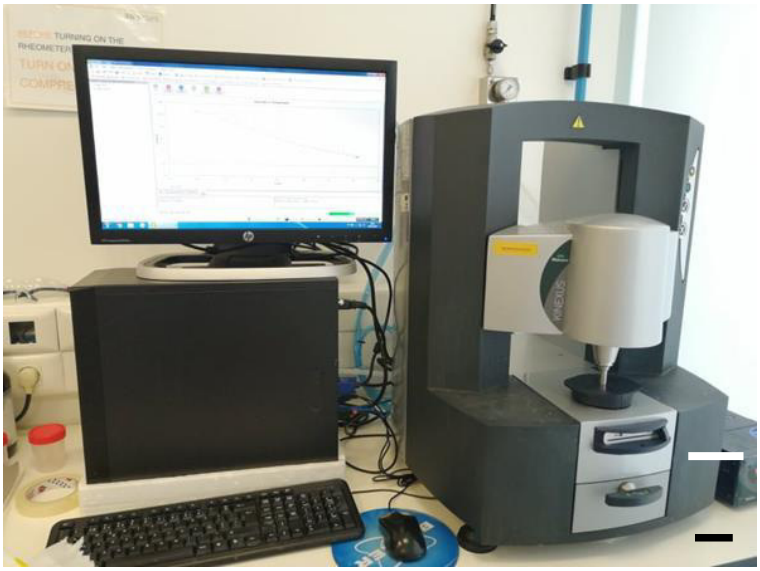

Figure IV-16 - Rheometer apparatus, Malvern Instruments. Scale bar: 10 cm.

IV-4.1.10. Injectability test

Injectability is an important parameter of any parenteral dosage form. This test refers to the capability of an injectable therapeutic to pass easily through a needle on transfer from a vial prior to injection. Injectability includes factors as pressure or force required for injection [91].

In **Chapter VI** and **Chapter VII**, the injectability tests were performed to Ty-GG and Ty-GG/SF hydrogels by means of injectability measurement equipment (PARALAB) **(Figure IV-17)**. The injectability measurements were performed using a syringe with a 27 G needle. The material was placed in the syringe that was placed in the equipment and then it applied a force that extruded the sample from the syringe at a rate of 1 mL min^{-1}. The force needed for each hydrogel condition was recorded. Triplicates of each sample were performed, and water was used as a control.

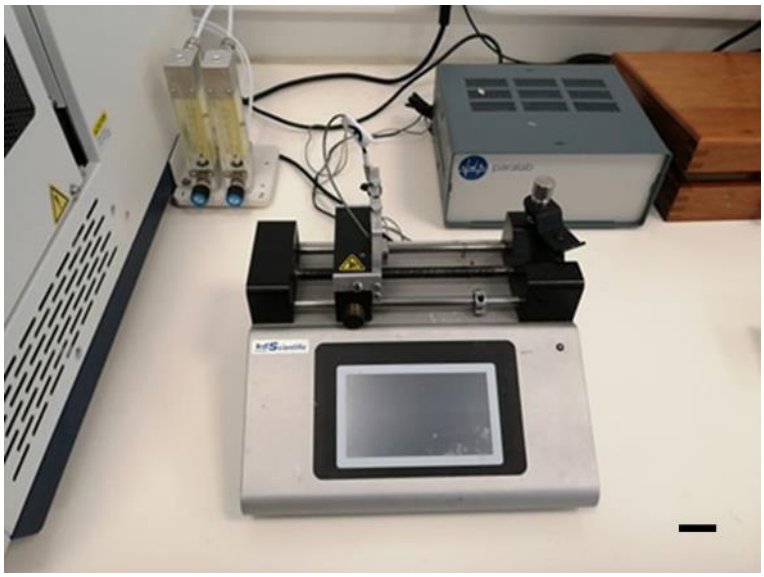

Figure IV-17 - Injectability measurement equipment, PARALAB instruments. Scale bar: 10 cm.

IV-4.1.11. Gelation time

The gelation time is amount of time it takes for the liquid form to transform into a gel. The gel form is a highly viscous material that can no longer flow into a thin coating. The sol–gel transition in a sample can be qualitatively verified by a simple assay without the need to use a rheometer. The tube inversion test includes only a visual observation. The hydrogel is prepared in a tube and its physical state is detected by tube inversion and then it is observed whether the sample flows [92], [93]. The is an important parameter for the formation of hydrogels in situ because a quick gelation time is beneficial to obtain high loading efficiency of drugs in hydrogels.

In **Chapter VI** and **VII**, the vial inversion test **(Figure IV-18)** was made to determine an approximate gelation time. Thus, after mix Ty-GG and Ty-GG/SF with HRP and H_2O_2, the vials were placed in the water bath at 37°C and then inverted to see how long it takes to turn to gel.

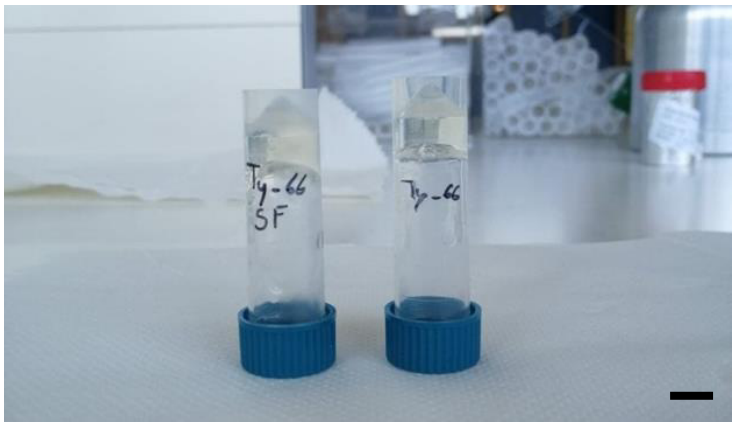

Figure IV-18 - Vial inversion test with Ty-GG and Ty-GG/Silk. Scale Bar: 10 cm.

IV-4.1.12. Water uptake

The water uptake behavior of the hydrogels can give a better understanding in terms of the performance of a biomaterial in contact with medium. This can predict the hydrogels interactions with the surrounding tissues where will be applied.

In **Chapter VI** and **VII**, the water uptake ratio of the Ty-GG and Ty-GG/SF hydrogels was performed in PBS solution at 37°C. The initial weight (w_i) of each sample was measured, and then the hydrogels were immersed in PBS solution. At the end of each time point (24 hours, 72 hours, 168 hours, 336 hours, and 504 hours), the samples were collected and placed in filter paper to remove excess liquid, and the wet weight (w_w) was measured. The percentage of water uptake was determined using **Equation IV-2**.

Equation IV-2- Water uptake.

$$\text{Water uptake (\%)} = \frac{W_w - W_i}{W_i} \times 100$$

IV-4.1.13. Degradation profile

The degradation rate of tissue engineering scaffolds and drug carriers should mirror the rate of new tissue formation or be adequate for the controlled release of bioactive molecules. The degradation rate of drug carriers should be adequate for the controlled release of bioactive molecules [94].

In **Chapter VI**, weight loss was assessed in parallel with water uptake, following the same protocol. The weight loss was quantified after the samples were dried under at 70°C and until they reached constant weight (wf), using the **Equation IV-3**.

In **Chapter VII**, the degradation of Ty-GG/SF hydrogels was evaluated by enzymatic degradation test. The enzyme, Protease from Streptomyces griseus Type XIV (Sigma-Aldrich, USA) was prepared at 1 U mL^{-1} and 3.3 U mL^{-1} by dissolution in PBS. The initial weight of each sample was measured, and then the hydrogels were immersed in a protease solution. The dry weight (wf) was evaluated after samples dried at 70°C and until they reached a constant weight. The study was made at 37°C at different time points, 3 replicates per time points, for 21 days. The weight loss was calculated using the **Equation IV-3**.

Equation IV-3- Weight loss.

$$\text{Weight loss (\%)} = \frac{W_i - W_f}{W_i} \times 100$$

IV-5. *IN VITRO* BIOLOGICAL TESTING

IV-5.1. Cell sources

The work performed in this thesis was carried out using different cell lines and a primary cell line. Cell lines are immortalized cells that show the capability to proliferate indeterminately either due to a programmed modification or a random mutation. These cells are useful models for doing research because they offer reliability in experimental results due to the possibility to acquire large amounts of cells for prolonged use [95]. Primary cells are directly isolated from organs or tissues of interest by enzymatic dissociation. These cell models are well established,

quite easy and cheap to operate, and offer several vital advantages. The main advantage of primary cells is that these they possess purposes and phenotypes close to those of *in vivo* tissues and organs. The effect of drug systems can be studied on isolated primary cells at the cellular level [96].

Furthermore, since this thesis was developed in the context of rheumatoid arthritis research, chondrogenic cells and inflammatory system cells were abundantly used.

IV-5.1.1. ATDC 5 cell line

Chondrogenic ATDC 5 cell line was purchased from the European Collection of Authenticated Cell Culture, England. ATDC 5 cell line was expanded in DMEM-12 medium (Dulbecco's Modified Eagle Medium: Nutrient Mixture F-12, Alfagene, Portugal), supplemented with 10% Heat Inactivated Fetal Bovine Serum (FBS) (Alfagene, Portugal), sodium bicarbonate (Sigma-Aldrich, USA) and 1% antibiotic/antimycotic (Alfagene, Portugal), under standard culture conditions (at 37°C in a 5% CO_2 incubator). Cells were regularly trypsinized (0.25% trypsin– Ethylenediaminetetraacetic acid (EDTA) solution; Life Technologies, Carlsbad, CA, USA) for 5 minutes at 37°C, centrifuged at 300 G for 5 minutes, and re-suspended at a density of $1x10^6$ cells in T150 cell culture flasks. This cell line was used in **Chapter V**.

IV-5.1.2. Jurkat cell line

Jurkat cell line was expanded in RPMI medium (RPMI 1640 Medium, GlutaMAX™ Supplement, HEPES, Gibco, Life Technologies, Grand Island, NY), supplemented with 10% Heat Inactivated Fetal Bovine Serum, 2 mM glutamine and 100 U mL^{-1} of penicillin/streptomycin (PAA; Pasching, Austria), under standard culture conditions (37° C in a humidified atmosphere, containing 5% CO_2). This cell line was used in **Chapter V**.

IV-5.1.3. Human monocytic cell line

Human monocytic cell line (THP-1) (SIGMA, USA) was expanded in RPMI 1640 Medium, GlutaMAX™ Supplement, HEPES (Thermo Fisher Scientific, USA), supplemented with 10% fetal bovine serum and 1% (v/v) of penicillin and streptomycin, under standard culture conditions (37°C in a humidified atmosphere containing 5 % CO_2). This cell line was used in **Chapter V**, **VI**, **VII**, **VIII** and **IX**.

IV-5.1.4. Rabbit chondrogenic primary cells

Chondrogenic primary cells were isolated from female New Zealand White rabbits (Damul Sci., Korea) with 1 kg and 6 weeks. Dulbecco's modified eagle medium (DMEM/ F12) (Gibco, USA) was used in chondrogenic cells. This culture medium was supplemented with 10% (v/v) fetal bovine serum (Gibco, USA) and 1% (v/v) antibiotic-antimycotic (Gibko /Thermo Fisher Scientific, South Korea) under standard conditions (37°C in a humidified atmosphere containing 5% CO_2). The knees were initially removed from the rabbit, and the samples were washed 3 times with PBS (1X) solution. The cartilage was scraped carefully with the blade, and small fragments were placed inside a conical tube with 1.5% (v/v) antibiotic-antimycotic. The sample was centrifuged at 300 G, 3 minutes and 4°C. The supernatant was discarded and refilled with an enzymatic cocktail (DMEM/F12 medium + collagenase A (Roche, USA). The solution was previously filter-sterilized through a 0.2 µm filter. The sample was placed in the CO_2 incubator at 37°C for 24 hours. The next day, cells were centrifuged at 300 G, for 3 minutes and at 4°C. The supernatant was removed, and the cells were plated on a cell culture dish, with a complete medium and kept in the CO_2 incubator at 37°C until they reach the desired confluence. Chondrogenic primary cells were used in **Chapter VI** and **VII**.

IV-5.1.5. Human chondrogenic primary cells

The human chondrogenic primary cells (hCH) (passage=3) previously isolated and characterized were used for these assays. Briefly, they were obtained from human cartilage during arthroscopic surgeries on male and female donors with ages between 19 and 56 years (Centro Hospitalar Póvoa do Varzim). The articular cartilage was removed from the bone and cut into small pieces. The samples were washed several times with 1% PBS/antibiotic-antimycotic (v/v) solution, digested with 0.08% collagenase type II (Sigma-Aldrich, USA)/DMEM-F12 medium 1:1 (v/v) and incubated at 37°C in a water bath overnight with gentle agitation. The digested tissue was filtered, and cell suspension centrifuged at 500 G for 5 minutes. hCH cells were expanded in DMEM/F12 medium (Dulbecco's Modified Eagle Medium: Nutrient Mixture F-12, Alfagene, Portugal), supplemented with 10% of Heat Inactivated Fetal Bovine Serum (FBS) (Alfagene, Portugal), sodium bicarbonate (Sigma-Aldrich, USA) and 1% (v/v) antibiotic-antimycotic (Alfagene, Portugal), under standard culture conditions (at 37°C in a 5% CO_2 incubator). Human chondrogenic primary cells were used in **Chapter IX**.

IV-5.2. Cryopreservation

The cryopreservation of the cells used in this thesis was achieved using a Statebourne Biosystem 24 cryogenic tank (Statebourne Cryogenics Ltd., UK). The cell suspensions of $1x10^6$ cells/mL were prepared in 10% (v/v) DMSO (N182, VWR, Radnor, PA, USA) in FBS, and transferred into 1.5 mL cryovials (479-6841, VWR, Radnor, PA, USA). Then, cell suspensions were put at -20°C for at least 2 hours and posteriorly kept to -80°C freezer for period of 12 hours. The cryovials were subsequently stored at -176°C in the cryogenic tank.

IV-5.3. Cell seeding techniques

IV-5.3.1. Cell culture in a Dual-chamber bioreactor

In **Chapter VIII**, THP-1 cells were seeded at a density of $5x10^5$ cells/well mL^{-1} in TCP coverslips in 24-well plates. For induction of THP-1 cell differentiation, cells were cultured under RPMI medium with 100 nM phorbol 12-myristate-13-acetate (PMA) (Sigma-Aldrich, USA). After 24 hours, the medium was replaced with RPMI medium without PMA and incubated for another 48 hours. Then cells were incubated with 100 ng mL^{-1} Lipopolysaccharide (LPS) (Sigma-Aldrich, USA) in RPMI medium and incubated for 5 hours to induce an inflammatory response. After LPS stimulation, the coverslips were transferred to the lower chamber of a dual-chamber bioreactor with RPMI medium contained LPS and the anti-inflammatory effect of developed release systems was evaluated.

IV-5.3.2. Seeding on microfluidic chip

In **Chapter IX**, to perform cell seeding, the microfluidic platform 3D Cell Culture Chips DAX-1 (Tebu-bio, Portugal) was used. The device consists of three compartments: two lateral channels, where THP-1 (left side) and hCH cells (right side) encapsulated in Matrigel mimic the cartilage inflammation microenvironment, and one central channel where the produced anti-TNF α mAb-CS/PAMAM dendrimer NPs loaded-Ty-GG hydrogel (NPs-hydrogel) was injected to treat the inflammatory environment. The appropriate culture medium was placed in the lateral channels with a volume differential (90 µL at inlet and 70 µL at the outlet) to allow fluid diffusion between the channels.

IV-5.3.3. Encapsulation of Gelatin in central channel of chip

Gelatin from porcine skin (Sigma-Aldrich, USA) at 2% (w/v) was dissolved in water at 50°C and added to the central channel of the microfluidic device. This polymer was used as sacrificial hydrogel, preventing the Matrigel® with encapsulated cells to leak into the central chamber. The device was placed at 4°C for 20 minutes for jellification.

IV-5.3.4. Encapsulation of hCH and THP-1 in lateral channels of chip

In **Chapter IX**, the hCH and THP-1 cells were centrifuged at 300 G for 5 minutes and diluted in a new cell suspension with appropriate media. Then, the THP-1 and hCH cells were encapsulated in Matrigel® at a density of $2x10^{6}$ cells mL^{-1}. THP-1 cells suspended in Matrigel® were injected in the left channel and hCH in the right channel of the microfluidic device, followed by incubation for 20 minutes at 37°C for crosslinking. After this, RPMI medium with 100 nM PMA was added to the channel with THP-1 cells and DMEM-F12 was added to the channel with hCH cells to prevent drying. A differential of cell culture medium was added to the inlet (90 µL) and outlet (70 µL) of the microchannel to allow perfusion and nutrition of the cells. The microfluidic devices were incubated for 24 hours, after which the medium was replaced with RPMI medium without PMA in the THP-1 channel and DMEM-F12 in hCH channel, followed by another 24 hours of incubation.

To enable an inflammatory response, THP-1 cells were incubated for 5 hours with 100 ng mL^{-1} of lipopolysaccharide (LPS) (SigmaAldrich, USA) in RPMI medium. After incubation time, gelatin was flushed from the central channel with PBS at 50°C, letting the channel free to add our formulation of NPs-Hydrogel, for 3 and 7 days. In parallel, a positive control chip comprising THP-1 stimulated with LPS in left channel, and hCH in the right channel without NPs-Hydrogel was used (hereafter designated $CTRL^{+}$). Additionally, a negative control chip with THP-1 differentiated with PMA in the left channel, and hCH cells in the right channel without NPs-hydrogel was used (hereafter designated $CTRL^{-}$).

IV-5.4. Metabolic activity and cell viability examination

IV-5.4.1. MTS assay

The MTS assay is a colorimetric assay frequently used for determining the number of viable cells in cytotoxicity tests. This method is intended to evaluate the short-term cytotoxicity of polymeric biomaterials. The MTS assay is based on bio-reduction of a tetrazolium compound, 3-(4,5-dimethylthiazol-2-yl)-5-(3-carboxymethoxyphenyl)-2-(4-sulfofenyl)-2H-tetrazolium (MTS), into a brown formazan product that is soluble in tissue culture medium. This conversion is accomplished by NADPH or NADH formed by dehydrogenase enzymes in metabolically active cells. The quantity of formazan product, as measured by the amount of 490 nm absorbance, is proportional to the number of living cells in culture [97].

In **Chapter V**, the ATDC 5 cells were seeded at a density of 1×10^4 cells per well and incubated with different concentrations of CS/PAMAM dendrimer NPs, for 72 hours. Cells cultured with regular medium (without CS/PAMAM dendrimer NPs) were used as a control. At each time point, cell culture medium (DMEM-F12) was replaced by culture medium without phenol red, containing MTS at a 5:1 ratio, and was incubated for 3 hours. Then, 100 µL from each well were passed into a 96-well plate and the absorbance was read at 490 nm. The Jurkat and (differentiated) THP-1 cell lines were seeded in a 96-well plate with a density of $3x10^4$ and $1x10^4$ cells per well, respectively. The CS/PAMAM dendrimer NPs were administrated in serial dilutions 1:2 starting with the concentrations of 0.5 mg mL^{-1}. The cells were incubated with the CS/PAMAM dendrimer NPs for 48 hours, in standard cell culture conditions. The remaining procedure was performed as previously mentioned for the ATDC 5 cell line. Furthermore, THP-1 cells were seeded at a density of 5×10^5 cells per well and incubated for 1 day, 3 days and 7 days with the anti-TNF α Abs-CS/PAMAM dendrimer NPs (0.5 mg mL^{-1}), to assess the effect of this conjugation on cells` viability and proliferation.

IV-5.4.2. MEM Extract test

The MEM Extract test is a cytotoxicity test which is intended to establish the rate of cytotoxicity of leachables from medical devices/materials. The cells are exposed to an extract, containing the potential leachables, after which the effect on the cells is measured. The principle of this method is based on a

monolayer of cells that is put in contact with an extract the of a medical device/material. As a function of time, the reaction of these cells on the presence of the extract is assessed. If the extract contains toxic leachables, originating from the material, cells can react with cell growth inhibition, decrease/ increase metabolism, intracellular granulation, cell death, or a change in cell morphology. To evaluate the cytotoxicity index, MTS and MTT assay were performed.

In **Chapter VI** and **VII** after following the MEM extract test was performed MTT assay.

IV-5.4.3. MTT assay

The MTT assay is used to measure cellular metabolic activity. This method is based on the reduction of a yellow tetrazolium salt 3-(4,5-dimethylthiazol-2-yl)-2,5-diphenyltetrazolium bromide (MTT) to purple formazan crystals by metabolically active cells. The viable cells contain NAD(P)H-dependent oxidoreductase enzymes which reduce the MTT to formazan. The insoluble formazan crystals are dissolved using a solubilization solution and the resulting colored solution is quantified by measuring absorbance at 500-600 nanometers using a multi-well spectrophotometer. The darker the solution, the greater the number of viable, metabolically active cells [98], [99].

In **Chapter VI** and **VII**, chondrogenic primary cells at a density of 10000 cells cm2 were cultured with extraction fluid of Ty-GG and Ty-GG/SF hydrogels and evaluated by MTT (Sigma, South Korea) at 24, 48 and 72 hours. At each time point, the DMEM/ F12 medium was replaced by culture medium containing MTT assay in a 9:1 ratio and incubated for 3 hours. When violet crystals were formed, they were melted using dimethyl sulfoxide solution (DMSO). Then, 100 µL of solution from each well was transferred to 96-well plates, and a microplate reader (EMax; Molecular Devices, Sunnyvale, CA, USA) was used at 570 nm optical density.

IV-5.4.4. Alamar Blue assay

Alamar blue assay is used to assess the metabolic activity of cells. The Alamar Blue is a cell viability reagent that works by using the reducing power of living cells to quantitatively measure their metabolic activity. When cells are metabolically active, they keep a reducing environment within the cytosol. Resazurin, is the active ingredient of AlamarBlue® reagent, blue in color, non-toxic and cell permeable. Within the cells, resazurin is reduced to resorufin, a compound that is red in color and

extremely fluorescent. Viable cells convert resazurin to resorufin, enhancing the overall fluorescence and color of the media around the cells [98].

In **Chapter VIII**, cells' metabolic activity was evaluated on days 1, 3, and 7 of culture with Alamar Blue at each time point. For that, RPMI culture medium containing 10% (v/v) of AlamarBlue® (BioRad, Oxford, UK) was added to the different conditions.

In **Chapter IX**, Alamar blue was performed to assess the effect of NPs-Hydrogel in terms of metabolic activity in THP-1 and hCH cells for 3 and 7 days. For the Alamar blue metabolic activity assay in 3D, cells encapsulated in Matrigel® were retrieved using Corning Cell Recovery Solution (Laborspirit, Portugal) for 40 minutes at 4°C. After complete Matrigel® release, cells were collected to an Eppendorf tube and centrifuged to a pellet (300 G for 5 minutes). The supernatant was removed and a culture medium containing 10% (v/v) of AlamarBlue® (BioRad, Oxford, UK) was added.

The culture plates were kept in the dark, at 37°C in the CO_2 incubator for 4 hours. Afterward, 100 µL of each well were transferred in triplicate to 96-well plates. The fluorescence was read at an excitation wavelength of 530/25 nm and an emission wavelength of 590/535 nm, using a microplate reader (Synergy HT, BioTek, Instruments, USA).

IV-5.4.5. Live/Dead staining assay

To visualize cell viability and death, Calcein-acetoxymethyl (Calcein-AM)/ ethidium homodimer (EthD-1) staining was performed. In this assay, cells are incubated with Calcein-AM, which is a non-fluorescent and cell-permeant derivative of calcein that becomes green fluorescent by intracellular esterase activity in live cells. However, it stays non-fluorescent when the acetoxymethyl ester is intact because of the non-active esterases of dead cells. The identification of dead cells can be performed by incubation with fluorescent EthD-1, which shows increased fluorescence when binding with high affinity to DNA. EthD-1 is membrane impermeant and consequently does not enter viable cells with intact membranes. When the cellular membrane is disrupted, EthD-1 binds to nucleic acids and the fluorescence increases intensely and is therefore used to identify dead cells [99],[100].

In **Chapter IX**, cell viability of THP-1 and hCH cells cultured in the microfluidic chip's lateral channels was assessed in the presence of NPs-Hydrogel for 3 and 7 days, using the live/dead assay. Initially, the NPs-Hydrogel was flushed with PBS at 50°C in the central channel to add the solution of Calcein-AM (1 mM; live cells in green) (Alfagene, Portugal) and ethidium homodimer (EthD-1 6 mM;

dead cells in red) (Laborspirit, Portugal). The chips were incubated for 40 minutes in the dark, at 37°C in the CO_2 incubator, to reach the cells in the lateral channels. After this, the central channel was washed with PBS three times. The chips were observed under fluorescence microscopy (EthD-1 ex/em 528/617 nm Calcein-AM; ex/em 495/515 nm) in the Fluorescence Inverted Microscope. Images were acquired using the Zen microscope processing software, connected to the digital camera Axio Observer. A Z-stack function was used to combine images at different depths into one final image.

IV-5.4.6. DNA quantification

DNA content was evaluated by the total double-stranded DNA (dsDNA) using the Pico- Green® dsDNA quantification assay. This colorimetric assay employs fluorescence to evaluate cell proliferation through the measurement of the dsDNA of samples. When the PicoGreen® fluorescent marker is added to the solution, it exactly links to the dsDNA emitting fluorescence, read at 480 nm (excitation) and 520 nm (emission) [101].

In **Chapter V**, the proliferation of the ATDC5 and THP-1 cells was evaluated. ATDC 5 cells were seeded at a density of 1×10^4 cells per well and incubated with different concentrations of CS/PAMAM dendrimer NPs for 24 hours, 48 hours and 72 hours and THP-1 cells were seeded at a density of 1×10^6 cells mL^{-1} and incubated with anti-TNF α Abs-CS/PAMAM dendrimer NPs (0.5 mg mL^{-1}) for 1 day, 3 days and 7 days.

In **Chapter VI** and **VII**, extraction solution of Ty-GG and Ty-GG/SF hydrogels (C1, C2, and C3) was incubated with chondrogenic cells at a density of 10000 cells cm^2 for 24 hours, 48 hours and 72 hours. In **Chapter VIII**, the proliferation of the THP-1 cells at days 1, 3, and 7 of culture was analyzed by dsDNA quantification. In **Chapter IX,** the proliferation of THP-1 and hCH cells in contact with NPs-Hydrogel for 3 and 7 days were analyzed by means of DNA quantification. For DNA quantification, cells encapsulated in Matrigel® were retrieved using Corning Cell Recovery Solution for 40 minutes at 4°C.

At each time-point, ultrapure water was added for cell lysis. The cells' lysate solution was stored at -80°C until further analysis. Quanti-IT PicoGreen dsDNA Assay Kit (Alfagene, Portugal) was used to quantify dsDNA, according to manufacturers' instructions. Then, the plate was incubated in the dark for 10 minutes and the fluorescence was read using excitation of 480/20 nm and emission of 528/20 nm,

in a microplate reader (SYNERGY HT, BIO-TEK). DNA concentration was determined using a standard curve in the range of 2 to 0 μL mL^{-1}.

IV-5.4.7. Flow cytometry analysis

Flow cytometry is a method that allow measure physical characteristics of a single cell such as size and granularity simultaneously, as the cell flows in suspension through a measuring device. This method depends on the light scattering features of the cells under study, which may be derived from monoclonal antibodies or dyes or targeting either extracellular molecules located on the surface or intracellular molecules inside the cells. The flow cytometry is an effective method for complete analysis of complex populations in a short period of time [104].

In **Chapter V**, for flow cytometry analysis the ATDC 5 cells were seeded at a density 4×10^5 cells per well (in a 24-well plate) and cultured with different concentrations of FITC-labelled CS/PAMAM NPs (0.01, 0.1 and 0.5 mg mL^{-1}), for 72 hours. ATDC5 cells cultured in DMEM-F12 without CS/PAMAM dendrimer NPs were used as control. The samples were measured using a FACSCalibur flow cytometer (BD Biosciences Immunocytometry Systems, CA, USA) and the results were analyzed by the Flowing Software 2. THP-1 cells were incubated for 3, 6 and 24 hours with 0.5 mg mL^{-1} of CS/PAMAM dendrimer NPs at a cell density of 1x105 cells per well, in a 24-well plate. THP-1 cells cultured with only RPMI medium were used as control. The samples were measured in a BD Accuri C6 flow cytometer (BD Biosciences, USA) and the analysis was performed in the cytometer software.

IV-5.4.8. Fluorescence microscopy

Fluorescence microscopy is a technique where samples stained with fluorescent dyes are observed with a fluorescent microscope. In fluorescence imaging, the fluorophores located near the site of interest are excited by an external source of light and then reemitted at another wavelength that can be detected. Therefore, the optical signal in fluorescence microscopy strongly depends on the fluorophore properties. The fluorescence microscopy, it is a main method with which to monitor cell physiology [102].

In **Chapter V**, the ATDC5 cells were seeded at a density of 1×10^4 cells per well in a 24-well plate, with different concentrations of FITC- labelled CS/PAMAM dendrimer NPs for 72 hours. Then, cells

were fixed with 10% formalin (Sigma-Aldrich, USA) and stained with 4,6-diamidino-2-phenylindole, dilactate (DAPI blue, VWR International, USA) for nuclei and Texas Red-X phalloidin (Sigma- Aldrich, USA) for actin filaments of the cytoskeleton. The cells were observed under the fluorescence microscope (AxioImager, Z1, Zeis Inc., Oberkochen, Germany). The differentiated THP-1 cells were seeded at a density of $4x10^4$ cells per well in a 24-well plate and incubated for 3 and 6 hours with FITC-labelled CS/PAMAM dendrimer NPs. At each time point the cells were stained with Hoechst 33342 (1:1000) (Immnochemistry Technologies) and observed under a Nikon Eclipse Ti2 microscope (Nikon Instruments, Inc.).

In **Chapter VI** and **VII,** the chondrogenic primary cells were seeded at a density of 10000 cells per cm^2 and incubated with extraction solution of Ty-GG and Ty-GG/SF hydrogels for periods of 24, 48 and 72 hours. Then, cells were fixed with 10% formalin (Sigma-Aldrich, USA) and stained with Texas Red-X phalloidin (Sigma-Aldrich, USA) for actin filaments of the cytoskeleton and 4,6-diamidino-2-phenylindole, dilactate (DAPI blue, VWR International, USA) for nuclei. At the end, cells were analyzed under the fluorescence microscope (AxioImager, Z1, Zeis Inc., Oberkochen, Germany).

IV-5.4.9. Hemolytic properties

Hemolytic property is one of the most common tests in studies of nanoparticle interaction with blood components. Hemolysis *in vivo* can lead to anemia and other pathological conditions; therefore, the hemolytic potential of all intravenously administered pharmaceuticals must be analyzed. The studies of particle-induced hemolysis evaluate the percent hemolysis by spectrophotometrically detecting plasma free hemoglobin derivatives after incubating the particles with blood and then separating undamaged cells by centrifugation [103].

In **Chapter V,** Erythrocytes from whole mouse blood were used to test the hemolytic properties of CS/PAMAM dendrimer NPs. The blood was extracted into a tube with EDTA and an aliquot of 5 mL was diluted with PBS (1:10) in a pre-weighted tube. After centrifugation and washing steps, the pellet was weighed and diluted with PBS to a final concentration of 3% (w/v). The CS/PAMAM dendrimer NPs were diluted in PBS and administrated in serial dilutions 1:2 starting with the concentrations of 0.5 mg mL^{-1}. PBS and Triton x-100 were used as negative control and positive control, respectively. The plates were incubated for 4 hours, centrifuged and the supernatant was collected. The samples were read at

588 nm absorbance using a microplate reader (Greiner Bio-one). The percentage of hemolysis in the samples was calculated according to the following **Equation IV-4.**

Equation IV-4- Hemolysis

$$\text{Hemolysis } (\%) = \frac{\text{Abs (sample)} - \text{Abs (PBS)}}{Abs\ (Triton) - Abs\ (PBS)} x100$$

Abs: Absorbance at 558 nm

IV-5.4.10. Assessment of binding to Plasma Protein by Fluorescence spectroscopy

Plasma protein binding is an important method for a drug therapy safety that needs to be investigated during each drug-development system. Human serum albumin (HSA) and fibrinogen are the most extensively examined proteins in plasma. HAS and fibrinogen have a high ligand binding capacity, providing a repository for a wide range of ligands that can exist in quantities beyond their plasma solubility [104], [105].

In **Chapter V**, Suspensions of HSA and fibrinogen (Sigma-Aldrich, USA) at 400 µg mL^{-1} and 40 µg mL^{-1}, respectively, were prepared in PBS. Different volumes of a CS/PAMAM dendrimer NPs solution at 0.5 mg mL^{-1}, or PBS as the control, were sequentially added to the cuvette (1, 5, 10 and 20 µL). The fluorescence spectra of the plasma proteins were recorded after each addition using the microplate reader. Fibrinogen was excited at 280 nm and HSA at 290 nm and the emission spectra were both collected from 300 nm to 450 nm. The spectra were obtained using the FluorEssenceTM software.

IV-5.4.11. Immunofluorescence

Immunofluorescence is a technique that uses fluorophores to visualize several cellular antigens. The principle of this technique consists in the incubation of biological samples of interest with an antibody specific linked to a fluorophore (direct fluorescence) or by a secondary antibody bonded to a fluorophore (indirect fluorescence) [106].

In **Chapter IX**, to evaluate the amount of Collagen Type II (Coll type II) present in hCH primary cells, immunofluorescence staining was performed. On the 7th day, the NPs-Hydrogel was flushed from the central channel of the chip with PBS at 50°C. For cell fixation, 10% formaldehyde was added and left to incubate for 15 minutes at RT. Then, the channel was washed twice with PBS. For permeabilization 0.1% Triton X-100 was added and incubated for 10 minutes at RT. Then, the channel was washed twice with PBS. For blocking, the PBS was removed and replaced with blocking buffer (2% BSA in PBS) and left to incubate for 2 hours at RT. The blocking buffer was removed from the central channel and mouse anti-human COL II monoclonal antibody (Laborspirit, Portugal) in PBS solution (1:250) was added and incubated overnight at 4°C. Then, the central channel was washed 3 times with PBS and the secondary antibody Alexa Fluor® 594 donkey anti-mouse (1:500) (Invitrogen, USA) with DAPI (1:1000) (VWR International, USA), in PBS solution and was left to incubate 1.5 hours. The samples were immediately analyzed by confocal microscopy (Leica, SP8, Germany) (Alexa Fluor 594: ex/em 590/617 nm; DAPI: ex/em 358/461 nm).

IV-5.5. Anti-inflammatory activity assay

IV-5.5.1. Assessment of TNF α decrease using different drug delivery systems in static conditions

In **Chapter V**, **VI**, **VII** and **VIII** the therapeutic efficacy of the anti-TNF α Abs-CS/PAMAM dendrimer NP`s, Betamethasone-loaded Ty-GG, Betamethasone-loaded Ty-GG/SF hydrogels and Ty-GG and Ty-GG/SF encapsulated with anti-TNF α mAb-CS/PAMAM dendrimer NPs was evaluated in a cell inflammation model to verify the ability that these systems have to decrease TNF α in the medium. Macrophage-differentiated THP-1 cells were stimulated with Lipopolysaccharide (LPS) (Sigma-Aldrich, USA) and used as *in vitro* model for cell inflammation. Firstly, THP-1 cells were seeded at a density of $1x10^6$ cells mL^{-1} in RPMI with 100 nM phorbol 12-myristate-13-acetate (PMA) (Sigma-Aldrich, USA). After 24 hours of incubation time, the medium in the wells was replaced with RPMI medium without PMA and incubated for another 48 hours. To induce an inflammatory response, 100 ng mL^{-1} of LPS in RPMI medium was added to the macrophage-differentiated THP-1 cells, and the plate was incubated for 5 hours. After LPS stimulation, 0.5 mg mL^{-1} anti-TNF α Abs-CS/PAMAM dendrimer NPs, different concentrations of Betamethasone-loaded Ty-GG and Betamethasone-loaded Ty-GG/SF hydrogels were added to the cells. Culture medium with only PMA was used as control. At each time point ((1 day, 3

days, 7 days) and 14 days in **Chapter VIII**), the culture medium was removed from the wells, centrifugated and the supernatants were stored at -80°C for further analysis.

To determine the degree of TNF α captured/decreased by the anti-TNF α Abs-CS/PAMAM dendrimer NPs, Betamethasone-loaded Ty-GG and Betamethasone-loaded Ty-GG/SF hydrogels and Ty-GG and Ty-GG/SF encapsulated with anti-TNF α mAb-CS/PAMAM dendrimer NPs, the TNF-α concentration in the samples was measured using the Human TNF-alpha DuoSet ELISA kit and the DuoSet Ancillary Reagent Kit 2. The ELISA assay followed the same protocol as described previously. The calibration curve was performed using TNF-α standard solutions, with concentrations ranging from 1000 to 0 pg mL^{-1}, which were also included in the ELISA plate. The samples were analyzed using a microplate reader, with an optical density of 450 nm.

IV-5.5.2. Anti-inflammatory effect in dynamic conditions: Dual-chamber bioreactor and microfluidic platform

In **Chapter VIII**, to evaluate the anti-inflammatory activity of the developed approaches under dynamic conditions, one condition of each delivery system was selected and added to the cells cultured on the lower chamber of the bioreactor. Then, the entire piping system was assembled, the syringes were filled with medium and connected to the syringe pump. The dual-chamber bioreactor was kept at 37°C in a humidified 5% CO_2 atmosphere and the compartment containing the cells and anti-TNF α mAb-CS/PAMAM dendrimer NPs into Ty-GG hydrogel and Ty-GG/SF hydrogels was perfused at a rate of 12.5 µL h^{-1}. After 1, 3,7, and 14 days of perfusion, the culture medium contained in the collection tubes was removed and stored at -80°C. Delivery systems cultured in THP-1 cell-based inflammation *in vitro* models under standard static conditions were used as control.

In **Chapter IX**, to assesses the therapeutic efficacy of NPs-Hydrogel, at each time point (3 and 7 days), the culture medium was collected and stored at -80°C until further analysis.

Human TNF-alpha DuoSET ELISA (R&D Systems, USA) kit and DuoSet Ancillary Reagent Kit 2 (R&D Systems, USA), for the optimum performance of the ELISA kit were used to evaluate the anti-inflammatory activity. TNFα standard solutions with concentrations from 1000 to 0 pg mL^{-1} were also assessed in the ELISA plate to perform the calibration curve. The optical density at 450 nm was read in a microplate reader (Synergy HT, BIO-TEK, Winooski, VT, USA).

IV-6. STATISTICAL ANALYSIS

Statistical analysis was performed using GraphPad Prism 8 version. All quantitative data are presented as mean ± standard deviation (SD). Statistical significances (∗p ≤ 0.05, ∗∗p ≤ 0.01 and ∗∗∗p ≤ 0.001) were determined using specific statistical tests described in the subsection of materials and methods in the different chapters.

In **Chapter V**, statistical analysis was performed using GraphPad Prism 8 version. Statistical significances were determined as *p < 0.05, ** p<0.01 and *** p<0.001. All assays were performed in triplicated and results were presented as mean ± standard deviation.

In **Chapter VI**, GraphPad Prism 8 version was used to conduct the statistical analysis, where a Shapiro-Wilk normality test was formerly performed to evaluate the data normality. Nonparametric Kruskal-Wallis test was applied in all assays, except for weight loss and MTT assay where One Way-ANOVA was used; since there was an absence of normality. Dunn's multiple comparison test was used to compare the mean rank of each condition with the mean rank of every other condition in nonparametric Krustal-Wallis. Turkey's multiple comparisons test was used to compare the mean of each condition with the mean of every other condition in One Way-ANOVA. Statistical significances were determined as * p<0.05, ** p<0.01 and *** p<0.001. All tests were performed in triplicated, and results were presented with mean ± standard deviation.

In **Chapter VII**, statistical analysis was done with GraphPad Prism 8 version, where a Shapiro–Wilk normality test was formerly performed to evaluate the data normality. Statistical significance was obtained as * p < 0.05, ** p < 0.01 or *** p < 0.001. Results are presented as means ± standard deviations, and all assays were performed in triplicate.

In **Chapter VIII**, statistical analysis was performed by GraphPad Prism 8 version, where a Shapiro-Wilk normality test was previously made to evaluate the data normality. Statistical significances were obtained as *p < 0.05. All assays were performed in triplicated and the results were presented with mean ± standard deviation.

In **Chapter IX**, statistical analysis was performed with GraphPad Prism 8 version, where a Shapiro–Wilk normality test was done to assess the data normality. Non-parametric Kruskal-Wallis test was applied to all assays. Statistical significance was obtained as * p<0.05. All results are presented as means ± standard deviations, and all assays were performed in triplicate.

IV-7. REFERENCES

1. Balagani, P., et al., *Dendrimer: a complete drug carrier.* International Journal of Pharmacy Review & Research, 2011. **1**: p. 25.
2. Li, Y. and D. Ju, *Chapter 12 - The Application, Neurotoxicity, and Related Mechanism of Cationic Polymers**Conflict of Interests: All the Figures and Table in "The application, neurotoxicity, and related mechanism of cationic polymers" are original, unpublished materials designed and prepared by Yubin Li and Dianwen Ju. The authors declared that there's no conflict of interests*, in *Neurotoxicity of Nanomaterials and Nanomedicine*, X. Jiang and H. Gao, Editors. 2017, Academic Press. p. 285-329.
3. Araújo, R.V.d., et al., *New Advances in General Biomedical Applications of PAMAM Dendrimers.* Molecules (Basel, Switzerland), 2018. **23**(11): p. 2849.
4. Sohail, I., et al., *Polyamidoamine (PAMAM) dendrimers synthesis, characterization and adsorptive removal of nickel ions from aqueous solution.* Journal of Materials Research and Technology, 2020. **9**(1): p. 498-506.
5. Santos, A., F. Veiga, and A. Figueiras, *Dendrimers as Pharmaceutical Excipients: Synthesis, Properties, Toxicity and Biomedical Applications.* Materials (Basel, Switzerland), 2019. **13**(1): p. 65.
6. Choudhary, S., et al., *Impact of Dendrimers on Solubility of Hydrophobic Drug Molecules.* Frontiers in pharmacology, 2017. **8**: p. 261-261.
7. Fruchon, S. and R. Poupot, *Pro-Inflammatory Versus Anti-Inflammatory Effects of Dendrimers: The Two Faces of Immuno-Modulatory Nanoparticles.* Nanomaterials (Basel, Switzerland), 2017. **7**(9): p. 251.
8. Avti, P.K. and A. Kakkar, *Dendrimers as anti-inflammatory agents.* Brazilian Journal of Pharmaceutical Sciences, 2013. **49**(SPE): p. 57-65.
9. Hayder, M., et al., *Anti-inflammatory properties of dendrimers per se.* The Scientific World Journal, 2011. **11**: p. 1367-1382.
10. Upadhaya, S.K., et al., *Analysis of polyamidoamine dendrimers by isoelectric focusing.* Analytical and bioanalytical chemistry, 2014. **406**(2): p. 455-458.
11. Bedini, E., et al., *Chondroitin, Dermatan, Heparan, and Keratan Sulfate: Structure and Functions*. 2019. p. 187-233.
12. Lindahl, U., et al., *Proteoglycans and sulfated glycosaminoglycans.* Essentials of glycobiology, 2015. **3**.
13. Schiraldi, C., D. Cimini, and M. De Rosa, *Production of chondroitin sulfate and chondroitin.* Applied microbiology and biotechnology, 2010. **87**(4): p. 1209-1220.
14. Malavaki, C., et al., *Recent advances in the structural study of functional chondroitin sulfate and dermatan sulfate in health and disease.* Connective tissue research, 2008. **49**(3-4): p. 133-139.
15. Lamari, F.N. and N.K. Karamanos, *Structure of chondroitin sulfate.* Advances in Pharmacology, 2006. **53**: p. 33-48.
16. Henrotin, Y., et al., *Chondroitin sulfate in the treatment of osteoarthritis: from in vitro studies to clinical recommendations.* Therapeutic advances in musculoskeletal disease, 2010. **2**(6): p. 335-348.
17. Mikami, T. and H. Kitagawa, *Biosynthesis and function of chondroitin sulfate.* Biochimica et Biophysica Acta (BBA)-General Subjects, 2013. **1830**(10): p. 4719-4733.

18. Mizumoto, S., S. Yamada, and K. Sugahara, *Molecular interactions between chondroitin-dermatan sulfate and growth factors/receptors/matrix proteins.* Current opinion in structural biology, 2015. **34**: p. 35-42.
19. Iozzo, R.V. and L. Schaefer, *Proteoglycan form and function: a comprehensive nomenclature of proteoglycans.* Matrix Biology, 2015. **42**: p. 11-55.
20. Susarla, B.T., et al., *Smad proteins differentially regulate transforming growth factor - β - mediated induction of chondroitin sulfate proteoglycans.* Journal of neurochemistry, 2011. **119**(4): p. 868-878.
21. Jerosch, J., *Effects of Glucosamine and Chondroitin Sulfate on Cartilage Metabolism in OA: Outlook on Other Nutrient Partners Especially Omega-3 Fatty Acids.* International journal of rheumatology, 2011. **2011**: p. 969012.
22. Zhou, X., et al., *Chondroitin sulfate and abnormal contact system in rheumatoid arthritis*, in *Progress in molecular biology and translational science*. 2010, Elsevier. p. 423-442.
23. Morales, M.E. and M.A. Ruiz, *16 - Microencapsulation of probiotic cells: applications in nutraceutic and food industry*, in *Nutraceuticals*, A.M. Grumezescu, Editor. 2016, Academic Press. p. 627-668.
24. Sworn, G., *9 - Gellan gum*, in *Handbook of Hydrocolloids (Second Edition)*, G.O. Phillips and P.A. Williams, Editors. 2009, Woodhead Publishing. p. 204-227.
25. Cui, S.W., Y. Wu, and H. Ding, *5 - The range of dietary fibre ingredients and a comparison of their technical functionality*, in *Fibre-Rich and Wholegrain Foods*, J.A. Delcour and K. Poutanen, Editors. 2013, Woodhead Publishing. p. 96-119.
26. Fallourd, M.J. and L. Viscione, *1 - Ingredient selection for stabilisation and texture optimisation of functional beverages and the inclusion of dietary fibre*, in *Functional and Speciality Beverage Technology*, P. Paquin, Editor. 2009, Woodhead Publishing. p. 3-38.
27. Cascone, M.G., et al., *Bioartificial polymeric materials based on polysaccharides.* Journal of Biomaterials Science, Polymer Edition, 2001. **12**(3): p. 267-281.
28. Mano, J.F., et al., *Natural origin biodegradable systems in tissue engineering and regenerative medicine: present status and some moving trends.* Journal of the Royal Society, Interface, 2007. **4**(17): p. 999-1030.
29. Bacelar, A., et al., *Recent progress on gellan gum hydrogels provided by functionalization strategies.* J. Mater. Chem. B, 2016. **4**.
30. Mahdi Aljeboury, M., I. Saleem, and A. Smith, *Gellan gum blends as an in situ gelling nasal delivery system*. 2013.
31. Muthukumar, T., J.E. Song, and G. Khang, *Biological Role of Gellan Gum in Improving Scaffold Drug Delivery, Cell Adhesion Properties for Tissue Engineering Applications.* Molecules (Basel, Switzerland), 2019. **24**(24): p. 4514.
32. Jana, S. and K. Sen, *Gellan gum/PVA Interpenetrating Network Micro-beads for Sustained Drug Delivery.* Materials Today: Proceedings, 2019. **11**: p. 614-619.
33. Matricardi, P., et al., *Preparation and Characterization of Novel Gellan Gum Hydrogels Suitable for Modified Drug Release.* Molecules (Basel, Switzerland), 2009. **14**: p. 3376-91.
34. Wang, K., et al., *Functional Hydrogels and Their Application in Drug Delivery, Biosensors, and Tissue Engineering.* International Journal of Polymer Science, 2019. **2019**: p. 3160732.
35. Coutinho, D.F., et al., *Modified Gellan Gum hydrogels with tunable physical and mechanical properties.* Biomaterials, 2010. **31**(29): p. 7494-502.
36. González-Jiménez, M., et al., *Mutagenic products are promoted in the nitrosation of tyramine.* Food Chemistry, 2017. **216**: p. 60-65.

37. Costa, M.R. and M.B.A. Glória, *MIGRAINE AND DIET*, in *Encyclopedia of Food Sciences and Nutrition (Second Edition)*, B. Caballero, Editor. 2003, Academic Press: Oxford. p. 3940-3947.
38. Finberg, J.P.M. and K. Gillman, *Selective inhibitors of monoamine oxidase type B and the "cheese effect"*, in *International Review of Neurobiology*, M.B.H. Youdim and P. Douce, Editors. 2011, Academic Press. p. 169-190.
39. Yang, J.-A., et al., *In situ-forming injectable hydrogels for regenerative medicine.* Progress in Polymer Science, 2014. **39**(12): p. 1973-1986.
40. Hou, J., et al., *Enzymatically crosslinked alginate hydrogels with improved adhesion properties.* Polymer Chemistry, 2015. **6**(12): p. 2204-2213.
41. Sofia, S.J., A. Singh, and D.L. Kaplan, *PEROXIDASE-CATALYZED CROSSlINKING OF FUNCTIONALIZED POLYASPARTIC ACID POLYMERS.* Journal of Macromolecular Science, Part A, 2002. **39**(10): p. 1151-1181.
42. Kurisawa, M., et al., *Injectable biodegradable hydrogels composed of hyaluronic acid–tyramine conjugates for drug delivery and tissue engineering.* Chemical communications, 2005(34): p. 4312-4314.
43. Jin, R., et al., *Enzyme-mediated fast in situ formation of hydrogels from dextran–tyramine conjugates.* Biomaterials, 2007. **28**(18): p. 2791-2800.
44. Oryan, A., et al., *Chemical crosslinking of biopolymeric scaffolds: Current knowledge and future directions of crosslinked engineered bone scaffolds.* International journal of biological macromolecules, 2018. **107**: p. 678-688.
45. Nilebäck, L., et al., *Silk–silk interactions between silkworm fibroin and recombinant spider silk fusion proteins enable the construction of bioactive materials.* ACS applied materials & interfaces, 2017. **9**(37): p. 31634-31644.
46. Koh, L.-D., et al., *Structures, mechanical properties and applications of silk fibroin materials.* Progress in Polymer Science, 2015. **46**: p. 86-110.
47. Kundu, B., et al., *Silk proteins for biomedical applications: Bioengineering perspectives.* Progress in Polymer Science, 2013. **39**.
48. Nguyen, T.P., et al., *Silk Fibroin-Based Biomaterials for Biomedical Applications: A Review.* Polymers, 2019. **11**(12): p. 1933.
49. Zafar, M.S., et al., *Functional material features of Bombyx mori silk light versus heavy chain proteins.* Biomacromolecules, 2015. **16**(2): p. 606-614.
50. Qi, Y., et al., *A review of structure construction of silk fibroin biomaterials from single structures to multi-level structures.* International journal of molecular sciences, 2017. **18**(3): p. 237.
51. Srisuwan, Y. and Y. Baimark, *Preparation of Biodegradable Silk Fibroin/Alginate Blend Films for Controlled Release of Antimicrobial Drugs.* Advances in Materials Science and Engineering, 2013. **2013**.
52. Seib, F.P., *Reverse-engineered silk hydrogels for cell and drug delivery.* Therapeutic delivery, 2018. **9**(6): p. 469-487.
53. Carissimi, G., et al., *Revealing the Influence of the Degumming Process in the Properties of Silk Fibroin Nanoparticles.* Polymers, 2019. **11**(12): p. 2045.
54. Johnston, E.R., et al., *Interplay between Silk Fibroin's Structure and Its Adhesive Properties.* ACS biomaterials science & engineering, 2018. **4**(8): p. 2815-2824.
55. Wray, L.S., et al., *Effect of processing on silk‐based biomaterials: Reproducibility and biocompatibility.* Journal of Biomedical Materials Research Part B: Applied Biomaterials, 2011. **99**(1): p. 89-101.
56. Kundu, S., *Silk biomaterials for tissue engineering and regenerative medicine*. 2014: Elsevier.

57. Tomeh, M.A., R. Hadianamrei, and X. Zhao, *Silk Fibroin as a Functional Biomaterial for Drug and Gene Delivery.* Pharmaceutics, 2019. **11**(10): p. 494.
58. Yin, Z., et al., *A silk fibroin hydrogel with reversible sol–gel transition.* RSC advances, 2017. **7**(39): p. 24085-24096.
59. Ribeiro, V.P., et al., *Rapidly responsive silk fibroin hydrogels as an artificial matrix for the programmed tumor cells death.* PloS one, 2018. **13**(4).
60. Pritchard, E.M. and D.L. Kaplan, *Silk fibroin biomaterials for controlled release drug delivery.* Expert opinion on drug delivery, 2011. **8**(6): p. 797-811.
61. Chae, M., et al., *3D bioprinting adipose tissue for breast reconstruction*, in *3D Bioprinting for Reconstructive Surgery*. 2018, Elsevier. p. 305-353.
62. Talbot, N.C. and T.J. Caperna, *Proteome array identification of bioactive soluble proteins/peptides in Matrigel: relevance to stem cell responses.* Cytotechnology, 2015. **67**(5): p. 873-883.
63. Funaki, M. and P.A. Janmey, *Chapter 23 - Technologies to Engineer Cell Substrate Mechanics in Hydrogels*, in *Biology and Engineering of Stem Cell Niches*, A. Vishwakarma and J.M. Karp, Editors. 2017, Academic Press: Boston. p. 363-373.
64. Gomillion, C.T. and K.J.L. Burg, *6.22 Adipose Tissue Engineering*, in *Comprehensive Biomaterials II*, P. Ducheyne, Editor. 2017, Elsevier: Oxford. p. 403-415.
65. Conboy, I., et al., *6.13 Tissue Engineering of Muscle Tissue☆*, in *Comprehensive Biomaterials II*, P. Ducheyne, Editor. 2017, Elsevier: Oxford. p. 216-235.
66. Tibbitt, M.W. and K.S. Anseth, *Hydrogels as extracellular matrix mimics for 3D cell culture.* Biotechnology and bioengineering, 2009. **103**(4): p. 655-663.
67. Nicolas, J., et al., *3D Extracellular Matrix Mimics: Fundamental Concepts and Role of Materials Chemistry to Influence Stem Cell Fate.* Biomacromolecules, 2020.
68. Dolcimascolo, A., et al., *Innovative Biomaterials for Tissue Engineering*, in *Biomaterial-supported Tissue Reconstruction or Regeneration*. 2019, IntechOpen.
69. Chen, F.-M. and X. Liu, *Advancing biomaterials of human origin for tissue engineering.* Progress in polymer science, 2016. **53**: p. 86-168.
70. Shaunak, S., et al., *Polyvalent dendrimer glucosamine conjugates prevent scar tissue formation.* Nature biotechnology, 2004. **22**: p. 977-84.
71. Rahman, M., et al., *Morphological Characterization of Hydrogels.* Polymers and Polymeric Composites: A Reference Series, 2019: p. 819-863.
72. Li, J. and D.J. Mooney, *Designing hydrogels for controlled drug delivery.* Nature reviews. Materials, 2016. **1**(12): p. 16071.
73. Maitra, J. and V. Shukla, *Cross-linking in hydrogels - a review.* Am J Polym Sci, 2014. **4**: p. 25-31.
74. Hu, W., et al., *Advances in crosslinking strategies of biomedical hydrogels.* Biomaterials science, 2019. **7**(3): p. 843-855.
75. Roberts, J.J., et al., *A comparative study of enzyme initiators for crosslinking phenol-functionalized hydrogels for cell encapsulation.* Biomaterials research, 2016. **20**: p. 30-30.
76. Prodanovic, O., et al., *Tyramine modified alginates via periodate oxidation for peroxidase induced hydrogel formation and immobilization.* Reactive and Functional Polymers, 2015. **93**: p. 77-83.
77. Finlayson, D., C. Rinaldi, and M.J. Baker, *Is infrared spectroscopy ready for the clinic?* Analytical chemistry, 2019. **91**(19): p. 12117-12128.
78. Baker, M.J., et al., *Using Fourier transform IR spectroscopy to analyze biological materials.* Nat Protoc, 2014. **9**(8): p. 1771-91.

79. Kitayama, T. and K. Hatada, *NMR spectroscopy of polymers*. 2013: Springer Science & Business Media.
80. Tognarelli, J.M., et al., *Magnetic Resonance Spectroscopy: Principles and Techniques: Lessons for Clinicians.* Journal of clinical and experimental hepatology, 2015. **5**(4): p. 320-328.
81. Ebnesajjad, S. and P.R. Khaladkar, *10 - Failure Analysis of Fluoropolymer Parts*, in *Fluoropolymer Applications in the Chemical Processing Industries (Second Edition)*, S. Ebnesajjad and P.R. Khaladkar, Editors. 2018, William Andrew Publishing. p. 357-400.
82. Farré, M. and D. Barceló, *Chapter 1 - Introduction to the Analysis and Risk of Nanomaterials in Environmental and Food Samples*, in *Comprehensive Analytical Chemistry*, M. Farré and D. Barceló, Editors. 2012, Elsevier. p. 1-32.
83. Sousa, F.D.B.d. and C.H. Scuracchio, *The use of atomic force microscopy as an important technique to analyze the dispersion of nanometric fillers and morphology in nanocomposites and polymer blends based on elastomers.* Polímeros, 2014. **24**(6): p. 661-672.
84. Nellist, P.D., *Scanning transmission electron microscopy*, in *Science of microscopy*. 2007, Springer. p. 65-132.
85. Maguire, C.M., et al., *Characterisation of particles in solution - a perspective on light scattering and comparative technologies.* Sci Technol Adv Mater, 2018. **19**(1): p. 732-745.
86. Mourdikoudis, S., R.M. Pallares, and N.T. Thanh, *Characterization techniques for nanoparticles: comparison and complementarity upon studying nanoparticle properties.* Nanoscale, 2018. **10**(27): p. 12871-12934.
87. Itagaki, H., *Chapter 3 - Fluorescence Spectroscopy*, in *Experimental Methods in Polymer Science*, T. Tanaka, Editor. 2000, Academic Press: Boston. p. 155-260.
88. Wiederschain, G.Y., *The ELISA guidebook*. 2009, Springer Nature BV.
89. Abraham, J., et al., *14 - Rheological characteristics of nanomaterials and nanocomposites*, in *Micro and Nano Fibrillar Composites (MFCs and NFCs) from Polymer Blends*, R.K. Mishra, S. Thomas, and N. Kalarikkal, Editors. 2017, Woodhead Publishing. p. 327-350.
90. Borzacchiello, A., F.D. Sala, and L.A. Ambrosio, *10 - Rheometry of polymeric biomaterials*, in *Characterization of Polymeric Biomaterials*, M.C. Tanzi and S. Farè, Editors. 2017, Woodhead Publishing. p. 233-253.
91. Cilurzo, F., et al., *Injectability evaluation: an open issue.* AAPS PharmSciTech, 2011. **12**(2): p. 604-9.
92. Ardebili, H. and M.G. Pecht, *Chapter 4 - Characterization of Encapsulant Properties*, in *Encapsulation Technologies for Electronic Applications*, H. Ardebili and M.G. Pecht, Editors. 2009, William Andrew Publishing: Oxford. p. 181-224.
93. Argenta, D.F., et al., *Chapter 3 - Hydrogel Nanocomposite Systems: Physico-Chemical Characterization and Application for Drug-Delivery Systems∗∗Dedicated to Professor Claudia Maria Oliveira Simões on the occasion of her retirement*, in *Nanocarriers for Drug Delivery*, S.S. Mohapatra, et al., Editors. 2019, Elsevier. p. 81-131.
94. Li, M. and J. Li, *12 - Biodegradation behavior of silk biomaterials*, in *Silk Biomaterials for Tissue Engineering and Regenerative Medicine*, S.C. Kundu, Editor. 2014, Woodhead Publishing. p. 330-348.
95. Kaur, G. and J.M. Dufour, *Cell lines: Valuable tools or useless artifacts.* Spermatogenesis, 2012. **2**(1): p. 1-5.
96. Li, Z., *5.43 - In Vitro Micro-Tissue and -Organ Models for Toxicity Testing*, in *Comprehensive Biotechnology (Second Edition)*, M. Moo-Young, Editor. 2011, Academic Press: Burlington. p. 551-563.

97. Riss, T.L., et al., *Cell viability assays*, in *Assay Guidance Manual [Internet]*. 2016, Eli Lilly & Company and the National Center for Advancing Translational Sciences.
98. Rampersad, S.N., *Multiple applications of Alamar Blue as an indicator of metabolic function and cellular health in cell viability bioassays.* Sensors, 2012. **12**(9): p. 12347-12360.
99. Uggeri, J., et al., *Calcein-AM is a detector of intracellular oxidative activity.* Histochemistry and cell biology, 2000. **122**(5): p. 499-505.
100. Tawakoli, P., et al., *Comparison of different live/dead stainings for detection and quantification of adherent microorganisms in the initial oral biofilm.* Clinical oral investigations, 2013. **17**(3): p. 841-850.
101. Dragan, A.I., et al., *Characterization of PicoGreen interaction with dsDNA and the origin of its fluorescence enhancement upon binding.* Biophysical journal, 2010. **99**(9): p. 3010-3019.
102. Atabaev, T.S. and N.H. Hong, *Chapter 4 - Silica-Based Nanostructures in Biomedicine*, in *Nano-Sized Multifunctional Materials*, N.H. Hong, Editor. 2019, Elsevier. p. 73-88.
103. Dobrovolskaia, M.A., et al., *Method for analysis of nanoparticle hemolytic properties in vitro.* Nano letters, 2008. **8**(8): p. 2180-2187.
104. Horbett, T.A., *Fibrinogen adsorption to biomaterials.* Journal of biomedical materials research. Part A, 2018. **106**(10): p. 2777-2788.
105. Shakya, A.K., et al., *Chapter 8 - First-Pass Metabolism Considerations in Pharmaceutical Product Development*, in *Dosage Form Design Considerations*, R.K. Tekade, Editor. 2018, Academic Press. p. 259-286.
106. Joshi, S. and D. Yu, *Chapter 8 - Immunofluorescence*, in *Basic Science Methods for Clinical Researchers*, M. Jalali, F.Y.L. Saldanha, and M. Jalali, Editors. 2017, Academic Press: Boston. p. 135-150.

SECTION 3

EXPERIMENTAL SECTION

Chapter V

PAMAM Dendrimers Functionalized with an Anti-TNF α Antibody and Chondroitin Sulfate for Treatment of Rheumatoid Arthritis

Chapter V

PAMAM Dendrimers Functionalized with an Anti-TNF α Antibody and Chondroitin Sulfate for Treatment of Rheumatoid Arthritis[4]

ABSTRACT

Rheumatoid arthritis is a chronic autoimmune disease characterized by joint synovial inflammation, along with cartilage and bone tissue destruction. Dendrimers can offer new opportunities as drug delivery systems of molecules of interest. Herein we aimed to develop poly(amidoamine) dendrimers (PAMAM), functionalized with chondroitin sulfate (CS), lined with anti-TNF α antibodies (Abs) to provide anti-inflammatory properties. Physicochemical characterization demonstrated that anti-TNFα Abs-CS/PAMAM dendrimer NPs were successfully produced. The in vitro studies revealed that CS/PAMAM dendrimer NPs did not affect the ATDC5 and THP-1 cell lines' metabolic activity and proliferation, presenting good cytocompatibility and hemocompatibility. Moreover, anti-TNFα Abs-CS/PAMAM dendrimer NPs showed suitable TNF α capture capacity, making them appealing for new immunotherapies in RA patients.

Keywords: Rheumatoid arthritis, inflamed joint, PAMAM dendrimer, Chondroitin sulfate, Anti-TNF α, Polyclonal antibody

[4]This chapter is based on the following publication:

Oliveira I. M., Gonçalves C., Oliveira E. P., Simón-Vasquez R., Silva-Morais A., González-Fernandez A., Reis R. L., Oliveira J. M. "PAMAM Dendrimers Functionalized with an Anti-TNF α Antibody and Chondroitin Sulfate for Treatment of Rheumatoid Arthritis" Materials Science and Engineering: C, 2021, 121. doi.org/10.1016/j.msec.2020.111845.

V-1. GRAPHICAL ABSTRACT

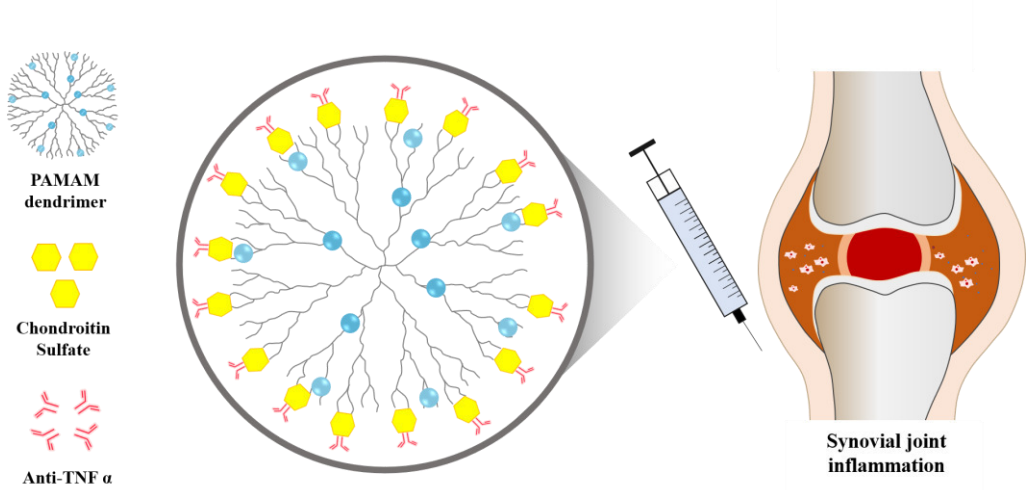

V-2. INTRODUCTION

Modern lifestyle has been accompanied by an increased incidence of age-related and autoimmune diseases. Autoimmune disorders have several etiologies, from genetic susceptibility or immune dysregulation to environmental factors [1, 2].

Rheumatoid arthritis (RA) is a systemic autoimmune disorder with undisclosed cause, characterized by polyarthritis and joint synovial inflammation, as well as cartilage and bone tissue destruction [3].

Currently, RA treatment strategies include disease-modifying anti-rheumatic drugs (DMARDs), typically supported by non-steroidal anti-inflammatory drugs (NSAIDs) and/or corticosteroids to reduce the pain and inflammation [4]. However, many side effects are associated with these treatments, limiting their therapeutic efficacy. Therefore, it is essential to develop and validate new drug delivery strategies for RA treatment that specifically target inflamed joints and attenuate the damage to healthy tissues [5].

High levels of the pro-inflammatory Tumor Necrosis Factor alfa (TNF α) are observed in the synovial fluid and the synovium of patients with RA, making this cytokine an appealing target for

treatment [6]. Targeting TNF α with anti-TNF α agents, such as antibodies (Abs) and fusion proteins, has shown to induce long-term improvements in RA manifestations and signs.[7] For this reason, several smart nanocarriers for delivering drugs have been developed and tested for RA treatment [8], [9].

Dendrimers offer new opportunities as drug delivery systems with improved effectiveness and specificity. These dendrimers NPs allow a time-controlled delivery, of single or multiple compounds, reducing the uptake of toxic agents and side effects of certain drugs, while improving and prolonging its bioavailability [10],[11]. In particular poly(amidoamine) (PAMAM) dendrimers, polymeric structures sphere-shaped with branches, have been studied as nanocarriers for targeted drug delivery. The functional groups on the surface allow their modification to conjugate small molecules and Abs [12]. The potential of PAMAM dendrimers in the treatment of RA has been increasingly explored, and literature demonstrated that these nanoparticles allow a controlled release of molecules of interest and have anti-inflammatory properties [13],[14]. Moreover, the combination of dendrimers with synthetic and natural biodegradable polymers could benefit a closer interaction with living cells, enhancing its biological performance [15]. Chondroitin sulfate (CS) is one of the main components of the extracellular matrix (ECM) and is abundant in several living tissues, such as cartilage. This sulfated glycosaminoglycan shows numerous appealing characteristics like antioxidant, antiatherosclerotic, antithrombosis, anticoagulant and non-immunogenic properties, and as a natural polymer, it is also biocompatible and biodegradable [16],[17],[18]. Moreover, considering this delivery system is intended to be administrated in the intra-articular space, and CS is one of the main components of the cartilage tissue, the functionalization of the PAMAM dendrimers with this natural polymer may increase its affinity with the tissue of interest (cartilage).

Herein it was hypothesized that PAMAM dendrimers functionalized with CS and linked to specific Abs could have advantageous properties for the treatment of RA. Thus, this work consists of the development and evaluation of an innovative approach for RA treatment, based on targeted delivery, using an anti-TNF α Abs linked to PAMAM dendrimers. The PAMAM were functionalized with CS and synthesized as nanocarriers, to help receptor-ligand interaction and low toxicity, while the covalently linked anti-TNF α Abs provides anti-inflammatory properties.

The successful functionalization of PAMAM dendrimer NPs was confirmed through their physicochemical characterization, using energy-dispersive X-ray spectroscopy, proton nuclear magnetic

resonance spectroscopy, Fourier transform infrared spectroscopy, Scanning Transmission Electron Microscope, Dynamic light scattering, electrophoretic light scattering, and Rheometer methodologies. In vitro studies were performed to analyze the effect of the PAMAM dendrimer NPs on the viability and proliferation of human chondrogenic, lymphocytic, and monocytic cells. The dendrimers' internalization, NPs-induced hemolysis, interaction with plasma proteins, and anti-inflammatory activity were also evaluated.

V-3. MATERIAL AND METHODS

V-3.1. Synthesis of the CS/PAMAM dendrimer NPs

Chondroitin sulfate A sodium salt from bovine trachea (463.363 g/mol) and PAMAM carboxylic-terminated dendrimers (generation 1.5, 20% methanolic solution), with an ethylenediamine core, were purchased from Sigma-Aldrich (USA). CS/PAMAM dendrimer NPs were prepared as referred by Shaunak et al., 2004, with some modifications. Briefly, 20 g mol^{-1} of (2-N-Morpholino)ethanesulfonic acid hydrate (MES) (Sigma-Aldrich) was added to 50 g L^{-1} of PAMAM (diluted in MES), then N-(3-Dimethylaminopropyl)-N′-ethylcarbodiimide hydrochloride (EDC) (Sigma-Aldrich, USA) (4 equivalents) and sulfo-NHS N-Hydroxysulfosuccinimide sodium salt ≥98% (HPLC) (Sigma-Aldrich, USA) (2 equivalents), also in MES, were mixed and stirred for 15 minutes, with the first solution of PAMAM. Then, chondroitin sulfate (20 equivalents) was added with EDC (4 equivalents) and the reactions were mixed and stirred for 15 minutes. The PAMAM mixture was added to the CS mixture and stirred for 24 hours. The solution was dialyzed against distilled water using a Dialysis Tubing membrane, benzoylated (Laborspirit, Loures), for 48 hours. CS/PAMAM dendrimer NPs were obtained by freezing the solution at -80°C and freeze-drying (Telstar- LyoAlfa 10/15) for approximately 7 days.

V-3.2. Labelling of CS/PAMAM dendrimer NPs with fluorescein isothiocyanate (FITC)

The CS/PAMAM dendrimer NPs were linked to Fluorescein isothiocyanate (FITC) (Sigma-Aldrich, USA). Firstly, 10 mg mL^{-1} of CS/PAMAM solution was prepared in a carbonate-bicarbonate coupled buffer (pH 9.2). Then 50 µL of the FITC (10 mg mL^{-1}) / DMSO (anhydrous dimethyl sulfoxide) solution

was added per each mL of CS/PAMAM dendrimer NPs solution under agitation and kept in the dark at 4°C for 8 hours. Lastly, the FITC-labelled CS/PAMAM dendrimer NPs were dialyzed in ultrapure water for 48 hours. The product was achieved after dialysis and freeze-drying.

V-3.3. Physicochemical characterization

V-3.3.1. Proton nuclear magnetic resonance spectroscopy (^{1}H-NMR)

CS/PAMAM dendrimer NPs was solubilized in deuterium water oxide (1 mg mL^{-1}) at room temperature and the sample was transferred to NMR tube. The NMR spectra were obtained on a Bruker AVANCE 400 spectrometer, at 50 °C using a resonance frequency of 400 MHz. To process and analyze the obtained spectra, MestReNova 9.0 Software was used.

V-3.3.2. Fourier transform infrared spectroscopy (FTIR)

The CS/PAMAM dendrimer NPs were mixed with potassium bromide and molded into a transparent pellet using a press. Transmission spectra were acquired on an IR Prestige-21 spectrometer (Shimadzu, Japan), using wavenumber range between 4400 and 400 cm^{-1}, 32 scans and a resolution of 4 cm^{-1}.

V-3.3.3. Energy-dispersive X-ray spectroscopy (EDS)

CS/PAMAM dendrimer NPs samples were coated with carbon (Fisons Instruments, Polaron SC 508, UK). The electric current was set at 18 mA with a coating time of 120 seconds. The sulfur, calcium, sodium, carbon, and oxygen elemental analysis were achieved through an X-ray detector (Pentafet model 5526, UK) attached to the S-360 microscope, and a voltage of 10 kV was used.

V-3.3.4. Dynamic light scattering (DLS) and electrophoretic light scattering (ELS)

Particle size and zeta potential of CS/PAMAM dendrimer NPs were measured in a particle analyzer (Zetasizer Nano ZS, Malvern Instruments, UK). Particle size analysis was made by DLS technique, in an

ultrapure water solution with 1 mg mL^{-1} of CS/PAMAM dendrimer NPs. Zeta potential of nanoparticles was evaluated by ELS, at pH 7.4 phosphate buffer saline (PBS) solution.

V-3.3.5. Atomic force microscopy (AFM)

The morphology of the nanoparticles was evaluated through AFM. The CS/PAMAM dendrimer NPs were dissolved in ultrapure water to achieve a final concentration of 1 mg mL^{-1} and transferred to the surface of a 9.9 mm mica disc (Agar Scientific, England). The samples were evaluated using the Tapping model TM with a MultiMode AFM connected to a NanoScope III controller (Veeco, USA) with noncontact silicon nanoprobes (ca. 300 kHz) from Nanosensors, Switzerland. Images were plane-fitted using the third-degree-flatten procedure included in NanoScope software version 1.5. The particle morphology and size were both analyzed with NanoScope 1.5 software.

V-3.3.6. Scanning Transmission Electron Microscope (STEM)

The size and morphology of CS/PAMAM dendrimer NPs were also obtained by STEM. The nanoparticles were diluted in ultrapure water to a final concentration of 0.1 mg mL^{-1} and then 2 µL were placed on copper grids at 37° C overnight for observation.

V-3.3.7. Rheometer methodologies

Rheological analyses were performed using Kinexus pro+rheometer with the acquisition software rSpace (Malvern). The rotational experiments were performed using a cone-plate measuring system composed by an upper stainless-steel cone of 40 mm of diameter and a cone angle of 4°. Shear viscosity was obtained as a function of the shear rate, from 0.001 to 0.1 s^{-1} at 37°C. The oscillatory experiments were made to obtain frequency sweep curves, after LVER determination.

V-3.4. TNF-α Abs linked to CS/PAMAM Dendrimer Nanoparticles

V-3.4.1. Functionalization

The CS/PAMAM dendrimer NPs linked to a rabbit polyclonal anti-TNF-α antibody (ab7742, Abcam, United Kingdom) was obtained through a crosslinking reaction. A 0.2 g L^{-1} solution of CS/PAMAM in 5 mL MES was mixed with EDC (4 equivalents) and NHS (2 equivalents) for 15 minutes. Next, 20 equivalents of anti-TNF α Abs were added with EDC (4 equivalents) and were stirred for 15 minutes. Then, CS/PAMAM dendrimer NPs mixture was added to anti-TNF α Abs mixture and stirred for 24 hours. The solution was dialyzed against distilled water for 48 hours. Anti-TNF α Abs-CS/ PAMAM dendrimer NPs were obtained through dialysis and freeze-drying.

V-3.4.2. Physicochemical characterization

The immobilization of the Abs by CS/PAMAM was evaluated by fluorescence spectrometer FP-8500 (Jasco). Briefly, anti-TNF α Abs-CS/PAMAM dendrimer NPs and CS/PAMAM dendrimer NPs were mixed with a secondary antibody anti-rabbit IgG-labelled with Alexa Fluor 488 dye (Molecular probes, USA), in PBS solution (1:1000) for 1 hour to detect the conjugation of anti-TNF α Abs to CS/PAMAM dendrimer NPs. The solutions were centrifuged, and the supernatants were visualized in the spectrometer.

The determination of the degree of TNF α captured by anti-TNF α Abs-CS/PAMAM dendrimer NPs was analyzed by the incubation of the dendrimers with 1000 pg mL^{-1} of TNF α (Peprotech, United Kingdom) for 6 hours at room temperature. After centrifugation, the supernatants were kept at -80 °C for further analysis. Then, the free TNF-α concentration in the samples after incubation was measured using a Human TNF-alpha DuoSET ELISA kit (R&D systems, USA) and a DuoSet Ancillary Reagent Kit 2 (R&D systems, USA). The calibration curve was prepared using TNF-α standard solutions, with concentrations from 0 to 1000 pg mL^{-1}, which were also included in the ELISA plate. The samples were measured in the microplate reader (Synergy HT, BIO-TEK) with an optical density of 450 nm.

V-3.5. *In vitro* studies

V-3.5.1. Cell cultures

Chondrogenic ATDC 5 cell line (European Collection of Authenticated Cell Culture, England), human monocytic cell line (THP-1) and differentiated human T lymphocyte cell line (Jurkat) were used to analyses the effects of CS/PAMAM dendrimer NPs in cartilage and immune system cells.

ATDC 5 cell line was expanded in DMEM medium (Dulbecco's Modified Eagle Medium: Nutrient Mixture F-12, Alfagene, Portugal). THP-1 and Jurkat cell lines were expanded in RPMI medium (RPMI 1640 Medium, GlutaMAX™ Supplement, HEPES, Gibco, Life Technologies, Grand Island, NY), supplemented with 10% Heat Inactivated Fetal Bovine Serum, 2 mM glutamine and 100 U mL^{-1} of penicillin/streptomycin (PAA; Pasching, Austria), under standard culture conditions (37 °C in a humidified atmosphere, containing 5 v/v CO_2).

The experiments with the THP-1 and Jurkat cells were carried out in the Immunology laboratory at the University of Vigo and for that reason, some experimental conditions differ from the ATDC 5 cell line. When the conditions or the equipment used were different, it was specifically mentioned.

V-3.5.2. MTS assay

Cell viability was evaluated by MTS [3-(4,5-dimethylthiazol-2-yl)-5-(3-carboxymethoxyphenyl)-2(4-sulfophenyl)-2H-tetrazolium] (VWR International, USA). The ATDC 5 cells were seeded at a density of 1×10^4 cells per well and incubated with different concentrations of CS/PAMAM dendrimer NPs, for 72 hours. Cells cultured with regular medium (without CS/PAMAM dendrimer NPs) were used as a control. At each time point, cell culture medium (DMEM-F12) was replaced by culture medium without phenol red, containing MTS at a 5:1 ratio, and was incubated for 3 hours. Then, 100 µL from each well were passed into a 96-well plate and the absorbance was read at 490 nm.

The Jurkat and (differentiated) THP-1 cell lines were seeded in a 96-well plate with a density of $3x10^4$ and $1x10^4$ cells per well, respectively. The CS/PAMAM dendrimer NPs were administrated in serial dilutions 1:2 starting with the concentrations of 0.5 mg mL^{-1}. The cells were incubated with the

CS/PAMAM dendrimer NPs for 48 hours, in standard cell culture conditions. The remaining procedure was performed as previously mentioned for the ATDC 5 cell line.

V-3.5.3. DNA quantification

The proliferation of the ATDC5 cells upon CS/PAMAM dendrimer NPs administration was analyzed by DNA quantification, using the Quanti-IT PicoGreen dsDNA Assay Kit (Alfagene, Portugal).

ATDC5 cells were seeded at a density of 1×10^4 cells per well and incubated with different concentrations of CS/PAMAM dendrimer NPs for 72 hours. Cells cultured with DMEM-F12 medium were used as control. After the incubation period, the cells were lysed in ultrapure water and stored at -80°C for further analysis. The calibration curve was performed using DNA standards, prepared with concentrations ranging from 2 to 0 μL mL^{-1}. Both the calibration curve and the cells` samples were quantified following the manufacturer's instructions. The fluorescence was acquired at 480/20 nm of excitation and emission of 528/20 nm, in a microplate reader. The DNA concentration on the cells samples was determined using the standard curve.

V-3.5.4. Flow cytometry

For flow cytometry analysis the ATDC 5 cells were seeded at a density 4×10^5 cells per well (in a 24-well plate) and cultured with different concentrations of FITC-labelled CS/PAMAM NPs (0.01, 0.1 and 0.5 mg mL^{-1}), for 72 hours. ATDC5 cells cultured in DMEM-F12 without CS/PAMAM dendrimer NPs were used as control. The samples were measured using a FACSCalibur flow cytometer (BD Biosciences Immunocytometry Systems, CA, USA) and the results were analyzed by the Flowing Software 2. THP-1 cells were incubated for 3, 6 and 24 hours with 0.5 mg mL^{-1} of CS/PAMAM dendrimer NPs at a cell density of $1x10^5$ cells per well, in a 24-well plate. THP-1 cells cultured with only RPMI medium were used as control. The samples were measured in a BD Accuri C6 flow cytometer (BD Biosciences, USA) and the analysis was performed in the cytometer software.

V-3.5.5. Fluorescence microscopy

For this assay the ATDC5 cells were seeded at a density of 1×10^4 cells per well in a 24-well plate, with different concentrations of FITC-labelled CS/PAMAM dendrimer NPs, using the previously tested time points. Then, cells were fixed with 10% formalin (Sigma-Aldrich, USA) and stained with 4,6-diamidino-2-phenylindole, dilactate (DAPI blue, VWR International, USA) for nuclei and Texas Red-X phalloidin (Sigma- Aldrich, USA) for actin filaments of the cytoskeleton. The cells were observed under the fluorescence microscope (Axiolmager, Z1, Zeis Inc., Oberkochen, Germany).

The differentiated THP-1 cells were seeded at a density of $4x10^4$ cells per well in a 24-well plate and incubated for 3 and 6 hours with FITC-labelled CS/PAMAM dendrimer NPs. At each time point the cells were stained with Hoechst 33342 (1:1000) (Immnochemistry Technologies) and observed under a Nikon Eclipse Ti2 microscope (Nikon Instruments, Inc.).

V-3.5.6. Hemolytic properties of CS/PAMAM dendrimer NPs

Erythrocytes from whole mouse blood were used to test the hemolytic properties of CS/PAMAM dendrimer NPs. The blood was extracted into a tube with EDTA and an aliquot of 5 mL was diluted with PBS (1:10) in a pre-weighted tube. After centrifugation and washing steps, the pellet was weighed and diluted with PBS to a final concentration of 3% w/v.

The CS/PAMAM dendrimer NPs were diluted in PBS and administrated in serial dilutions 1:2 starting with the concentrations of 0.5 mg mL^{-1}. PBS and Triton x-100 were used as negative control and positive control, respectively. The plates were incubated for 4 hours, centrifuged and the supernatant was collected. The samples were read at 588 nm absorbance using a microplate reader (Greiner Bio-one). The percentage of hemolysis in the samples was calculated according to the following Equation:

$$\text{Hemolysis } (\%) = \frac{\text{Abs (sample)} - \text{Abs (PBS)}}{Abs\ (Triton) - Abs\ (PBS)} x100$$

Abs: Absorbance at 558 nm

V-3.5.7. Assessment of binding to Plasma Protein by Fluorescence spectroscopy

Suspensions of human albumin (HSA) and fibrinogen (Sigma-Aldrich, USA) at 400 μg mL^{-1} and 40 μg mL^{-1}, respectively, were prepared in PBS. Different volumes of a CS/PAMAM dendrimer NPs solution at 0.5 mg mL^{-1}, or PBS as the control, were sequentially added to the cuvette (1, 5, 10 and 20 μL). The fluorescence spectra of the plasma proteins were recorded after each addition using the microplate reader. Fibrinogen was excited at 280 nm and HSA at 290 nm and the emission spectra were both collected from 300 nm to 450 nm. The spectra were obtained using the FluorEssenceTM software.

V-3.5.8. Assessment of TNF α capture by anti-TNF α Abs-CS/PAMAM dendrimer NPs

The therapeutic efficacy of the NPs was evaluated in a cell inflammation model, by assessing the anti-TNF α Abs-CS/PAMAM dendrimer NP`s ability to capture TNF α in the medium. Macrophage-differentiated THP-1 cells were stimulated with Lipopolysaccharide (LPS) (Sigma-Aldrich, USA) and used as in vitro model for cell inflammation. Firstly, THP1 cells were seeded at a density of $1x10^6$ cells/mL in RPMI with 100 nM phorbol 12-myristate-13-acetate (PMA) (Sigma-Aldrich, USA). After 24 hours of incubation time, the medium in the wells was replaced with RPMI medium without PMA and incubated for another 48 hours. In order to induce an inflammatory response, 100 ng mL^{-1} of LPS in RPMI medium were added to the macrophage-differentiated THP-1 cells, and the plate was incubated for 5 hours. After LPS stimulation, 0.5 mg mL^{-1} of anti-TNF α Abs-CS/PAMAM dendrimer NPs were added to the cells, using a medium with only PMA were used as control. At each time point (1 day, 3 days, and 7 days), the culture medium was removed from the wells, centrifugated and the supernatants were stored at -80 °C for further analysis.

To determine the degree of TNF α captured by the anti-TNF α Abs-CS/PAMAM dendrimer NPs, the TNF-α concentration in the samples was measured using the Human TNF-alpha DuoSET ELISA kit (R&D systems, USA) and the DuoSet Ancillary Reagent Kit 2 (R&D systems, USA). The calibration curve was performed using TNF-α standard solutions, with concentrations ranging from 1000 to 0 pg mL^{-1}, which were also included in the ELISA plate. The samples were analysed using a microplate reader, with an optical density of 450 nm (Synergy HT, BIO-TEK).

V-3.6. Statistical analysis

Statistical analysis was performed using GraphPad Prism 8 version. Statistical significances were determined as *p < 0.05, ** p<0.01 and *** p<0.001. All assays were performed in triplicated and results were presented as mean ± standard deviation.

V-4. RESULTS AND DISCUSSION

V-4.1. Physicochemical characterization

V-4.1.1. Chemical analysis of CS/PAMAM dendrimer NPs

This study focused on the functionalization of PAMAM with CS, conjugated to an anti-TNF α Abs. It was hypothesized that this strategy can be used for RA treatment, by helping receptor-ligand interaction, reducing toxicity, and providing anti-inflammatory properties. The first steps consisted of the functionalization of PAMAM dendrimer NPs with CS and, later on, with anti-TNF α Abs. Then, it was followed by the physicochemical characterization and further evaluation of their biological effect.

Firstly, the successful functionalization of the PAMAM with CS was confirmed through chemical analysis. **Figure V-1** shows EDS analysis, ^{1}H-NMR and FTIR spectra of the CS/PAMAM dendrimer NPs.

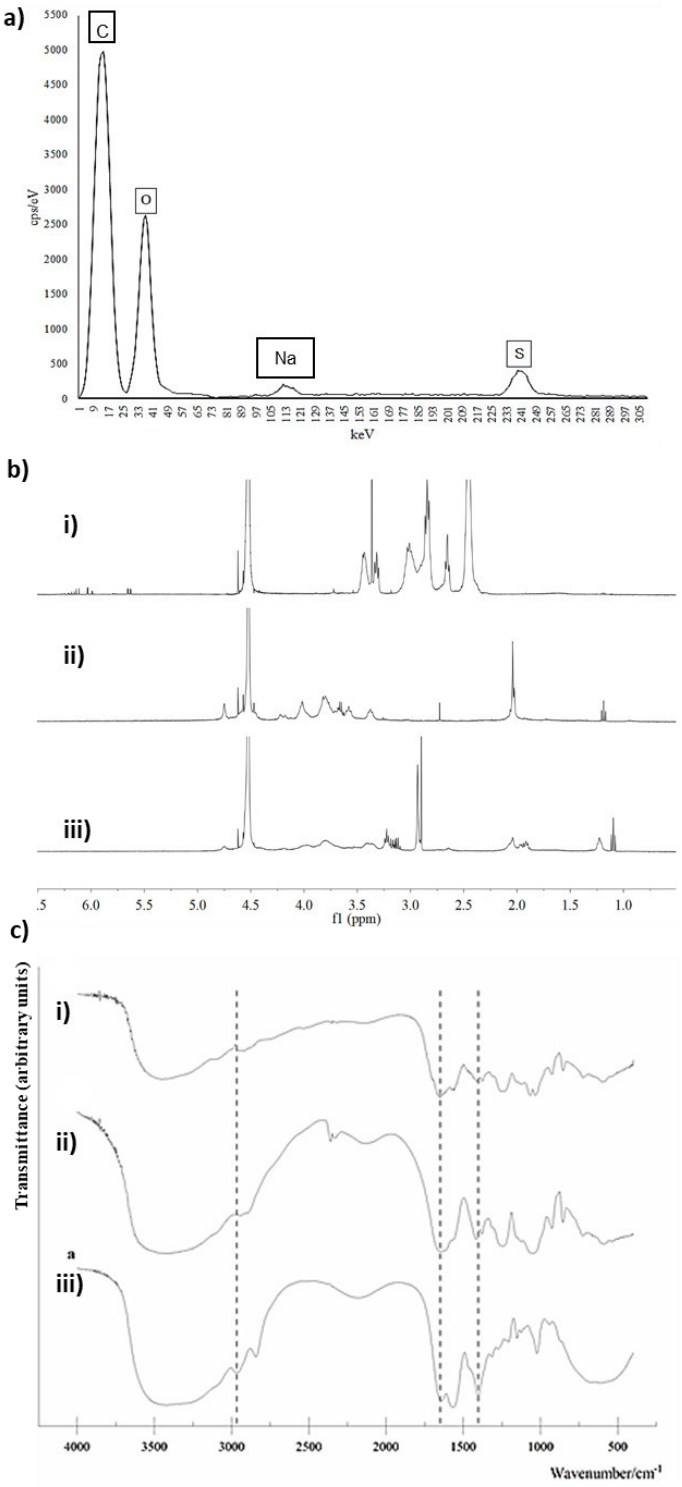

Figure V-1 - EDS analysis (a) of CS/PAMAM dendrimer and ^{1}H-NMR in D_2O at 50°C (b) and FTIR (c), of PAMAM dendrimer (G=1.5) (i), CS (ii) and the CS/PAMAM dendrimer NPs (iii).

The EDS analysis showed the presence of C, O, and Na atoms at a percentage of 58.3%, 34.5% and 0.3%, respectively (Figure 1a). The analysis of functionalized PAMAM also detected a sulfur group (6.9%) that does not exist on the PAMAM structure but is a characteristic chemical element of chondroitin sulfate, suggesting the PAMAM dendrimer`s modification with CS was accomplished [19],[20].

The PAMAM dendrimer is a branched polymer with an abundance of protons, making the identification of full structure on the ^{1}H-NMR and FTIR spectrum a challenge. Nevertheless, some characteristic chemical shifts can be identified, such as the well-defined signals visible on the ^{1}H-NMR spectra (Figure 1 b). Typical shifts of PAMAM dendrimer were observed at 2.4, 2.6, 2.7, 2.8 and 3.5 ppm [21],[22] but also chemical shifts of chondroitin sulfate (CS-A sodium salt from bovine trachea) were found. The signal at 2.04 ppm corresponds to the CH3 and at 4.75 ppm to the ^{1}H signal of the 4-sulfated site of the galactosamine unit of chondroitin sulfate, following the literature [23],[24]. Therefore, in the functionalized NPs it was observed the presence of characteristics peaks from both the PAMAM and CS, indicating the modification was successful. Some EDC residues were also observed specifically the chemical shifts of 1.1 ppm and 1.9 ppm. The modification was further confirmed by the FTIR analysis of the chondroitin sulfate, PAMAM dendrimer, and CS/PAMAM dendrimer NPs (Figure 1 c). In the spectra of CS/ PAMAM dendrimer NPs it was visible the strong and broad peak of absorption at around 3400 cm^{-1}, assigned to the stretching vibration of the structural N-H overlapping the O-H stretching [25]. Other characteristic absorption bands are noticeable, for instance: 1650 cm^{-1} for amide bands, 1240 cm^{-1} for S=O stretching vibration, 1415 cm^{-1} and 1379 cm^{-1} for the coupling of the C–O stretching vibration and O–H variable-angle vibration of –COOH, as described in the literature [26]. The absorption band assigned to the α-(1,4) glycoside bond was observed at 925 cm^{-1} [25]. Regarding the PAMAM G1.5 spectra, it was also detectable the leading characteristic bands such as a characteristic –C = O stretching vibrations around 1645 cm^{-1} due to the presence of a free ester (C = O) group. At the end, expected on half the generation material, [27] and a peak at 1560 cm^{-1} assigned to an O–H or N–H stretching vibration. Moreover, peaks at 2970 cm^{-1} and 2840 cm^{-1} assigned to –CH3 and –CH2– stretching vibrations as well as the broad peak around 3430 cm^{-1} attributed to an O–H stretching vibration were also observed.[25],[28] The CS/PAMAM dendrimer NPs spectrum showed a very similar spectrum to the CS, which is expected from a successful modification, due to the

surface coverage allowed by such a large molecule. However, CS is a large molecule able to cover the PAMAM surface, being possible that it hides some of the PAMAM characteristic peaks.

V-4.1.2. Morphology, size and zeta potential of CS/PAMAM NPs

The morphology of the CS/PAMAM dendrimer NPs was evaluated in dry conditions, using AFM and STEM techniques, and in wet conditions by DLS and ELS, **Figure V-2**.

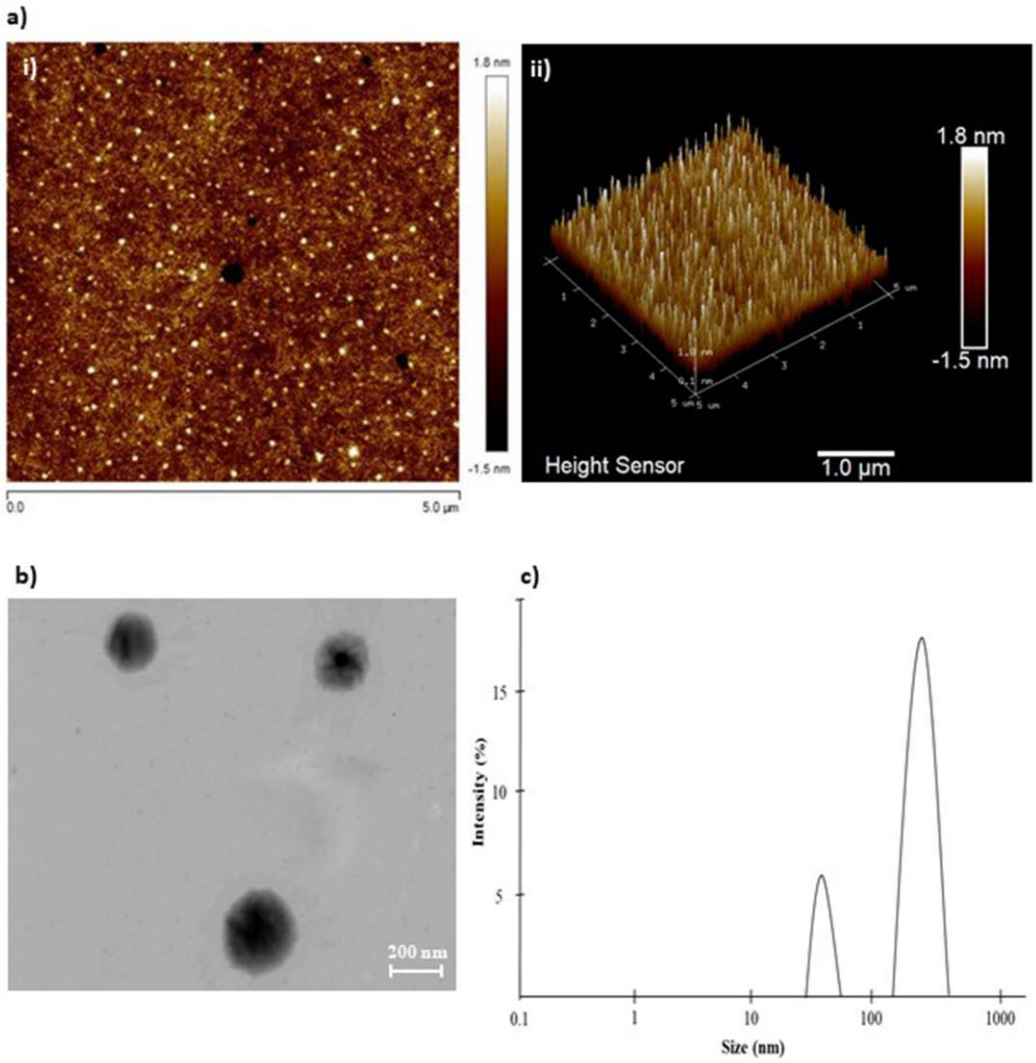

Figure V-2 – (a) AFM analysis (i) 2D, (ii) 3D (b) STEM analysis of the CS/PAMAM dendrimer NPs and (c) DLS analysis.

The characterization clearly showed that CS/PAMAM dendrimer NPs had a globular shape, were monodisperse and presented a polymer coating around PAMAM dendrimer NPs, which is in accordance with the data found in literature, with/using modified PAMAM dendrimer NPs [24],[29].

DLS and ELS were also used to analyze the CS/PAMAM dendrimer NPs. The data obtained by DLS (Figure 2 c) showed the presence of two peaks, one small peak with an intensity of approximately 48 nm corresponding to the modified dendrimer (i) and a second peak with an intensity of approximately 300 nm that corresponds to aggregated NPs (ii). The aggregation NPs can be caused by the interactions between noncovalent free sulfur groups/carboxyl groups of Chondroitin sulfate and/or not functionalized PAMAM dendrimer NPs (carboxyl-terminal dendrimer) and amino groups of Chondroitin sulfate [30]. Moreover, zeta potential data indicated that CS/PAMAM dendrimer NPs in PBS, at neutral pH, presented negative charge of approximately -15 mV. The data showed that the negatively charged sulfur groups in CS/PAMAM dendrimer NPS were mostly distributed at the surface of the nanoparticles, as observed in other studies, [31] which once again reveals the effectiveness of the functionalization of PAMAM dendrimer NPs with CS.

V-4.1.3. Rheological properties of CS/PAMAM dendrimer NPs

Drug delivery requires minimally invasive deployment strategies, therefore, the biomaterial used needs to have a suitable flow rate (even at the maximum pressure applicable), and be easily injected without being affected or deformed [32]. The rheological examination was performed using the rotational and oscillatory modes, resulting in flow behavior and mechanical analysis of the produced NPs. Flow behavior is described by the fitting of the experimental data with the power-law model: $\tau=k\cdot\gamma n$, where τ is the shear stress (Pa), γ is the shear rate (s^{-1}), k is the consistency coefficient (Pa.sn) and n is the flow behavior index, being n = 1 for Newtonian liquid, n < 1 for shear-thinning fluid (non-Newtonian) and n > 1 for swelling plastic fluid [33]. **Figure V-3** shows the rheological analysis of the CS/PAMAM at 0.1 mg mL^{-1} and 0.5 mg mL^{-1}, from rotational and oscillatory experiments.

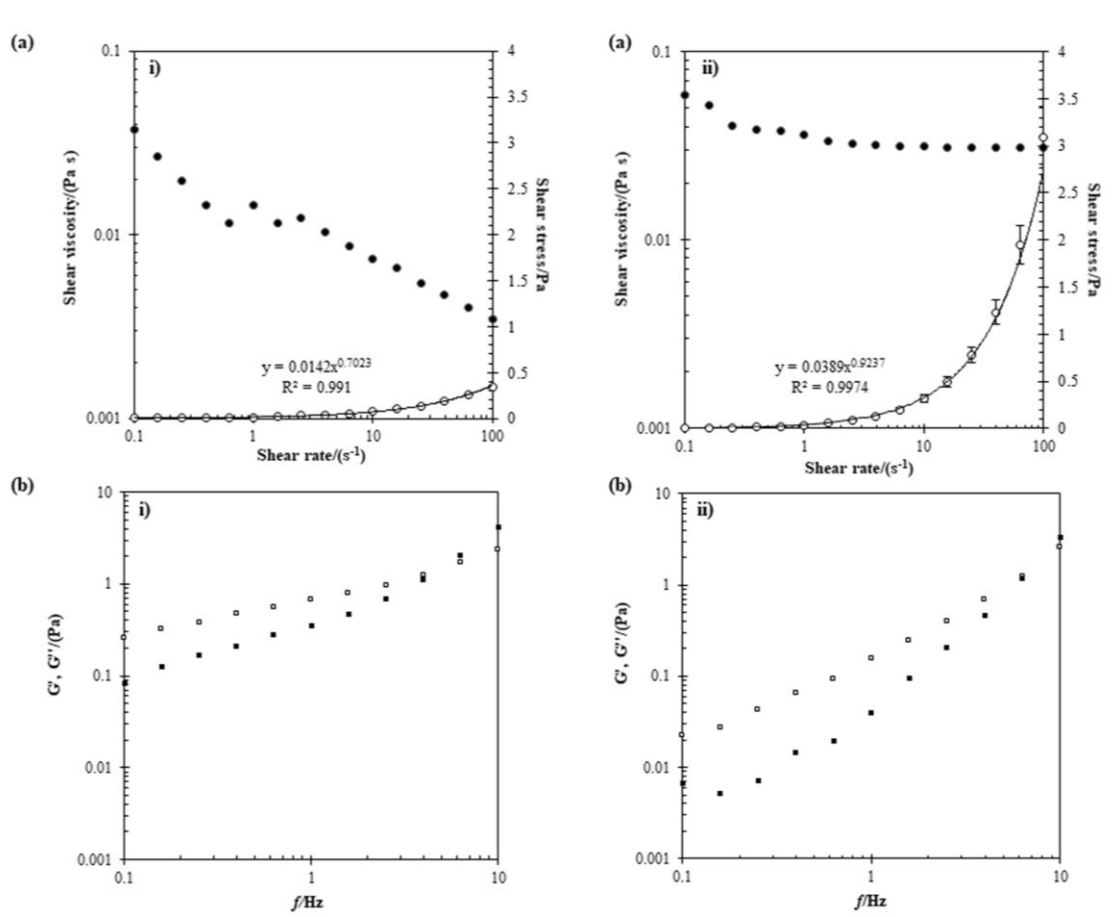

Figure V-3 - Rheological rotational (a) and oscillatory (b) assays performed at concentrations 0.1 mg mL^{-1} (i) and 0.5 mg mL^{-1} (ii) of CS/PAMAM dendrimers.

The shear-thinning behavior of both solutions was clearly shown by the plot of the viscosity in the function of shear rate curves. Moreover, from the flow curves it was obtained the flow behavior index for each solution, which is approximately 0.70 and 0.92 for 0.1 mg mL^{-1} and 0.5 mg mL^{-1} CS/PAMAM solutions, respectively. These values categorize the samples as shear-thinning fluid, having the highest concentration a more stable behavior when higher stress was applied. Usually, shear-thinning fluids are characterized by high viscosity in static conditions and in dynamic conditions with a viscosity close to water (n=1), thus decreasing the pressure during injection and facilitating their administration [34]. The obtained results are in accordance with the previous experiments because CS/PAMAM dendrimer NPs have a viscosity close to the water, mainly at the highest concentration (0.5 mg mL^{-1}). Thus, nanoparticles have a good flow behavior to be injected.

V-4.1.4. Anti-TNF-α binding determination

The CS/PAMAM dendrimer NPs were conjugated to a polyclonal rabbit anti-TNF-α Abs, and to evaluate their effectiveness, fluorescence spectroscopy was performed using CS/PAMAM dendrimer NPs with and without linked Abs, in the presence of secondary antibodies labelled with Alexa Fluor 488 dye, **Figure V-4**.

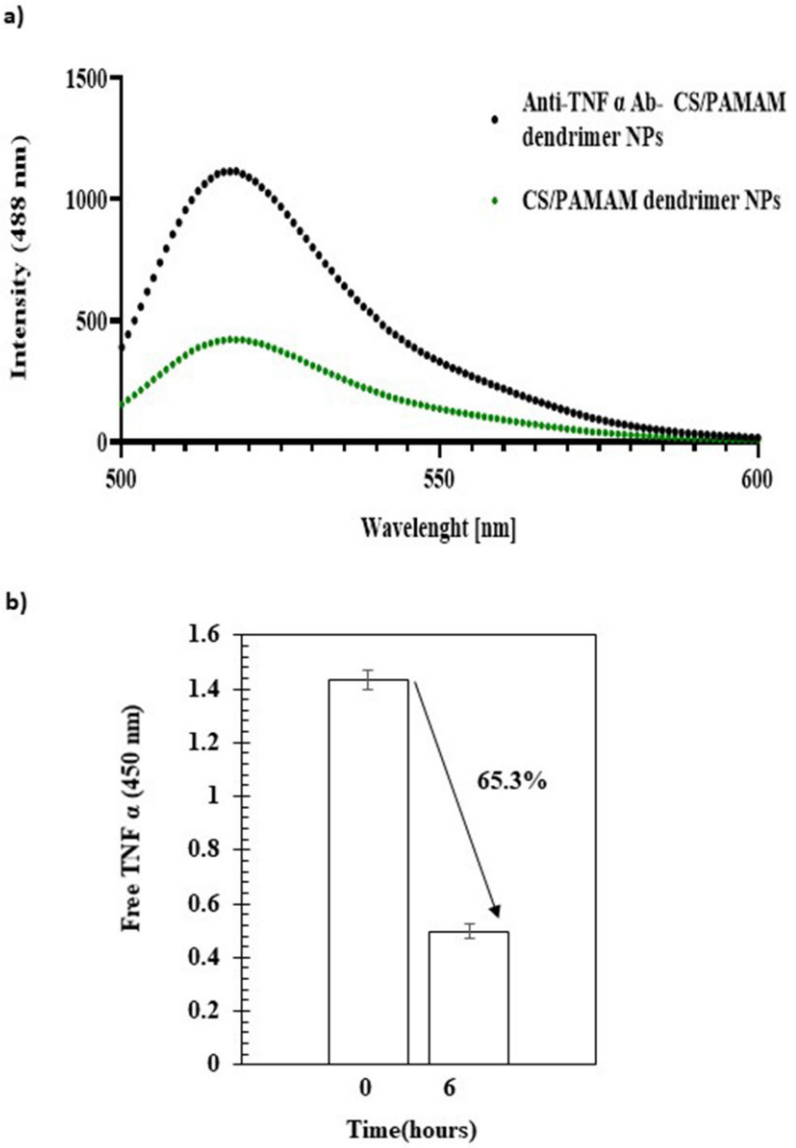

Figure V-4 - a) Fluorescence spectroscopy of CS/PAMAM dendrimer NPs and anti-TNF α Abs-CS/ PAMAM dendrimer NPs. b) Percentage of TNF α captured by anti-TNF α Abs-CS/ PAMAM dendrimer NPs.

The emission spectra of Alexa 488 (between 500 and 600 nm) for the CS/PAMAM dendrimer NPs without anti-TNF α Abs showed a low fluorescence intensity (≃400), indicative of some unspecific secondary Abs binding. However, the fluorescence of the anti-TNF α Ab-CS/PAMAM dendrimer NPs was significantly higher (≃1100), thus suggesting the conjugation with the anti-TNF α Abs was accomplished.

The anti-TNF α Abs-CS/PAMAM dendrimer NP`s capacity to capture TNF α was evaluated by the difference between the initial and the final amount of free TNF α in solution, after adding the dendrimer NPs. The results demonstrated that after 6 hours of reaction, between TNF α and anti-TNF α Abs-CS/PAMAM dendrimer NPs, the degree of capture was 65.27%, Figure 4 b. By maintaining this capture rate, the maximum can be reached in less than 24 hours. The size of the CS/PAMAM dendrimers NPs after antibody binding was 58 ± 2.3 nm and the zeta potential -8.3 ± 5.7 mV, indicating the NPs increased in size and became less negative after binding with antibody. Literature reports that positively charged particles are typically internalized by cells more extensively than negatively charged nanoparticles [35],[36]. On the other hand, positive nanoparticles are more toxic [37]. For that reason, the negatively charged surface of the NPs would favor the cytocompatibility, and in turn, the NPs could be specifically internalized or bound to TNF α expressing cells, avoiding unspecific cell entry.

V-4.2. *In vitro* studies

V-4.2.1. Influence of CS/PAMAM dendrimer NPs of ATDC 5, THP1 and Jurkat on cell viability and proliferation

The influence of CS/PAMAM dendrimer NPs on cell viability and proliferation was evaluated by MTS and DNA quantification assays (**Figures V-5** (a) (i) and (ii), respectively), using three different concentrations of NPs (0.01, 0.1 and 0.5 mg mL^{-1}) on the ATDC5 cell line for 3 days.

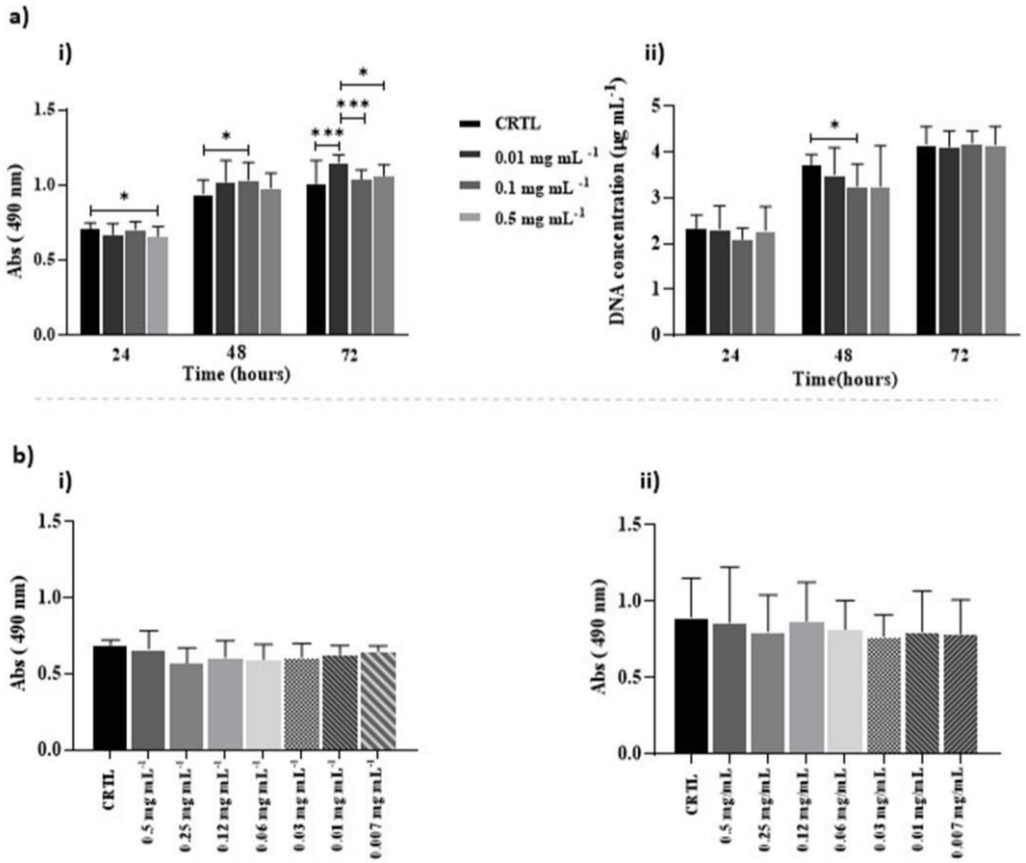

Figure V-5 - MTS assay (a, i) and DNA quantification (a, ii) of the ATDC 5 cells. THP1 cells (b, i) and Jurkat cells' (b, ii) MTS assay. In image a) the cells were incubated with media (CTRL) and different CS/PAMAM dendrimer NPs concentrations C1, C2 and C3 (0.01, 0.1 and 0.5 mg mL^{-1}) at different time points (24, 48 and 72 hours). In b) the cells were incubated with the CS/PAMAM dendrimer NPs at 0.5 mg mL^{-1} for 48 hours. Significant differences * p<0.001 and *p< 0.05, by non-parametric Kruskal-Wallis test (a,i), (a,ii) and (b,ii); Ordinary one-way ANOVA (b,i). THP1 and Jurkat cells have not significant differences.

The MTS and DNA quantification results demonstrated that although there were some significant differences between the tested NPs concentrations, the cell viability and proliferation increased over time in a similar trend than control cells. The cytotoxicity of PAMAM dendrimer depends actively on their generation and nature of functional surface groups, where high generations and cationic terminal groups often exhibit high toxicity, whereas anionic and neutral dendrimers show small or no toxic effects. Furthermore, modification of the dendrimer`s surface with negatively charged or neutral moieties decreases its cytotoxicity [38]. The obtained results are in the accordance with data reported in the literature, as the produced negatively charged CS/PAMAM dendrimer NPs demonstrated no harmful effects on both cell viability and proliferation in the ATDC 5 cell line.

Besides evaluating the metabolic activity and cell proliferation of NPs in ATDC 5 cells, it is vital to study their effect on the immune system. When immune cells are exposed to the stimulation they can activate several signaling pathways that promote different responses, such as proliferation, differentiation, migration, and inflammatory and immune response [39]. Macrophages are relevant cells of the innate immune system, implicated in the recognition of foreign pathogens, such as nanoparticles, via interaction of their surface structures with different types of Pattern Recognition Receptors (PRRs). These cells are also responsible for the production of pro-inflammatory and anti-inflammatory cytokines and pathogen clearance by phagocytosis [40]. In fact, TNF-α is released by immune cells such as macrophages or lymphocytes [41]. Having this in mind, the effect of CS/PAMAM dendrimer NPs on THP-1 and Jurkat cell line was assessed (Figure 5b). The results obtained in the MTS assay indicated that CS/PAMAM dendrimer NPs were cytocompatible at all the tested concentrations, in both cell lines. Moreover, there were no significant differences in the cells` metabolic activity after dendrimer administration, when compared with the control cells.

V-4.2.2. Internalization of the CS/PAMAM NPs by ATDC 5 and THP-1 cell lines

The quantitative and qualitative analysis of the internalization of FITC-labelled dendrimer NPs by cells was performed by flow cytometry assay and fluorescence microscopy, using ATDC 5 and THP-1 cell lines, **Figure V-6**.

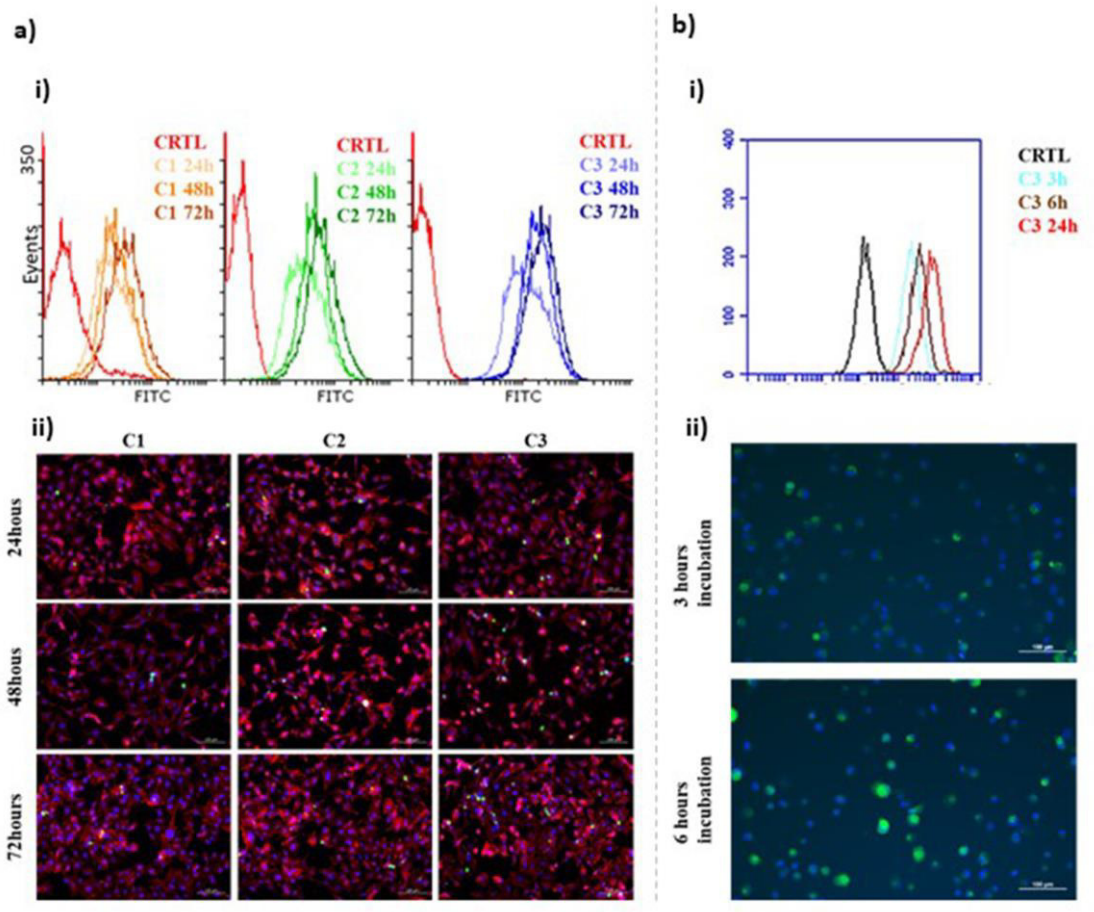

Figure V-6 - Flow cytometry histograms (a) (i) and Fluorescence microscopy images (a) (ii) of the ATDC 5 cell line cultured in presence of different concentrations (C1 (0.01mg mL^{-1}), C2 (0.1 mg mL^{-1}) and C3 (0.5 mg mL^{-1})) of FITC labelled CS/PAMAM dendrimer NPs for 72 hours. Flow cytometry (b) (i) and Fluorescence microscopy (b) (ii) of differentiated THP-1 cells with CS/PAMAM dendrimer NPs incubation at different time points (3 and 6 hours). Cell nuclei are stained in blue (Hoechst) and CS/PAMAM dendrimer NPs in green (FITC). Scale bar: 100 µm (b).

ATDC 5 cells were cultured with different concentrations of fluorescently labelled dendrimer NPs and flow cytometry analysis showed that all concentrations obtained a high percentage of internalization at 72 hours (Figure 6 (a) (i)). NPs at 0.5 mg mL^{-1} reached the highest and constant rate of internalization over time (**Table V-1**).

Table V-1 - Percentage of internalization of FITC labelled CS/PAMAM dendrimer NPs by ATDC5 cells at different concentrations of dendrimer and time points.

INTERNALIZATION (%)			
CONDITIONS/ TIME (H)	**24 h**	**48 h**	**72 h**
C1: 0.01 mg/ml	45.98%	56.08%	74.19%
C2: 0.1 mg/ml	66.90%	91%	95.32%
C3: 0.5 mg/ml	98.99%	99.36%	99.88%

Qualitative images obtained with a fluorescence microscope showed typical morphology of the cells (marked by DAPI and phalloidin), suggesting survival and healthy proliferation in all the tested concentrations (Figure 6 (a) (ii)). The results showed that C3 (0.5 mg mL^{-1}) obtained almost the maximum internalization rate at 24 hours. For that reason, henceforth the experiments were performed with only the concentration of 0.5 mg mL^{-1} of CS/PAMAM dendrimer NPs.

The macrophage-differentiated THP-1 cell line was also analyzed as they are phagocytic cells and can internalize dendrimers on a large scale. The FITC-labelled CS/PAMAM dendrimer NPs at 0.5 mg mL^{-1} were incubated with THP-1 cells at different time points. The flow cytometry analysis showed that the internalization rate was high after 3 hours of incubation, in comparison with the control, and increased throughout the incubation time (Figure 6 (b) (i)). The internalization of the CS/PAMAM dendrimer NPs by the macrophage cells was further confirmed by fluorescence microscopy, as depicted in Figure 6 (b) (ii).

Fluorescence microscopy confirmed the internalization of the CS/PAMAM dendrimer NPs, detected also by flow cytometry. The microscopy images showed that after 3 hours and 6 hours of incubation the cells internalized the dendrimers in a high rate and that the CS/PAMAM dendrimer NPs were present in both the nucleus and cytoplasm of the cells. Despite the high internalization rate of the dendrimers in ATDC 5 and macrophage-differentiated THP-1 cells, there was not a reduction on the cell viability, as seen in Figure 5. Hence, the use of the CS/PAMAM dendrimer NPs for the targeted delivery of anti-TNF α Abs antibody could be a promising strategy to reduce the inflammation, based on the high

internalization rate and the absence of negative effects on the macrophage viability. Moreover, CS/PAMAM dendrimer NPs could be used to explore other therapies targeting inflammatory macrophages.

V-4.2.3. Hemolytic properties and interaction of the CS/PAMAM dendrimer NPs with plasma proteins

Nanoparticles for medical applications must be subjected to biocompatibility assessments before their approval for administration in patients. The in vitro evaluation of the hemocompatibility is an essential part of preclinical development for NPs that will be injected through the intravenous route, or any other route in which they can be in contact with blood [42]. According to the American Society for Testing and Materials (ASTM), medical devices that have direct or indirect blood contact must not be hemolytic [43]. Following the ASTM guidelines, a biomaterial that induces the lysis of about 0% to 2% of the red blood cells is not considered hemolytic. When the burst of blood cells is about 2% to 5%, the material is partially hemolytic. For values superior to 5%, it indicates an apparent hemolytic effect [44].

The physicochemical properties of nanoparticles can also drastically influence plasm protein`s functions and might originate adverse effects, such as conformational changes, which can affect their stability and loss of protein functionality, alter the interaction with other elements or induce an inflammatory or autoimmune response [45],[46].

Human plasma is constituted of many proteins such as albumin (HSA) and fibrinogen, two of the most representative plasma proteins that are attached to the surface of several nanoparticles after entering the blood circulation [47]. For this reason, it is essential to analyses the effect of the dendrimers on those proteins, to ensure there will be no deleterious or unexpected effects upon interaction.

The hemolysis properties and interaction of the CS/PAMAM dendrimer NPs with plasma proteins are represented in **Figures V-7** (a) and (b), respectively.

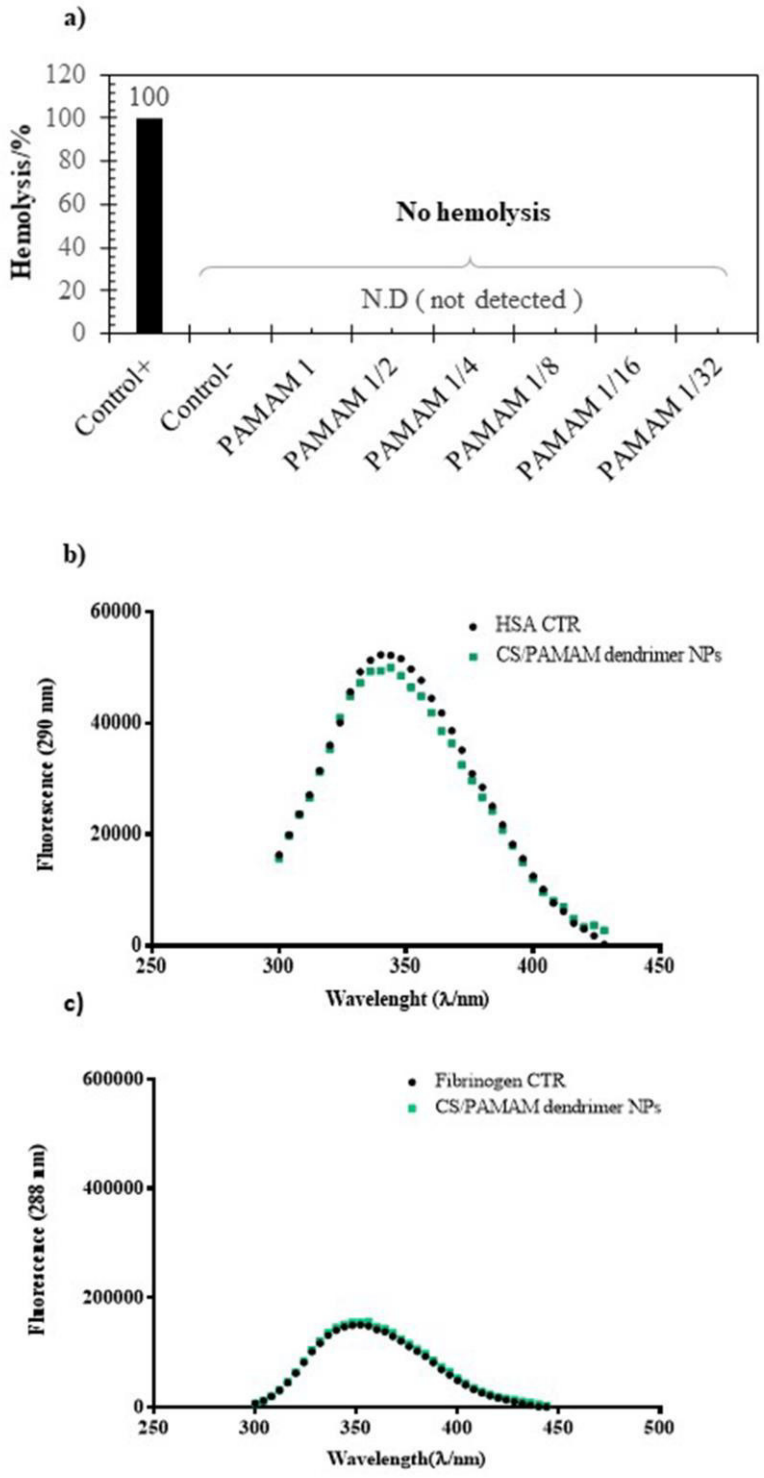
a)
Hemolysis/%
120
100
80
60
40
20
0
100
No hemolysis
N.D (not detected)
Control+
Control-
PAMAM 1
PAMAM 1/2
PAMAM 1/4
PAMAM 1/8
PAMAM 1/16
PAMAM 1/32
b)
Fluorescence (290 nm)
60000
40000
20000
0
HSA CTR
CS/PAMAM dendrimer NPs
250
300
350
400
450
Wavelenght (λ/nm)
c)
Fluorescence (288 nm)
600000
400000
200000
0
Fibrinogen CTR
CS/PAMAM dendrimer NPs
250
300
350
400
450
500
Wavelength(λ/nm)

Figure V-7 - Percentage of Hemolysis induced by the CS/PAMAM dendrimer NPs at different dilutions in contact with blood cells (a) and tryptophan emission spectra of an HSA (b) and fibrinogen (c) protein suspension in PBS, before and after incubation with CS/PAMAM dendrimer NPs at 20 μg mL^{-1}.

The analysis of the CS/PAMAM dendrimer NPs showed the absence of hemolysis at any of the concentrations tested (Figure 7 (a)). The absorbance in the supernatant of the samples was similar to the absorbance of the negative control (only PBS). Hence, the CS/PAMAM dendrimer NPs are biocompatible with red blood cells.

Then it was evaluated the NPs interactions with plasm protein (Figures 7 (b) and (c)).

The comparison of the protein spectra, after incubation with the NPs, with the spectra of the proteins alone showed the absence of relevant spectral shifts, even at the highest concentration tested, namely 20 μL of the sample. Only a minor change was observed for HSA, probably associated with an interaction between the NPs and the protein. Hence, the NPs are safe regarding protein structure, although alterations in other plasma proteins cannot be ruled out from this experiment. However, the lack of cytotoxicity, hemolytic effect, or major protein structural changes showed the excellent hemocompatibility of the NPs and their suitability for an in vivo administration.

V-4.2.4. Assessment of metabolic activity, cell proliferation and TNF α capture by anti-TNF α Abs-CS/PAMAM dendrimer NPs in THP-1 cell line

The influence of anti-TNF α Abs conjugation to PAMAM dendrimer NPs on metabolic activity and cell proliferation was evaluated using the THP-1 cell line. The previous experiments were performed with CS/ PAMAM dendrimer NPs without anti-TNF α and the results did not show significant toxicity, in the different concentrations tested. In this assay, the THP-1 cells were incubated for 7 days with the anti-TNF α Abs-CS/PAMAM dendrimer NPs (0.5 mg mL^{-1}), to assess the effect of this conjugation on cells` viability and proliferation.

The anti-TNF α Abs-CS/PAMAM dendrimer NPs' capacity to decrease the levels of TNF α present in the medium was evaluated using differentiated THP-1 cells, which were stimulated with LPS to induce an inflammatory scenario. Upon establishment of the inflammation, 4 conditions were tested: 1) cells without treatment, 2) cells with anti-TNF α Abs-CS/ PAMAM dendrimer NPs, 3) cells with CS/PAMAM dendrimer NPs without Abs and 4) cells with anti-TNF α Abs alone. Cells differentiated with PMA but without LPS stimulation were used as control. **Figure V-8** shows the metabolic activity and cell

proliferation of THP-1 cells upon NPs administration and the quantity of free TNF α (uncaptured) over time of incubation with the NPs.

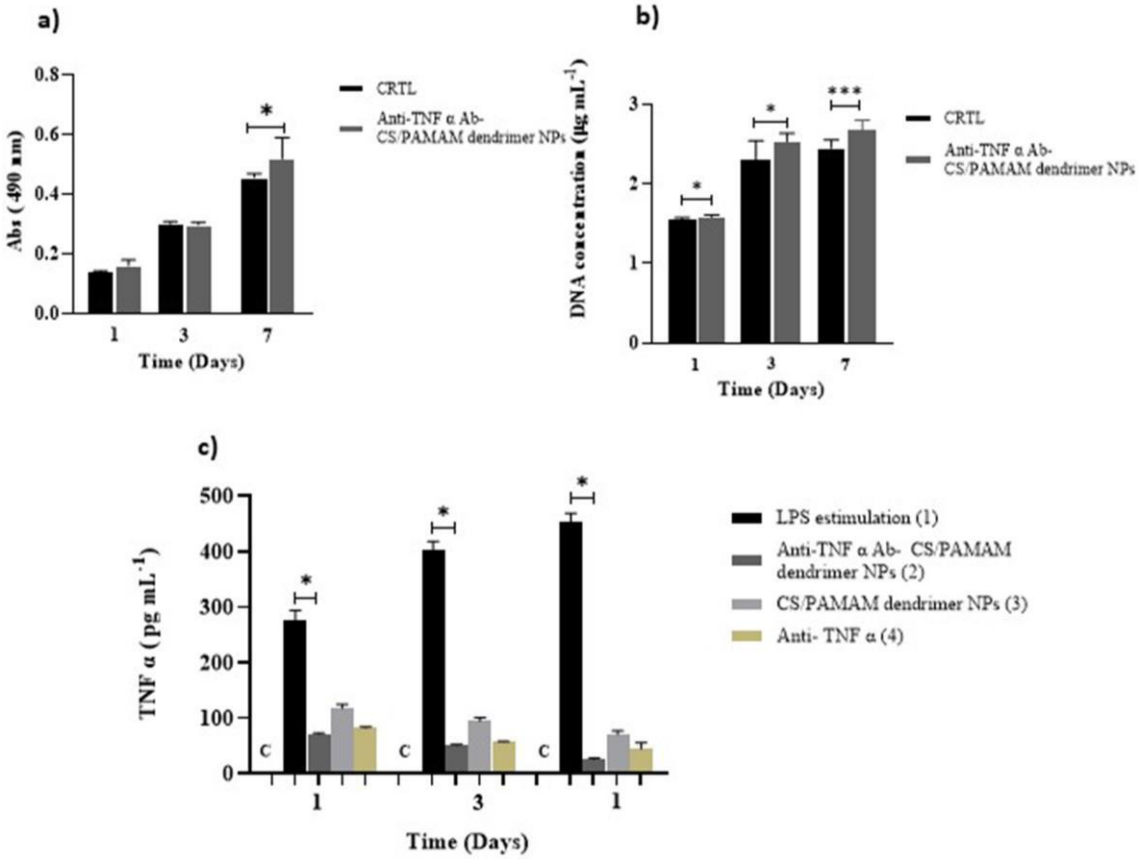

Figure V-8 - Metabolic activity (a), Cell proliferation (b) and amount of uncaptured TNF α (c) under different conditions: cells differentiated with PMA but without LPS stimulation (C); cells stimulated with LPS ,without treatment (1), anti-TNF α Abs-CS/ PAMAM (2), CS/PAMAM, without Abs conjugated (3) and anti-TNF α Abs (4). Significant differences *** p<0.001 and *p< 0.05. Mann-Whitney test (a), Unpaired t test (b) nonparametric Kruskal-Wallis test (c).

The cells` metabolic activity (Figure V-8 a) and cell proliferation (Figure 8b) were not affected by the presence of anti-TNF α Abs-CS/PAMAM dendrimer NPs when compared to control cells.

The TNF α capture by anti-TNF α Abs-CS/PAMAM dendrimer NPs and the capacity of the CS-modified dendrimer NPs to inhibit the release of TNF α were also evaluated. The results obtained showed that untreated LPS-stimulated cells presented high levels of free TNF α in the medium, compared to the remaining conditions, as expected. The levels of TNF α dropped significantly in the cells treated with anti-TNF α Abs CS/PAMAM dendrimer NPs, being even lower than the CS/PAMAM

dendrimer NPs or the anti-TNF α Abs alone. Moreover, this trend was maintained throughout the time tested, as the TNF α levels continued decreasing up to 7 days (Figure 8c).

The CS/PAMAM dendrimer NPs without anti-TNF α Abs also showed the ability to reduce TNF α levels significantly. These results are consistent with the literature that indicates that CS administration has an inhibitory effect on the release of TNF-α release, due to the anti-inflammatory activity of this sulfated glycosaminoglycan [48],[49],[50]. The combination of both effects, namely the anti-inflammatory effect of the CS and the presence of the anti-TNF α Abs, has probably increased the therapeutic efficacy of anti-TNF α Abs-CS/PAMAM dendrimer NPs by reducing the production and enhancing the capture of the pro-inflammatory cytokine. Although no statistically significant differences were observed, a trend was visible as the free TNF α decreases over time, with a more pronounced effect on the dendrimers with Abs, indicating a combined effect of the CS with the Abs.

Rheumatoid arthritis is characterized by an imbalance between a pro-inflammatory and anti-inflammatory cytokines, that is, upregulation of pro-inflammatory cytokines and downregulation of anti-inflammatory cytokines [51],[52]. Since the pro-inflammatory phenotype is more evident in the synovial joints of patients with RA [53],[53] only the pro-inflammatory cytokines were evaluated and more specifically TNF-α.

In fact, the model used in this study is a model of inflammation however, the inflammatory environment is a usual condition in rheumatoid arthritis. Through this model, it is possible to verify the anti-inflammatory effect of the anti-TNF α Abs-CS/PAMAM dendrimer NPs that can potentially be used in the treatment of several inflammatory pathologies including rheumatoid arthritis.

V-5. CONCLUSION

In this work, an innovative therapeutic approach comprising anti-TNF α Abs-CS/PAMAM dendrimer NPs was developed, to provide a more targeted and effective anti-inflammatory effect for the management of several inflammatory including RA disease. The main goal of this approach was to develop a therapeutic and efficient strategy, through the maximum capture of TNF α by anti-TNF α Abs-CS/PAMAM dendrimer NPs and the synergistic inhibition of the inflammation by the CS. The proposed formulation showed appropriate mechanical and rheological properties and exhibited higher TNF α

capture capacity than the anti-TNF α Abs alone, showing that this system could be useful for controlled and sustained drug delivery. The in vitro studies demonstrated that CS/PAMAM dendrimer NPs presence did not produce a deleterious effect on the tested cells` metabolic activity and proliferation, thus presenting a suitable cytocompatibility and hemocompatibility. The anti-TNF α Abs-CS/PAMAM dendrimer NPs properties owe them the potential to complement or improve current strategies in the treatment of rheumatoid arthritis.

V-6. FUTURE PERSPECTIVE

Recent studies using dendrimers show their great specificity in the delivery of the drugs to the site of interest. Having this in mind, it was hypothesized that PAMAM dendrimer functionalized with CS and linked to specific antibodies (anti-TNF α) could help in the treatment of RA. The combinatory approach presented here showed a synergistic effect of capture ability of the target agent over time and reduction of this production, showing great potential to be used as a specific and sustained treatment in RA patients. Despite the encouraging results showed in this work, further studies are required to clarify the underlying mechanisms. Therefore, future work will comprise the proof of concept of this system in vivo, through an animal model of RA. In the future, dendrimers will undoubtedly have an important role in the world of nanopharmaceuticals, and in particular, in patient-specific approaches for RA treatment.

V-7. CONFLICTS OF INTEREST

There are no conflicts to declare.

V-8. ACKNOWLEDGMENTS

The authors thank the financial support under the Norte2020 project ("NORTE-08-5369-FSE-000044") and BD/137726/2018/J621340zkMF. The FCT distinction attributed to J. M. O. under the Investigator FCT program (No. IF/00423/2012) is also greatly acknowledged. C. G. also wished to acknowledge FCT for supporting her research (No. SFRH/BPD/94277/2013). RS and AG-F thank

Xunta de Galicia (Grupo de Referencia Competitiva, ED431C 2016041) and Centro de Investigaciones Biomédicas (CINBIO), Vigo, Spain, for supporting their research.

V-9. REFERENCES

1. Singh, J.A., et al., *2015 American College of Rheumatology guideline for the treatment of rheumatoid arthritis.* Arthritis & rheumatology, 2016. **68**(1): p. 1-26.
2. Gerlag, D.M., J.M. Norris, and P.P. Tak, *Towards prevention of autoantibody-positive rheumatoid arthritis: from lifestyle modification to preventive treatment.* Rheumatology, 2016. **55**(4): p. 607-614.
3. Yang, M., et al., *Nanotherapeutics relieve rheumatoid arthritis.* Journal of Controlled Release, 2017.
4. Guidelli, G., et al., *One year in review: novelties in the treatment of rheumatoid arthritis.* Clinical and experimental rheumatology, 2015. **33**(1): p. 102-108.
5. Boulaiz, H., et al., *Nanomedicine: application areas and development prospects.* International journal of molecular sciences, 2011. **12**(5): p. 3303-3321.
6. Oliveira, I.M., et al., *Engineering nanoparticles for targeting rheumatoid arthritis: Past, present, and future trends.* Nano Research, 2018. **11**(9): p. 4489-4506.
7. Radner, H. and D. Aletaha, *Anti-TNF in rheumatoid arthritis: an overview.* Wiener Medizinische Wochenschrift, 2015. **165**(1-2): p. 3-9.
8. Lombardo, D., M.A. Kiselev, and M.T. Caccamo, *Smart nanoparticles for drug delivery application: development of versatile nanocarrier platforms in biotechnology and nanomedicine.* Journal of Nanomaterials, 2019. **2019**.
9. Patra, J.K., et al., *Nano based drug delivery systems: recent developments and future prospects.* Journal of nanobiotechnology, 2018. **16**(1): p. 71.
10. Gorain, B., et al., *The use of nanoscaffolds and dendrimers in tissue engineering.* Drug Discovery Today, 2017.
11. Wang, H., et al., *Stimuli-responsive dendrimers in drug delivery.* Biomaterials science, 2016. **4**(3): p. 375-390.
12. Qi, R., et al., *Folate receptor-targeted dendrimer-methotrexate conjugate for inflammatory arthritis.* Journal of biomedical nanotechnology, 2015. **11**(8): p. 1431-1441.
13. Chandrasekar, D., et al., *Folate coupled poly (ethyleneglycol) conjugates of anionic poly (amidoamine) dendrimer for inflammatory tissue specific drug delivery.* Journal of Biomedical Materials Research Part A, 2007. **82**(1): p. 92-103.
14. Thomas, T.P., et al., *Folate‐targeted nanoparticles show efficacy in the treatment of inflammatory arthritis.* Arthritis & Rheumatism, 2011. **63**(9): p. 2671-2680.
15. van Rijt, S. and P. Habibovic, *Enhancing regenerative approaches with nanoparticles.* Journal of the Royal Society Interface, 2017. **14**(129): p. 20170093.
16. Cerqueira, S.R., et al., *Multifunctionalized CMCht/PAMAM dendrimer nanoparticles modulate the cellular uptake by astrocytes and oligodendrocytes in primary cultures of glial cells.* Macromolecular bioscience, 2012. **12**(5): p. 591-597.
17. Bahadır, E.B. and M.K. Sezgintürk, *Poly (amidoamine)(PAMAM): An emerging material for electrochemical bio (sensing) applications.* Talanta, 2016. **148**: p. 427-438.

18. Nurunnabi, M., et al., *Polysaccharide based nano/microformulation: an effective and versatile oral drug delivery system*, in *Nanostructures for Oral Medicine*. 2017, Elsevier. p. 409-433.
19. Nagasawa, K., H. Uchiyama, and N. Wajima, *Chemical sulfation of preparations of chondroitin 4-and 6-sulfate, and dermatan sulfate. Preparation of chondroitin sulfate E-like materials from chondroitin 4-sulfate.* Carbohydrate research, 1986. **158**: p. 183-190.
20. Zaręba, M., et al., *Mixed-Generation PAMAM G3-G0 Megamer as a Drug Delivery System for Nimesulide: Antitumor Activity of the Conjugate Against Human Squamous Carcinoma and Glioblastoma Cells.* International journal of molecular sciences, 2019. **20**(20): p. 4998.
21. Yellepeddi, V.K., A. Kumar, and S. Palakurthi, *Biotinylated poly (amido) amine (PAMAM) dendrimers as carriers for drug delivery to ovarian cancer cells in vitro.* Anticancer research, 2009. **29**(8): p. 2933-2943.
22. Choi, J.S., et al., *Enhanced transfection efficiency of PAMAM dendrimer by surface modification with L-arginine.* Journal of controlled release, 2004. **99**(3): p. 445-456.
23. Khanlari, A., T.C. Suekama, and S.H. Gehrke. *Structurally versatile glycosaminoglycan hydrogels for biomedical applications*. in *Macromolecular Symposia*. 2015. Wiley Online Library.
24. Pomin, V.H., *NMR chemical shifts in structural biology of glycosaminoglycans.* Analytical chemistry, 2014. **86**(1): p. 65-94.
25. Fajardo, A.R., et al., *Hydrogel based on an alginate–Ca 2+/chondroitin sulfate matrix as a potential colon-specific drug delivery system.* Rsc Advances, 2012. **2**(29): p. 11095-11103.
26. Lü, S., et al., *Injectable and self-healing carbohydrate-based hydrogel for cell encapsulation.* ACS applied materials & interfaces, 2015. **7**(23): p. 13029-13037.
27. Wang, Y., et al., *Dendrimer modified magnetic nanoparticles for immobilized BSA: a novel chiral magnetic nano-selector for direct separation of racemates.* Journal of Materials Chemistry B, 2013. **1**(38): p. 5028-5035.
28. Zheng, X., et al., *Incorporation of Carvedilol into PAMAM-functionalized MWNTs as a sustained drug delivery system for enhanced dissolution and drug-loading capacity.* asian journal of pharmaceutical sciences, 2013. **8**(5): p. 278-286.
29. Duan, Y., et al., *Chondroitin sulfate-functionalized polyamidoamine-mediated miR-34a delivery for inhibiting the proliferation and migration of pancreatic cancer.* RSC Advances, 2016. **6**(75): p. 70870-70876.
30. Carvalho, M.R., et al., *A semiautomated microfluidic platform for real-time investigation of nanoparticles' cellular uptake and cancer cells' tracking.* Nanomedicine, 2017. **12**(6): p. 581-596.
31. Imamura, M., et al., *Ternary complex of plasmid DNA electrostatically assembled with polyamidoamine dendrimer and chondroitin sulfate for effective and secure gene delivery.* Biological and Pharmaceutical Bulletin, 2014. **37**(4): p. 552-559.
32. Cilurzo, F., et al., *Injectability evaluation: an open issue.* AAPS PharmSciTech, 2011. **12**(2): p. 604-609.
33. Wei, B., L. Romero-Zerón, and D. Rodrigue, *Mechanical properties and flow behavior of polymers for enhanced oil recovery.* Journal of Macromolecular Science, Part B, 2014. **53**(4): p. 625-644.
34. Yaich, H., et al., *Impact of extraction procedures on the chemical, rheological and textural properties of ulvan from Ulva lactuca of Tunisia coast.* Food hydrocolloids, 2014. **40**: p. 53-63.
35. Wang, W., et al., *The impact of nanoparticle shape on cellular internalisation and transport: what do the different analysis methods tell us?* Materials Horizons, 2019. **6**(8): p. 1538-1547.

36. Gustafson, H.H., et al., *Nanoparticle uptake: the phagocyte problem.* Nano today, 2015. **10**(4): p. 487-510.
37. Huang, Y.-W., M. Cambre, and H.-J. Lee, *The toxicity of nanoparticles depends on multiple molecular and physicochemical mechanisms.* International journal of molecular sciences, 2017. **18**(12): p. 2702.
38. Janaszewska, A., et al., *Cytotoxicity of dendrimers.* Biomolecules, 2019. **9**(8): p. 330.
39. Simon-Vazquez, R., et al., *Metal oxide nanoparticles interact with immune cells and activate different cellular responses.* International journal of nanomedicine, 2016. **11**: p. 4657.
40. Chanput, W., J.J. Mes, and H.J. Wichers, *THP-1 cell line: an in vitro cell model for immune modulation approach.* International immunopharmacology, 2014. **23**(1): p. 37-45.
41. Arango Duque, G. and A. Descoteaux, *Macrophage cytokines: involvement in immunity and infectious diseases.* Frontiers in immunology, 2014. **5**: p. 491.
42. Dobrovolskaia, M.A., et al., *Method for analysis of nanoparticle hemolytic properties in vitro.* Nano letters, 2008. **8**(8): p. 2180-2187.
43. Boutrand, J.-P., *Biocompatibility and performance of medical devices*. 2019: Woodhead Publishing.
44. Henkelman, S., et al., *Standardization of incubation conditions for hemolysis testing of biomaterials.* Materials Science and Engineering: C, 2009. **29**(5): p. 1650-1654.
45. Simón-Vázquez, R., et al., *Conformational changes in human plasma proteins induced by metal oxide nanoparticles.* Colloids and Surfaces B: Biointerfaces, 2014. **113**: p. 198-206.
46. Canoa, P., et al., *A quantitative binding study of fibrinogen and human serum albumin to metal oxide nanoparticles by surface plasmon resonance.* Biosensors and Bioelectronics, 2015. **74**: p. 376-383.
47. Van Hong Nguyen, B.-J.L., *Protein corona: a new approach for nanomedicine design.* International journal of nanomedicine, 2017. **12**: p. 3137.
48. Ronca, F., et al., *Anti-inflammatory activity of chondroitin sulfate.* Osteoarthritis and Cartilage, 1998. **6**: p. 14-21.
49. Tully, S.E., M. Rawat, and L.C. Hsieh-Wilson, *Discovery of a TNF-α antagonist using chondroitin sulfate microarrays.* Journal of the American Chemical Society, 2006. **128**(24): p. 7740-7741.
50. Campo, G.M., et al., *Efficacy of treatment with glycosaminoglycans on experimental collagen-induced arthritis in rats.* Arthritis Res Ther, 2003. **5**(3): p. R122.
51. Mateen, S., et al., *Understanding the role of cytokines in the pathogenesis of rheumatoid arthritis.* Clin Chim Acta, 2016. **455**: p. 161-71.
52. Soler Palacios, B., et al., *Macrophages from the synovium of active rheumatoid arthritis exhibit an activin A-dependent pro-inflammatory profile.* J Pathol, 2015. **235**(3): p. 515-26.
53. Yang, X., Y. Chang, and W. Wei, *Emerging role of targeting macrophages in rheumatoid arthritis: Focus on polarization, metabolism and apoptosis.* Cell Proliferation, 2020: p. e12854.

Chapter VI

Enzymatically crosslinked Tyramine-Gellan Gum Hydrogels as Drug Delivery System for Rheumatoid Arthritis Treatment

Chapter VI

Enzymatically crosslinked Tyramine-Gellan Gum Hydrogels as Drug Delivery System for Rheumatoid Arthritis Treatment[5]

ABSTRACT

Rheumatoid arthritis (RA) is a chronic inflammatory disease characterized by joint synovial inflammation, as well as cartilage and bone tissue destruction. Current strategies for the treatment of RA can reduce joint inflammation, but the treatment options still represent stability concerns since they are not sufficient and present a fast clearing. Thus, several drug delivery systems (DDS) have been advanced to tackle this limitation. Injectable Gellan Gum (GG) hydrogels, reduced by physical crosslinking methods, also being proposed as DDS, but this kind of crosslinking can produce hydrogels that become weaker in physiological conditions. Nevertheless, enzymatic crosslinking emerged as an alternative to increase mechanical strength, which can be adjusted by the degree of enzymatic crosslinking. In this study, tyramine-modified Gellan Gum (Ty-GG) hydrogels were developed via horseradish peroxidase (HRP) crosslinking; and Betamethasone was encapsulated within, to increase the specificity and safety in the treatment of patients with RA. Physicochemical results showed that it was possible to modify GG with Tyramine, with a degree of substitution of approximately 30%. They showed high mechanical strength and resistance, presenting a controlled Betamethasone release profile over time. Ty-GG hydrogels also exhibited no cytotoxic effects, do not negatively affected the metabolic activity and proliferation of chondrogenic primary cells. Furthermore, the main goal was achieved since Betamethasone-loaded Ty-GG hydrogels demonstrated to have a more effective therapeutic effect when compared to the administration of Betamethasone alone. Therefore, the

[5] [1]This chapter is based on the following publication:

Oliveira I. M., Gonçalves C., Shin, M. E., Lee S. , Reis R. L., Khang, G., Oliveira J. M. "Enzymatically crosslinked tyramine-gellan gum hydrogels as drug delivery system for rheumatoid arthritis treatment". Drug Delivery and Translational Research 2020. doi: 10.1007/s13346-020-00855-9.

developed Ty-GG hydrogels represent a promising DDS and a reliable alternative to traditional treatments in patients with RA.

Keywords: Rheumatoid arthritis, hyperplasic synovium, Ty-GG hydrogels, horseradish peroxidase, drug delivery.

VI-1. GRAPHICAL ABSTRACT

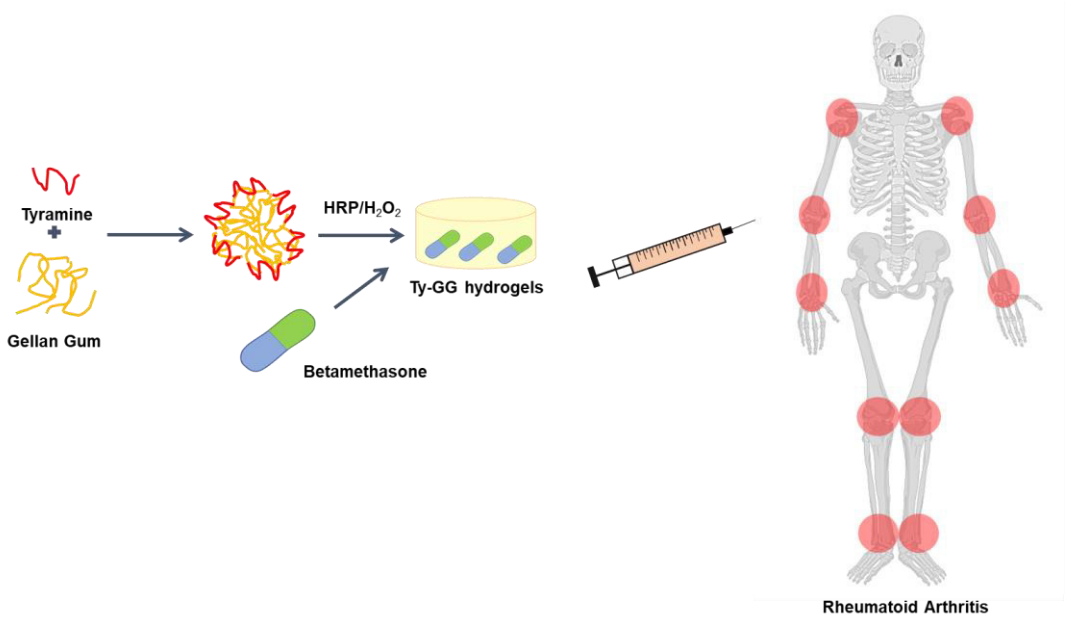

VI-2. INTRODUCTION

Rheumatoid arthritis (RA) is a chronic autoimmune disease, with a complex pathology that affects about 1% of the worldwide population [1],[2]. It is characterized by progressive chronic inflammation of joints, the proliferation of the synovium leading to pannus formation, bones, and cartilage destruction. It is associated with persistent arthritic pain, swelling, stiffness, and work disability. RA is also responsible for the decreased expectancy and quality of life, being more prevalent in women than men [3],[4].

Despite the recent advances in medical therapeutics, currently, it is only possible to slow down the progression of the disease and attempt to increase the quality of life, being not possible to cure RA. The most commonly used therapeutic agents for RA include disease-modifying anti-rheumatic drugs, glucocorticoids, non-steroidal anti-inflammatory drugs, and biological agents. However, such therapies

have several drawbacks due to quite a few side effects, such as headaches, dizziness, and insomnia, damage to the skin and hair, cytopenia, transaminase elevation among others; mainly caused by the lack of selectivity of the drugs and also frequent and long-term dosing, that lead to patient non-compliance [5],[6].

A possible solution to avoid the undesired side effects, is the drug delivery directly to the affected site, via intra-articular injection.

Compared to traditional methods currently used for the administration of drugs, the use of biomaterials as drug delivery systems present many advantages. Those advantages are related, for instance, with the improvement of the insoluble drug delivery, maximizing the bioavailability, and the treatment efficacy. Furthermore, the use of biomaterials can help to reduce secondary effects and enhance the plasma half-life of peptide drugs by protecting them from degradation caused by the environment [7],[8].

Hydrogels are three-dimensional, crosslinked networks of water-soluble polymers that have physiochemical similarities to the extracellular matrix, namely mechanical and composition properties. The particular physical properties of hydrogels have encouraged the interest in their use in drug delivery applications. The porosity of the hydrogels also enables the charging of drugs into the gel matrix and posterior controlled drug release [9],[10].

An injectable hydrogel is a class of hydrogel, which can convert from solution to gel in situ upon physical or chemical stimuli. Therefore, these hydrogels can be introduced into a defined position of the body through a minimally invasive method [11],[12].

Gellan Gum (GG) is a bacterial polysaccharide obtained from Sphyngomonas elodea, and its glycosidic backbone is a repeating tetrasaccharide unit with one L-glycerate per repeating unit and one acetate, occurring every two sequences as esterified substituents [13]. GG is biodegradable, biocompatible and nontoxic. In tissue engineering, the versatility of this polysaccharide has been studied to develop drug delivery systems such as the development of injectable hydrogels [14]. Physical crosslinking methods can produce GG hydrogels that become weaker in physiological conditions since a switch of divalent cations by monovalent ones and physically crosslinked hydrogels occur, leading to the loss of in vivo stability after implantation [15],[16]. Enzymatically crosslinked hydrogels, including covalent bonds between the polymer chains, are produced via radical polymerization and non-enzymatic

or enzymatic crosslinking of complementary groups [17],[18]. Enzyme-mediated hydrogel formation is a suitable method of crosslinking materials in the aqueous medium due to the reaction condition desirable near physiological pH and room temperature. Furthermore, enzymatic hydrogelation prevent the production of undesirable by-products or cytotoxic composite because enzymes only work with distinct substrates [19],[20].

Enzymatic crosslinking of polymer–phenol conjugates in the presence of horseradish peroxidase (HRP) and H_2O_2 has emerged as a valuable method to synthesize in situ-forming (injectable hydrogels) due to fast gelation and controllable crosslinking density [21],[22]. Furthermore, HRP has moderate substrate specificity and can easily be a tuned hydrogel network by adjusting the concentration of enzyme and subtract [23],[19]. Several research groups reported the *in situ* formation of hydrogels through the functionalization of polymers with Tyramine. The hydrogels are chemically crosslinked and consequently possess superior characteristics in terms of stability and mechanical resistance when compare to physically crosslinked, been widely used in drug delivery [24].

In this work, it was developed tyramine-modified gellan gum (Ty-GG) hydrogels (crosslinked by both physical and chemical mechanisms) in the presence of horseradish peroxidase (HRP) and hydrogen peroxide (H_2O_2). The Ty-GG hydrogels were loaded with Betamethasone in order to provide its sustain release and improve the treatment safety in patients with RA. Physicochemical characterization was performed to evaluate the successful functionalization of Ty-GG using nuclear magnetic resonance (^{1}H-NMR) and Fourier transform infrared (FTIR) spectroscopic techniques. Furthermore, the Betamethasone-loaded Ty-GG hydrogels water uptake, weight loss, gelation time, injectability, and rheological properties were assessed. The Betamethasone release profile from the Ty-GG hydrogels was also evaluated *in vitro. In vitro* studies for cell viability such as 3-(4,5-dimethylthiazol-2-yl)-2,5-diphenyl-2H-tetrazolium bromide and DNA proliferation on chondrogenic primary cells and anti-inflammatory activity by enzyme-linked immunosorbent in THP-1 cell line were performed.

VI-3. MATERIALS AND METHODS

VI-3.1. Synthesis of Tyramine-Gellan Gum (Ty-GG)

The functionalization of gellan gum with Tyramine was carried out following the method reported by Prodanović et al. [25], with minor changes. Briefly, gellan gum from Gelzan™ CM (Sigma-Aldrich, USA) was dissolved in water at 90°C to a final concentration of 1% (w/v). Sodium (meta)periodate (Sigma-Aldrich, USA) was added to a final concentration of 1 mM in GG at 1% (w/v). The reaction was kept in the dark for 24 hours at 4°C. The reaction was then stopped by adding glycerol (500 mM) and incubated for 30 minutes in the dark at 4°C. The Oxidized GG was precipitated from the reaction mixture by adding NaCl at 1% (w/v) and 2 volumes of 99% (v/v) ethanol. This precipitation step was repeated two times, using the same procedure after dissolving oxidized GG at 1% (w/v) concentration in water. In the end, the precipitate was separated, dried, and dissolved in 0.1 M sodium-phosphate buffer pH 6. When dissolved at 1% (w/v) concentration, tyramine hydrochloride (Sigma-Aldrich, USA) was added by molecular equivalents (number of mol equivalents of GG to number of mol equivalents of Tyramine) and the solution was stirred for 30 minutes. Subsequently, solid cyanoborohydride was added at 0.5% (w/v) final concentration, and the reaction mixture was left in the dark for 24 hours at 4°C. Modified Gellan Gum was precipitated by adding NaCl to 1 M final concentration and two volumes of 96% (v/v) ethanol. Precipitation was repeated two times using the same procedure after dissolving modified GG at 1% (w/v) concentration in water. Ty-GG powder was obtained by lyophilization, at 0.08 mbar and -77.7°C, during approximately 4 days.

VI-3.2. Physicochemical characterization

VI-3.2.1. Fourier-transform infrared (FTIR) spectroscopy

Powder samples of Ty-GG, GG, and Tyramine were mixed with potassium bromide and, using a manual press, a transparent pellet was obtained. The transmission spectra of the samples were obtained on an IR Prestige-21 spectrometer (Shimadzu, Japan), using 32 scans, a resolution of 4 cm^{-1} and a wavenumber range between 4400 and 400 cm^{-1}.

VI-3.2.2. Assessment of the degree of substitution of Tyramine in Gellan Gum

The chemical modification of GG with Ty was evaluated and quantified by proton nuclear magnetic resonance spectroscopy (^{1}H-NMR). Ty-GG was solubilized in deuterium water oxide (D_2O) (2 mg mL^{-1}) at room temperature. Then, 1 mL of the sample was transferred to an NMR tube. The NMR spectra were obtained on a Bruker AVANCE 400 spectrometer, at 50 °C using a resonance frequency of 400 MHz. To process and analyze the obtained spectra, MestReNova 9.0 Software was used. The degree of substitution (DS, the fraction of modified hydroxyl groups per repeating unit) was determined by the relative integration of the tyramine peaks ($I_{T1,T2}$) of the modified groups to methyl protons of the internal standard (I_{CH3}), according to **(Equation 1)**, adapted from another DS calculation as reported in several studies [26], [27]. The n_{HT1}, $_{T2}$, and n_{HCH3} correspond to the number of tyramine protons and the methyl protons of GG monomer, respectively. n_{OH} corresponds to the number of reactive -OH sites in the GG structure.

$$DS = \left(\frac{\frac{I_{T_1T_2}}{I_{CH_3}}}{\frac{n_{HT_1T_2}}{n_{CH_3}}} \Big/ n_{OH} \right) \times 100 \qquad \textbf{(Equation 1)}$$

VI-3.2.3. Horseradish peroxidase to induce Tyramine-Gellan Gum hydrogels formation

Horseradish peroxidase (HRP) solution (0.84 mg mL^{-1}) (Sigma-Aldrich, USA) and hydrogen peroxide solution (H_2O_2) (0.36% (v/v)) (VWR, USA) were both prepared in water. Tyramine-Gellan Gum solution of 1% (w/v) was used for the hydrogel preparation. Tyramine-Gellan gum hydrogels were prepared by mixing of Ty-GG solution with different amounts of HRP and H_2O_2 solutions **(Table VI-1)**. Ty-GG hydrogels discs were prepared by adding 200 µL of the mixture solutions in a polypropylene mold at 37°C.

Table VI-1- Ty-GG conditions (C1, C2 and C3) with different amounts of HRP and H_2O_2 solutions.

	Ty-GG	HRP	H_2O_2
C1	167 µL	16.6 µL	10.83 µL
C2	167 µL	18.3 µL	15 µL

C3	167 µL	20 uL	13.3 µL

VI-3.2.4. Water uptake and weight loss of the Tyramine-Gellan Gum hydrogels

Weight loss and water uptake of Ty-GG hydrogels were performed. Hydrogels were soaked into a PBS solution at 37°C, for up to 21 days, in triplicate. Then, specimens were removed after the different time points of immersion. The initial weight (w_i) of each sample was measured, and then Ty-GG hydrogels were immersed in PBS solution. At each time point, the samples were removed and put in filter paper to remove the excess of the solution, and the wet weight (w_w) was measured. The water uptake was determined as shown by **(Equation 2)**.

$$\text{Water uptake } (\%) = \frac{w_w - w_i}{w_i} \times 100 \qquad \textbf{(Equation 2)}$$

The weight loss was quantified after the samples were dried under at 70°C and until they reached constant weight (w_f), using the **(Equation 3)**.

$$\text{Weight loss } (\%) = \frac{w_i - w_f}{w_i} \times 100 \qquad \textbf{(Equation 3)}$$

VI-3.2.5. Investigation of gelation time, injectability tests and rheological properties

The vial inversion test was routinely used to determine an approximate gelation time. Thereby, after mix Ty-GG with HRP and H_2O_2, the vials were placed in the water bath at 37°C and then inverted to see how long it takes to turn to gel.

The injectability tests were also investigated by means of injectability measurement equipment (PARALAB). The injectability measurements were performed using a syringe with a 27 G needle. The

material was placed in the syringe that was placed in the equipment and then it applied a force that extruded the sample from the syringe at a rate of 1 ml min^{-1}. The force needed for each hydrogel condition was recorded. Triplicates of each sample were performed, and water was used as a control.

The mechanical properties of Ty-GG hydrogels were evaluated by using a rheometer (Kinexus pro+rheometer, software rSpace, from Malvern). The oscillatory experiments were performed using a stainless-steel plate-plate measuring system. This system is composed of an upper stainless-steel plate of 8 mm of diameter, with a rough finish to prevent the sample from slipping. Frequency sweep curves, also known as mechanical spectra, were obtained from 0.01 Hz to 1 Hz of frequency, at a shear strain of 0.1% (from LVER determination) for 5 minutes at 37°C. These curves were obtained in three independent tests, with different samples of the same condition.

VI-3.3. Drug release profile of the Betamethasone-loaded Tyramine-Gellan Gum hydrogels

To assess the drug release system, one corticosteroid, Betamethasone, was incorporated in Ty-GG hydrogels. Ty-GG hydrogels loaded with Betamethasone (Sigma-Aldrich, USA) were prepared by mixing Ty-GG solution, with 5 mg mL^{-1} of Betamethasone in PBS and the enzymatic crosslinking was made by adding of HRP and H_2O_2. Betamethasone release profile in Ty-GG 1% hydrogels was evaluated immersing each hydrogel in PBS at 37°C. After each time point (3 hours, 6 hours, 24 hours, 72 hours, 168 hours, 336 hours and 504 hours), the supernatant was removed and kept at -80°C until the end of the experiment. Three samples per condition were used at each time point. To formulate the calibration curve, Betamethasone dilutions were prepared (from 0 mg mL^{-1} to 5 mg mL^{-1}). The UV absorbance at 245 nm was read in a microplate reader (EMax; Molecular Devices, Sunnyvale, CA, USA) to measure the Betamethasone release.

VI-3.4. *In vitro* studies

VI-3.4.1. Cell cultures

Chondrogenic primary cells isolated from female New Zealand White rabbits (Damul Sci., Korea) with 1 kg and 6 weeks, were used. Dulbecco's modified eagle medium (DMEM/ F12) (Gibco, USA) was

used in chondrogenic cells. This culture medium was supplemented with 10% (v/v) fetal bovine serum (Gibco, USA) and 1% (v/v) antibiotic-antimycotic (Gibko /Thermo Fisher Scientific, South Korea) under standard conditions (37°C in a humidified atmosphere containing 5% CO_2). Human monocytic cell line (THP-1) (SIGMA, USA) was expanded in RPMI 1640 Medium, GlutaMAX™ Supplement, HEPES (Thermo Fisher Scientific, USA), supplemented with 10% fetal bovine serum and 1% (v/v) of penicillin and streptomycin, under standard culture conditions (37°C in a humidified atmosphere containing 5 vol% CO_2).

VI-3.4.2. Chondrogenic cells isolation

Chondrogenic primary cells were isolated from rabbit cartilage. The knees were initially removed from the rabbit, and the samples were washed 3 times with PBS (1X) solution. The cartilage was scraped carefully with the blade, and small fragments were placed inside a conical tube with 1.5% (v/v) antibiotic-antimycotic. The sample was centrifuged at 300 G, 3 minutes and 4°C. The supernatant was discarded and refilled with an enzymatic cocktail (DMEM/F12 medium + collagenase A (Roche, USA). The solution was previously filter-sterilized through a 0.2 µm filter. The sample was placed in the CO2 incubator at 37°C for 24 hours. The next day, cells were centrifuged at 300 G, for 3 minutes and at 4°C. The supernatant was removed, and the cells were plated on a cell culture dish, with a complete medium and kept in the CO_2 incubator at 37°C until they reach the desired confluence.

VI-3.4.3. Metabolic activity

The metabolic activity of chondrogenic primary cells was assessed by MTT assay following the MEM extract test. The MEM extract test protocol followed was established according to European and international standards.

The Ty-GG hydrogels (C1, C2 and C3 (previously described)) were prepared with a thickness ranging from 0.5 mm to 1 mm a minimum area of 60 cm^2. The samples were placed in a sterile tube with 10/20 mL of cell culture medium, and they were kept in the water bath at 37°C and 60 rpm for 24 hours. Parallel 200 µL cell suspension was transferred into 96 well plates to obtain a cell density of 10000 cells per cm^2. After 24h of incubation, the extraction fluid was passed through a 0.45 µm

membrane filter and the medium of cells was removed and replaced with the extraction fluid. Cells with DMEM-F12 medium were used as Control.

The cell cultures were evaluated by 3-(4,5-dimethylthiazol-2-yl) -2,5-diphenyltetrazolium bromide (MTT, Sigma, South Korea) at 24, 48 and 72 hours. At each time point, the DMEM/ F12 medium was replaced by culture medium containing MTT assay in a 9:1 ratio and incubated for 3 hours. When violet crystals were formed, they were melted using dimethyl sulfoxide solution (DMSO). Then, 100 µL of solution from each well was transferred to 96-well plates, and a microplate reader (EMax; Molecular Devices, Sunnyvale, CA, USA) was used at 570 nm optical density.

VI-3.4.4. DNA quantification

The total amount of DNA was assessed using DNA quantification kit (Quant-iT™ PicoGreen® dsDNA Assay Kit, Invitrogen, USA), to evaluate the effect of Ty-GG hydrogels in chondrogenic primary cells. The cells were seeded at a density of 10000 cells per cm2 and incubated with extraction solution of Ty-GG hydrogels (C1, C2 and C3) for periods of 24, 48 and 72 hours. After the incubation period of the cells, they were washed with PBS solution and were lysed with ultrapure water. The cell solution was placed into microtubes, incubated for 1 hour in a water bath at 37°C, and then they were stored at -80°C for further analysis. Cells cultured with DMEM-F12 medium were used as a positive control. Several solutions were prepared, with concentrations ranging from 2 to 0 µL mL^{-1} to plot a DNA calibration curve. In each well (of the 96 well opaque plate), 28.7 µL of each sample or standard, was mixed with 71.3 µL of PicoGreen solution and 100 µL 1X TE. Then, the plate was incubated in the dark for 10 minutes, the fluorescence was read using excitation of 480/20 nm and emission of 528/20 nm, in a microplate reader and DNA concentration was determined from the standard curve.

VI-3.4.5. Fluorescence microscopy

Chondrogenic primary cells were seeded using the same protocol and conditions described above. Then, cells were fixed with 10% formalin (Sigma-Aldrich, USA) and stained with Texas Red-X phalloidin (Sigma-Aldrich, USA) for actin filaments of the cytoskeleton and 4,6-diamidino-2-phenylindole, dilactate (DAPI blue, VWR International, USA) for nuclei. At the end, cells were analyzed under the fluorescence microscope (AxioImager, Z1, Zeis Inc., Oberkochen, Germany).

VI-3.4.6. Anti-inflammatory activity of Betamethasone-loaded Ty-GG hydrogels

The anti-inflammatory activity of Betamethasone-loaded Ty-GG hydrogels was investigated with a THP-1 cell line. For this assay, the two concentrations that obtained the best results in metabolic activity and cell proliferation were evaluated. First, THP-1 cell line was seeded ($1x10^6$ cells per mL) and differentiated into macrophage phenotype with 100 nM phorbol 12-myristate-13-acetate (PMA) (Sigma-Aldrich, USA) for 1 day. The next day, the non-adhered cells were removed, the medium replaced and new RPMI medium without PMA was added, for 2 days. THP-1 cells were incubated for 5 hours with 100 ng mL^{-1} of Lipopolysaccharide (LPS) (Sigma-Aldrich, USA) in RPMI medium to enable the inflammatory response. After incubation time, cells were cultured with two concentrations of Betamethasone-loaded Ty-GG hydrogels (C1 and C2) for 7 days. Cells without treatment and differentiated with PMA and without LPS stimulation were used as Control. At each time point (1 day, 3 days and 7 days), the solution was collected and kept at -80°C for further analysis. Human TNF-alpha DuoSET ELISA (R&D Systems, USA) kit and DuoSet Ancillary Reagent Kit 2 (R&D Systems, USA), for the optimum performance of the ELISA kit, were used to assess the anti-inflammatory activity. The assay was performed to evaluate the system effectiveness through cytokine TNF α. The TNF α standards were prepared with concentrations ranging from 1000 to 0 pg mL^{-1} to make a TNF α calibration curve. A microplate reader set (Synergy HT, BIO-TEK) at 450 nm was used to determine the optical density of each well.

VI-3.4.7. Statistical analysis

GraphPad Prism 8 version was used to conduct the statistical analysis, where a Shapiro-Wilk normality test was formerly performed to evaluate the data normality. Nonparametric Kruskal-Wallis test was applied in all assays, except for weight loss and MTT assay where One Way-ANOVA was used; since there was an absence of normality. Dunn's multiple comparison test was used to compare the mean rank of each condition with the mean rank of every other condition in nonparametric Krustal-Wallis. Turkey's multiple comparisons test was used to compare the mean of each condition with the mean of every other condition in One Way-ANOVA. Statistical significances were determined as * $p<0.05$, ** $p<0.01$ and *** $p<0.001$. All tests were performed in triplicated, and results were presented with mean ± standard deviation.

VI-4. RESULTS AND DISCUSSION

VI-4.1. Physicochemical properties

Ty-GG hydrogels were obtained via enzymatic crosslinking with HRP and H_2O_2 and encapsulated with Betamethasone to increase the specificity and safety in the treatment of chronic inflammation of synovial joints in the patients suffering of RA. Ty-GG was synthesized by amide bond formation between the amine group of Tyramine and the carboxyl group of GG. After the modification of GG with Ty, its efficacy was evaluated by NMR and FTIR analysis. **Figure VI-1** shows a representative NMR spectrum (a) and FTIR spectra (b) of Gellan Gum, Tyramine and Ty-GG.

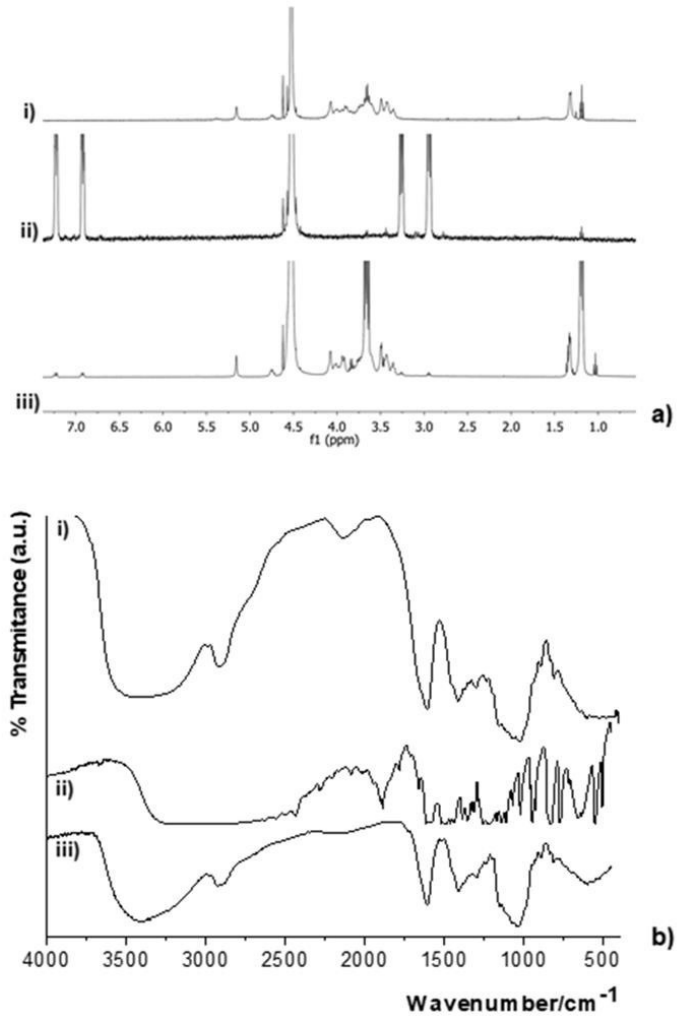

Figure VI-1 - ^{1}H-NMR spectra (a) of: GG (i), tyramine (ii), and the obtained Ty-GG (iii), in D_2O at 50°C. FTIR spectra (b) of: GG (i), tyramine (ii), and Ty-GG (iii).

From Figure 1a, it is possible to see that Ty-modified gellan gum (Ty-GG) (iii) showed additional peaks not appearing in the unsubstituted GG (i). The tyramine spectrum (ii) showed the distinctive signals for both pairs of aromatic ring protons (β pair and λ pair between 7.4 and 7.1 ppm) and aliphatic side chain protons between 3.4 and 3.1 ppm (α pair). These peaks are seen in Ty-GG spectrum and confirm the presence of Tyramine on Ty-GG [28],[29].

The degree of substitution of GG with Tyramine was calculated using Equation 1. The obtained degree of substitution for Ty-GG is (30.2 ± 1.3) %. This value of the degree of substitution is higher when compared with other molecules modified with tyramine [30],[31].

From Figure 1b, the GG and Ty-GG spectra within the region 1800–1200 cm^{-1} also indicated the efficient modification of tyramine-gellan gum. From the spectra analysis, it was possible to confirm the presence of the aromatic rings, due to the appearance of a peak of C-C (in-ring) stretching vibrations at 1517 cm^{-1} and 1417 cm^{-1}, only in the spectra of modified Gellan Gum, which is accordance with the spectra found in the literature [25],[32].

It is known that ionic crosslinked hydrogels present weak mechanical proprieties [33]. This limitation can be overcome by modification of GG with Tyramine, by enzymatic crosslinking. Therefore, enzymatic- but also physical- and chemical-crosslinking were combined to produce Ty-GG hydrogels with tunable mechanical proprieties.

Ty-GG hydrogels were produced via enzymatic crosslinking, with the enzyme HRP. Different conditions of Ty-GG hydrogels were produced and assessed (C1, C2, and C3) regarding water absorption capacity and weight loss. **Figure VI-2** shows the water uptake and weight loss of C1, C2 and C3 of Ty-GG hydrogels after soaking up to 504 hours.

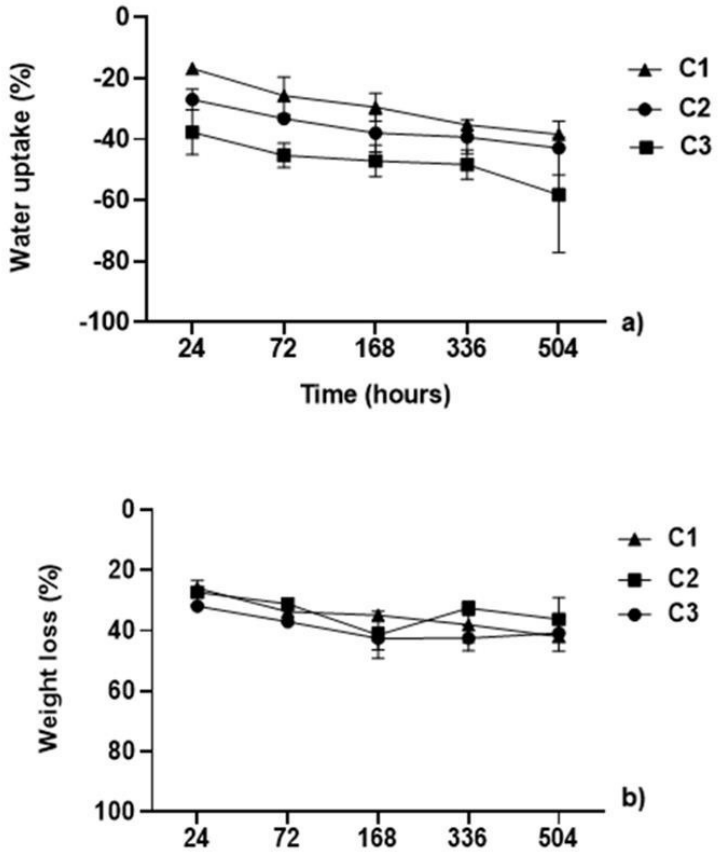

Figure VI-2 - Water uptake (a) and Weight loss (b) of: Ty-GG hydrogels after 24 hours, 72 hours, 168 hours, 336 hours, and 504 hours of soaking. Significant differences ***p<0.001, **p<0.01 and *p<0.05. Water uptake, significant differences between (C2 vs C3) *p< 0.05 at time point 1 day and 3 days, nonparametric Kruskal-Wallis test. Weight loss, significant differences between (C1 vs C2) **p<0.01 at time point 3 days, one way-ANOVA.

It was possible to verify that all conditions of Ty-GG hydrogels showed negative values of water uptake. The swelling ratios of gels ranged from (-42.89 ± 6.25) %, (-47.25 ± 1.47) %, (-39.21 ± 1.53) % in the C1, C2 and C3, respectively. Some studies [11],[26] demonstrated that the crosslinking degree, the formation of ionic bonds and hydrophilicity of network of hydrogels influence the swelling. In the swelling kinetics assays, the hydrogel behavior is powerfully influenced by the presence of cations in the immersion solution [11]. These cations form ionic bonds that increase the crosslinking degree and lower the water uptake ratio. Interactions between the carboxylic group on GG and calcium ions can reduce the hydrogen binding donors and receptors free for interaction with water, thereby decreasing the quantity of water-related with the hydrogel network [34].

The results are in agreement with the previously mentioned studies [26],[34],[35] the Ty-GG hydrogels produced by enzymatic crosslinking, after immersion in PBS (ionic crosslinking) did not present water absorption capability. Thus, it is possible to consider this test as an indirect method to assume a high crosslinking degree in the produced gels, thus showing that the properties of GG improved after modification.

The degradation profile of hydrogels in this study was obtained by exposing the Ty-GG hydrogels in PBS at different points (Figure 2b). The weight loss results show that all concentrations had approximately the same degradation profile over time. The weight loss ratio was (40.8 ± 4.1) %, (36.2 ± 0.7) % and (41.9 ± 1.6) %, for C1, C2 and C3, respectively. Ty-GG hydrogels are relatively stable in PBS due to the ionic crosslinking, being possible to observe a similar weight loss rate over time. The osmotic forces influence this process, such as the external ionic aqueous solution and the elastic force executed by the crosslinked polymeric structure [36]. When the external solution is ionically more concentrated than the hydrogels, promote ions to penetrate the hydrogels, stabilizing and increasing the hydrogel crosslinking degree, as well, stimulates water molecule expulsion and consequently the decrease of weight loss. Furthermore, the ionic crosslink, when combined with chemical crosslink mechanisms extend the rate of degradation, as reported by several studies [26],[35].

The gelation time is a crucial parameter for the formation of hydrogels in situ and is widely connected with the crosslinking rate of the HRP- catalyzed reaction [23]. The gelation time was determined by the vial inversion test. After adding Ty-GG with HRP and H_2O_2, the vials were placed at 37°C in the water bath and then inverted. It was possible to verify that all concentrations (C1, C2, and C3) had a gelation time about 30 seconds.

Several studies reported that HRP catalysis the crosslinking reaction of polymer-phenol conjugates in the presence of H_2O_2, resulting in hydrogels with tunable gelation rate [20]. The HRP and H_2O_2 concentrations are essential parameters to control the crosslinking rate of phenol-rich polymers. The association between these parameters and gelation time has been well-known. It has been described that the gelation time reduces with rising HRP concentration [37],[38]. In order to use injectable hydrogels for bio-applications, a suitable gelation time is desired. A short gelation time (ten seconds to a few minutes) is essential for efficient local delivery of drugs [31],[39]. While a quick gelling time is beneficial to obtain high loading efficiency of drugs in hydrogels, in a real clinical setting, rapid administration can be more challenging. The use of appropriate syringes, with more than one channel,

in which the mixture is made while the injection is given, would be the most appropriate form of administration. Through the results obtained, it was possible to confirm that the produced gels fulfill the necessary characteristics.

The injectability (formulation performance during injection, including pre-filled syringes) is a very important parameter to determine the force required to extrude the material through a device [40]. The injectability analysis was performed for the three conditions of hydrogels (C1, C2 and C3) and water was used as Control. The syringe was loaded with the Ty-GG solution, HRP and H2O2 to form the hydrogels and the injection was performed using a rate of 1 mL min-1. The force needed for each injection was measured, together with the Control (water), and is presented in **(Figure VI-3)**.

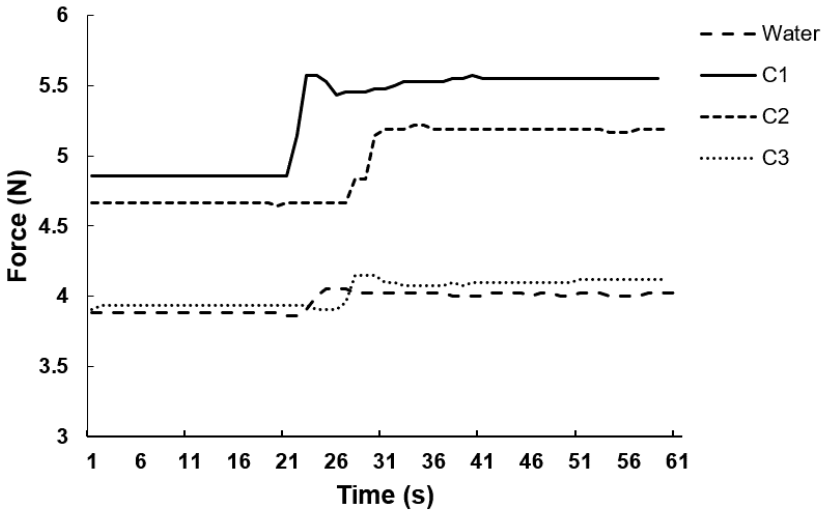

Figure VI-3 - Injectability test of Ty-GG hydrogels, C1, C2, and C3 and water (Control). Significant differences *** p<0.001 (water vs C1) and (water vs C2), nonparametric Kruskal-Wallis test.

In Figure 3, it was visible that the force needed to inject the condition 1 (5.2 ± 0.3 N) and condition 2 (4.9 ± 0.2 N) is greater than the force required to inject water (3.9 ± 0.1 N). However, the force required to inject condition 3 (4 ± 0.1 N) is comparable to the force required to inject water. Initially, in condition 1, there was a lower value in the injectability force, with that force increasing around 23 seconds, possibly due to the beginning of the crosslinking in the reaction, and then the value remained constant until the end of the analysis. In condition 2, the same profile of injectability as in condition 1 was observed, although the values of the injectable force were lower, and the increase of force occurred around 31 seconds. This result may be due to condition 1 has a slightly higher degree of crosslinking when compared to condition 2; therefore, this slight difference in behavior. In condition 3

there was an injectability force value similar to the value obtained with water. However, in condition 3 there was also an increase in the injectable force around 31 seconds. Which, like the other conditions, maybe due to the beginning of the crosslinking of the reaction. Taking this into account, condition 3 has presented an injectable force more similar to that found in water, meaning that it can become easier and less painful to inject into the patient. However, conditions 2 and 3, despite having higher injectable force values, may have other advantages as was verified in other characterization tests.

The mechanical properties of Ty-GG hydrogels were assessed after enzymatic crosslinking via HRP and stabilized at different time points in PBS. The hydrogels were evaluated through oscillatory rheology experiment at 37°C. The oscillatory shear flow has been extensively used to measure viscoelastic properties of materials. The storage modulus, elastic solid-like behavior, (G`) provide a small amplitude of oscillatory shear and loss modulus, the viscous response, (G``) assess stress amplitude and the time lag between the stress and strain. The phase angle ($\delta$, $0 \leq \delta \leq 90^{o}$) is a representative physical property that estimates the viscoelasticity of a material. G`, G`` and δ are determined by a single function of the frequency (f). These materials are often called linear viscoelastic properties. A general form of the shear stress subjected to oscillatory shear ($\lambda = \lambda 0 \sin \omega t$) [41]. **Figure VI-4** shows the mechanical spectra of Ty-GG hydrogels (C1, C2 and C3), after different time points.

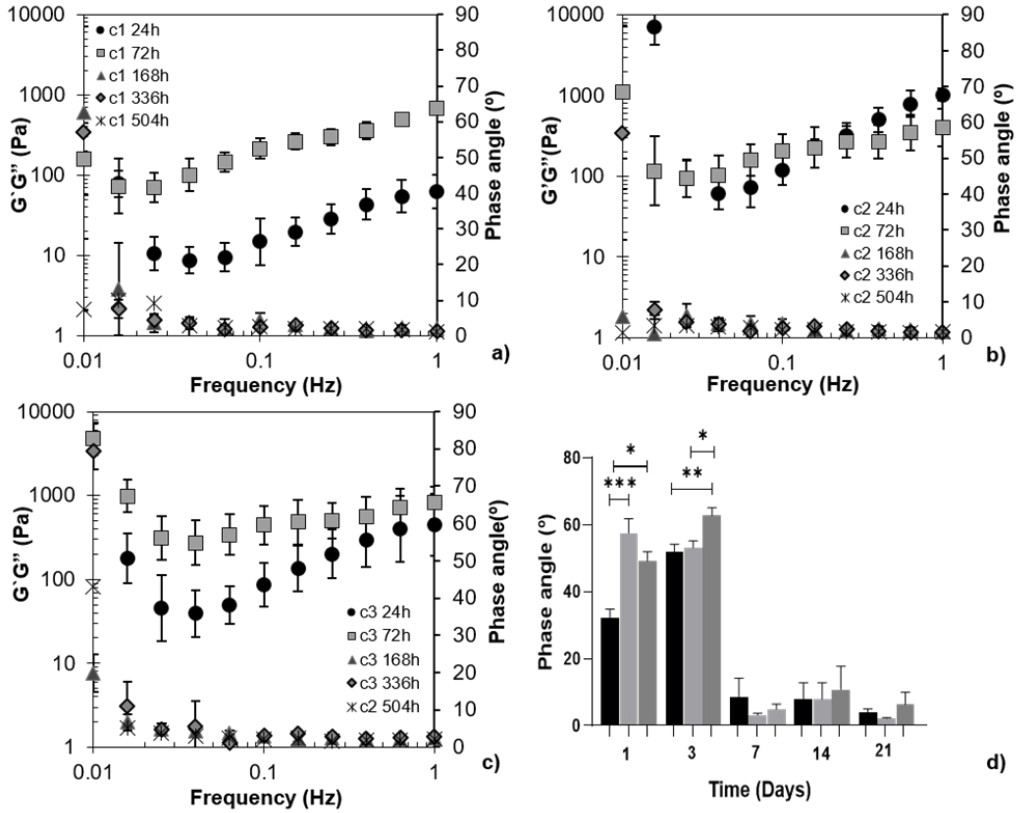

Figure VI-4 – Mechanical spectra of Ty-GG hydrogels: C1 (a), C2 (b) and C3 (c) at different timepoints (24 hours, 72 hours, 168 hours, 336 hours, and 504 hours). Significant differences *** p<0.001, **p<0.01 and *p<0.05, nonparametric Kruskal-Wallis test.

The spectrum of mechanical proprieties of Ty-GG hydrogels showed that at 24 hours and 72 hours, all conditions of Ty-GG hydrogels demonstrated a G`` > G`, and consequently presented a high phase angle, that is, a viscous component higher than the solid. In the following time points, 168 hours, 336 hours and 504 hours, it was possible to observe that the phase angle decreased, G`>G``, so the elastic component is higher than the viscous component, showing that the material has a viscoelastic behavior, with superior elastic character [41],[42]. The Ty-GG hydrogels are intended to be injected in the synovial cavity filled with synovial fluid. This fluid has highly viscous (G`` > G`) properties, and the hydrogels obtained showed viscoelastic behavior with high viscosity after formation, similar to the synovial liquid. Thus, Ty-GG hydrogels achieved the desired mechanical properties [43],[44]. Viscoelastic materials, such as the proposed Ty-GG hydrogels, can be injected directly into the knee joint of patients with RA and, in addition to function as a drug carrier, surrounding the deficient cartilage joints and acting as a lubricant and shock absorber [45], as well as reducing pain and slowing down the disease progress.

Controlled drug delivery is revealing great importance over conventional drug delivery methods. In traditional drug administration, drug concentration in the blood rises instantly after the drug is taken and then decreases over time. Plasma drug concentration is a vital parameter for any drug since there is an optimum concentration above which it is toxic and below which it is not effective. The conventional drugs are also very limited concerning their short half-lives and their stability only under physiological conditions. Therefore, drug delivery at a constant rate is generally better compared to the traditional methods of drug administration [46], [47], [48].

Betamethasone suspensions were approved for intraarticular injection to provide adjuvant therapy in Rheumatoid Arthritis. Normal intraarticular doses of Betamethasone suspensions differ with the size of the joint, from 1.5 mg to 12 mg [49]. In this work, it was used 5 mg mL^{-1} of Betamethasone because it was the average value found in the literature to have a therapeutic effect. The Betamethasone has a short half-life about 36-54 hours [50], which means that the drug must be injected more frequently to have the desired therapeutic effect. It was possible to verify that the Ty-GG hydrogels, allowed a controlled release profile of Betamethasone over 21 days, not reaching the maximum of release in any of the concentrations, C1 released (64 ± 1.5) % of the drug, C2 released (51 ± 0.8)% and C3 released approximately (82 ± 0.05)%, **(Figure VI- 5)**. Intraarticular corticosteroid therapy has been used for the treatment of RA. Corticosteroid therapy is effective at temporarily alleviating joint symptoms associated with inflammatory disorders. However, long term adverse effects of corticosteroids on chondrocyte of the articular cartilage are a concern. Thus, the number of injections is usually restricted [51], [52]. The use of Ty-GG hydrogels loaded with Betamethasone allow the drug to be administered less frequently, providing lower and continuous dosages of the drug, thus decreasing the levels of toxicity. In addition, constant injections can become painful and uncomfortable for patients. Thus, the use of Ty-GG hydrogels to Betamethasone release can improve the failures of the traditional models, allowing a better quality of patient's life during the treatment period.

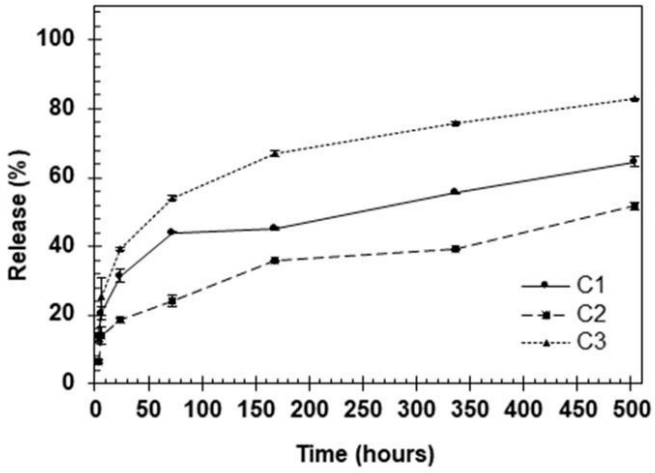

Figure VI-5 - Drug release profile of Ty-GG hydrogels (C1, C2, and C3) with encapsulated Betamethasone for 3 hours, 6 hours, 24 hours, 72 hours, 168 hours, 336 hours, and 504 hours. Significant differences *** p<0.001, **p<0.01 and *p<0.05, by nonparametric Kruskal-Wallis test. At time point 1day, significant differences between (C2 vs C3) * p<0.05, at time point 3 days, (C2 vs C3) * p<0.05, at time point 14 days, (C1 vs C2) * p<0.05.

VI-4.2. *In vitro* studies

Cell viability and proliferation of Ty-GG hydrogels were assessed in chondrogenic primary cells, and therapeutic efficacy was evaluated using the THP-1 cell line.

MTT assay was made to investigate the influence of Ty-GG hydrogels. Thus, the metabolic activity of cells up to 72 hours of culturing **(Figure VI-6**a**)** was evaluated. DNA quantification was also performed to assess cell proliferation (Figure 6b).

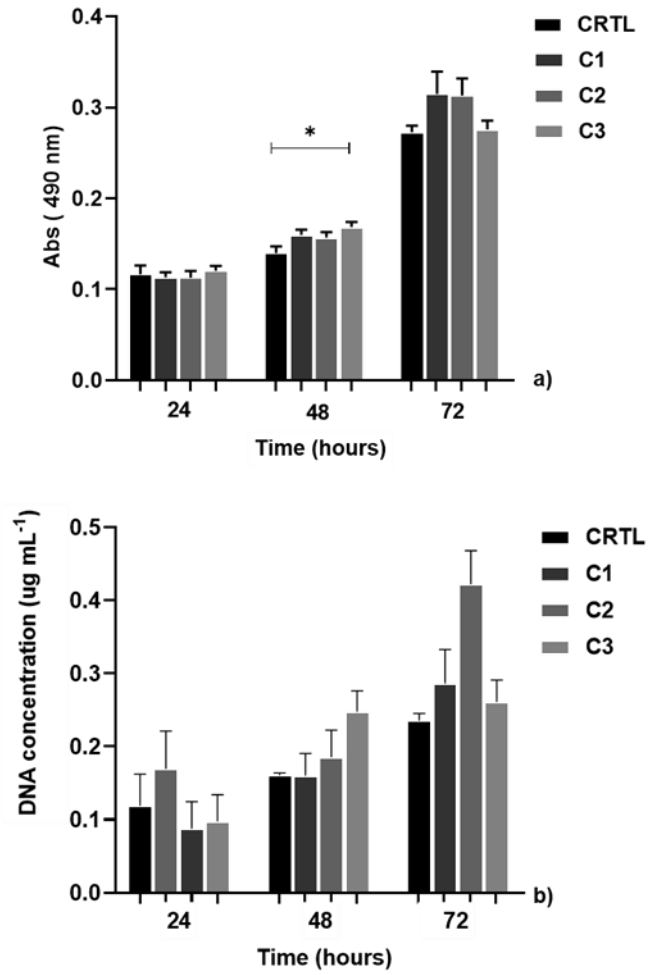

Figure VI-6 - MTT assay (a) and DNA quantification (b) of chondrogenic primary cells with Control (cells with DMEM-12 medium) and different conditions (C1, C2, and C3) of Ty-GG hydrogels, after 24 hours, 48 hours, and 72 hours of culturing. Significant differences *** p<0.001, **p<0.01 and *p<0.05. Ordinary One-Way ANOVA (MTT assay) and nonparametric Kruskal-Wallis test (DNA quantification).

From day 1 to day 3, all cells with different conditions of Ty-GG hydrogels shown an increase of metabolic activity, not presenting significant differences between them. However, on day 2, cells with C3 demonstrated significant differences as compared with Control (*p<0.05).

In parallel, DNA quantification was performed to assess cell proliferation for 72 hours. It was observed that there was a decrease in the first time point in C2 and C3 samples, although there were no significant differences. At the following time points, there was an increase in cell proliferation in all conditions, and no significant differences were found between conditions.

These results are in line with those found in the literature, i.e., modified GG is not cytotoxic over different cell types [53], [54], [55].

Qualitative analysis of the morphology of chondrogenic primary cells in contact with Ty-GG hydrogel extracts was obtained by fluorescence microscopy **(Figure VI-7)**.

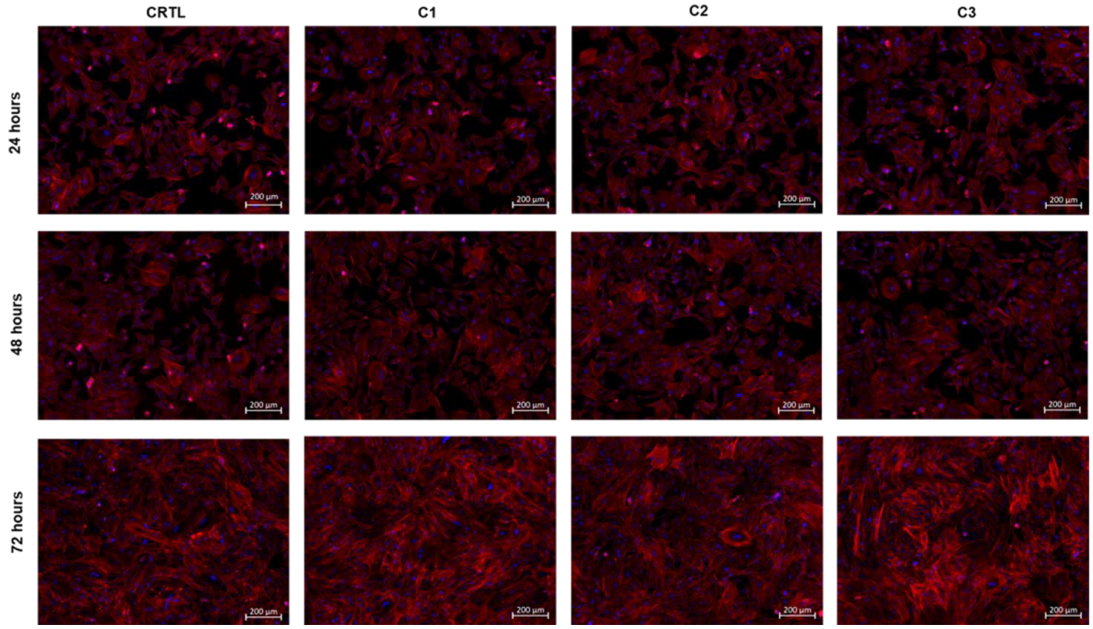

Figure VI-7 - Fluorescence microscopy images of chondrogenic primary cells cultured in the presence of CRTL (RMPI medium) and C1, C2, and C3 of Ty-GG hydrogels for 72 hours. Scale bar: 200 µm.

Chondrogenic primary cells were cultured with different conditions of extraction fluid of Ty-GG hydrogels. It was possible to verify that none of the conditions produced affected the typical morphology of the chondrogenic cells (marked by DAPI and phalloidin), suggesting healthy proliferation and survival.

Then, the rates of the pro-inflammatory Tumor Necrosis Factor alfa (TNF α), present in the medium after being in contact with Ty-GG hydrogels, were assessed. This cytokine is found in large quantities in patients with RA and has been studied with a therapeutic target. THP-1 cell line was differentiated with PMA and stimulated with LPS to assess the capacity of Ty-GG hydrogels encapsulated with Betamethasone to decrease the levels of TNF α present in the medium. Only C1 and C2 were analyzed regarding the neutralizing capacity since these were the best conditions in previous metabolic activity and cell proliferation. After the inflammation is manifested, 7 conditions were established to test, cells stimulated with LPS, without treatment, Betamethasone alone, Ty-GG hydrogels

(C1 and C2) without Betamethasone encapsulated and Ty-GG hydrogels (C1 and C2) encapsulated with Betamethasone. Cells differentiated with PMA but without LPS stimulation were used as Control.

Figure VI-8 shows the graphs of C1 (a) and C2 (b) separately, regarding the amount of TNF α present in RPMI medium for 1 day, 3 days, and 7 days of culturing.

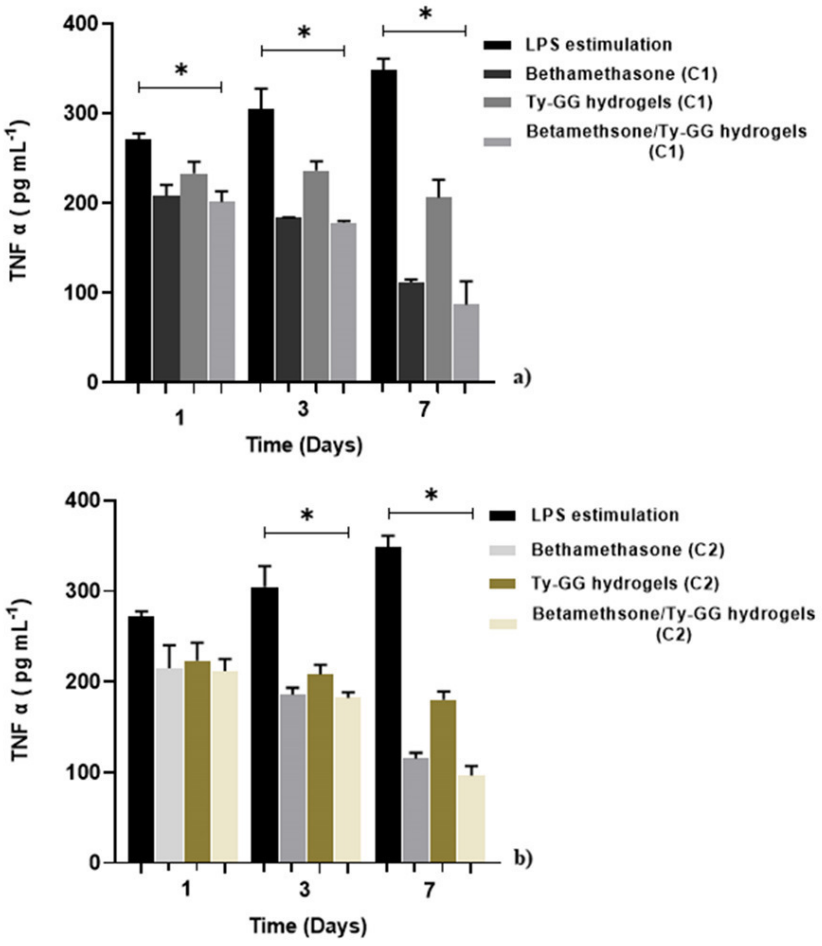

Figure VI-8 – Amount of TNF α present in the medium, in contact with different conditions, cells stimulated with LPS, Betamethasone (C1); Ty-GG hydrogels (C1) and Ty-GG hydrogels (C1) encapsulated with Betamethasone (a). Cells stimulated with LPS, Betamethasone (C2), Ty-GG hydrogels (C2) and Ty-GG hydrogels (C2) encapsulated with Betamethasone (b). Significant differences *** p<0.001, **p<0.01 and *p<0.05, nonparametric Kruskal-Wallis test.

The results showed that cells stimulated with LPS but without treatment demonstrated high levels of free TNF α in the RPMI medium, compared to the other conditions. Furthermore, it was possible to verify a higher neutralization of TNF α in THP-1 cells treated with Ty-GG hydrogels encapsulated with Betamethasone (C1 and C2) than with Ty-GG (C1 and C2) and Betamethasone alone (C1 and C2).

Significant differences were found between cells stimulated with LPS without treatment and cells that were treated Ty-GG hydrogels encapsulated with Betamethasone (*$p<0.05$). This significant difference was more evident in C1 than C2, at the first timepoint.

The higher ability to neutralize the TNF α becomes more noticeable on the seventh day, which may be because hydrogels are degrading, so a higher amount of drug is released.

Ty-GG hydrogels loaded with Betamethasone can bring more advantages in the treatment of the inflammatory environment than the drug alone. This approach may allow a prolonged action, due to the controlled rate of drug release over time, and treat inflammation more effectively in patients with RA. Furthermore, as mentioned earlier, it can reduce frequent administration of the drug to patients, decreasing the level of toxicity caused by recurrent administrations.

The data is in agreement with the previously reported literature, where it was shown that the great potential of GG for finding application as a controlled drug release system [56], [57], [58].

VI-5. CONCLUSION

This study developed tyramine-substituted Gellan gum hydrogels via enzymatic and physical crosslinking, with Betamethasone encapsulated can increase the specificity and safety in the treatment of patients with RA. The Gellan gum was effectively modified with Tyramine, presenting a substitution degree of about 30%. Tyramine-substituted Gellan gum hydrogels showed rapid gelation time and demonstrated a good strength and resistance, ideal to be applied in the intra-articular cavity. The tyramine-substituted Gellan gum hydrogels presented low water absorption capacity, a constant weight loss profile, and a controlled Betamethasone release profile over time. Thus, it can be considered that the properties of Gellan gum were improved after modification. Furthermore, the tyramine-substituted Gellan gum hydrogels did not show to cause toxic effects on metabolic activity, morphology, and cell proliferation and tyramine-substituted Gellan gum hydrogels with Betamethasone encapsulated demonstrated more effective therapeutic efficacy over time than Betamethasone alone. Therefore, tyramine-substituted Gellan gum hydrogel has excellent potential to be used as a drug delivery system for the treatment of rheumatoid arthritis.

VI-6. FUNDING INFORMATION AND ACKNOWLEDGEMENTS

I. Oliveira thanks the financial support under the Norte2020 project ("NORTE-08-5369-FSE-000044"), REMIX project (G.A. 778078 — REMIX — H2020-MSCA-RISE-2017) and Gilson Lab, Chonbuk National University, Republic of Korea. The FCT distinction attributed to J. Miguel Oliveira under the Investigator FCT program (IF/01285/2015) is also greatly acknowledged. C. Gonçalves also wish to acknowledge FCT for supporting her research (No. SFRH/BPD/94277/2013).

VI-7. CONFLICTS OF INTEREST

There are no conflicts to declare.

VI-8. REFERENCES

1. Wang, M., et al., *Leptin Upregulates Peripheral CD4+ CXCR5+ ICOS+ T Cells via Increased IL-6 in Rheumatoid Arthritis Patients.* Journal of Interferon & Cytokine Research, 2018. **38**(2): p. 86-92.
2. Guo, Q., et al., *Rheumatoid arthritis: pathological mechanisms and modern pharmacologic therapies.* Bone research, 2018. **6**(1): p. 1-14.
3. Pirmardvand Chegini, S., J. Varshosaz, and S. Taymouri, *Recent approaches for targeted drug delivery in rheumatoid arthritis diagnosis and treatment.* Artificial cells, nanomedicine, and biotechnology, 2018. **46**(sup2): p. 502-514.
4. Andersen, N.S., et al., *Methotrexate prodrugs sensitive to reactive oxygen species for the improved treatment of rheumatoid arthritis.* European journal of medicinal chemistry, 2018. **156**: p. 738-746.
5. Gouveia, V.M., et al., *Non-biologic nanodelivery therapies for rheumatoid arthritis.* Journal of biomedical nanotechnology, 2015. **11**(10): p. 1701-1721.
6. Yang, M., et al., *Nanotherapeutics relieve rheumatoid arthritis.* Journal of Controlled Release, 2017. **252**: p. 108-124.
7. Prosperi, D., et al. *Drug nanocarriers to treat autoimmunity and chronic inflammatory diseases*. in *Seminars in immunology*. 2017. Elsevier.
8. Feng, X. and Y. Chen, *Drug delivery targets and systems for targeted treatment of rheumatoid arthritis.* Journal of drug targeting, 2018. **26**(10): p. 845-857.
9. Hoare, T.R. and D.S. Kohane, *Hydrogels in drug delivery: Progress and challenges.* Polymer, 2008. **49**(8): p. 1993-2007.
10. Li, J. and D.J. Mooney, *Designing hydrogels for controlled drug delivery.* Nature Reviews Materials, 2016. **1**(12): p. 1-17.

11. Xu, Y., et al., *Injectable and self-healing chitosan hydrogel based on imine bonds: design and therapeutic applications.* International journal of molecular sciences, 2018. **19**(8): p. 2198.
12. Yang, J.-A., et al., *In situ-forming injectable hydrogels for regenerative medicine.* Progress in Polymer Science, 2014. **39**(12): p. 1973-1986.
13. Harding, N.E., Y.N. Patel, and R.J. Coleman, *Organization of genes required for gellan polysaccharide biosynthesis in Sphingomonas elodea ATCC 31461.* Journal of Industrial Microbiology and Biotechnology, 2004. **31**(2): p. 70-82.
14. Shin, H., B.D. Olsen, and A. Khademhosseini, *Gellan gum microgel-reinforced cell-laden gelatin hydrogels.* Journal of Materials Chemistry B, 2014. **2**(17): p. 2508-2516.
15. Hu, W., et al., *Advances in crosslinking strategies of biomedical hydrogels.* Biomaterials science, 2019. **7**(3): p. 843-855.
16. Li, X., et al., *Functional hydrogels with tunable structures and properties for tissue engineering applications.* Frontiers in chemistry, 2018. **6**: p. 499.
17. Parhi, R., *Cross-Linked Hydrogel for Pharmaceutical Applications: A Review.* Advanced pharmaceutical bulletin, 2017. **7**(4): p. 515-530.
18. Akhtar, M.F., M. Hanif, and N.M. Ranjha, *Methods of synthesis of hydrogels... A review.* Saudi Pharmaceutical Journal, 2016. **24**(5): p. 554-559.
19. Khanmohammadi, M., et al., *Horseradish peroxidase-catalyzed hydrogelation for biomedical applications.* Biomaterials science, 2018. **6**(6): p. 1286-1298.
20. Lee, F., K.H. Bae, and M. Kurisawa, *Injectable hydrogel systems crosslinked by horseradish peroxidase.* Biomedical Materials, 2015. **11**(1): p. 014101.
21. Ribeiro, V.P., *Multifunctional silk fibroin-based constructs for tissue engineering and regenerative medicine applications.* 2018.
22. Ribeiro, V.P., et al., *Combinatory approach for developing silk fibroin scaffolds for cartilage regeneration.* Acta biomaterialia, 2018. **72**: p. 167-181.
23. Bae, J.W., et al., *Horseradish peroxidase‐catalysed in situ‐forming hydrogels for tissue‐engineering applications.* Journal of tissue engineering and regenerative medicine, 2015. **9**(11): p. 1225-1232.
24. Oryan, A., et al., *Chemical crosslinking of biopolymeric scaffolds: Current knowledge and future directions of crosslinked engineered bone scaffolds.* International journal of biological macromolecules, 2018. **107**: p. 678-688.
25. Prodanovic, O., et al., *Tyramine modified alginates via periodate oxidation for peroxidase induced hydrogel formation and immobilization.* Reactive and Functional Polymers, 2015. **93**: p. 77-83.
26. Coutinho, D.F., et al., *Modified Gellan Gum hydrogels with tunable physical and mechanical properties.* Biomaterials, 2010. **31**(29): p. 7494-7502.
27. Reys, L.L., et al., *Fucoidan hydrogels photo-cross-linked with visible radiation as matrices for cell culture.* ACS Biomaterials Science & Engineering, 2016. **2**(7): p. 1151-1161.
28. Kim, K., et al., *Injectable hyaluronic acid–tyramine hydrogels for the treatment of rheumatoid arthritis.* Acta biomaterialia, 2011. **7**(2): p. 666-674.
29. Darr, A. and A. Calabro, *Synthesis and characterization of tyramine-based hyaluronan hydrogels.* Journal of Materials Science: Materials in Medicine, 2009. **20**(1): p. 33-44.
30. Loebel, C., et al., *Precise tailoring of tyramine-based hyaluronan hydrogel properties using DMTMM conjugation.* Carbohydrate polymers, 2015. **115**: p. 325-333.
31. Wennink, J.W., et al. *Injectable Hydrogels by Enzymatic Co‐Crosslinking of Dextran and Hyaluronic Acid Tyramine Conjugates*. in *Macromolecular symposia*. 2011. Wiley Online Library.

32. Prokopijevic, M., et al., *Tyramine-modified pectins via periodate oxidation for soybean hull peroxidase induced hydrogel formation and immobilization.* Applied microbiology and biotechnology, 2017. **101**(6): p. 2281-2290.
33. Jagur‐Grodzinski, J., *Polymeric gels and hydrogels for biomedical and pharmaceutical applications.* Polymers for Advanced Technologies, 2010. **21**(1): p. 27-47.
34. Huang, Y., H. Yu, and C. Xiao, *pH-sensitive cationic guar gum/poly (acrylic acid) polyelectrolyte hydrogels: Swelling and in vitro drug release.* Carbohydrate Polymers, 2007. **69**(4): p. 774-783.
35. da Silva, L.P., et al., *Engineering cell-adhesive gellan gum spongy-like hydrogels for regenerative medicine purposes.* Acta biomaterialia, 2014. **10**(11): p. 4787-4797.
36. Flory, P.J., *Thermodynamics of high polymer solutions.* The Journal of Chemical Physics, 1941. **9**(8): p. 660-660.
37. Jin, R., et al., *Enzyme-mediated fast in situ formation of hydrogels from dextran–tyramine conjugates.* Biomaterials, 2007. **28**(18): p. 2791-2800.
38. Nguyen, Q.V., J.H. Park, and D.S. Lee, *Injectable polymeric hydrogels for the delivery of therapeutic agents: A review.* European Polymer Journal, 2015. **72**: p. 602-619.
39. Jin, R., c. lin, and A. Cao, *Enzyme-mediated fast injectable hydrogels based on chitosan-glycolic acid/tyrosine: Preparation, characterization, and chondrocyte culture.* Polym. Chem., 2013. **5**.
40. Buitrago-Vásquez, M. and C.P. Ossa-Orozco, *Degradation, mater uptake, injectability and mechanical strength of injectable bone substitutes composed of silk fibroin and hydroxyapatite nanorods.* Revista Facultad de Ingeniería, 2018. **27**(48): p. 49-60.
41. Nam, J.G., et al., *Phase angle of the first normal stress difference in oscillatory shear flow.* Korea-Australia Rheology Journal, 2010. **22**(4): p. 247-257.
42. Ngan, C.L., et al., *Comparison of process parameter optimization using different designs in nanoemulsion-based formulation for transdermal delivery of fullerene.* International journal of nanomedicine, 2014. **9**: p. 4375.
43. Cai, Z., et al., *Shear-thinning hyaluronan-based fluid hydrogels to modulate viscoelastic properties of osteoarthritis synovial fluids.* Biomaterials science, 2019. **7**(8): p. 3143-3157.
44. Galesso, D., et al., *Viscoelastic properties and elastic recovery of HYADD® 4 hydrogel compared to crosslinked HA-based commercial viscosupplements.* Osteoarthritis and Cartilage, 2012. **20**: p. S292.
45. Lawless, B.M., et al., *Viscoelasticity of articular cartilage: analysing the effect of induced stress and the restraint of bone in a dynamic environment.* Journal of the mechanical behavior of biomedical materials, 2017. **75**: p. 293-301.
46. Risbud, M.V. and R.R. Bhonde, *Polyacrylamide-chitosan hydrogels: in vitro biocompatibility and sustained antibiotic release studies.* Drug Delivery, 2000. **7**(2): p. 69-75.
47. Li, J. and D.J. Mooney, *Designing hydrogels for controlled drug delivery.* Nature Reviews Materials, 2016. **1**(12): p. 16071.
48. Zhang, J. and P.X. Ma, *Cyclodextrin-based supramolecular systems for drug delivery: recent progress and future perspective.* Advanced drug delivery reviews, 2013. **65**(9): p. 1215-1233.
49. Dreyer, S.J. and W.J. Beckworth, *2 - Commonly Used Medications in Procedures*, in *Pain Procedures in Clinical Practice (Third Edition)*, T.A. Lennard, et al., Editors. 2011, Hanley & Belfus: Saint Louis. p. 5-12.
50. Jacobs, J.W.G. and J.W.J. Bijlsma, *Chapter 60 - Glucocorticoid Therapy*, in *Kelley and Firestein's Textbook of Rheumatology (Tenth Edition)*, G.S. Firestein, et al., Editors. 2017, Elsevier. p. 932-957.e5.

51. Wernecke, C., H.J. Braun, and J.L. Dragoo, *The Effect of Intra-articular Corticosteroids on Articular Cartilage: A Systematic Review.* Orthopaedic journal of sports medicine, 2015. **3**(5): p. 2325967115581163-2325967115581163.
52. Østergaard, M. and P. Halberg, *Intra-Articular Corticosteroids in Arthritic Disease.* BioDrugs, 1998. **9**(2): p. 95-103.
53. Silva‐Correia, J., et al., *Gellan gum‐based hydrogels for intervertebral disc tissue‐engineering applications.* Journal of tissue engineering and regenerative medicine, 2011. **5**(6): p. e97-e107.
54. Khang, G., et al., *Biological evaluation of intervertebral disc cells in different formulations of gellan gum‐based hydrogels.* Journal of tissue engineering and regenerative medicine, 2015. **9**(3): p. 265-275.
55. Silva-Correia, J., et al., *Mechanical performance and biocompatibility study of methacrylated Gellan gum hydrogels with potential for nucleus pulposus regeneration.* 2012.
56. Kesavan, K., G. Nath, and J. Pandit, *Preparation and in vitro antibacterial evaluation of gatifloxacin mucoadhesive gellan system.* Daru: journal of Faculty of Pharmacy, Tehran University of Medical Sciences, 2010. **18**(4): p. 237.
57. Carmona-Moran, C., et al., *Development of gellan gum containing formulations for transdermal drug delivery: Component evaluation and controlled drug release using temperature responsive nanogels.* International Journal of Pharmaceutics, 2016. **509**.
58. Norazemi, N., et al., *Coated gellan gum hydrogel as a drug carrier for colon targeted drug delivery.* Journal of Sustainability Science and Management, 2017. **2**: p. 36-41.

Chapter VII

Anti-Inflammatory Properties of Injectable Betamethasone- Loaded Tyramine-Modified Gellan Gum/Silk Fibroin Hydrogels

Chapter VII

Anti-Inflammatory Properties of Injectable Betamethasone - Loaded Tyramine-Modified Gellan Gum/Silk Fibroin Hydrogels[6]

ABSTRACT

Rheumatoid arthritis is a rheumatic disease for which a healing treatment does not presently exist. Silk fibroin has been extensively studied for use in drug delivery systems due to its uniqueness, versatility and strong clinical track record in medicine. However, in general, natural polymeric materials are not mechanically stable enough, and have high rates of biodegradation. Thus, natural materials such as gellan gum can be used to produce composite structures with biological signals to promote tissue-specific interactions while providing the desired mechanical properties. In this work, we aimed to produce hydrogels of tyramine-modified gellan gum with silk fibroin (Ty–GG/SF) via horseradish peroxidase (HRP), with encapsulated betamethasone, to improve the biocompatibility and mechanical properties, and further increase therapeutic efficacy to treat rheumatoid arthritis (RA). The Ty–GG/SF hydrogels presented a β-sheet secondary structure, with gelation time around 2–5 min, good resistance to enzymatic degradation, a suitable injectability profile, viscoelastic capacity with a significant solid component and a betamethasone controlled release profile over time. *In vitro* studies showed that Ty–GG/SF hydrogels did not produce a deleterious effect on cellular metabolic activity, morphology or proliferation. Furthermore, Ty–GG/SF hydrogels with encapsulated betamethasone revealed greater therapeutic efficacy than the drug applied alone. Therefore, this strategy can provide an improvement in therapeutic efficacy when compared to the traditional use of drugs for the treatment of rheumatoid arthritis.

[6]This chapter is based on the following publication:

Oliveira I. M., Gonçalves C., Shin, M. E., Lee S. , Reis R. L., Khang, G., Oliveira J. M. "Anti-inflammatory Properties of Injectable Betamethasone-loaded Tyramine-modified Gellan Gum/Silk Fibroin Hydrogels" Biomolecules 2020, 10(10), 1456. doi: 10.3390/biom10101456.

Keywords: Ty–GG/SF hydrogels, enzymatic crosslinking, betamethasone, inflammation, rheumatoid arthritis

VII-1. GRAPHICAL ABSTRACT

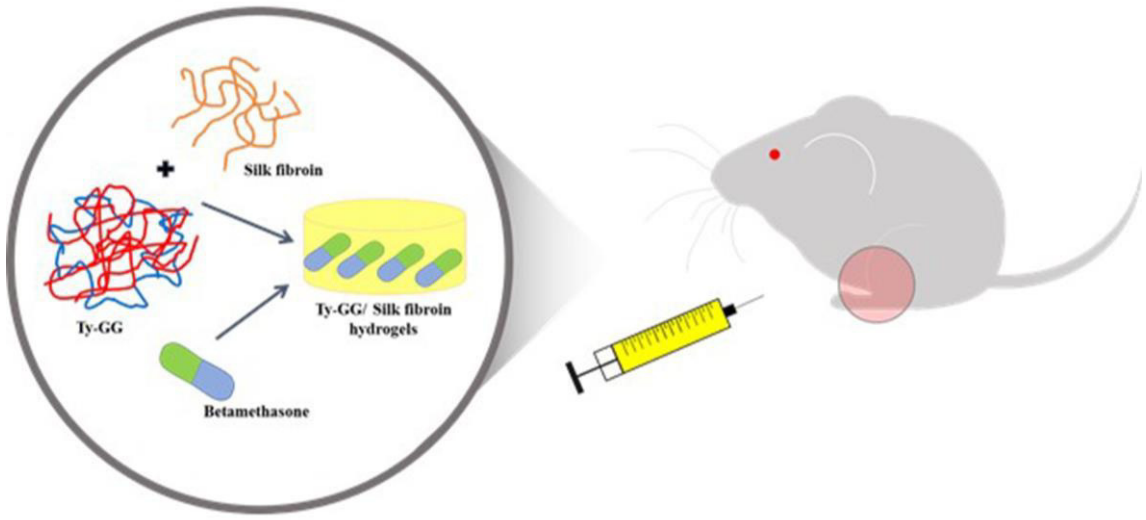

VII-2. INTRODUCTION

Among the several types of chronic inflammatory disorders, rheumatoid arthritis (RA) is a debilitating condition with severe physical, emotional and socioeconomic burdens. This disease affects 1% of the adult population worldwide, and there are approximately 5–50 new cases per 100,000 adults per year. The prevalence increases with age and occurs four times more often in women than men [1]. The disease starts with an inflammatory process that is characterized by inflammation in the synovial membrane, induced by leucocyte infiltration; joint swelling and pain; and at the same time, systemic inflammation registered by elevated serum levels of autoantibodies and acute phase protein; and later on, cartilage and bone tissue destruction [2]. The most common treatments for rheumatoid arthritis comprise nonsteroidal anti-inflammatory drugs, corticosteroids, disease-modifying antirheumatic drugs and some biological agents [3]. These drugs have improved quality of life for a significant number of RA patients. Corticosteroids, such as betamethasone, are inflammation suppressors that have been mainly used for the treatment of RA [4]. However, there are some concerns regarding the long-term use of

corticosteroids because of the high doses, and consequently, the side effects. Therefore, it is necessary to develop and test new approaches to specifically target inflamed joints and attenuate damage to healthy tissues [5],[6].

Injectable hydrogels have been widely studied, particularly in the tissue engineering and regenerative medicine field. These promising biomaterials present several advantages, such as convenient injectability with minimal invasiveness, and the ability to fill irregular and defective areas entirely and produce three-dimensional, intensely hydrated structures [7]. Furthermore, the injectable hydrogels can also be suitable for non-invasive applications; they are applied in the local delivery of a wide range of therapeutic agents, including biomolecules and drugs. Injectable hydrogels derived from natural polymers, such as silk fibroin, alginate, hyaluronic acid and collagen, have been regularly used and show great potential for biomedical applications, including the delivery of local therapeutic agents [8]. The promising advantages of these biomaterials come from their adaptability and versatility due to their properties and components being similar to those of the physiological extracellular matrix [9].

Natural polymers are often used as hydrogels for controlled drug delivery vehicles. The hydrogels can be prepared with natural and controlled compositions and morphologies. The properties can be influenced to enhance biocompatibility, immune compatibility, cellular uptake, stability and solubility [10]. Silk is a natural fiber produced by silkworm (Bombyx mori) cocoons, and it is composed of two types of protein (fibroin and sericin). Silk fibroin has been extensively studied as a drug delivery system for its unique and highly versatile structure and its strong clinical track record. Silk hydrogels have unlimited applications and have several advantages, such as high biocompatibility, tunable biodegradation and low immunogenicity [11],[12]. Silk fibroin solution has been used to produce hydrogels as injectable systems for load-bearing of cartilage tissue [13]. Most silk fibroin hydrogels are formed in a sol–gel transition, with a conformation transition from the amorphous structure to β-sheet, through different physical and chemical procedures. Enzymatically crosslinking methods have been used to produce in situ hydrogels [14],[15]. Compared to other systems, enzyme-mediated crosslinking can present several advantages; for instance, gelation time can be easily adjusted to be fast, favoring drug delivery. The enzymatic crosslinking via horseradish peroxidase (HRP) has shown great potential once the phenol groups in tyrosine, tyramine and/or aminophenol can be conjugated in the presence of hydrogen peroxide (H_2O_2) [16],[17]. Since the silk protein contains tyrosine amino acids, this natural polymer has great advantages for producing SF hydrogels [18].

Nevertheless, usually, natural polymeric materials are not mechanically stable enough, and the rate of biodegradation is high [19]. Thus, to increase mechanical stability, natural or synthetic materials can be used to produce composite structures with biological cues to promote tissue-specific interactions [20].

Gellan Gum is a water-soluble extracellular polysaccharide produced by the aerobic fermentation process of Sphingomonas elodea. According to the degree of acyl substitution, it is available in two forms, high acyl and low acyl, the low acyl form being the most common and commercially available one [21]. The GG has properties that provide great versatility, such as biocompatibility, biodegradability, easy bio-fabrication, tunable mechanical properties, cell adhesion and easy functionalization. These appealing properties make GG a promising material in different tissue engineering fields, such as drug delivery [22],[21].

Previously, Gellan Gum was successfully modified with tyramine (Ty–GG), to produce hydrogels enzymatically crosslinked by HRP [23]. The Ty–GG hydrogels showed good strength and resistance, did not interfere with metabolic activity and cell proliferation, and presented good therapeutic efficiency; i.e., Ty–GG hydrogels with a corticosteroid encapsulated showed a great decrease in inflammation as compared to the administration of the corticosteroid alone. Therefore, the Ty–GG was used to increase the mechanical stability of silk fibroin and further enhance the therapeutic effect as a drug delivery system.

In this work, we developed Ty–GG/SF (silk fibroin) hydrogels with encapsulated betamethasone to be injected into intra-articular cavities to further increase therapeutic efficacy in the inflamed joints of patients with RA.

VII-3. MATERIAL AND METHODS

VII-3.1. Physicochemical characterization

VII-3.1.1. Preparation of Silk Fibroin Solution

The silk fibroin solution was obtained based on a previously reported procedure [24],[25].Silkworm cocoons (Rural Development Administration, Jeonju, Korea and Portuguese Association of Parents and

Friends of Mentally Disabled Citizens (APPACDM, Castelo Branco, Portugal)) were cut into fragments and boiled in 0.02 M Sodium carbonate (Na_2CO_3) solution (Showa Chemical, Tokyo, Japan) for 30 min to remove sericin. Boiled silkworm cocoons were washed with distilled water three times and dried inside an oven at 70°C. The dry silkworm cocoons were then dissolved in the oven with 9.3 M LiBr (lithium bromide; Kanto Chemical, Tokyo, Japan) at 70°C for 4 h. The dissolved solution was dialyzed using a SnakeSkin Dialysis Tubing 3500 MWCO (ThermoScientific, Waltham, MA, USA), over 48 h, against distilled water, to remove LiBr. Silk fibroin was kept at 4°C until use.

VII-3.1.2. Horseradish Peroxidase to Induce Ty–GG/SF Hydrogel Formation

Ty–GG previously produced by the authors was used to obtain Ty–GG/SF hydrogels [23]. Briefly, Gellan Gum from Gelzan™ CM (Sigma-Aldrich, St. Louis, MO, USA) was dissolved in water to a final concentration of 1% (w/v) and sodium (meta)periodate (Sigma-Aldrich, St. Louis, MO, USA) was added to a final concentration of 1 mM in GG at 1% (w/v). The reaction was stopped by adding glycerol (500 mM) and oxidized GG was precipitated from the reaction mixture by adding NaCl at 1% (w/v) and 2 volumes of 99% (v/v) ethanol. The precipitate was separated, dried and dissolved in 0.1 M sodium phosphate buffer, pH 6, and tyramine hydrochloride (Sigma-Aldrich, St. Louis, MO, USA) was added through molecular equivalents (number of mol equivalents of GG to number of mol equivalents of tyramine). The solid cyanoborohydride was added at 0.5% (w/v) final concentration and modified Gellan Gum was precipitated by adding NaCl to 1 M final concentration and two volumes of 96% (v/v) ethanol. Ty–GG was obtained after dialysis for 7 days and lyophilized for approximately 4 days.

Horseradish peroxidase (HRP) solution (0.84 mg mL^{-1}) (Sigma-Aldrich, St. Louis, MO, USA) and hydrogen peroxide solution (H_2O_2, 0.36% (v/v)) (VWR, Radnor, PA, USA) were both prepared in water. Tyramine-Gellan Gum/SF hydrogels were prepared by mixing the 1% (w/v) Ty–GG and 2% (w/v) SF (1:1) solutions with different amounts of HRP and H_2O_2 solutions (**Table VII-1**). Ty–GG/SF hydrogels were prepared by adding 200 µL of the mixture solutions in a polypropylene mold at 37 °C.

Table VII-1- Ty-GG and SF conditions (C1, C2 and C3) with different amounts of HRP and H_2O_2 solutions.

	Ty–GG	SF	HRP	H_2O_2
C1	83.5 µL	83.5 µL	16.6 µL	10.83 µL

C2	83.5 µL	83.5 µL	18.3 µL	15 µL
C3	83.5 µL	83.5 µL	20 µL	13.3 µL

VII-3.1.3. Analysis of the Secondary Protein Structure of Silk Fibroin

The secondary structure of the SF in the Ty–GG/SF hydrogels was recorded by Fourier transform infrared (FTIR) spectroscopy (IRPrestige 21, Shimadzu, Japan). Measurements were made with attenuated total reflection (ATR) over a Germanium crystal. Transmission spectra were acquired on an IR Prestige-21 spectrometer (Shimadzu, Japan), using 32 scans, a resolution of 4 cm^{-1} and a wavenumber range between 4400 and 400 cm^{-1}. The SF absorbance spectra were calculated using **Equation 1**.

$$Abs(absorbance) = 2\text{-}\log_{10} T(transmittance/\%) \quad \textbf{(Equation 1)}$$

To quantify secondary structure composition, Origin Pro 2018 Software was used. The deconvolution of the amine I region (1750–1600 cm^{-1}) was performed using a Gaussian Peak shape and the bands were identified by the area integral (Area IntgP) analysis with the points of interest. Baseline treatment was performed on the deconvolution spectrum. A maximum entropy Gaussian curve fitting algorithm was executed on the deconvolution spectrum using the peak positions identified in the Area IntgP, maximum peak and variable peak height. Peak positions were attained using wavenumber ranges described by Litvinov et al. [26]. The structural composition was measured by relative areas of the fit curve in the amine I region.

VII-3.1.4. Water uptake and Enzymatic Degradation of Ty–GG/SF Hydrogels

The water uptake ratio of the Ty–GG/SF hydrogels was measured in PBS solution at 37°C. The initial weight (wi) of each sample was measured, and then the hydrogels were immersed in PBS solutions. At the end of each time point (24, 72, 168, 336 and 504 hours), the samples were collected

and placed in filter paper to remove excess liquid, and the wet weight (ww) was measured. The percentage of water uptake was determined using **Equation 2**.

$$\text{Water uptake (\%)} = (ww - wi)/(wi) \times 100 \qquad \textbf{(Equation 2)}$$

The durability of Ty–GG/SF hydrogels was evaluated by enzymatic degradation test. The enzyme, protease from Streptomyces griseus type XIV (Sigma-Aldrich, St. Louis, MOI, USA) was prepared at 1 and 3.3 U mL^{-1} by dissolution in PBS. The initial weight of each sample was measured, and then the hydrogels were immersed in a protease solution. The dry weight (wf) was evaluated after samples were dried at 70°C and until they reached a constant weight. The study was done at 37°C at different time points, 3 replicates per time points, for 21 days. The weight loss was calculated using **Equation 3**.

$$\text{Weight Loss (\%)} = (wi - wf)/(wi) \times 100 \qquad \textbf{(Equation 3)}$$

VII-3.1.5. Gelation Time, Injectability and Rheological Properties of the Ty–GG/SF Hydrogels

The gelation time was assessed after mixing Ty–GG/SF (1:1) with HRP and H_2O_2 in a vial at 37 °C in a water bath, which then was inverted to better analyze the hydrogel fixed in the bottom and measure how long hydrogel formation takes.

The injectability measurements were made utilizing a syringe with a 27 G needle in injectability equipment (PARALAB, Porto, Portugal). The syringe was filled with Ty–GG/SF that was then injected at a rate of 1 mL min^{-1} through the needle by applying the force exerted by the injectability machine. The injection force needed for each hydrogel condition was assessed, and water was used as control.

The mechanical properties of Ty–GG/SF hydrogels were assessed through an oscillatory mode in a rheometer (Kinexus pro+rheometer, software rSpace, from Malvern, Worcestershire, UK)). The oscillatory experiments were performed using a plate–plate measuring system compound via an upper stainless-steel plate 8 mm in diameter, with a rough finish, so that the samples did not slip. The mechanical spectra (frequency sweep curves) were obtained from 0.1 to 10 Hz of frequency, at a shear strain of 0.3% for 5 minutes. All experiments were repeated 3 times at 37°C. The shear strain used was within the linear viscoelastic region (LVER) of the material, previously obtained through strain sweep

curves. By using a value from LVER it is ensured that the applied stress did not cause microstructural breakdowns (called yielding), and the hydrogel properties could be accurately determined.

VII-3.1.6. Betamethasone Release Studies of the Ty–GG/SF Hydrogels

To evaluate anti-inflammatory drug release systems, betamethasone was loaded in Ty–GG/SF hydrogels. The Ty–GG/SF hydrogels with encapsulated betamethasone (Sigma-Aldrich, St. Louis, MO, USA) were prepared by mixing Ty–GG/SF solution with 5 mg mL^{-1} of betamethasone in PBS, and the enzymatic crosslinking was obtained using the enzyme HRP and substrate H_2O_2. Each hydrogel was immersed in 1 mL of PBS to evaluate the betamethasone release profile. The samples were put in an incubator at 37°C and removed after 3, 6, 24, 72, 168, 336 and 504 hours. The supernatant was removed and kept at −80°C until further analysis. The same hydrogels were used throughout the experiment.

A sequence of betamethasone dilutions was prepared (from 0 to 5 mg mL^{-1} in PBS) to obtain a calibration curve and assesses the amount of betamethasone released. The UV absorbance at 245 nm [27] was read in a microplate reader to measure the betamethasone release (EMax; Molecular Devices, Sunnyvale, CA, USA). Three samples per condition were evaluated at each time point.

VII-3.2. *In vitro* studies

VII-3.2.1. Chondrogenic Cell Isolation

Firstly, after quarantine time for the New Zealand white rabbits, they were injected subcutaneously with a mixture of ketamine (15 mg/kg) and metedomidine (0.25 mg/kg) for anesthesia. The animals were euthanized by intravenous injection of an overdose of pentobarbital sodium (200 mg/kg). The knees from rabbits were removed, and the samples were washed 3 times with a PBS (1X) solution. The cartilage was cut into small pieces and placed inside a conical tube with 1.5% (*v/v*) antibiotic–antimycotic. The sample was centrifugated at 300 G for 3 min at 4°C, and the supernatant was discarded and replaced with a solution with DMEM/F12 medium and collagenase A (0.2% in PBS) (Roche, USA), previously sterilized. The sample was kept in the CO_2 incubator at 37°C for 24 hours. After incubation time, cells were centrifuged at 300 G for 3 min at 4 °C. The supernatant was removed,

and cells were seeded on a flask with medium and kept in the CO_2 incubator at 37°C until they are ready to be used [28],[29]. The institutional and national guidelines and certification for animal experimentation were followed.

VII-3.2.2. Cell Culture

In this work were used chondrogenic cells, isolated from female New Zealand white rabbits (Damul Sci., Jeonju, Korea) with 6 weeks old. The cells were cultured with Dulbecco' s modified eagle medium (DMEM/F12) (Gibco, Waltham, MA, USA) and supplemented with 10% (*v/v*) fetal bovine serum (Gibco, Waltham, MA, USA) and 1% (*v/v*) antibiotic-antimycotic (Gibco, Seoul, South Korea) under standard conditions (37°C in a humidified atmosphere containing 5% CO_2).

The therapeutic effect was assessed in a human monocytic cell line (THP-1) (Sigma -Aldrich, St. Louis, MO, USA) (Sigma -Aldrich, St. Louis, MO, USA). RPMI 1640 Medium, GlutaMAX™ Supplement, HEPES (Thermo Fisher Scientific, Waltham, MA , USA) was used and supplemented with 10% (*v/v*) fetal bovine serum and 1% (*v/v*) of penicillin and streptomycin, under standard culture conditions (37°C in a humidified atmosphere containing 5 vol% CO_2).

VII-3.2.3. Metabolic Activity

The MTT assay was made to evaluate the metabolic activity of chondrogenic primary cells following MEM extract test.

The Ty–GG/SF hydrogels (C1, C2 and C3) were produced with a width ranging from 0.5 to 1 mm, with a minimum area of 60 cm^2. The hydrogels were placed in a sterile tube with 10 mL of cell culture medium (DMEM-F12) for 24 hours, in the water bath at 37°C and 60 rpm. Simultaneously, 200 µL cell suspensions of chondrogenic primary cells were seeded into 96 well plates to achieve a cell density of 10,000 cells per cm^2. After incubation time, the medium that was in contact with the Ty–GG/SF hydrogels (extraction fluid) was passed through a 0.45 µm membrane filter and added to chondrogenic primary cells. Cells with DMEM-F12 medium were used as controls. Test samples were incubated in triplicate. The cell culture medium was evaluated by 3-(4,5-dimethylthiazol-2-yl)-2,5-diphenyltetrazolium bromide (MTT, Sigma-Aldrich, Seoul, South Korea) at 24, 48 and 72 hours. At each time point, the cell

culture was refilled with a new culture medium, an MTT assay was done in a 9:1 ratio and the cell culture was incubated for 3 hours. After violet crystals were produced, they were melted using dimethyl sulfoxide solution (DMSO), and 100 µL of solution from each well was transferred to 96-well plates. The optical density was read at 570 nm via microplate reader (EMax; Molecular Devices, Sunnyvale, CA, USA).

The MEM extract test was applied laid down in European and international standards (ISO10993-5).

VII-3.2.4. DNA Quantification

The total amount of DNA was assessed using a DNA quantification kit (Quant-iT™ PicoGreen® dsDNA Assay Kit, Invitrogen, Waltham, MA, USA), to evaluate the effects of Ty–GG/SF hydrogels on chondrogenic primary cells. The protocol used for the seeding of cells and the handling of the Ty–GG/SF hydrogels was the same as that described in the previous section (MEM extract test). Briefly, extraction solution of Ty–GG/SF hydrogels (C1, C2 and C3) was incubated with chondrogenic cells at a density of 10,000 cells cm^{2} for 24, 48 and 72 hours. Cells cultured with DMEM-F12 medium were used as a positive control. After incubation time, the cells were washed with PBS solution and lysed with pure water. The cell solution was incubated for 1 hour in a water bath at 37°C and kept at –80 °C until further analysis. Several concentrations between 2 and 0 µL ml^{-1} were prepared to make the DNA calibration curve. The fluorescence was read using excitation of 480/20 nm and emission of 528/20 nm in a microplate reader, and DNA concentration was obtained from the standard curve.

VII-3.2.5. Fluorescence Microscopy

Chondrogenic primary cells were seeded using the same protocol and conditions described above. After that, cells were fixed with 10% (v/v) formalin (Sigma-Aldrich, St. Louis, MOI, USA) and stained with 4,6-diamidino-2-phenylindole, dilactate (DAPI blue, VWR International, USA) for nuclei and Texas Red-X phalloidin (Sigma-Aldrich, St. Louis, MOI, USA) for actin filaments of the cytoskeleton. Cells were observed through the fluorescence microscope (Axiolmager, Z1, Zeis Inc., Oberkochen, Germany).

VII-3.2.6. The Therapeutic Efficacy of Ty–GG/SF with Betamethasone Encapsulated

To assess anti-inflammatory activity, a THP-1 cell line stimulated with lipopolysaccharide (LPS) (Sigma-Aldrich, St. Louis, MOI, USA) was used as an *in vitro* model. From the 3 conditions tested, the two that had the best results in metabolic activity and cell proliferation were evaluated (C1 and C3). THP-1 cells were seeded at a density of 1×10^6 cells/mL in RPMI medium with 100 nM phorbol 12-myristate-13 acetate (PMA) (Sigma-Aldrich, St. Louis, MOI, USA) for 24 hours. After incubation time, the medium in the wells was refilled with RPMI medium without PMA and incubated for another 48 hours. Cells were incubated with 100 ng mL^{-1} of LPS in RPMI medium and incubated for 5 hours, to induce the inflammatory response. After this period, cells were cultured with the conditions previously mentioned (C1 and C3) for 7 days. At each time point, 1, 3 and 7 days, the culture medium was removed and stored at −80 °C for further analysis.

This test was done to evaluate the concentration of the cytokine TNFα in the medium after being in contact with the hydrogels. Human TNF-alpha DuoSET ELISA (R&D Systems, Minneapolis, MN, USA) kit and DuoSet Ancillary Reagent Kit 2 (R&D Systems, Minneapolis, MN, USA) were used. TNF-α standard solutions with concentrations from 1000 to 0 pg mL^{-1} were also evaluated in the ELISA plate to formulate the calibration curve. The optical density at 450 nm was read in a microplate reader (Synergy HT, BIO-TEK, Winooski, VT, USA).

VII-3.2.7. Statistical Analysis

Statistical analysis was done with GraphPad Prism 8 version, where a Shapiro–Wilk normality test was formerly performed to evaluate the data normality. Statistical significance was obtained as * $p < 0.05$, ** $p < 0.01$ or *** $p < 0.001$. Results are presented as means ± standard deviations, and all assays were performed in triplicate.

VII-4. RESULTS AND DISCUSSION

VII-4.1. Physicochemical Characterization

This study focused on the production of Ty–GG/SF hydrogels via enzymatic crosslinking with HRP and H_2O_2 with encapsulated betamethasone to increase therapeutic efficacy in the treatment of inflammation in patients with rheumatoid arthritis.

Initially, a 1% (*w/v*) Ty–GG solution was mixed with a 2% (*w/v*) of SF solution to produce Ty–GG/SF hydrogels, followed by physicochemical characterization by FTIR. FTIR methodology was followed to predict the secondary structure of SF in hydrogels. The deconvolution method was made to quantitatively estimate the conformational ratio in the amide I region. The IR spectral region of amine I (1700–1600 cm^{-1}) absorption had already been frequently used for the analysis of different secondary structures of SF. The intensity ratios of the β-sheet structure over the α-helix and random coils were calculated to study the relationship between the crystalline and amorphous phases in the SF [30]. The conformational transitions and crystalline content of SF highly influence its physiochemical properties, affecting its biological properties and applications. The secondary structure (Silk II) has an important role in its physicochemical properties and supports its mechanical stabilities [31]. **Figure VII-1** shows the secondary structure of SF 2% (*w/v*) alone and after mixing with Ty–GG solution, HRP and H_2O_2 (C1, C2 and C3).

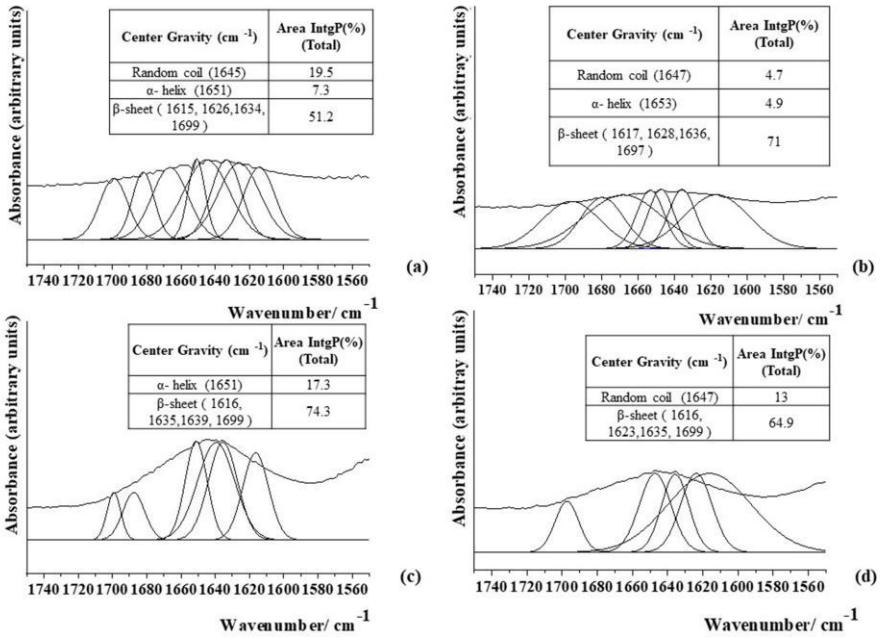

Figure VII-1 - FTIR spectra of secondary structure of the 2% SF solution alone (a) and after producing Ty–GG/SF hydrogels via HRP and H_2O_2, C1 (b), C2 (c) and C3 (d).

The spectrum of 2% (*w/v*) SF protein (Figure 1a) revealed an absorption band at 1651 cm^{-1} (7.3%), which is a characteristic peak for an α-helix, and another absorption peak located at 1645 cm^{-1} (19.5%) for a random coil structure (corresponding to Silk I structure). The absorption bands at 1615, 1626, 1634 and 1699 cm^{-1} (51.2%) are features of the β-sheet structure (corresponding to Silk II crystal structure). Quantitative analysis showed—after Ty–GG/SF hydrogels were produced—that the β-sheet structure was the dominant conformation in all conditions (C1 (71%), C2 (74.3%) and C3 (64.9%)), demonstrating that the tested conditions produce more crystalline phases than amorphous; see Figure 1b–d. That is, SF acquired a more stable structure after the formation of Ty–GG/SF hydrogels. The results obtained indicate that the presence of Ty–GG to do enzymatic crosslinking via HRP may have increased the number of β-sheets in the structure of SF.

These results are in line with other studies that showed that modified SF and enzymatic crosslinks were marked by increases of the β-sheet content, that is, improved mechanical properties when compared with SF alone [31],[32]. The other studies hypothesized that once SF acquires its mobility within the structure, it is natural to return toward the more stable secondary structure, which is the β-sheet the in the case of SF [33].

After analyzing the secondary structure of SF, Ty–GG/SF hydrogels (C1, C2, and C3) were evaluated regarding water uptake capacity and enzymatic degradation; see **Figure VII-2.**

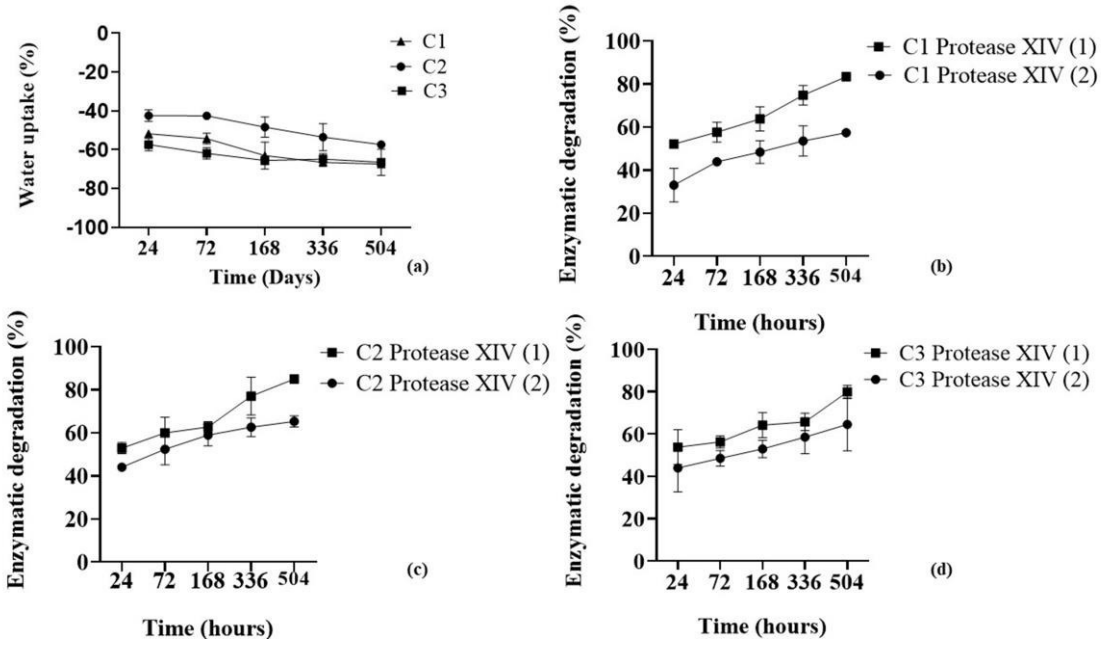

Figure VII-2 - Water uptake (a) and enzymatic degradation profiles of C1 (b), C2 (c) and C3 (d) with Protease XIV at 3.3 U mL^{-1} (1) and 1 U mL^{-1} (2) and after 24, 72, 168, 336 and 504 hours.

The swelling kinetics of Ty–GG/SF hydrogels (Figure 2a) were evaluated after they were immersed in PBS solutions (physical crosslinking) for 21 days to maximize crosslinking of the polymeric networks and reach the equilibrium. The water absorption graph showed that all conditions present a negative absorption rate over time, C1 (–57.37% ± 1.12%), C2 (–68.82% ± 5.19%) and C3 (–67.41% ± 0.62%). Regarding the water uptake statistical analysis, there were only significant differences between C1 and C2 ($p < 0.05$) at timepoints 24 and 72 hours, by nonparametric Kruskal–Wallis test. The mass swelling ratio has an important role in the mechanical performance, and the combination of chemical and physical leads to the production of hydrogels with high versatility of mechanical properties [34]. The swelling properties are significantly influenced by crosslinking density and ionic osmotic pressure [35]. The chemical crosslink network is highly flexible, allowing the extension of the polymeric network without breaking it. In contrast, the exposure to the physical crosslinking allows the diffusion of monovalent cations within the inner polymeric network and the formation of strong ionic bonds between the chains. These bonds are less flexible, so the capability of the polymer to retain the solvent is decreased by the physical crosslinking. The combination of both crosslinking mechanisms leads to obtaining hydrogels that significantly decrease their mass swelling ratio in PBS [36],[37]. The results

are in agreement with the studies previously mentioned, which showed that if an external solution is ionically more concentrated than structure, it will promote the entry of ions into the hydrogels, and water molecule expulsion. This allows stabilization and increases the crosslinking of the polymeric chains. [38],[39]. Hence, the Ty–GG/SF hydrogels showed a high degree of crosslinking and consequently a good mechanical property. The enzymatic degradation profile was obtained by immersion of Ty–GG/SF hydrogels in PBS solution with sodium azide and diluting the enzyme protease from *Streptomyces griseus* Type XIV, ≥3.5 U mg^{-1} at 1 and 3.3 U mL^{-1}; see Figure 2b–d. The results of the enzymatic degradation showed that condition 1 had a more significant difference in the degree of degradation using the enzyme concentrations 1 U mL^{-1} (57.37% ± 1.2%) and 3 U mL^{-1} (83.41% ± 0.6%). The same degradation pattern was also found in C2 (66.23% ± 2.12% at 1 U mL^{-1} and 84.97% ± 0.86% at 3.3 U mL^{-1}) and C3 (66.23% ± 8.82% at 1 U mL^{-1} and 79.89% ± 2.18% at 3.3 U mL^{-1}). C1, C2 and C3 have similar degradation profiles, but although the differences were not significant, C1 and C3 showed lower degradation profiles over time; that is, those conditions may be slightly more resistant to degradation. Regarding the enzymatic degradation statistical analysis , there were only significant differences between C1, 1 vs. 3.3 U mL^{-1} ($p < 0.01$) at time point 504 h, C2, 1 vs. 3.3 U mL^{-1} ($p < 0.05$) at time point 24 hours, and $p < 0.01$ at timepoint 504 h, by unpaired *t* test. These results may be due to the ratio between the HRP enzyme and H_2O_2, which can influence the degree of reticulation of the sample consequently, the degradation profile. Even so, no conditions exposed to the concentration of protease at 1 and 3 U mL^{-1} showed a total degradation profile after 21 days of study. Considering the hydrogels' degradation profiles, during the time of study, in approximately 1 month the hydrogels could be completely degraded.

Bearing in mind the degradation profiles of Ty–GG/SF hydrogels, it was possible to verify that they are highly resistant to enzymatic degradation when compared to the degradation profiles from other studies, carried out with the same enzyme at different concentrations [13],[40].

The gelation time was measured by the inverted tube method. Each condition of Ty–GG/SF hydrogels was produced at room temperature in a tube and monitored by repeat inversion. The gelation time was noted when the solution was no longer flowing upon inversion by the force of gravity, demonstrating the production of a stable gel network. It was possible to observe that all concentrations (C1, C2 and C3) had gelation times around 3–5 minutes. Gelation time is an essential component for developing the in situ-forming hydrogels, and it is associated with the crosslinking rate of the HRP-

catalyzed reaction. HRP and H_2O_2 concentrations are crucial criteria to control the crosslinking rate. The gelation time decrease with increasing HRP concentration and vice versa have been studied [41],[42]. A slow gelation rate may provoke the heterogeneous distribution of encapsulated entities, so controlled gelation is necessary for efficient local delivery of drugs [43]. Considering the obtained results, it was possible to verify that Ty–GG/SF hydrogels presented a rapid gelation time which may be due to a high degree of enzymatic crosslinking promoted by the HRP enzyme and its H_2O_2 substrate.

Since the hydrogels are intended to be injected into intra-articular cavities, it is crucial to evaluate the injectability profiles of the gels. The injectability, the force required for injection, is a key-product performance parameter to evaluate the performance of the formulation during the injection. The injectability was performed in all conditions, C1, C2 and C3, and as a control water was used. The syringe was filled with the Ty–GG/SF solution, HRP and H_2O_2 to produce the hydrogels, and the injection was performed using a rate of 1 mL min^{-1}. The obtained injection force profile per condition and that for water (control) are presented in **Figure VII-3.**

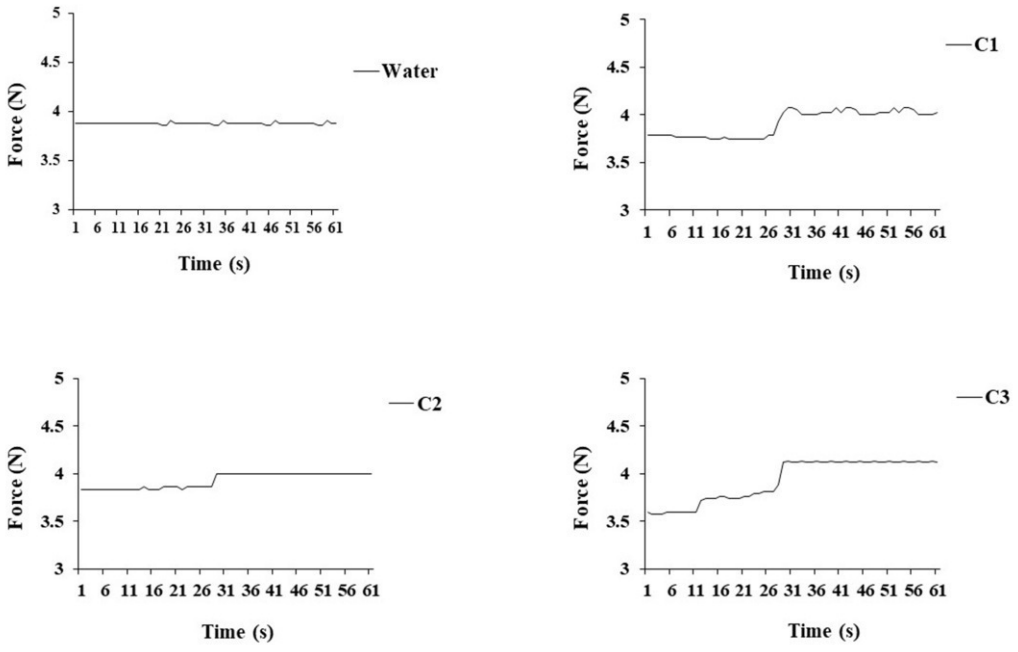

Figure VII-3 – Injectability profiles of Ty–GG/SF hydrogels, C1, C2 and C3 and water (control). There are not significant differences.

It was possible to verify that the forces needed to inject all conditions were similar—C1 (3.9 N ± 0.13 N), C2 (3.9 N ± 0.07 N) and C3 (3.9 N ± 0.2 N)—as was the control with the water (3.8 N ± 0.01

N). Firstly, all conditions presented low values of injectability, and at around 30 s, there was an increase in force. This change in values may have been due to the beginning of the crosslinking between molecules, leading to the need for the higher force to inject. However, the value of the force required for each condition remained similar to that of water. This indicated that all conditions have an adequate injectability profile to be used as injectable hydrogels.

To evaluate the mechanical properties of Ty–GG/SF hydrogels, they were produced, via enzymatic crosslinking, and immersed in PBS, physical crosslinking, for 21 days. At each time point (24, 72, 168, 336, and 504 h), they were removed and evaluated through the oscillatory rheology experiment at 37 °C. The oscillatory shear flow was used extensively to characterize the viscoelastic capacities of materials and to relate them to the polymer structures. The small-amplitude oscillatory shear determines storage modulus (G′) and loss modulus (G″) in terms of stress amplitude and lag between the stress and strain. The phase and amplitude of the relevant portion of the resulting spectra of the stress and strain are used to calculate the storage modulus (G′), loss modulus (G″) and phase angle (δ) for the hydrogel. The phase angle ($0 \leq \delta \leq 90°$) is a representative physical property that measures the material viscoelasticity and G′, G″ and δ are determined by equation ($\varepsilon(t) = \varepsilon o \sin \omega t$), εo (amplitudes of the sinusoidal strain curves) [44],[45]. A phase angle of 0° is characteristic of elastic solids; on the other hand, 90° is characteristic of viscous liquids, and between 0° and 90° represents the viscoelastic materials [46]. The mechanical properties of the Ty–GG/SF hydrogels are shown in **Figure VII-4.**

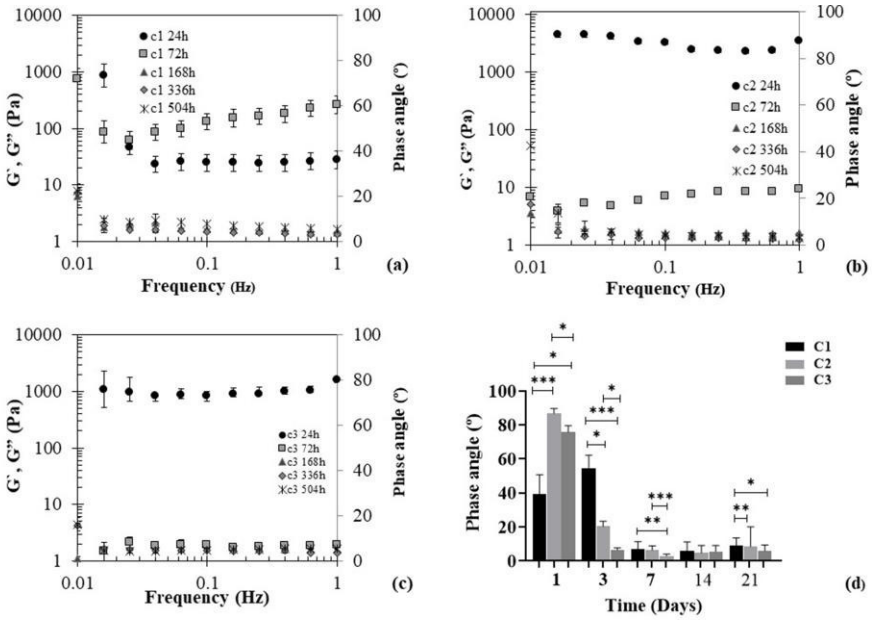

Figure VII-4 – Mechanical spectra of Ty-GG/SF hydrogels C1 (a), C2 (b) and C3 (c) and phase angle values (d) at different timepoints (24, 72, 168, 336 and 504 hours). G′ (elastic moduli) and G″ (viscous moduli). Significant differences ***p<0.001, **p<0.01 and *p<0.05, by nonparametric Kruskal–Wallis test. There are not significant differences.

The mechanical proprieties resulting from conditions 1 and 2 of Ty–GG/SF hydrogels showed that at time points 24 and 72 hours the G″ > G′, and consequently there was a high phase angle, that is, a viscous component higher than the solid. The same pattern was verified in condition 3 at time point 24 h, however, from the third day to last time point G′ > G″, meaning that the solid component was higher than the viscous. The same profile can also be seen in conditions 1 and 2, where there was a higher solid than viscous component from the third day; see (Figure 4d). Regarding these results, it was possible to verify that Ty–GG/SF hydrogels had a viscoelastic behavior with a higher elastic component. The cartilage presents viscoelastic mechanical behavior and Ty–GG/SF hydrogels had a mechanical profile similar to the tissue where they will be injected (intra-articular injection); consequently, this material demonstrated a good mechanical capacity for the proposed objective [47]. This equipment could also be used to measure the exact time of gelation by finding the gel point, where the G′ and G″ curves cross. However, the reaction is swift, and the samples quickly acquire the gel character.

Traditional drug delivery approaches present some side effects, such as systemic toxicity and repeating doses. Betamethasone suspensions can be used for intraarticular injection in the inflamed joint. Normal intraarticular doses of betamethasone suspensions vary with the size of the joint, from 1.5

to 12 mg [48]. In the present work, we used 5 mg mL^{-1} of betamethasone since it was the average value found in the literature to have anti-inflammatory activity [23]. Betamethasone has a short half-life of about 36–54 hours [49], which means that the drug must be injected more frequently to treat inflammation in the patient. However, hydrogels are suitable drug delivery vehicles to minimize these effects and optimize therapeutic benefits from the drug. The hydrogels have tunable physical properties that confer great controlled drug release and drug protection from degradation. Thus, hydrogels emerged as a very efficient drug delivery system [50, 51].

Drug release results showed that after 21 days, C1 presented a betamethasone release profile of 75% ± 0.3% (approximately 3.75 mg mL^{-1}), C3 a rate of 80% ± 0.5% (approximately 4 mg mL^{-1}) and C2 a rate of betamethasone release of 38% ± 3.3% (approximately 1.9 mg mL^{-1}) (**Figure VII-5**); that is, no concentration reached the maximum release after 21 days. Significant differences were found at time points 1h and 3 h between C1 and C2 $p < 0.05$, at time point 72 hours between C1 and C2 $p < 0.05$, at time point 168 between C2 and C3 $p < 0.05$ and at time point 336 hours between C1 and C2 * $p < 0.05$, by nonparametric Kruskal–Wallis test. Considering these results, it was possible to state that all conditions had a controlled release profile of betamethasone, which allows prolonged treatment and less frequent drug administration to the patient. Furthermore, this approach can help reduce the toxic effects of drugs. Thus, Ty–GG/SF hydrogels presented the great potential to be used as a betamethasone delivery system.

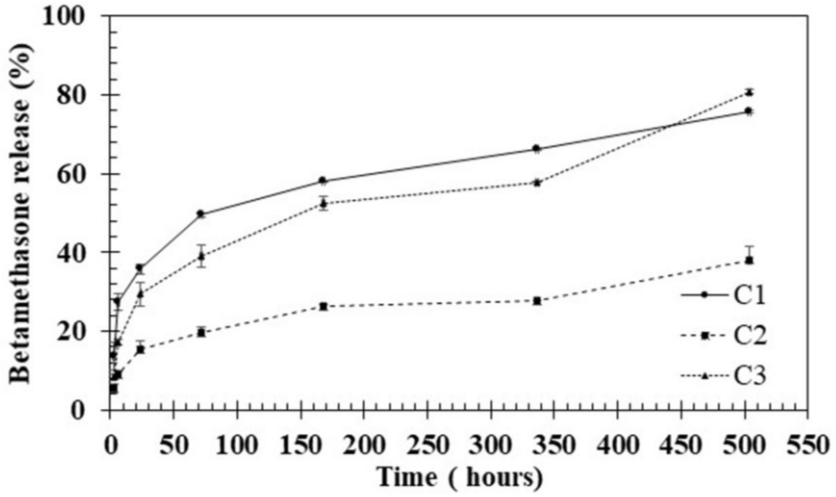

Figure VII-5 – Percentage of betamethasone release from Ty–GG/SF hydrogels (C1, C2 and C3) for 1, 3, 24, 72, 168, 336 and 504 hours.

VII-4.2. *In vitro* studies

The MTT assay and DNA quantification were performed in order to assess the metabolic activity and cell proliferation of chondrogenic primary cells with different conditions of Ty–GG/SF hydrogels (C1, C2 and C3) for 72 hours; see **Figure VII-6.**

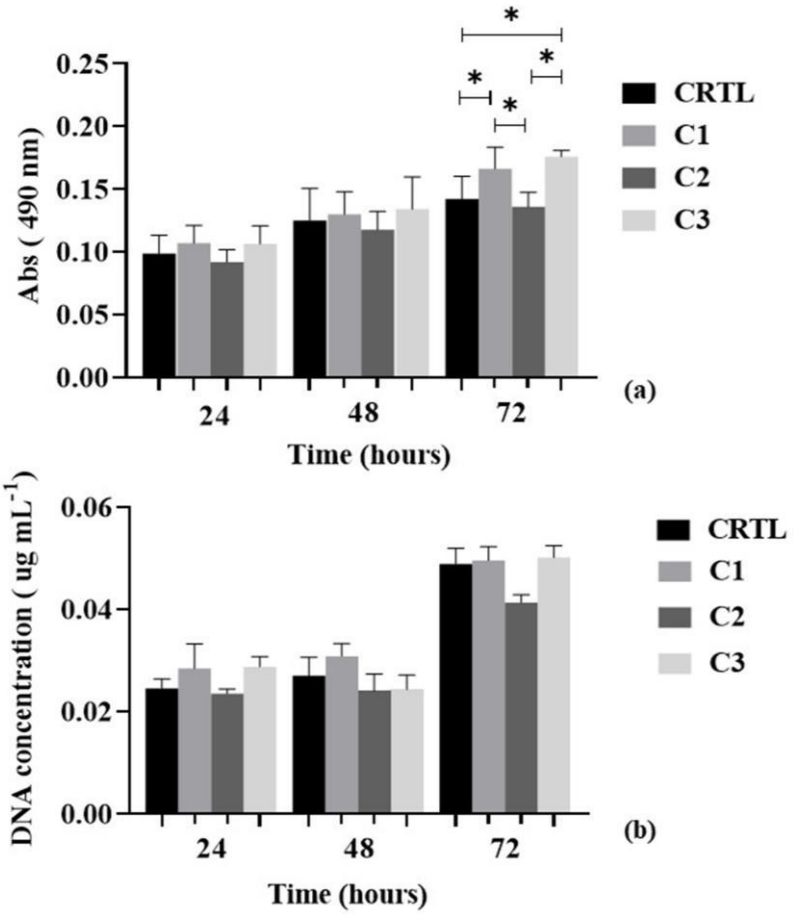

Figure VII-6 – MTT assay (a) and DNA quantification (b) of chondrogenic primary cells with control (cells with DMEM-12 medium) and different Ty–GG hydrogels conditions (C1, C2 and C3) for 24, 48 and 72 hours. Significant differences ***p< 0.001, **p<0.01 and *p<0.05. Nonparametric Kruskal–Wallis test (MTT assay) and Ordinary one-way ANOVA (DNA quantification).

At time points 24 and 48 hours, chondrogenic primary cells showed an increase of metabolic activity and we did not observe significant differences between any conditions ($p > 0.05$). At 72 hours, there continued to occur an increase in metabolic activity, but we found significant differences between control and C1 (* $p < 0.05$), control and C3 (* $p < 0.05$), C1 and C2 (* $p < 0.05$) and C2 and C3 (* $p < 0.05$)—Figure 6a.

DNA proliferation was quantified using the cell content based on dsDNA quantification; see Figure 6b. An increase in the cell number was observed in the control and C1 for 48 hours, and C2 showed approximately the same values in cell proliferation between 24 and 48 hours. However, in C3, there was a decrease in cell proliferation between 24 and 48 hours, increasing again at 72 hours. At the last time point, all conditions demonstrated an increase in cell proliferation and significant differences were

not observed. However, the most evident difference was between the (control, C1 and C3) and C2; despite the increase in the number of cells from 48 to 72 hours, cell proliferation was lower.

These results are in agreement with the studies found in the literature where the hydrogels of GG and SF do not produce cytotoxic effects on cells [52, 53].

The morphology of chondrogenic primary cells, in contact with Ty–GG hydrogel extract, was analyzed by fluorescence microscopy, **(Figure VII-7).**

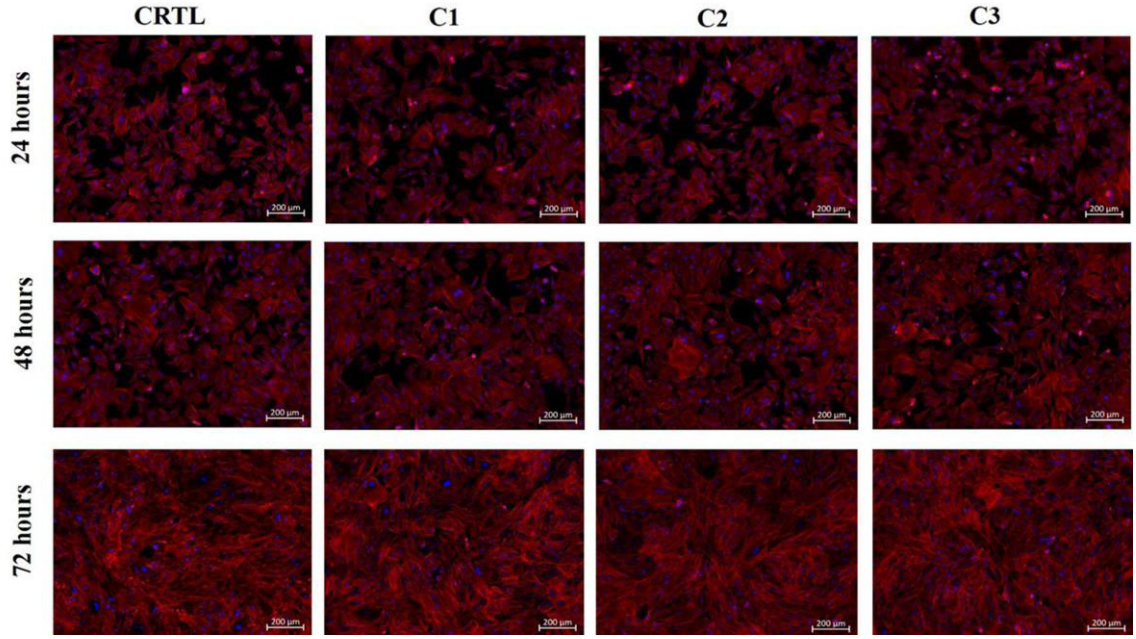

Figure VII-7 – Fluorescence microscopy images of chondrogenic primary cells cultured in the presence of CRTL (RPMI medium) and Ty–GG/SF hydrogels made in different conditions (C1, C2 and C3) for 72 hours.

Chondrogenic primary cells were incubated with C1, C2 and C3 of Ty–GG/SF hydrogels. It was possible to see that all conditions presented the typical morphology of chondrogenic primary cells, blue (nuclei) and red (cytoskeleton), suggesting healthy proliferation and survival when compared with control.

To assess the therapeutic efficacy of Ty–GG/SF hydrogels, the levels of tumor necrosis factor alpha (TNFα) were quantified. In patients with RA, high levels of this cytokine were observed in the synovial fluid, making TNFα an exciting target for RA treatment [5].

Firstly, THP-1 cells were differentiated with PMA and stimulated with LPS to evaluate the capacity of Ty–GG/SF with encapsulated betamethasone to decrease the levels of TNFα present in the RPMI

medium. The ability of each of C1 and C3 to decrease TNFα was evaluated because they were the best conditions in metabolic activity and cell proliferation.

After the inflammation was activated, several conditions were evaluated: betamethasone alone (5 mg mL^{-1}), and Ty–GG/SF hydrogels (C1 and C3) with and without betamethasone encapsulated (5 mg mL^{-1}). Cells differentiated with PMA were used as the negative control and cells stimulated with LPS as the positive control.

Figure VII-8 shows the amount of TNFα present in RPMI medium in contact with C1 and C3 of Ty–GG/SF hydrogels for 7 days.

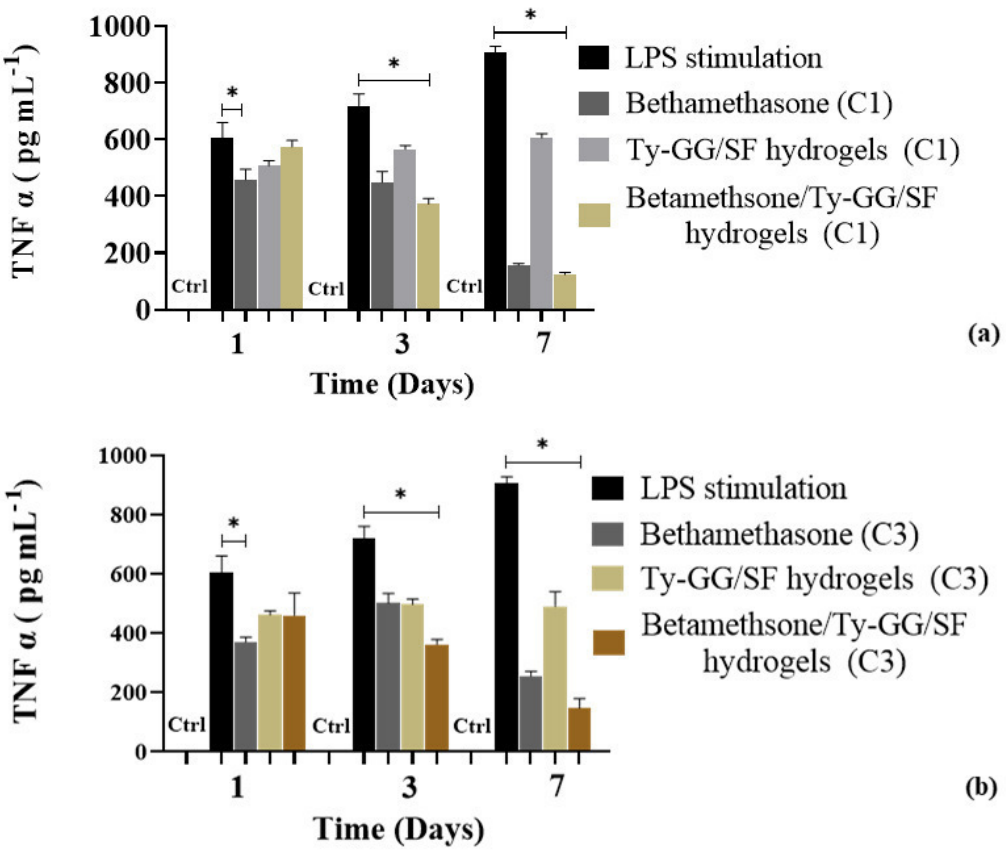

Figure VII-8 – Amount of uncaptured TNF α under different conditions; cells with PMA without LPS stimulation (Ctrl), cells stimulated with LPS, betamethasone (C1), Ty – GG/SF hydrogels (C1) and Ty – GG/SF hydrogels with encapsulated betamethasone (C1) (a). Cells with PMA without LPS stimulation (Ctrl), cells stimulated with LPS, betamethasone (C3), Ty–GG/SF hydrogels (C3) and Ty–GG/SF hydrogels with encapsulated betamethasone (C3) (b). Significant differences *** $p < 0.001$, ** $p < 0.01$ and * $p < 0.05$, nonparametric Kruskal–Wallis test.

The results obtained showed that untreated LPS-stimulated cells showed increasing amounts of TNF over the study period, thereby demonstrating that the stimulation of cells with LPS was achieved. Furthermore, it was possible to verify that the Ty–GG/SF hydrogels (C1 and C3) without encapsulated betamethasone had no effect on decreasing the amount of TNFα. On the other hand, it was observed that the decrease of the TNFα concentration was higher in cells treated with Ty–GG/SF hydrogels, in both conditions (C1 and C3), when compared with betamethasone alone (C1 and C2). This trend continued throughout the study period, and the difference between the therapeutic efficacy of Ty–GG/SF hydrogels with betamethasone encapsulated and the drug alone became more evident at the last point of time, 7 days. This more evident difference may be due to the fact that the hydrogels were being degraded, so there was a higher release of betamethasone at 7 days than at the initial time points, 1 and 3 days.

These results are in agreement with the studies found in the literature where they describe that GG and SF have several unique properties that become favorable for the incorporation and delivery of a range of the therapeutic agents [54],[55].

VII-5. CONCLUSION

In this study, drug-loaded, injectable Ty–GG/SF hydrogels were produced to increase therapeutic efficacy in an inflammatory environment. The results obtained are promising enough to envisage a possible application of this product in the inflamed joints of patients with RA. The Ty–GG/SF hydrogels presented a dominant conformation of β-sheet structure (crystalline phase), thereby indicating that the use of Ty–GG increased the number of β-sheets, that is, a more stable structure when compared with SF alone. The Ty–GG/SF hydrogels showed low water absorption capacity due to the high degree of enzymatic and physical crosslinking. The enzymatic degradation demonstrated that Ty–GG/SF hydrogels exposed to the concentrations of protease of 1 and 3 U mL^{-1} demonstrated good resistance to

degradation—not reaching its maximum after 21 days of study. Furthermore, the hydrogels showed rapid gelation time, good strength and a controlled betamethasone release profile over time, which are appropriate physicochemical characteristics for the final application. The *in vitro* studies demonstrated that Ty–GG/SF hydrogels did not produce any deleterious effect on cellular metabolic activity, morphology or proliferation. Furthermore, the Ty–GG/SF hydrogels with betamethasone encapsulated revealed greater therapeutic efficacy than the drug alone, and although the difference was not significant, showed that if the study time is increased, the therapeutic effect of hydrogels with betamethasone encapsulated can be even more visible. Therefore, Ty–GG/SF hydrogels can provide an improvement in therapeutic efficacy through controlled drug delivery, thereby overcoming the disadvantages of current strategies for treating rheumatoid arthritis.

VII-6. Author Contributions

Isabel Oliveira: Formal analysis, Investigation, Visualization, Writing-Original draft, address revisions; Cristiana Gonçalves: Conceptualization, Physical-Chemical Methodology, Writing–Review & Editing; Myeong Eun Shin: Investigation, *In vitro* Methodology; Sumi Lee: Investigation, *In vitro* Methodology; Rui Luis Reis: Project administration, Resources, Review, Validation; Gilson Khang:: Project administration, Resources, Review, Validation; Joaquim Miguel Oliveira: Supervision, Project administration, Resources, Review & Editing.

Funding: Norte2020 project ("NORTE-08-5369-FSE-000044") and REMIX project (GA 778078—REMIX—H2020-MSCA-RISE-2017)

VII-7. Acknowledgments

The authors thank the financial support under the Norte2020 project ("NORTE-08-5369-FSE-000044"), REMIX project (GA 778078—REMIX—H2020-MSCA-RISE-2017) Gilson Lab, Chonbuk National University, Republic of Korea and the Frontiers of technology for theranostics of cancer, metabolic and neurodegenerative diseases (FROnTHERA), Structural Project NORTE-01-0145-FEDER-000023. The FCT distinction attributed to J.M.O. under the Investigator FCT program (number

IF/01285/2015) is also greatly acknowledged. C.G. also wishes to acknowledge FCT for supporting her research (number SFRH/BPD/94277/2013).

VII-8. CONFLICTS OF INTEREST

The authors declare no conflict of interest.

VII-9. REFERENCES

1. Chancay, M.G., S.N. Guendsechadze, and I. Blanco, *Types of pain and their psychosocial impact in women with rheumatoid arthritis.* Women's Midlife Health, 2019. **5**(1): p. 3.
2. Sardar, S. and Å. Andersson, *Old and new therapeutics for rheumatoid arthritis: in vivo models and drug development.* Immunopharmacology and immunotoxicology, 2016. **38**(1): p. 2-13.
3. Kesharwani, D., et al., *Rheumatiod arthritis: an updated overview of latest therapy and drug delivery.* Journal of Pharmacopuncture, 2019. **22**(4): p. 210.
4. Yasir, M. and S. Sonthalia, *Corticosteroid Adverse Effects*. 2019, StatPearls Publishing, Treasure Island (FL).
5. Oliveira, I.M., et al., *Engineering nanoparticles for targeting rheumatoid arthritis: Past, present, and future trends.* Nano Research, 2018. **11**(9): p. 4489-4506.
6. Guo, Q., et al., *Rheumatoid arthritis: pathological mechanisms and modern pharmacologic therapies.* Bone research, 2018. **6**: p. 15-15.
7. Lee, J.H., *Injectable hydrogels delivering therapeutic agents for disease treatment and tissue engineering.* Biomaterials research, 2018. **22**(1): p. 1-14.
8. Kim, H.-S., et al., *Biodegradable and injectable hydrogels as an immunosuppressive drug delivery system.* Materials Science and Engineering: C, 2019. **98**: p. 472-481.
9. Liang, K., K.H. Bae, and M. Kurisawa, *Recent advances in the design of injectable hydrogels for stem cell-based therapy.* Journal of Materials Chemistry B, 2019. **7**(24): p. 3775-3791.
10. Onaciu, A., et al., *Hydrogels Based Drug Delivery Synthesis, Characterization and Administration.* Pharmaceutics, 2019. **11**(9): p. 432.
11. Spicer, C.D., *Hydrogel scaffolds for tissue engineering: the importance of polymer choice.* Polymer Chemistry, 2020.
12. Seib, F.P., *Reverse-engineered silk hydrogels for cell and drug delivery.* Therapeutic delivery, 2018. **9**(6): p. 469-487.
13. Ribeiro, V.P., et al., *Combinatory approach for developing silk fibroin scaffolds for cartilage regeneration.* Acta biomaterialia, 2018. **72**: p. 167-181.
14. Ribeiro, V.P., et al., *Rapidly responsive silk fibroin hydrogels as an artificial matrix for the programmed tumor cells death.* PloS one, 2018. **13**(4).
15. Yin, Z., et al., *A silk fibroin hydrogel with reversible sol–gel transition.* RSC advances, 2017. **7**(39): p. 24085-24096.
16. Khanmohammadi, M., et al., *Horseradish peroxidase-catalyzed hydrogelation for biomedical applications.* Biomaterials science, 2018. **6**(6): p. 1286-1298.

17. Lee, F., K.H. Bae, and M. Kurisawa, *Injectable hydrogel systems crosslinked by horseradish peroxidase.* Biomedical Materials, 2015. **11**(1): p. 014101.
18. Liu, H., et al., *A dopamine-functionalized aqueous-based silk protein hydrogel bioadhesive for biomedical wound closure.* New Journal of Chemistry, 2020.
19. Tan, H., et al., *Gelatin/chitosan/hyaluronan scaffold integrated with PLGA microspheres for cartilage tissue engineering.* Acta Biomaterialia, 2009. **5**(1): p. 328-337.
20. Zhu, L., D. Luo, and Y. Liu, *Effect of the nano/microscale structure of biomaterial scaffolds on bone regeneration.* International Journal of Oral Science, 2020. **12**(1): p. 1-15.
21. Milivojevic, M., et al., *Chapter 6 - Gellan gum in drug delivery applications*, in *Natural Polysaccharides in Drug Delivery and Biomedical Applications*, M.S. Hasnain and A.K. Nayak, Editors. 2019, Academic Press. p. 145-186.
22. Muthukumar, T., J.E. Song, and G. Khang, *Biological Role of Gellan Gum in Improving Scaffold Drug Delivery, Cell Adhesion Properties for Tissue Engineering Applications.* Molecules, 2019. **24**(24): p. 4514.
23. Oliveira, I.M., et al., *Enzymatically crosslinked tyramine-gellan gum hydrogels as drug delivery system for rheumatoid arthritis treatment.* Drug Delivery and Translational Research, 2020: p. 1-13.
24. Rockwood, D.N., et al., *Materials fabrication from Bombyx mori silk fibroin.* Nature protocols, 2011. **6**(10): p. 1612.
25. Lee, D.H., et al., *Enhanced osteogenesis of β-tricalcium phosphate reinforced silk fibroin scaffold for bone tissue biofabrication.* International Journal of Biological Macromolecules, 2017. **95**: p. 14-23.
26. Litvinov, R.I., et al., *The α-helix to β-sheet transition in stretched and compressed hydrated fibrin clots.* Biophysical journal, 2012. **103**(5): p. 1020-1027.
27. Wulandari, L. and G. Indrayanto, *HPTLC determination of betamethasone in tablets and its validation.* Journal of liquid chromatography & related technologies, 2003. **26**(16): p. 2709-2717.
28. Manning, W.K. and W.M. Bonner Jr, *Isolation and culture of chondrocytes from human adult articular cartilage.* Arthritis & Rheumatism: Official Journal of the American College of Rheumatology, 1967. **10**(3): p. 235-239.
29. Jeon, H.Y., et al., *Evaluation of saponin loaded gellan gum hydrogel scaffold for cartilage regeneration.* Macromolecular Research, 2018. **26**(8): p. 724-729.
30. Yan, C., B. Yang, and Z. Yu, *Retracted Article: Determination of silk fibroin secondary structure by terahertz time domain spectroscopy.* Analytical Methods, 2013. **6**(1): p. 248-252.
31. Johari, N., L. Moroni, and A. Samadikuchaksaraei, *Tuning the conformation and mechanical properties of silk fibroin hydrogels.* European Polymer Journal, 2020: p. 109842.
32. Wei, W., et al., *Gellable silk fibroin-polyethylene sponge for hemostasis.* Artificial Cells, Nanomedicine, and Biotechnology, 2020. **48**(1): p. 28-36.
33. Taketani, I., et al., *The secondary structure control of silk fibroin thin films by post treatment.* Applied surface science, 2005. **244**(1-4): p. 623-626.
34. Vedadghavami, A., et al., *Manufacturing of hydrogel biomaterials with controlled mechanical properties for tissue engineering applications.* Acta biomaterialia, 2017. **62**: p. 42-63.
35. Huang, Y., H. Yu, and C. Xiao, *pH-sensitive cationic guar gum/poly (acrylic acid) polyelectrolyte hydrogels: Swelling and in vitro drug release.* Carbohydrate Polymers, 2007. **69**(4): p. 774-783.
36. Xu, Y., et al., *Injectable and self-healing chitosan hydrogel based on imine bonds: design and therapeutic applications.* International journal of molecular sciences, 2018. **19**(8): p. 2198.

37. Mihaila, S.M., et al., *Photocrosslinkable kappa‐carrageenan hydrogels for tissue engineering applications.* Advanced healthcare materials, 2013. **2**(6): p. 895-907.
38. da Silva, L.P., et al., *Engineering cell-adhesive gellan gum spongy-like hydrogels for regenerative medicine purposes.* Acta biomaterialia, 2014. **10**(11): p. 4787-4797.
39. Coutinho, D.F., et al., *Modified Gellan Gum hydrogels with tunable physical and mechanical properties.* Biomaterials, 2010. **31**(29): p. 7494-7502.
40. Ribeiro, V.P., et al., *Enzymatically cross-linked silk fibroin-based hierarchical scaffolds for osteochondral regeneration.* ACS applied materials & interfaces, 2019. **11**(4): p. 3781-3799.
41. Jin, R., et al., *Enzyme-mediated fast in situ formation of hydrogels from dextran–tyramine conjugates.* Biomaterials, 2007. **28**(18): p. 2791-2800.
42. Park, K.M., et al., *In situ forming hydrogels based on tyramine conjugated 4-Arm-PPO-PEO via enzymatic oxidative reaction.* Biomacromolecules, 2010. **11**(3): p. 706-712.
43. Bae, J.W., et al., *Horseradish peroxidase‐catalysed in situ‐forming hydrogels for tissue‐engineering applications.* Journal of tissue engineering and regenerative medicine, 2015. **9**(11): p. 1225-1232.
44. Byju, A.G., A. Kulkarni, and N. Gundiah, *Mechanics of gelatin and elastin based hydrogels as tissue engineered constructs.* 13th International Conference on Fracture 2013, ICF 2013, 2013. **6**: p. 4406-4415.
45. Yan, C., et al., *Injectable solid hydrogel: mechanism of shear-thinning and immediate recovery of injectable β-hairpin peptide hydrogels.* Soft matter, 2010. **6**(20): p. 5143-5156.
46. Franck, A. and T.I. Germany, *Viscoelasticity and dynamic mechanical testing.* TA Instruments, New Castle, DE, USA AN004, 1993.
47. Lawless, B.M., et al., *Viscoelasticity of articular cartilage: analysing the effect of induced stress and the restraint of bone in a dynamic environment.* Journal of the mechanical behavior of biomedical materials, 2017. **75**: p. 293-301.
48. Dreyer, S.J. and W.J. Beckworth, *Commonly Used Medications in Procedures.* Pain Procedures in Clinical Practice E-Book, 2011: p. 2.
49. Firestein, G.S., et al., *Kelley and Firestein's Textbook of Rheumatology E-Book*. 2016: Elsevier Health Sciences.
50. Narayanaswamy, R. and V.P. Torchilin, *Hydrogels and their applications in targeted drug delivery.* Molecules, 2019. **24**(3): p. 603.
51. Li, J. and D.J. Mooney, *Designing hydrogels for controlled drug delivery.* Nature Reviews Materials, 2016. **1**(12): p. 1-17.
52. Khang, G., et al., *Biological evaluation of intervertebral disc cells in different formulations of gellan gum‐based hydrogels.* Journal of tissue engineering and regenerative medicine, 2015. **9**(3): p. 265-275.
53. Kim, M.H. and W.H. Park, *Chemically cross-linked silk fibroin hydrogel with enhanced elastic properties, biodegradability, and biocompatibility.* International journal of nanomedicine, 2016. **11**: p. 2967-2978.
54. Wenk, E., H.P. Merkle, and L. Meinel, *Silk fibroin as a vehicle for drug delivery applications.* Journal of Controlled Release, 2011. **150**(2): p. 128-141.
55. D'Arrigo, G., et al., *Gellan gum nanohydrogel containing anti-inflammatory and anti-cancer drugs: a multi-drug delivery system for a combination therapy in cancer treatment.* European Journal of Pharmaceutics and Biopharmaceutics, 2014. **87**(1): p. 208-216.

Chapter VIII

Bioengineered nanoparticles loaded-hydrogels to target TNF alpha in inflammatory diseases

Chapter VIII

Hydrogels in the treatment of Rheumatoid Arthritis: Drug delivery systems and artificial matrices for dynamic *in vitro* models[7]

ABSTRACT

Most of the current treatments addressing inflammatory-related diseases such as Rheumatoid Arthritis (RA) may decrease the pain and improve outcomes of joint damage and disability but do still present some shortcomings. RA begins with an inflammatory condition that leads to cartilage and bone tissue destruction so, it is vital to develop therapies that immediately target the inflammation. The encapsulation of nanoparticles into hydrogels represents an attractive approach for controlled release that presents higher effectiveness and fewer drawbacks. In this reasoning, the present study describes the development of monoclonal anti-TNF α antibody (anti-TNF α Ab) linked to chondroitin sulfate (CS) modified poly(amidoamine) (CS/PAMAM) dendrimer nanoparticles (NPs) and loaded into Tyramine-Gellan Gum (Ty-GG) hydrogels and Tyramine-Gellan Gum/Silk Fibroin (Ty-GG/SF) hydrogels. The therapeutic efficacy was evaluated using a THP-1 cells-based inflammation *in vitro* model under standard static conditions and dynamic conditions using a bioreactor. The results showed that anti-TNF α Ab was effectively linked to CS/PAMAM dendrimer NPs, which enabled a high immobilization degree of TNF α. Furthermore, anti-TNF α Ab-CS/PAMAM dendrimer NPs encapsulated within Ty-GG and Ty-GG/SF hydrogels presented a controlled drug release profile over time. The *in vitro* studies demonstrated that the proposed approach did not present any toxic effect on the THP-1 cells' metabolic activity and proliferation. Moreover, the anti-TNF α Ab-CS/PAMAM dendrimer NPs encapsulated within Ty-GG and Ty-GG/SF hydrogels presented a good anti-inflammatory activity over time, enabling to retain a high percentage of TNF α present within the inflammatory *in vitro* model, in a sustainable way along

[7]This chapter is based on the following publication:

Oliveira I.M., Fernandes, D.C., Maia, F. R., Canadas, R.F., Reis, R.L., and Oliveira, J.M. "Bioengineered nanoparticles loaded-hydrogels to target TNF alpha in inflammatory diseases" (Submitted)

the 14 days of culture. Overall, the anti-TNF α Ab-CS/PAMAM dendrimer NPs encapsulated within Ty-GG and Ty-GG/SF hydrogels present an excellent potential to be used as a powerful therapeutic tool against inflammatory arthritis.

Keywords: Nanocomposite hydrogels, Anti-inflammatory properties, Static conditions, Dynamic conditions, Bioreactor.

VIII-1. GRAPHICAL ABSTRACT

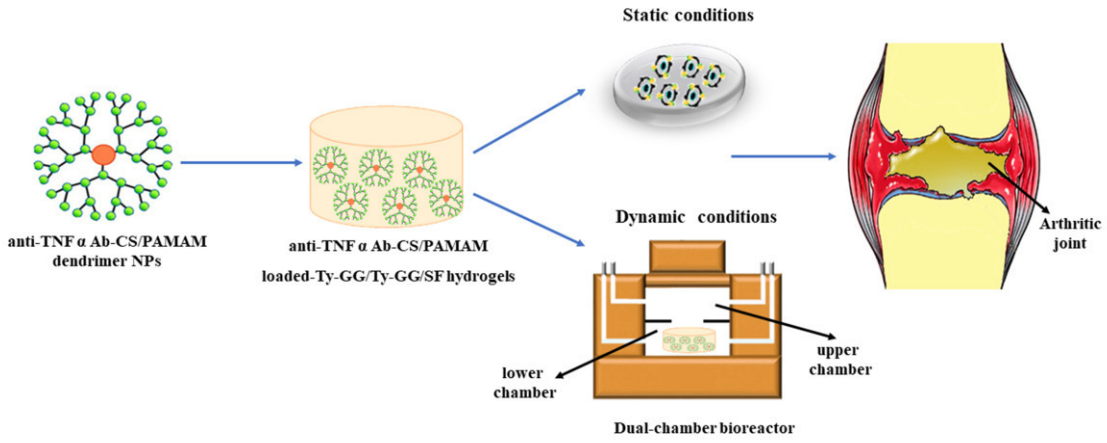

VIII-2. INTRODUCTION

Inflammatory arthritis is a term used to classify a group of conditions such as Rheumatoid Arthritis (RA), which affects the immune system, causing pain, stiffness, and joint damage [1, 2]. Different therapeutic strategies for RA have rapidly advanced over the past years to decrease the pain and improve outcomes of joint damage and disability.

The TNF α has an important role in the pathogenesis of RA since it is overexpressed in the synovial joints of patients [3]. Therefore, anti-TNF α monoclonal antibody therapies have been pursued to target TNF α and treat RA. These therapies have been effective in most treated RA patients, however, there is a percentage of patients that fail to respond to the therapy or present adverse effects [4]. Traditional drug administration frequently involves high dosage or repeated administration to have a therapeutic

effect. However, this can result in a decrease in overall efficacy and patient compliance, causing severe side effects [5]. Thus, to overcome the existing limitations, new and advanced therapies to tackle inflammatory arthritis are strongly required [6, 7].

Nanotechnology, as nanoparticle-based delivery systems, provides a unique series of advantages for the development of delivery systems, including high loading capacity, controlled release, prolonged circulation, and target delivery [8]. Even so, those systems have been showing an unpredictable drug release, depending on their polymer structure, production conditions, and particle size [9]. In order to tune drug release, nanoparticles have been combined with different biomaterials [10-13]. Amongst the studied biomaterials, hydrogels are the ones presenting the most attractive outcomes. Hydrogels are a particularly appealing type of delivery system. In fact, they can provide controlled release of nanoparticles over time, offer controllable degradability, and the capacity to protect loaded drugs from degradation [14, 15].

Despite being relatively simple and effective, such approaches have been struggling to be translated into the clinic. One of the reasons may rely on the settings selected for its study. The current *in vitro* cellular methods applied in several areas of drug discovery comprise the use of static conditions, which do not emulate the dynamic natural physiological environment found in the human body, falling in producing reliable data [16, 17]. For so, new dynamic methods need to be established to more precisely assess the effectiveness of drugs in an in vivo system. Bioartificial devices, as flow bioreactors, are highly promising tools for tissue engineering and regenerative medicine applications [18]. They can be used for cell culture, therapeutic approaches, and for *in vitro* organ modeling, offering a more physiologically appropriate environment compared to traditional static conditions [19, 20]. Current works have shown that the use of bioreactors to maintain the culture of cell-laden scaffolds enabled a proper flow of nutrients, and increased the diffusion of oxygen through the 3D structures, thereby mimicking specific aspects of native tissues [20, 21].

In previous works, Tyramine-Gellan Gum (Ty-GG) hydrogels [22] and Tyramine-Gellan Gum/Silk Fibroin (Ty-GG/SF) hydrogels [23] showed good resistance to degradation, high mechanical strength, and a suitable drug controlled release to treat inflammatory conditions such as RA. Monoclonal anti-TNF α antibody (anti-TNF α Ab) linked to chondroitin sulfate (CS) modified poly(amidoamine) (CS/PAMAM) dendrimer nanoparticles (NPs) were developed and demonstrated a more targeted and effective anti-inflammatory effect for the management of RA disease [24]. Herein, with the aforementioned in mind, it

was hypothesized that, by combining the two approaches, an improved delivery system would be achieved with a sustained release that would last for longer periods. For so, a system based on anti-TNF α Ab-CS/PAMAM dendrimer NPs loaded into Ty-GG and Ty-GG/ SF hydrogels was developed, as a promising drug delivery vehicle with improved therapeutic efficacy for the treatment of RA. The evaluation of the developed system was performed in a THP-1 cells-based inflammation *in vitro* model under static and dynamic conditions.

VIII-3. MATERIAL AND METHODS

VIII-3.1. Anti-TNF α Ab-CS/PAMAM dendrimer NPs

VIII-3.1.1. Functionalization

Mouse Monoclonal antibody [2C8] (26000 g mol^{-1}) (ab8348, Abcam, United Kingdom) was linked to CS/PAMAM dendrimer NPs previously produced by the authors [24]. The linkage was obtained through a typical carbodiimide chemistry reaction. Briefly, a 2 g L^{-1} solution of CS/PAMAM in 19.52 g L^{-1} 2-N-Morpholinoethanesulfonic acid hydrate (MES) (Sigma-Aldrich, USA) was mixed with N-(3-Dimethylaminopropyl)-N′-ethylcarbodiimide hydrochloride (EDC) (Sigma-Aldrich, USA) (4 equivalents) and NHS sulfo-NHS N-Hydroxysulfosuccinimide sodium salt ≥98% (HPLC) (Sigma-Aldrich, USA) (2 equivalents) for 15 minutes. At the same time, 20 equivalents of anti-TNF α Ab were added with EDC (4 equivalents) and were stirred for 15 minutes. Then, CS/PAMAM dendrimer NPs mixture was added to the anti-TNF α mAb mixture and stirred for 24 hours. Upon this time, the solution was dialyzed against distilled water for 48 hours. Anti-TNF α Ab-CS/ PAMAM dendrimer NPs were obtained by freezing the solution at -80°C and freeze-drying (Telstar- LyoAlfa 10/15) up to 48 hours.

VIII-3.1.2. Evaluation of anti-TNF α Ab conjugation efficacy and retention of biological activity

The efficacy of the modification was assessed by fluorescence spectrometer FP-8500 (Jasco). For that, anti-TNF α Ab-CS/PAMAM dendrimer NPs and CS/PAMAM dendrimer NPs were allowed to react with a secondary antibody Alexa Fluor 488 rabbit anti-mouse IgG (H+L) (Molecular Probes, USA), in

PBS solution (1:1000) for 1 hour. Then, the solutions were centrifuged, and the presence of non-bonded anti-TNF α Ab in the supernatants was analyzed in the fluorescence spectrometer.

The capacity of anti-TNF α Ab-CS/PAMAM dendrimer NPs to capture TNF α was also evaluated. For so, modified dendrimers were incubated with 1000 pg mL^{-1} of TNF α (Peprotech, United Kingdom) for 4 hours at room temperature. As controls, non-modified dendrimers were also incubated. After the time of reaction, the solutions were centrifuged, and the supernatants were kept at -80°C for further analysis. The concentration of free TNF-α in the supernatant samples was determined using a Human TNF-alpha DuoSET ELISA kit (R&D Systems, USA) and a DuoSet Ancillary Reagent Kit 2 (R&D Systems, USA), following manufacturer's instructions. The samples were measured at an optical density of 450 nm using a microplate reader (Synergy HT, BIO-TEK). Absorbance values were converted into concentrations using a standard curve of TNF-α in the range of 0 to 1000 pg mL^{-1}.

VIII-3.1.3.Production of anti-TNF α Ab-CS/PAMAM dendrimer NPs loaded Ty-GG and Ty-GG/SF hydrogels

Ty-GG previously produced by the authors [22] was used to obtain the investigated hydrogels. Considering Ty-GG/SF hydrogels, the silk fibroin [23] was extracted from silkworm cocoons (Portuguese Association of Parents and Friends of Mentally Disabled Citizens (APPACDM, Castelo Branco, Portugal). Briefly, the cocoons were cut into fragments and boiled for 30 minutes in 0.02 M Sodium carbonate solution (Laborspirit, Loures) to remove sericin. Boiled silkworm cocoons were washed with distilled water and dried at 70°C. The dry silkworm cocoons were then dissolved in the oven with 9.3 M Lithium bromide (Laborspirit, Loures) for 4 hours at 70°C. The dissolved solution was dialyzed using a dialysis tubing, benzoylated (Laborspirit, Loures) for 48 hours against distilled water, to remove LiBr. Silk fibroin was kept at 4°C until further use.

To prepare the hydrogels, first a solution of horseradish peroxidase (HRP) (0.84 mg mL^{-1}) (Sigma-Aldrich, USA) in PBS, and a solution of hydrogen peroxide (H_2O_2) (0.36% (v/v)) (VWR, USA) in distilled water were prepared. Then, 1% Ty-GG solution (w/v) was prepared in distilled water and used for the preparation of Ty-GG hydrogels and Ty-GG/SF hydrogels. To obtain the Ty-GG/SF hydrogels, 1% (w/v) of Ty-GG solution was mixed with 2% (w/v) SF (1:1) solution. At this point, anti-TNF α Ab-CS/PAMAM dendrimer NPs were mixed in the Ty-GG and Ty-GG/SF solutions at a final concentration of 0.5 mg mL^{-1}. Then, two different crosslinking levels were tested by adding different amounts of HRP and H_2O_2

solutions to Ty-GG and Ty-GG/SF solutions, hereafter denominated C1, C2, C3, and C4, as described in **Table VIII-1**. Each condition without anti-TNF α Ab-CS/PAMAM dendrimer NPs were used as control (hereafter designated C1 CTRL, C2 CTRL, C3 CTRL, and C4 CTRL). Then, the mixtures were transferred into polypropylene molds and incubate at 37°C until complete gelation.

Table VIII-1- Anti-TNF α Ab-CS/PAMAM loaded-Ty-GG and Ty-GG/SF hydrogels with different crosslinking levels.

Designation	Ty-GG (1% w/v)	SF (2% w/v)	Dendrimer NPs (1 mg mL^{-1})	HRP (0.84 mg mL-1)	H_2O_2 (0.36% v/v)
C1	167 µL	-	97 µL	16.6 µL	10.83 µL
C2	167 µL	-	100 µL	18.3 µL	15 µL
C3	83.5 µL	83.5 µL	97 µL	16.6 µL	10.83 µL
C4	83.5 µL	83.5 µL	100 µL	20 µL	13.3 µL

VIII-3.1.4.Distribution of FITC-CS/PAMAM dendrimer NPs throughout Ty-GG and Ty-GG/SF hydrogels

To assess the distribution profile of CS/PAMAM dendrimer NPs within Ty-GG and Ty-GG/SF hydrogels, the nanoparticles were labelled with Fluorescein isothiocyanate (FITC) (Sigma-Aldrich, USA). Initially, 10 mg mL^{-1} of CS/PAMAM dendrimer NPs solution was prepared in a carbonate-bicarbonate coupled buffer (pH 9.2). Then, 50 µL of 10 mg mL^{-1} of FITC in anhydrous dimethyl sulfoxide (DMSO) (VWR, USA) solution was added per each mL of CS/PAMAM dendrimer NPs solution under agitation and kept in the dark at 4°C for 8 hours. In the end, the FITC-labelled CS/PAMAM dendrimer NPs were dialyzed in ultrapure water for 48 hours and freeze-dried. Then, FITC-CS/PAMAM dendrimer NPs at a final concentration of 0.1 mg mL^{-1} were mixed with Ty-GG and Ty-GG/SF solutions, and HRP and H_2O_2 solutions as described in **Table VIII-1**. After crosslinking, the hydrogels were immersed in PBS and kept in a water bath at 37°C for 24 hours to remove free FITC. The hydrogels were observed under a confocal microscope (Leica TCS SP8).

VIII-3.1.5. Release profile of anti-TNF α Ab-CS/PAMAM dendrimer NPs from Ty-GG and Ty-GG/SF hydrogels

To evaluate the release profile of anti-TNF α Ab-CS/PAMAM dendrimer NPs, each release system developed, C1, C2, C3, and C4 (more details in **Table VIII-1**) were immersed in PBS at 37°C. After 3 hours, 24 hours, 72 hours, 168 hours, 336 hours, and 504 hours, the supernatant was removed and kept at -80° C until further analysis. To formulate the calibration curve, anti-TNF α Ab-CS/PAMAM dendrimer NPs dilutions were prepared ranging from 0 mg mL^{-1} to 0.5 mg mL^{-1}. The UV absorbance of dendrimers NPs was read at 280 nm in a microplate reader to quantify the anti-TNF α Ab-CS/PAMAM dendrimer release (EMax; Molecular Devices, Sunnyvale, CA, USA). Three samples per condition were evaluated at each time point. The absorbance values were converted into concentrations using the calibration curve.

VIII-3.2. THP-1 cells-based inflammation *in vitro* model: Static conditions

VIII-3.2.1. Cell culture

The Human monocytic cell line (THP-1) (SIGMA, USA) was expanded in RPMI 1640 Medium, GlutaMAX™ Supplement, HEPES (Thermo Fisher Scientific, USA), supplemented with 10% fetal bovine serum (PAA; Pasching, Austria) and 1% (v/v) of penicillin and streptomycin (Gibco, Life Technologies, Grand Island, NY), under standard culture conditions, i.e. at 37°C in a humidified atmosphere containing 5 vol% CO2. When ≈80% confluence was reached, cells were trypsinized and seeded in a well of a 24-well plate at a density of $5x10^5$ cells per well. For induction of THP-1 cells' differentiation into macrophages, cells were cultured under RPMI with 100 nM phorbol 12-myristate-13-acetate (PMA) (Sigma-Aldrich, USA), hereafter designated healthy cells. After 24 hours, the medium was replaced with RPMI medium without PMA and incubated for another 48 hours. At this point, to develop an inflammation *in vitro* model, cells were incubated with 100 ng mL^{-1} Lipopolysaccharide (LPS) (Sigma-Aldrich, USA) in RPMI medium and incubated for 5 hours to induce an inflammatory response.

Cells under LPS stimulation were incubated with each release system developed, C1, C2, C3, and C4 (more details in **Table VIII-1**), respective controls (C1 CTRL, C2 CTRL, C3 CTRL, and C4 CTRL) and 0.5 mg mL^{-1} anti-TNF α Ab-CS/PAMAM dendrimer NPs. Only cells under LPS stimulation were also

studied (hereafter designated LPS stimulation). Cells' metabolic activity and proliferation were monitored along 7 days of culture. The TNF α neutralization was assessed along 14 days of culture.

VIII-3.2.2.Cells' metabolic activity

Cells' metabolic activity was evaluated on days 1, 3, and 7 of culture with Alamar Blue at each time point. For that, RPMI culture medium containing 10% (v/v) of AlamarBlue® (BioRad, Oxford, UK) was added to the different conditions.

The culture plates were kept in the dark, at 37°C in the CO_2 incubator for 4 hours. Afterward, 100 µL of each well were transferred in triplicate to 96-well plates. The fluorescence was read at an excitation wavelength of 530/25 nm and an emission wavelength of 590/535 nm, using a microplate reader (Synergy HT, BioTek, Instruments, USA).

VIII-3.2.3.Cells' proliferation

The proliferation of the THP-1 cells at days 1, 3, and 7 of culture was analyzed by dsDNA quantification. At each time-point, cells were washed with PBS solution and lysed with ultrapure water. The cells' lysate solution was placed into 1.5 mL microtubes, and then they were stored at -80°C for further analysis. Quanti-IT PicoGreen dsDNA Assay Kit (Alfagene, Portugal) was used to quantify dsDNA, accordingly with manufacturers' instructions. Briefly, 28.7 µL of each sample was mixed with 71.3 µL of PicoGreen solution and 100 µL 1X TE buffer in a well of a 96-well white microplate. Then, the plate was incubated in the dark for 10 minutes, the fluorescence was read using excitation of 480/20 nm and emission of 528/20 nm, in a microplate reader. DNA concentration was determined using a standard curve in the range of 2 to 0 µL mL^{-1}.

VIII-3.2.4.Assessment of TNF α neutralization

The neutralization of TNF α as evaluated at 1, 3, 7, and 14 days of culture. At these time-points, the medium of each condition was recovered and stored at -80 °C. To determine the levels of TNF α captured, the TNF-α concentration in the samples was measured using the Human TNF-alpha DuoSET ELISA kit and the DuoSet Ancillary Reagent Kit 2, following manufacturers' instruction. The optical

density was measured at 450 nm using the microplate reader and the values were converted into concentration using a TNF-α calibration curve ranging from 1000 to 0 pg mL^{-1}.

VIII-3.3. THP-1 cells-based inflammation *in vitro* model: Dynamic conditions

VIII-3.3.1. Cell culture in a Dual-chamber bioreactor

THP-1 cells were seeded at a density of $5x10^5$ cells/well in TCP coverslips in 24-well plates. As done under static conditions, for induction of THP-1 cell differentiation, cells were cultured under RPMI with 100 nM PMA. After 24 hours, the medium was replaced with RPMI medium without PMA and incubated for another 48 hours. Then cells were incubated with 100 ng mL^{-1} of LPS in RPMI medium and incubated for 5 hours to induce an inflammatory response. After LPS stimulation, the coverslips were transferred to the lower chamber of a dual-chamber bioreactor [25] with RPMI medium contained LPS and the anti-inflammatory effect of developed release systems was evaluated.

VIII-3.3.2. Anti-inflammatory effect of developed release systems

To evaluate the anti-inflammatory activity of the developed approaches under dynamic conditions, one condition of each delivery system was selected and added to the cells cultured on the lower chamber of the bioreactor. Then, the entire piping system was assembled, the syringes were filled with medium and connected to the syringe pump. The dual-chamber bioreactor was kept at 37°C in a humidified 5% CO_2 atmosphere and the compartment containing the cells and hydrogels was perfused at a rate of 12.5 µL h^{-1}. After 1, 3,7, and 14 days of perfusion, the culture medium contained in the collection tubes was removed and stored at -80°C to analyze of the amount of TNF α present, through ELISA assay, as described above. Delivery systems cultured in THP-1 cell-based inflammation *in vitro* models under standard static conditions were used as control.

VIII-3.4. Statistical analysis

Statistical analysis was performed by GraphPad Prism 8 version, where a Shapiro-Wilk normality test was previously made to evaluate the data normality. Statistical significances were obtained as *p <

0.05. All assays were performed in triplicated and the results were presented with mean ± standard deviation.

VIII-4. Results and Discussion

The present work is focused on the development of anti-TNF α Ab-CS/PAMAM dendrimer NPs loaded into Ty-GG and Ty-GG/ SF hydrogels as a promising delivery system. This way, hydrogels would increase the controlled and sustained release of anti-TNF α Ab-CS/PAMAM dendrimer NPs at the target site, improving their therapeutic efficacy, while requiring less frequent administrations [14]. With this in mind, the developed NPs loaded-hydrogels were evaluated in a THP-1 cells-based inflammation *in vitro* model (**Figure VIII-1 in the Supplementary Information**) under static standard conditions and dynamic conditions using a bioreactor.

VIII-4.1.1. Evaluation of anti-TNF α Ab conjugation efficacy and retention of biological activity

Firstly, monoclonal anti-TNF α antibody was linked to CS/PAMAM dendrimer NPs and the efficacy of the conjugation, as well as, the preservation of its biological activity, i.e. its ability to capture TNF α, was evaluated **(Figure VIII-1)**. To assess the success of conjugation, fluorescence spectroscopy was performed **(Figure VIII-1a)**. The CS/PAMAM dendrimer NPs with and without linked Ab was mixed with a secondary antibody labeled with Alexa Fluor 488 dye. The intensity of the emission spectra of Alexa 488 between 500 and 600 nm for the anti-TNF α Ab-CS/PAMAM dendrimer NPs was significantly higher (≃3500) than CS/PAMAM dendrimer NPs without anti-TNF α Ab (≃800). The results indicated that the conjugation of CS/PAMAM dendrimer NPs with the anti-TNF α Ab was successfully achieved, despite some unspecific secondary Ab binding was observed, as expected.

Considering the anti-TNF α Ab-CS/PAMAM dendrimer NPs effectiveness to neutralize TNF α, it was measured by assessing the difference between the initial and the final amount of free TNF α in solution, after adding the dendrimer NPs **(Figure VIII- 1 b)**. The data showed that after 4 hours of reaction, the degree of capture was 56.8%. One of the main hurdles of using antibody conjugated therapies is the lack of control of the antibody conjugation site, which can lead to a remarkable decrease in targeting efficacy [26]. Nevertheless, the immobilization process followed during this study

did not compromise the biological activity of the anti-TNF α Ab, as demonstrated by the retention of its capacity to capture TNF α.

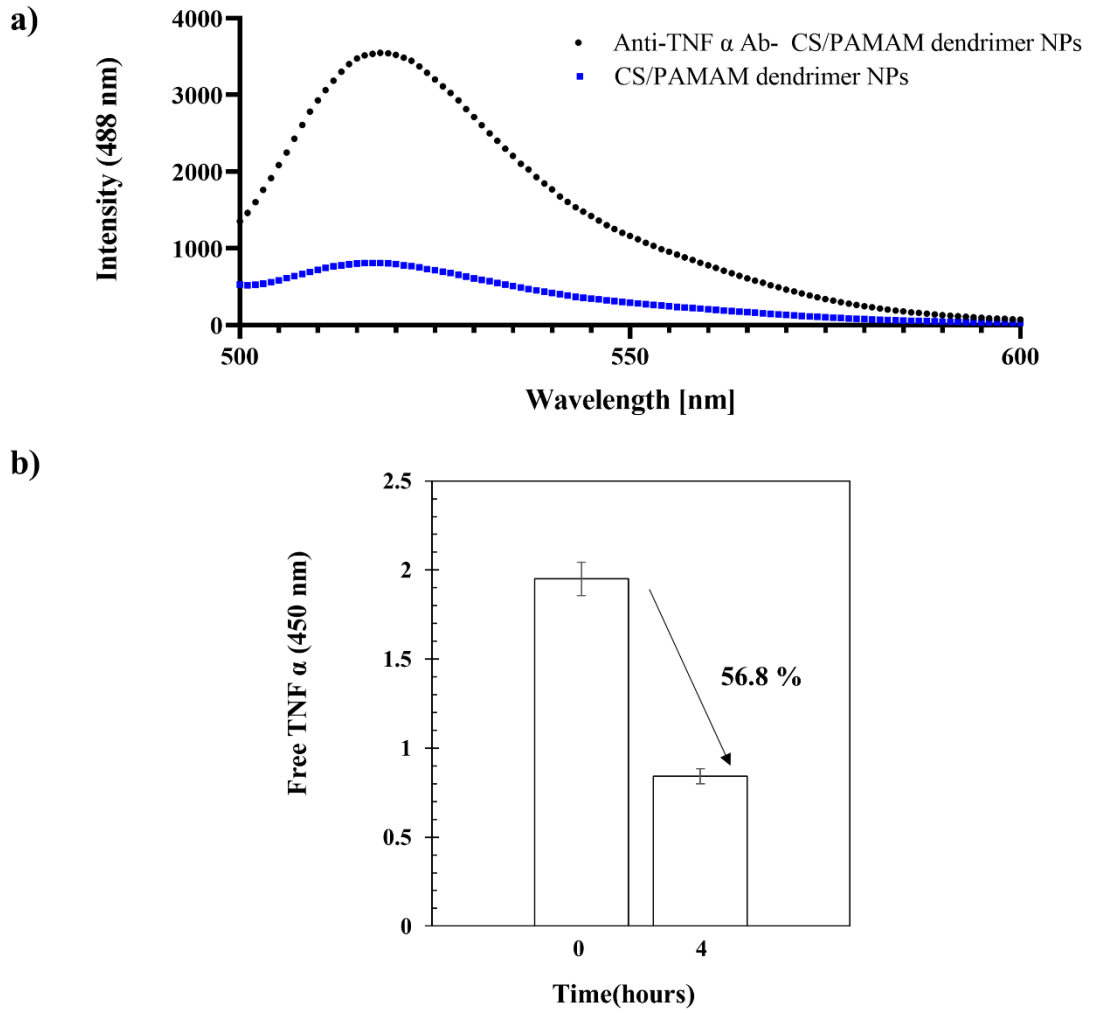

Figure VIII-1 - Anti-TNF α antibody conjugation to CS/PAMAM dendrimer NPs. a) Fluorescence spectroscopy of CS/PAMAM dendrimer NPs and anti-TNF α Ab-CS/PAMAM dendrimer NPs. b) Percentage of TNF α captured by anti-TNF α Ab-CS/PAMAM dendrimer NPs. Data shown as Mean ± SD.

VIII-4.1.2.Production of anti-TNF α Ab-CS/PAMAM dendrimer NPs loaded-Ty-GG and Ty-GG/SF hydrogels: dendrimer NPs distribution and release profile

At this point, anti-TNF α Ab-CS/PAMAM dendrimer NPs were loaded into Ty-GG and Ty-GG/SF solutions, and disc hydrogels were produced **(Figure VIII-2)**. The gelation of Ty-GG and Ty-GG/SF

solutions within polypropylene molds produced discs with similar sizes. But it was clear that the addition of SF resulted in less clear hydrogels **(Figure VIII- 2 a)**. To assess the distribution of dendrimer NPs throughout the hydrogels, they were labelled with FITC and observed using confocal microscopy (Figure 2 b). It was possible to observe that CS/PAMAM dendrimers NPs were uniformly dispersed across the hydrogel network with only a few aggregates, showing that the use of hydrogels to deliver nanoparticles minimizes their aggregation [27]. Furthermore, a higher dispersion guarantees a larger exposure of the surface of the nanoparticle and consequently a better performance as a therapeutic agent [28].

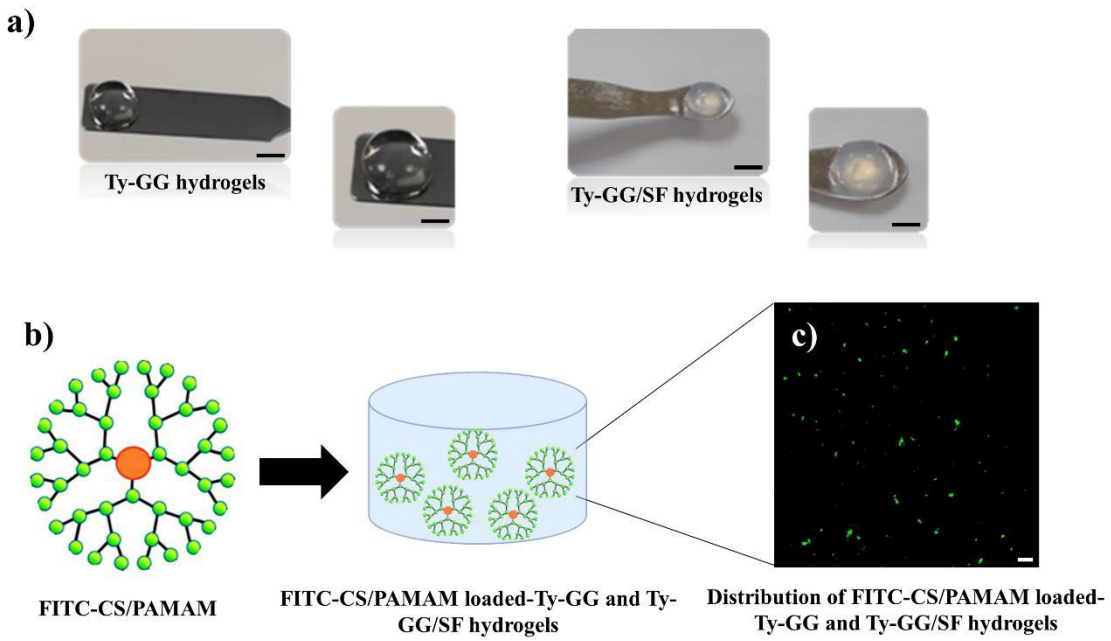

Figure VIII-2 - Anti-TNF α Ab-CS/PAMAM dendrimer NPs loaded-Ty-GG and Ty-GG/SF hydrogels. a) Representative images of Ty-GG hydrogels and Ty-GG/SF hydrogels. Scale bar: 10 cm. b) Schematic representation of FITC-CS/PAMAM dendrimer NPs and FITC-CS/PAMAM dendrimer NPs loaded-Ty-GG and Ty-GG/SF hydrogels. Scale bar: 5 μm. c) Representative fluorescence image of FITC-CS/PAMAM dendrimer NPs distributed within Ty-GG and Ty-GG/SF hydrogels, showing the NPs in green.

Then the release of anti-TNF α Ab-CS/PAMAM dendrimer NPs from Ty-GG and Ty-GG/SF hydrogels produced using different crosslinking levels was assessed **(Figure VIII-3)**. Ty-GG hydrogels, denominated C1 (more details at **Table VIII-1**), presented a release rate of 73.65% ± 1.85%, while the same hydrogels but with higher amounts of crosslinking (C2) showed a rate of 67.12% ± 4.03%. A similar profile was observed for Ty-GG/SF hydrogels, C3 condition showed a rate of 88.13% ± 2.36%, while the condition with higher crosslinking levels, C4, showed a lower release rate of 67.28% ± 1.47%. When analyzing the conditions with lower levels of crosslinking (C1 and C3), Ty-GG/SF hydrogels showed a higher release

profile as compared to Ty-GG hydrogels. But, when comparing the conditions with higher crosslinking levels, C2 and C4, no statistical differences were observed. On one hand, these observations indicated that the increase of crosslinking level may contract the hydrogel mesh, slowing the release of the dendrimer NPs. On the other hand, SF seems to interfere with Ty-GG hydrogels mesh, resulting in a higher release of dendrimer NPs, but this effect fades away with the increase of crosslinking levels. Noteworthy, none of the conditions reached a maximum drug release after 21 days of evaluation. Considering the results obtained, it was possible to verify that hydrogels can be fine-tuned to present a controlled drug release profile over time. This can allow a prolonged therapeutic effect of anti-TNF α Ab. In this reasoning, less frequent administration of drugs would be necessary, improving the quality of life of patients.

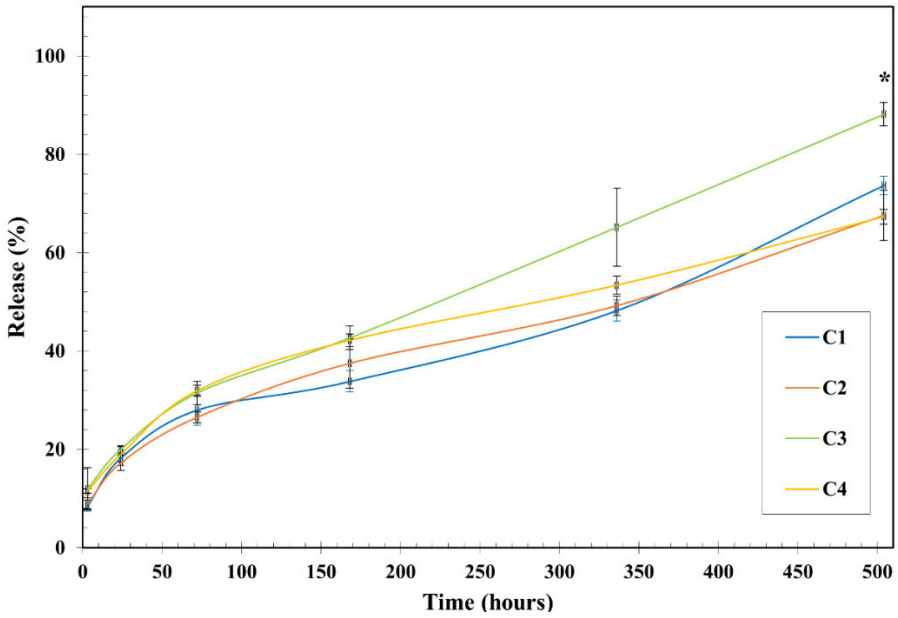

Figure VIII-3 - Release profile of anti-TNF α Ab-CS/ PAMAM dendrimer NPs. Release profile of anti-TNF α Ab-CS/ PAMAM dendrimer NPs from Ty-GG (C1 and C2) and Ty-GG/SF hydrogels (C3 and C4) with different crosslinking levels after 3, 24, 48, 72, 168, 336, and 504 hours. Data shown as Mean ± SD. * indicates significant differences when comparing C3 and C4 at time point 504 hours.

VIII-4.1.3.Evaluation of anti-TNF α Ab-CS/ PAMAM dendrimer NPs loaded-Ty-GG and Ty-GG/SF hydrogels effects on THP-1 cells-based inflammation *in vitro* models: static conditions

In RA, there is a disproportion between pro-inflammatory and anti-inflammatory cytokines, resulting in a more pronounced pro-inflammatory phenotype, than an anti-inflammatory phenotype [29-32]. For this reason, most therapies developed to decrease inflammation by inhibiting pro-inflammatory

cytokines are evaluated using cell inflammation *in vitro* models [6, 33]. As well, the influence of the different conditions of anti-TNF α Ab-CS/ PAMAM dendrimer NPs loaded-Ty-GG (C1 and C2) and Ty-GG/SF (C3 and C4) hydrogels were evaluated using an inflammation *in vitro* model created by induction of THP-1 cells. Ty-GG and Ty-GG/SF hydrogels without dendrimer NPs (C1 CTRL, C2 CTRL, C3 CTRL, and C4 CTRL) and dendrimer NPs were used as controls. First, the effect of loaded hydrogels on LPS stimulated THP-1 cells' metabolic activity and proliferation were quantified for 7 days using Alamar blue and DNA quantification assays, respectively (Figure 4). From day 1 up to day 7, THP-1 cells under all the different conditions of Ty-GG and Ty-GG/SF hydrogels showed to be metabolic activity over time. THP-1 cells under dendrimer NPs was the only condition to present higher metabolic activity at the first time point (24 hours) when compared with LPS stimulated cells. The enhanced metabolic activity observed can be explained by the increase of energy necessary for the internalization of dendrimers. In fact, considering the conditions that contained dendrimer NPs, they were released in a controlled and sustainable away from the hydrogels, while in this condition, dendrimer NPs were easily accessible, being internalized at higher amounts.

DNA quantification was also analyzed to assess THP-1 cells' proliferation in contact with the different conditions. Significant differences were observed in C1, C2, and C3, when compared with LPS stimulated cells. But differences were also observed between C4 CTRL and LPS stimulated cells, indicating that they may be related to the interaction of cells with the hydrogels. Moreover, the results showed that cells submitted to conditions C1 and C2 were less proliferative at day 1, comparing to its controls, which demonstrated that the effects can be due to the presence of the dendrimer NPs. However, no differences were observed along the remained time of culture, showing that the initial adverse effects fade away over time. These results are in agreement with other studies [34, 35]. In fact, PMA induces cells' differentiation, and the increase in adhesion properties is correlated with a progressive reduction in proliferative activity. Moreover, while cells are spending energy to differentiate, they do not spend energy to proliferate, resulting in the diminishing of cells' proliferation rates as the tendency observed on day 7.

Overall, the results of metabolic activity and cell proliferation analysis provided evidence regarding the safety of these materials for biomedical applications.

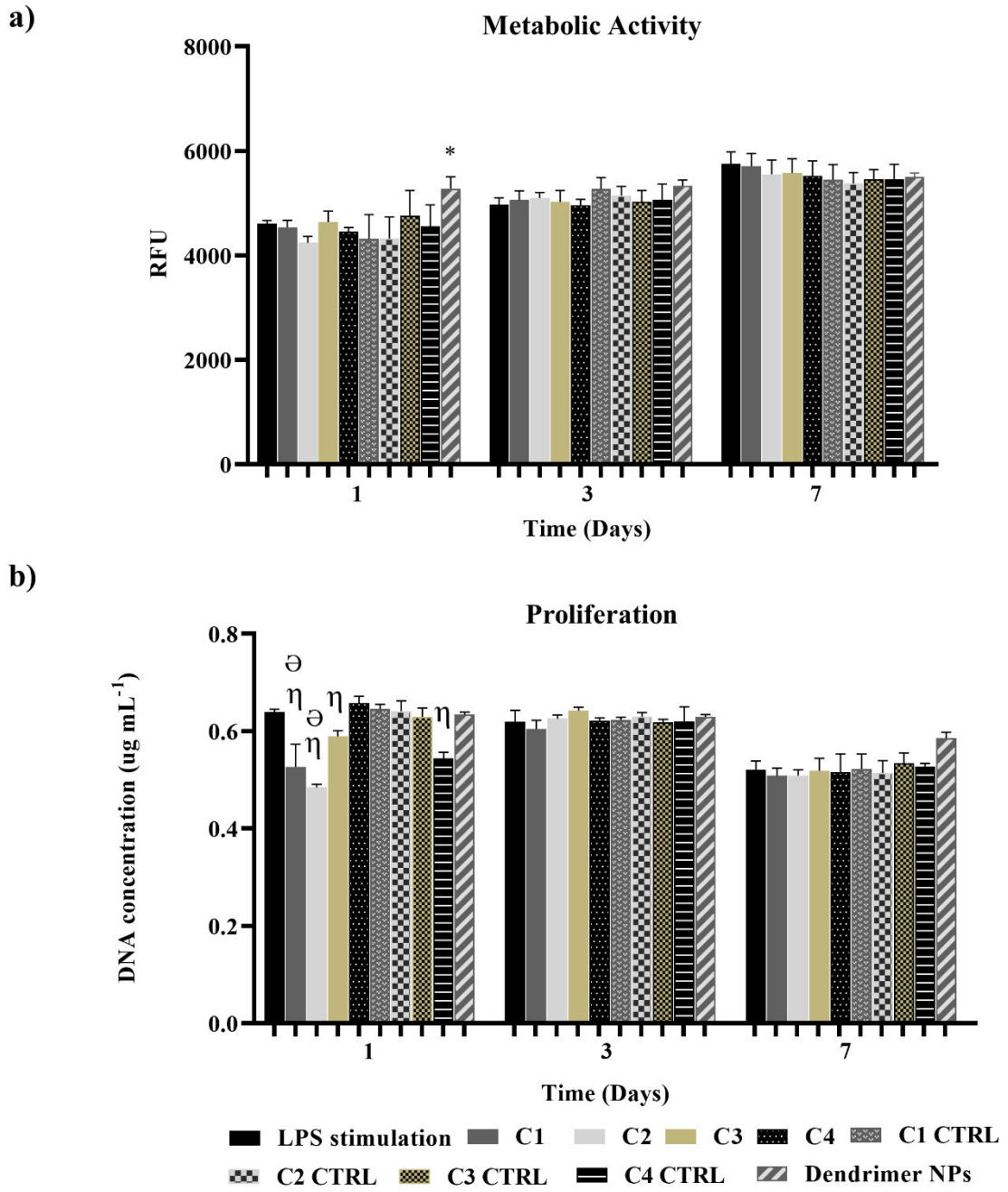

Figure VIII-4 - Evaluation of anti-TNF α Ab-CS/ PAMAM dendrimer NPs loaded-Ty-GG and Ty-GG/SF hydrogels effects on cells metabolic activity and proliferation. a) THP-1 cells' metabolic activity upon culture with anti-TNF α Ab-CS/ PAMAM dendrimer NPs loaded-Ty-GG (C1 and C2) and Ty-GG/SF (C3 and C4) hydrogels and controls along 7 days of culture. (* indicates significant differences when comparing Dendrimer NPs with LPS stimulation at time point 1 day); and b) THP-1 cells' proliferation by DNA quantification of THP-1 cells upon culture with anti-TNF α Ab-CS/ PAMAM dendrimer NPs loaded-Ty-GG (C1 and C2) and Ty-GG/SF (C3 and C4) hydrogels and controls along 7 days of culture. (η indicates significant differences when comparing with LPS stimulation. Ə indicates significant differences when comparing with respective CTRL). Data shown as Mean ± SD.

In order to evaluate the therapeutic efficacy of anti-TNF α Ab-CS/PAMAM dendrimer NPs loaded within Ty-GG (C1 and C2) and Ty-GG/SF (C3 and C4) hydrogels, the level of free TNF α in the culture medium along 14 days of culture was quantified (Figure 5). Again, Ty-GG and Ty-GG/SF control hydrogels without dendrimer NPs (C1 CTRL, C2 CTTRL, C3 CTRL, and C4 CTRL) and dendrimer NPs were analysed. Although at the beginning of culture only anti-TNF α Ab-CS/PAMAM dendrimer NPs loaded within Ty-GG hydrogels (C1 and C2) showed significant differences from their respective controls in the neutralization of free TNF α, after 14 days, all the conditions (C1, C2, C3, and C4) showed to neutralize significantly amounts. Moreover, the neutralization levels at day 14 were significantly different from day 1 for all the studied conditions. Considering free dendrimer NPs, they neutralized higher amounts of TNF α comparing with controls since day 1, as expected, reaching its maximum at day 7. Comparing with the studied conditions, no differences were observed until day 7, indicating that anti-TNF α Ab-CS/PAMAM dendrimer NPs were released along the time and successfully neutralized the free TNF α. On day 14, differences between studied conditions and dendrimer NPs were observed since the levels of free TNF α abruptly increased for dendrimer NPs, while studied conditions retained their capacity to neutralize TNF α. Noteworthy, dendrimer NPs at day 14 showed levels of free TNF α similar to the controls, corroborating dendrimer NPs' low capacity to neutralize after 14 days. The results indicated that in an in vivo scenario, it would be necessary repeated administrations of dendrimer NPs, but less frequent administrations would be necessary in the case of anti-TNF α Ab-CS/PAMAM dendrimer NPs loaded within Ty-GG (C1 and C2) and Ty-GG/SF (C3 and C4) hydrogels. So, this approach may allow the reduction of secondary side effects, providing a better quality of life to the patient, as seen in other studies using Gellan Gum and SF as drug delivery systems [36, 37].

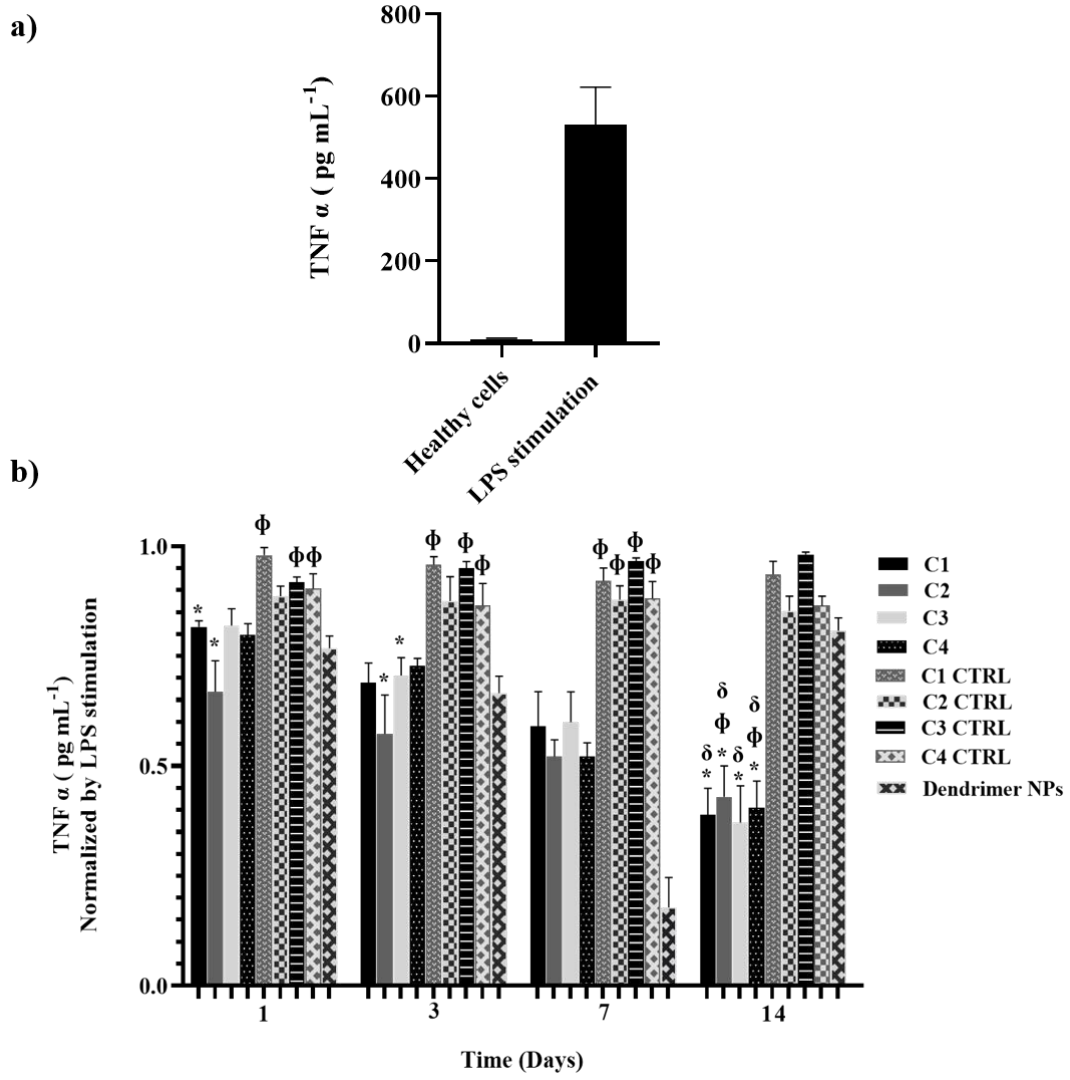

Figure VIII-5 - Quantification of TNF α free in the culture medium along 14 days of culture. a) Amount of free TNF α in medium in THP-1 cells culture without LPS stimulation, designated healthy cells, and with LPS stimulation after 1 day, confirming the successful development of THP-1 cells-based inflammation *in vitro* model. b) Results were normalized by the TNF α values obtained in cultures stimulated by LPS. Data shown as Mean $\pm$ SD. *indicates significant differences when comparing with respective CTRL. ϕ indicates significant differences when comparing with Dendrimer NPs at each time-point. δ indicates significant differences when comparing with day 1.

VIII-4.1.4.Evaluation of anti-TNF α Ab-CS/ PAMAM dendrimer NPs loaded-Ty-GG and Ty-GG/SF hydrogels effects on THP-1 cell-based inflammation *in vitro* models: dynamic conditions

To mimic the dynamic physiological environment found in the human body and obtain more reliable data concerning the anti-inflammatory effects of the developed approach a dual-chamber

bioreactor was used. In this sense, anti-TNF α Ab-CS/ PAMAM dendrimer NPs loaded-Ty-GG and Ty-GG/SF hydrogels were tested for 14 days using a THP-1 cell-based inflammation *in vitro* model under dynamic conditions (Figure 6). At this point, the condition C3 that presented higher release levels and higher ability to decrease TNF α in the medium during *in vitro* static evaluation was selected. In addition, it was also selected a condition with slower release to ensure a prolonged effect in an in vivo scenario and less frequent administrations. The two conditions presenting slower release profiles were C2 and C4, presenting very similar profiles. For so, since the first condition selected comprised the dendrimer NPs loading into Ty-GG/SF hydrogel, it was decided to select C2 to include a condition comprising dendrimer NPs loading into Ty-GG hydrogel. Additionally, THP-1 cell-based inflammation *in vitro* models under standard static conditions was used as control.

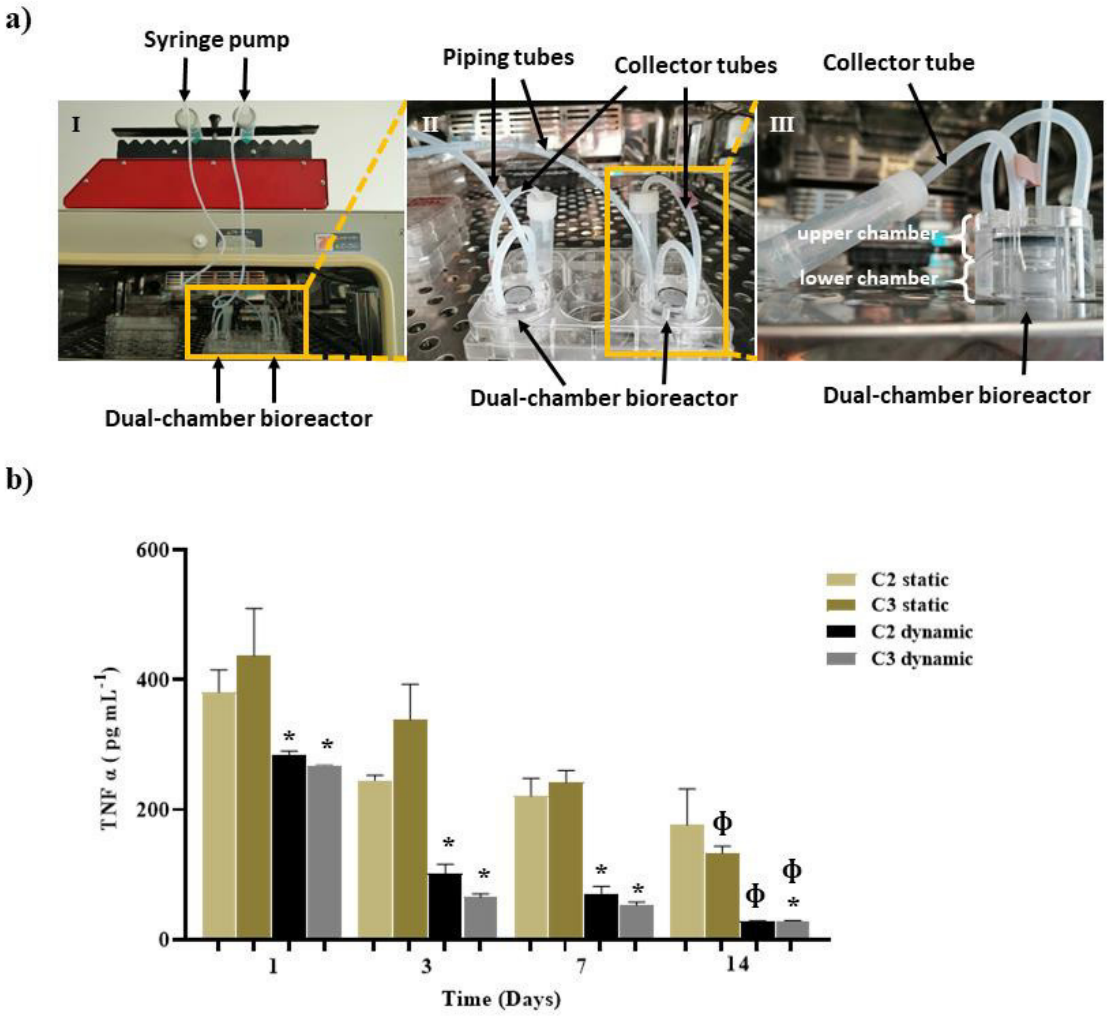

Figure VIII-6 - Evaluation of anti-TNF α Ab-CS/ PAMAM dendrimer NPs loaded-Ty-GG and Ty-GG/SF hydrogels effects under dynamic conditions. a) Representative images of Dynamic culture of THP-1 cell-based inflammation in vitro model using a dual-chamber bioreactor showing the I) Dual-chamber bioreactor connected to a syringe

pump; II) Higher amplification of the bioreactor inserted in a 6-well plate showing the piping tubes and collector tubes; III) Enlarged image of the dual-chamber bioreactor where it is possible to see the upper and lower chamber. b) Amount of TNF α present in the medium, in contact with C2 and C3 in static and dynamic conditions. Data shown as Mean ± SD. *indicates significant differences when comparing dynamic conditions with static conditions, ϕ indicates significant differences when comparing with day 1.

It was possible to verify that the TNF α concentration present in the supernatant medium significantly decreased along the 14 days of culture under dynamic and control conditions. The condition C2 under static conditions was the only one presenting no differences, as expected. In fact, this result is in accordance with the results obtained previously release profile evaluation. When analyzing the results obtained for static and dynamic conditions, it was observed that the concentration of TNF α was always lower in dynamic conditions. Furthermore, in dynamic conditions, on day 14, the levels of free TNF α were really low, indicating that all anti-TNF α Ab-CS/ PAMAM dendrimer NPs were released from the hydrogels. Under static conditions, a less accentuated decrease of TNF α was observed indicating a slower release of dendrimer NPs over time. Noteworthy, no significant differences were observed between the dendrimer NPs-loaded-hydrogels tested.

VIII-5. CONCLUSION

In this study, it was developed an improved system based on anti-TNF α Ab-CS/ PAMAM dendrimer NPs loaded into Ty-GG and Ty-GG/SF hydrogels to tackle inflammatory diseases such as RA. The produced anti-TNF α Ab- CS/PAMAM dendrimer NPs, showed to maintain the Ab biological activity enabling a high immobilization degree of TNF α. Furthermore, it was possible to fine-tune anti-TNF α Ab-CS/ PAMAM dendrimer NPs loaded-Ty-GG and Ty-GG/SF hydrogels by altering crosslinking levels, enabling the control of the dendrimer NPs release profile over time. The *in vitro* studies conducted using the THP-1 cell-based inflammation model under static conditions demonstrated that cells cultured with the developed dendrimer NPs-loaded hydrogels were metabolic active and proliferative along the culture time. When their capacity to capture TNF α was evaluated, it was showed that developed systems retained their capacity to neutralize TNF α even after 14 days. Finally, dynamic studies performed with the THP-1 cell-based inflammation model showed that the dendrimer NPs-loaded hydrogels maintained an even high anti-inflammatory activity over time, as compared with static, demonstrating the importance of using a physiologically mimetic environment. These relevant results support the successful use of these drug delivery systems in several inflammatory diseases, including

RA, in in vivo settings. Overall, the developed approaches making use of bioengineered nanoparticles-loaded hydrogels can fill the current gaps concerning traditional therapies, providing a more targeted and thus more effective treatment, while enabling less frequent administration and thus reducing the side effects caused by overdosing of drugs.

VIII-6. Acknowledgments

The authors thank the financial support under the Norte2020 project (NORTE-08-5369-FSE000044). D.C.F. acknowledges Portuguese Foundation for Science and Technology (FCT) for her phD scholarship (PD/BD/143081/2018) and F.R.M. for her contract under the Transitional Rule DL 57/2016 (CTTI-57/18-I3BS(5)),. The FCT distinction attributed to J.M.O. under the Investigator FCT program (number IF/01285/2015) is also greatly acknowledged.

VIII-7. References

1. Guo, Q., et al., *Rheumatoid arthritis: pathological mechanisms and modern pharmacologic therapies.* Bone research, 2018. **6**: p. 15-15.
2. Demoruelle, M.K., K.D. Deane, and V.M. Holers, *When and where does inflammation begin in rheumatoid arthritis?* Current opinion in rheumatology, 2014. **26**(1): p. 64-71.
3. Farrugia, M. and B. Baron, *The role of TNF-α in rheumatoid arthritis: a focus on regulatory T cells.* Journal of clinical and translational research, 2016. **2**(3): p. 84-90.
4. Köhler, B.M., et al., *Current Therapeutic Options in the Treatment of Rheumatoid Arthritis.* Journal of clinical medicine, 2019. **8**(7): p. 938.
5. Wen, H., H. Jung, and X. Li, *Drug Delivery Approaches in Addressing Clinical Pharmacology-Related Issues: Opportunities and Challenges.* The AAPS journal, 2015. **17**(6): p. 1327-1340.
6. Pisetsky, D.S. and M.M. Ward, *Advances in the treatment of inflammatory arthritis.* Best practice & research. Clinical rheumatology, 2012. **26**(2): p. 251-261.
7. Demoruelle, M.K. and K.D. Deane, *Treatment strategies in early rheumatoid arthritis and prevention of rheumatoid arthritis.* Current rheumatology reports, 2012. **14**(5): p. 472-480.
8. Gonçalves, C., P. Pereira, and M. Gama, *Self-assembled hydrogel nanoparticles for drug delivery applications.* Materials, 2010. **3**(2): p. 1420-1460.
9. Sethi, M., et al., *Effect of drug release kinetics on nanoparticle therapeutic efficacy and toxicity.* Nanoscale, 2014. **6**(4): p. 2321-2327.
10. Farokhzad, O.C. and R. Langer, *Impact of nanotechnology on drug delivery.* ACS nano, 2009. **3**(1): p. 16-20.
11. Timko, B.P., et al., *Advances in drug delivery.* Annual Review of Materials Research, 2011. **41**: p. 1-20.

12. Place, E.S., N.D. Evans, and M.M. Stevens, *Complexity in biomaterials for tissue engineering.* Nature materials, 2009. **8**(6): p. 457-470.
13. Huebsch, N. and D.J. Mooney, *Inspiration and application in the evolution of biomaterials.* Nature, 2009. **462**(7272): p. 426-432.
14. Li, J. and D.J. Mooney, *Designing hydrogels for controlled drug delivery.* Nature reviews. Materials, 2016. **1**(12): p. 16071.
15. Narayanaswamy, R. and V.P. Torchilin, *Hydrogels and Their Applications in Targeted Drug Delivery.* Molecules (Basel, Switzerland), 2019. **24**(3): p. 603.
16. Chaicharoenaudomrung, N., P. Kunhorm, and P. Noisa, *Three-dimensional cell culture systems as an in vitro platform for cancer and stem cell modeling.* World journal of stem cells, 2019. **11**(12): p. 1065-1083.
17. Edmondson, R., et al., *Three-dimensional cell culture systems and their applications in drug discovery and cell-based biosensors.* Assay and drug development technologies, 2014. **12**(4): p. 207-218.
18. Ginai, M., et al., *The use of bioreactors as in vitro models in pharmaceutical research.* Drug Discov Today, 2013. **18**(19-20): p. 922-35.
19. Ahmed, S., et al., *New generation of bioreactors that advance extracellular matrix modelling and tissue engineering.* Biotechnology letters, 2019. **41**(1): p. 1-25.
20. Martin, I., D. Wendt, and M. Heberer, *The role of bioreactors in tissue engineering.* Trends in Biotechnology, 2004. **22**(2): p. 80-86.
21. Gaspar, D.A., V. Gomide, and F.J. Monteiro, *The role of perfusion bioreactors in bone tissue engineering.* Biomatter, 2012. **2**(4): p. 167-175.
22. Oliveira, I.M., et al., *Enzymatically crosslinked tyramine-gellan gum hydrogels as drug delivery system for rheumatoid arthritis treatment.* Drug Delivery and Translational Research, 2020.
23. Oliveira, I.M., et al., *Anti-Inflammatory Properties of Injectable Betamethasone-Loaded Tyramine-Modified Gellan Gum/Silk Fibroin Hydrogels.* Biomolecules, 2020. **10**(10): p. 1456.
24. Oliveira, I.M., et al., *PAMAM Dendrimers Functionalised with an Anti-TNF α Antibody and Chondroitin Sulphate for Treatment of Rheumatoid Arthritis.* Materials Science and Engineering: C, 2021: p. 111845.
25. Canadas, R.F., et al., *Biochemical Gradients to Generate 3D Heterotypic ‐ Like Tissues with Isotropic and Anisotropic Architectures.* Advanced Functional Materials, 2018. **28**(48): p. 1804148.
26. Li, M., et al., *Controlling Conjugated Antibodies at the Molecular Level for Active Targeting Nanoparticles toward HER2-Positive Cancer Cells.* Molecular Pharmaceutics, 2021.
27. Thoniyot, P., et al., *Nanoparticle-Hydrogel Composites: Concept, Design, and Applications of These Promising, Multi-Functional Materials.* Advanced science (Weinheim, Baden-Wurttemberg, Germany), 2015. **2**(1-2): p. 1400010-1400010.
28. Dannert, C., B.T. Stokke, and R.S. Dias, *Nanoparticle-Hydrogel Composites: From Molecular Interactions to Macroscopic Behavior.* Polymers, 2019. **11**(2): p. 275.
29. Mateen, S., et al., *Understanding the role of cytokines in the pathogenesis of rheumatoid arthritis.* Clinica Chimica Acta, 2016. **455**: p. 161-171.
30. Maruotti, N., et al., *Macrophages in rheumatoid arthritis.* Histology and histopathology, 2007.
31. Yang, X., Y. Chang, and W. Wei, *Emerging role of targeting macrophages in rheumatoid arthritis: Focus on polarization, metabolism and apoptosis.* Cell Proliferation, 2020: p. e12854.
32. Laria, A., et al., *The macrophages in rheumatic diseases.* Journal of inflammation research, 2016. **9**: p. 1.

33. Rein, P. and R.B. Mueller, *Treatment with Biologicals in Rheumatoid Arthritis: An Overview.* Rheumatology and therapy, 2017. **4**(2): p. 247-261.
34. Spano, A., S. Barni, and L. Sciola, *PMA withdrawal in PMA-treated monocytic THP-1 cells and subsequent retinoic acid stimulation, modulate induction of apoptosis and appearance of dendritic cells.* Cell Prolif, 2013. **46**(3): p. 328-47.
35. Richter, E., et al., *Induction of Macrophage Function in Human THP-1 Cells Is Associated with Rewiring of MAPK Signaling and Activation of MAP3K7 (TAK1) Protein Kinase.* Front Cell Dev Biol, 2016. **4**: p. 21.
36. D'Arrigo, G., et al., *Gellan gum nanohydrogel containing anti-inflammatory and anti-cancer drugs: a multi-drug delivery system for a combination therapy in cancer treatment.* Eur J Pharm Biopharm, 2014. **87**(1): p. 208-16.
37. Dyakonov, T., et al., *Design and Characterization of a Silk-Fibroin-Based Drug Delivery Platform Using Naproxen as a Model Drug.* Journal of Drug Delivery, 2012. **2012**: p. 490514.

Chapter IX

Modulation of inflammation by anti-TNF α mAb-dendrimer nanoparticles loaded in tyramine-modified Gellan gum hydrogels in a cartilage-on-a-chip model

Chapter IX

Modulation of inflammation by anti-TNFα mAb-dendrimer nanoparticles loaded in tyramine-modified Gellan gum hydrogels in a cartilage-on-a-chip model[8]

ABSTRACT

Rheumatoid arthritis (RA) is an autoimmune and chronic inflammatory disease characterized by joint inflammation that can induce cartilage and bone destruction. Since the inflammatory condition plays an important role in the disease process, it is important to develop and test new therapeutic approaches that specifically target and treat joint inflammation, allowing overcome the limitations of the current treatments. In this study, a human 3D inflammatory cartilage-on-a-chip model was established to test the therapeutic efficacy of anti-TNFα mAb-CS/PAMAM dendrimer NPs loaded-Tyramine-Gellan Gum in the treatment of inflammation. The results showed that human monocyte cell line (THP-1) and human chondrogenic primary cells (hCH) cultured with anti-TNFα mAb-CS/PAMAM dendrimer NPs loaded-Ty-GG hydrogel were metabolically active and proliferative along the study time. Furthermore, the proposed therapeutic approach applied to the THP-1 and hCH cell-based inflammation system revealed an anti-inflammatory capacity that increased over 14 days. It was also possible to observe that Coll type II was highly expressed by hCH of the cell-based inflammation system cultured with anti-TNF α mAb-CS/PAMAM dendrimer NPs, indicating that in addition to modulating the inflammatory environment, the hCH cells were able maintain their biological functions. The developed preclinical model allowed us to provide more robust data on the potential therapeutic effect of anti-TNF α mAb-CS/PAMAM dendrimer NPs loaded-Ty-GG hydrogel in a physiologically relevant model.

[8]This chapter is based on the following publication:

Oliveira I.M., Carvalho, M. R., Fernandes, D.C., Abreu, C.M., Maia, F. R., Pereira H., Caballero, D., Kundu, S.C., Reis, R.L., and Oliveira, J.M. "Modulation of inflammation by anti-TNF α mAb-dendrimer nanoparticles loaded in tyramine-modified Gellan gum hydrogels in a cartilage-on-a-chip model " (Submitted)

Keywords: Cartilage-on-a-chip, Microfluidics, Inflammatory, Drugs screening, Ty-GG Hydrogel, Dendrimer nanoparticles.

IX-1. GRAPHICAL ABSTRACT

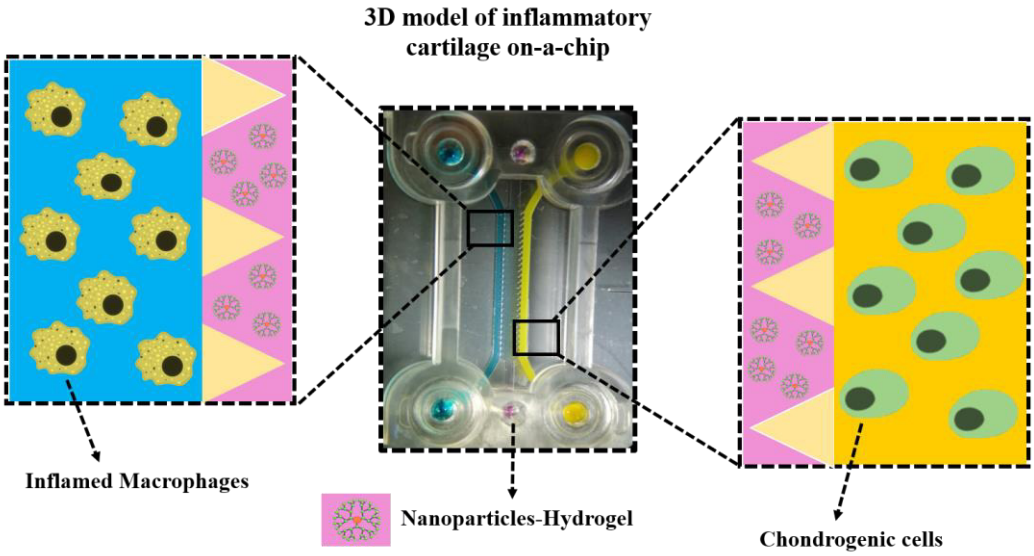

IX-2. INTRODUCTION

Rheumatoid arthritis (RA) is an autoimmune and chronic inflammatory disease characterized by joint inflammation. In the inflammatory scenario, inflammatory cytokines such as Tumor necrosis factor (TNFα) lead to macrophages activation, which can cause stiffness and swelling of joints, damage to cartilage and erosion of bone [1],[2]. Several therapies are currently available for RA treatment, including glucocorticoids, disease-modifying antirheumatic drugs, non-steroidal anti-inflammatory drugs, and biological agents to relieve pain and control inflammation [3],[4]. Despite the great advances, due to heterogeneity of RA, many patients do not reach continued clinical remission or become resistant to drug therapy [5],[6].

In vivo animal models are considered the gold standard in preclinical studies of pathophysiological mechanisms of RA [7],[8]. Although animal models present many aspects of human arthritic diseases and are highly useful for testing new therapeutic approaches, they show some limitations, such as the development of arthritis only in predisposed strains of rodents [9],[10]. They present limited

development of arthritis, and pathophysiology in animals does not fully mimic the human pathogenic disease [11],[12]. Furthermore, an increased amount of evidence suggest that current animal models are inadequate for wide drug screening due to their low reproducibility in clinical trials due to interspecies variations [13],[14]. Thus, better models are crucial to help improve our knowledge on the pathological mechanisms of RA at pre-clinical level, as well as to develop and test new therapeutic approaches in order to meet patient and medical needs [15],[16]. Having these considerations in mind, research has evolved into the next-generation *in vitro* screening platform based on the development of microphysiologically relevant systems, such as tissue- and organs-on-chips [17]. That models are generally based on primary or patient-derived cells, and can better mimic the disease and its treatment, therefore promoting the translational process to humans, while decreasing the number of animals experiments [18],[19]. The purpose of such type of *in vitro* technology is to provide an artificial testing system that fully mimics an tissue, organ, or the human body [20]. The chip platform can allow regulating indirect and direct cell-cell communication as well as biomechanical signals using several strategies such as the generation of a gradient flow [21]. The use of microfluidic-based technology thus can address the handicaps between *in vitro* and *in vivo* models presenting new promising approaches to research in medicine [22],[23].

In our previous work, monoclonal anti-TNFα antibody (anti-TNFα Ab) linked to chondroitin sulfate (CS) modified poly(amidoamine) (CS/PAMAM) dendrimer nanoparticles (NPs) [24] and loaded into Tyramine-Gellan Gum (Ty-GG) hydrogels were developed as a promising drug delivery vehicle to improve therapeutic efficacy in the treatment of inflammatory conditions such as RA. The therapeutic efficacy was evaluated using an inflammation *in vitro* model under standard static conditions and dynamic conditions using a bioreactor. In static and dynamic conditions, the Ty-GG hydrogel encapsulated with anti-TNFα mAb-CS/PAMAM dendrimer NPs exhibited good anti-inflammatory activity over time, motivating us to study the efficacy of this approach in the treatment of inflammation in a more physiologically relevant *in vitro* system, such as a 3D microfluidic platform. In this context, a new *in vitro* human 3D inflammatory cartilage-on-a-chip model was developed aiming to be used as a drug screening platform. An inflammatory environment was established by means of culturing human primary chondrocytes exposed to active pro-inflammatory macrophages, and the anti-TNFα mAb-CS/PAMAM dendrimer NPs loaded-Ty-GG hydrogel was used to test its anti-inflammatory therapeutic efficacy.

IX-3. MATERIAL AND METHODS

IX-3.1. *In vitro* studies under a 3D microfluidic platform

To mimic the human cartilage inflammation microenvironment, a complex 3D microfluidic chip-based *in vitro* model was developed. In this sense, human monocyte cell line (THP-1) and human chondrogenic primary cells (hCH) were used in this study, by means of encapsulation in Matrigel® and further perfuse in the microfluidic platform.

IX-3.1.1. Chondrogenic cell isolation

The hCH cells (passage=3) previously isolated and characterized (kindly provided by Raphael Canadas) were used for these assays [25]. Briefly, they were obtained from human cartilage during arthroscopic surgeries on male and female donors with ages between 19 and 56 years (Centro Hospitalar Póvoa do Varzim). The articular cartilage was removed from the bone and cut into small pieces. The samples were washed several times with 1% PBS/antibiotic-antimycotic (v/v) solution, digested with 0.08% collagenase type II (Sigma-Aldrich, USA)/DMEM-F12 medium 1:1 (v/v) and incubated at 37°C in a water bath overnight with gentle agitation. The digested tissue was filtered, and cell suspension centrifuged at 500 G for 5 minutes. The isolated cells were then plated in flasks cultured in DMEM-F12 medium and kept in the CO_2 incubator at 37°C until they reach the desired confluence.

IX-3.1.2. Cell culture

hCH cells were expanded in DMEM/F12 medium (Dulbecco's Modified Eagle Medium: Nutrient Mixture F-12, Alfagene, Portugal), supplemented with 10% of Heat Inactivated Fetal Bovine Serum (FBS) (Alfagene, Portugal), sodium bicarbonate (Sigma-Aldrich, USA) and 1% (v/v) antibiotic-antimycotic (Alfagene, Portugal), under standard culture conditions (at 37°C in a 5% CO_2 incubator).

THP-1 cells (SIGMA, USA) were expanded in RPMI 1640 Medium, GlutaMAX™ Supplement, HEPES (Thermo Fisher Scientific, USA), supplemented with 10% of FBS and 1% of antibiotic-antimycotic, under standard culture conditions (37°C in a humidified atmosphere containing 5% CO_2).

IX-3.1.3. Production and encapsulation of anti-TNF α mAb-CS/PAMAM dendrimer NPs into Ty-GG hydrogel

Ty-GG Anti-TNFα mAb-CS/PAMAM dendrimer NPs and Ty-GG were produced as previously described [26],[27].

Herein, these systems were used to obtain anti-TNFα mAb-CS/PAMAM dendrimer NPs loaded-Ty-GG hydrogel. The hydrogel was prepared by mixing 1% (w/v) of Ty-GG solution with anti-TNFα mAb-CS/PAMAM dendrimer NPs at a final concentration of 0.5 mg mL^{-1}. Then, the enzymatic crosslinking was made by adding horseradish peroxidase (HRP) solution (0.84 mg mL^{-1}) (Sigma-Aldrich, USA) and hydrogen peroxide solution (H_2O_2) (0.36% (v/v)) (VWR, USA) prepared in PBS and water, respectively. mAb-CS/PAMAM dendrimer NPs loaded-Ty-GG hydrogel (hereafter designated NPs-Hydrogel) was used in the subsequent assays.

IX-3.1.4. Seeding on microfluidic chip

To perform cell seeding, the microfluidic platform 3D Cell Culture Chips DAX-1(Aim Biotech, Singapore) was used. The device consists of three compartments: two lateral channels, where THP-1 (left side) and hCH cells (right side) encapsulated in Matrigel mimic the cartilage inflammation microenvironment, and one central channel where the produced NPs-Hydrogel was injected to treat the inflammatory environment. The appropriate culture medium was placed in the lateral channels with a volume differential (90 µL at inlet and 70 µL at the outlet) to allow fluid diffusion between the channels.

IX-3.1.5. Encapsulation of Gelatin in central channel

Gelatin from porcine skin (Sigma-Aldrich, USA) at 2% (w/v) was dissolved in water at 50°C and added to the central channel of the microfluidic device. This polymer was used as sacrificial hydrogel, preventing the Matrigel® with encapsulated cells to leak into the central chamber. The device was placed at 4°C for 20 minutes for jellification.

IX-3.1.6. Validation of the co-culture by fluorescence imaging

Before the seeding in the microfluidic device, THP-1 and hCH cells were made fluorescent by means of CellTracker CM-DiI Dye (Alfagene, Irland) and CellTracker Green CMFDA Dye, respectively. hCH confluent cells were detached from the cell culture flasks using trypsin (0.25% (v/v) trypsin–EDTA solution), centrifuged at 300 G for 5 minutes, and diluted in a new cell suspension. THP-1 non-adherent cells were also centrifuged at 300 G for 5 minutes and diluted in 1 mL of PBS. After this, the THP-1 and hCH cells were used at a density of $2x10^6$ cells mL^{-1}. THP-1 were incubated with CellTracker CM-DiI Dye (2 μM) (Alfagene, Irland) and hCH with CellTracker Green CMFDA Dye (1 μM) (Alfagene, Irland), for 30 minutes at 37°C. Cells were then centrifuged, encapsulated in Matrigel® and placed in the lateral channels of the chip. RPMI medium with 100 nM phorbol 12-myristate-13-acetate (PMA) (Sigma-Aldrich, USA) was added to the channel with THP-1 cells, to differentiate them into macrophage phenotype, and DMEM-F12 was added to the channel with hCH cells. The microfluidic device was incubated for 72 hours and observed under fluorescence microscopy (DiI tracker ex/em 553/570 nm Green tracker ex/em 492/517 nm) in the Fluorescence Inverted Microscope (Axio Observer, Zeiss). Images were acquired using the Zen microscope processing software, connected to the digital camera Axio Observer.

IX-3.1.7. Encapsulation of hCH and THP-1 in lateral channels to stimulate an inflammatory environment

The hCH and THP-1 cells were centrifuged at 300 G for 5 minutes and diluted in a new cell suspension with appropriate media. Then, the THP-1 and hCH cells were encapsulated in Matrigel® at a density of $2x10^6$ cells mL^{-1}. THP-1 cells suspended in Matrigel® were injected in the left channel and hCH in the right channel of the microfluidic device, followed by incubation for 20 minutes at 37°C for crosslinking. After this, RPMI medium with 100 nM PMA was added to the channel with THP-1 cells and DMEM-F12 was added to the channel with hCH cells to prevent drying. A differential of cell culture medium was added to the inlet (90 μL) and outlet (70 μL) of the microchannel to allow perfusion and nutrition of the cells. The microfluidic devices were incubated for 24 hours, after which the medium was replaced with RPMI medium without PMA in the THP-1 channel and DMEM-F12 in hCH channel, followed by another 24 hours of incubation.

To enable an inflammatory response, THP-1 cells were incubated for 5 hours with 100 ng mL^{-1} of lipopolysaccharide (LPS) (SigmaAldrich, USA) in RPMI medium. After incubation time, gelatin was flushed from the central channel with PBS at 50°C, letting the channel free to add our formulation of NPs-Hydrogel, for 3 and 7 days. In parallel, a positive control chip comprising THP-1 stimulated with LPS in left channel, and hCH in the right channel without NPs-Hydrogel was used (hereafter designated $CTRL^{+}$). Additionally, a negative control chip with THP-1 differentiated with PMA in the left channel, and hCH cells in the right channel without NPs-hydrogel was used (hereafter designated $CTRL^{-}$).

IX-3.1.8. Alamar blue assay

Alamar blue was performed to assess the effect of NPs-Hydrogel in terms of metabolic activity in THP-1 and hCH cells for 3 and 7 days. For the Alamar blue metabolic activity assay in 3D, cells encapsulated in Matrigel® were retrieved using Corning Cell Recovery Solution (Laborspirit, Portugal) for 40 minutes at 4°C. After complete Matrigel® release, cells were collected to an Eppendorf tube and centrifuged to a pellet (300 G for 5 minutes). The supernatant was removed and a culture medium containing 10% (v/v) of AlamarBlue® (BioRad, Oxford, UK) was added. The tubes were kept in the dark, at 37°C in the CO_2 incubator for 4 hours. Afterwards, 100 µL of each condition were transferred to 96-well plates. The fluorescence was read at an excitation wavelength of 530/25 nm and at an emission wavelength of 590/535 nm, using a microplate reader (Synergy HT, BioTek, Instruments, USA).

IX-3.1.9. DNA quantification

The proliferation of THP-1 and hCH cells in contact with NPs-Hydrogel for 3 and 7 days were analyzed by means of DNA quantification. For DNA quantification, cells encapsulated in Matrigel® were retrieved using Corning Cell Recovery Solution for 40 minutes at 4°C and the subsequent protocol was performed as previously described. After centrifugation, the supernatant was removed, and ultrapure water was added. The cells' lysate solution was stored at -80°C until further analysis. Quanti-IT PicoGreen dsDNA Assay Kit (Alfagene, Portugal) was used to quantify dsDNA, according to manufacturers' instructions. Then, the plate was incubated in the dark for 10 minutes and the fluorescence was read using excitation of 480/20 nm and emission of 528/20 nm, in a microplate

reader (SYNERGY HT, BIO-TEK). DNA concentration was determined using a standard curve in the range of 2 to 0 μL mL^{-1}.

IX-3.1.10. Live/Dead staining

Cell viability of THP-1 and hCH cells cultured in the microfluidic chip's lateral channels was assessed in the presence of NPs-Hydrogel for 3 and 7 days, using the live/dead assay. Initially, the NPs-Hydrogel was flushed with PBS at 50°C in the central channel to add the solution of Calcein-AM (1 mM; live cells in green) (Alfagene, Portugal) and ethidium homodimer (EthD-1 6 mM; dead cells in red) (Laborspirit, Portugal). The chips were incubated for 40 minutes in the dark, at 37°C in the CO_2 incubator, to reach the cells in the lateral channels. After this, the central channel was washed with PBS three times. The chips were observed under fluorescence microscopy (EthD-1 ex/em 528/617 nm Calcein-AM; ex/em 495/515 nm) in the Fluorescence Inverted Microscope. Images were acquired using the Zen microscope processing software, connected to the digital camera Axio Observer. A Z-stack function was used to combine images at different depths into one final image.

IX-3.1.11. Anti-inflammatory activity of anti-TNF α mAb-CS/PAMAM dendrimer NPs loaded-Ty-GG hydrogel

To assesses the therapeutic efficacy of NPs-Hydrogel, at each time point (3 and 7 days), the culture medium was collected and stored at -80°C until further analysis. Human TNF-alpha DuoSET ELISA (R&D Systems, USA) kit and DuoSet Ancillary Reagent Kit 2 (R&D Systems, USA), for the optimum performance of the ELISA kit were used to evaluate the anti-inflammatory activity. TNFα standard solutions with concentrations from 1000 to 0 pg mL^{-1} were also assessed in the ELISA plate to perform the calibration curve. The optical density at 450 nm was read in a microplate reader (Synergy HT, BIO-TEK, Winooski, VT, USA).

IX-3.1.12. Immunofluorescence staining

To evaluate the amount of Collagen Type II (Coll type II) present in hCH primary cells, immunofluorescence staining was performed. On the 7th day, the NPs-Hydrogel was flushed from the

central channel of the chip with PBS at 50°C. For cell fixation, 10% formaldehyde was added and left to incubate for 15 minutes at RT. Then, the channel was washed twice with PBS. For permeabilization 0.1% Triton X-100 was added and incubated for 10 minutes at RT. Then, the channel was washed twice with PBS. For blocking, the PBS was removed and replaced with blocking buffer (2% BSA in PBS) and left to incubate for 2 hours at RT. The blocking buffer was removed from the central channel and mouse anti-human COL II monoclonal antibody (Laborspirit, Portugal) in PBS solution (1:250) was added and incubated overnight at 4°C. Then, the central channel was washed 3 times with PBS and the secondary antibody Alexa Fluor® 594 donkey anti-mouse (1:500) (Invitrogen, USA) with DAPI (1:1000) (VWR International, USA), in PBS solution and was left to incubate 1.5 hours. The samples were immediately analyzed by confocal microscopy (Leica, SP8, Germany) (Alexa Fluor 594: ex/em 590/617 nm; DAPI: ex/em 358/461 nm).

IX-3.2. Statistical Analysis

Statistical analysis was performed with GraphPad Prism 8 version, where a Shapiro–Wilk normality test was done to assess the data normality. Non-parametric Kruskal-Wallis test was applied to all assays. Statistical significance was obtained as * $p<0.05$. All results are presented as means ± standard deviations, and all assays were performed in triplicate.

IX-4. RESULTS AND DISCUSSION

IX-4.1.1. Development of a 3D inflammatory cartilage-on-a-chip model

In this study, an *in vitro* 3D inflamed cartilage model-on-a-chip to test the therapeutic efficacy of NPs-Hydrogel was established. The first steps consisted in the encapsulation of pro-inflammatory THP-1 cells in Matrigel® in one of the lateral channels of the chip to mimic the intended inflammatory environment, while hCH cells encapsulated in Matrigel® were seeded on the other microchannel, as target cells. NPs-Hydrogel was added to be used as a treatment option. In the sense, mAb-CS/PAMAM dendrimer NPs are released from the hydrogel and the biological effect was evaluated.

In order to achieve this, the traditional "sandwich" microfluidic design was chosen [28]. The selected microfluidic has a central chamber and two perfusable lateral channels. THP-1 cells encapsulated in Matrigel® were seeded in the left channel, hCH were seeded in the right channel, and NPs-Hydrogel was added in the central channel (**Figure IX-1** a).

To assess the achievement and maintenance of the culture for 3 days, THP-1 cells encapsulated in Matrigel® were labelled with CellTracker CM-DiI Dye (Blue) and hCH with CellTracker Green CMFDA Dye (Green), as shown in (Figure 1 b). It was possible to observe that the cells remained in the lateral channels and were well distributed along the channel in the Matrigel® after 3 days of culture.

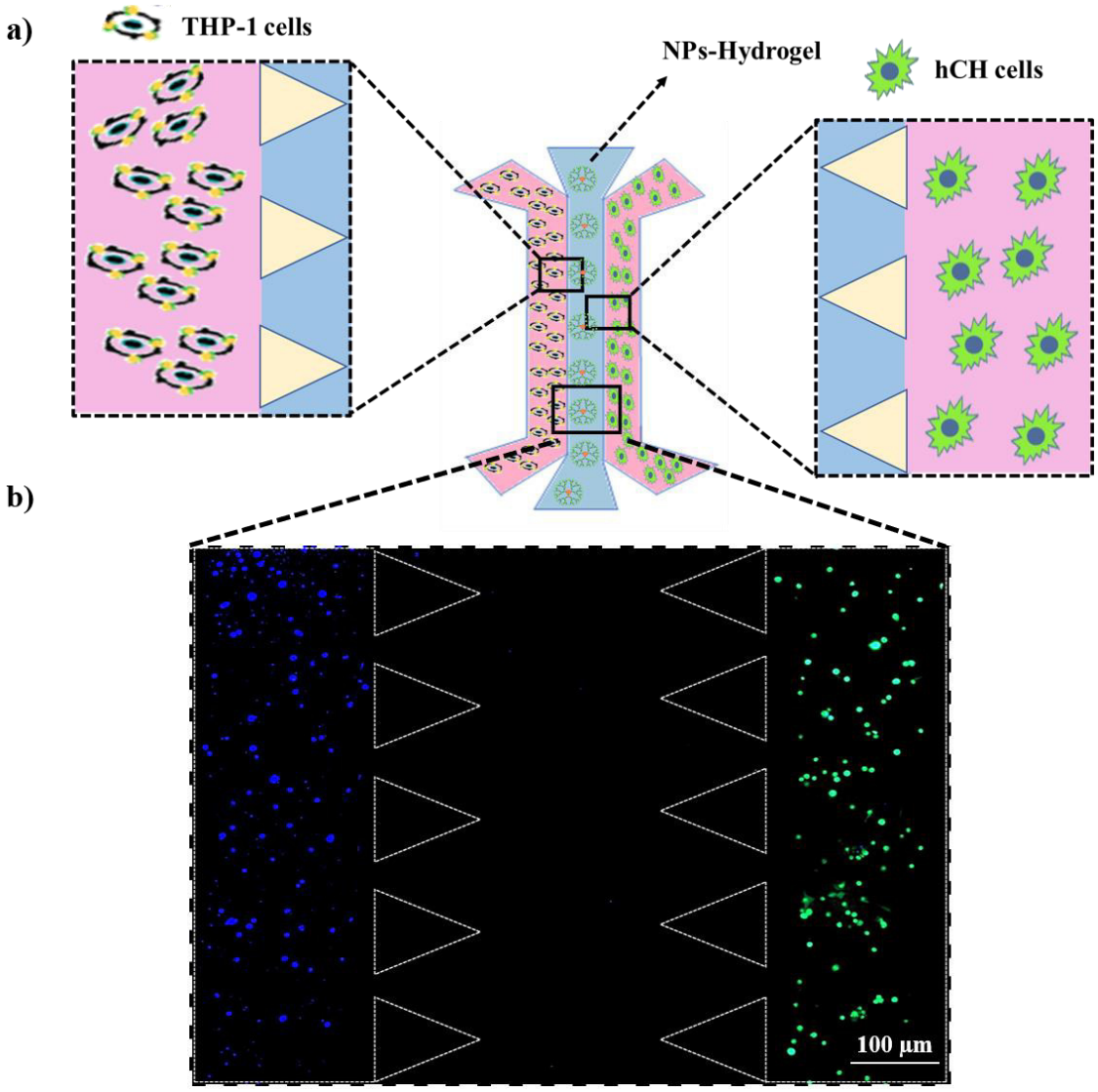

Figure IX-1 - Design of microfluidic chip. a) Schematic representation of a 3D inflamed cartilage model-on-a-chip. b) Fluorescence microscopy image of microfluidic lateral channel mimicking inflamed cartilage comprising

THP1 cells embedded in Matrigel® (left channel, stained with blue) and hCH cells (right channel, stained with green), after 3 days of culture (scale bar = 100 μ m).

IX-4.1.2. Influence of anti-TNF α mAb-CS/PAMAM dendrimer NPs loaded-Ty-GG hydrogel on metabolic activity and cell proliferation of THP-1 and hCH cells

Cells' metabolic activity and proliferation were determined by means of performing Alamar blue and DNA quantification assays, respectively, for 3 and 7 days (**Figure IX-2**). As depicted in Figure 2 a, at the first time point, THP-1 cells differentiated with PMA (healthy cells CTRL$^-$), stimulated with LPS (inflamed cells CTRL$^+$) and inflamed THP-1 cells with NPs-Hydrogel showed high metabolic activity with no significant differences between conditions. In addition, it was possible to verify that the healthy THP-1 cells did not negatively affect the metabolic activity of chondrocytes. However, inflamed THP-1 cells negatively and significantly affected the metabolic activity of chondrocytes as compared to the previous condition, as expected [29],[30]. In inflamed THP-1 cells with NPs-Hydrogel, despite a slight decrease, there was no significant difference in metabolic activity. On the seventh day of culture, there was a slight increase in metabolic activity in all conditions with THP-1 cells, with no significant differences between them. As expected, there was an increase in the metabolic activity in the chondrocytes when were in contact with healthy THP-1 cells and inflamed THP-1 cells with NPs-Hydrogel. Nevertheless, inflamed THP-1 cells induced a significant decrease in the metabolic activity of chondrocytes, when compared with healthy THP-1 cells.

DNA quantification was also analyzed to assess THP-1 and hCH cells' proliferation in contact in the different conditions for 3 and 7 days. As depicted in Figure 2 b, none of the conditions negatively affected the proliferation of THP-1 cells after 3 days of culture. However, it was observed a decrease in the proliferation of THP-1 cells in all conditions, after 7 days of culture. These results are in agreement with other studies [31],[32] wherein PMA induces differentiation of cells and while cells are spending energy to differentiate. Furthermore, it was possible to verify that healthy THP-1 cells also did not affect the chondrocytes metabolic activity, observing an increase in proliferation over time. The hCH cells in contact with inflamed THP-1 cells with NPs-Hydrogel maintain a constant profile of proliferation over time. In addition, inflamed THP-1 cells significantly decreased cell proliferation of chondrocytes as compared to healthy cells over time, corroborating the results obtained from Alamar blue observations.

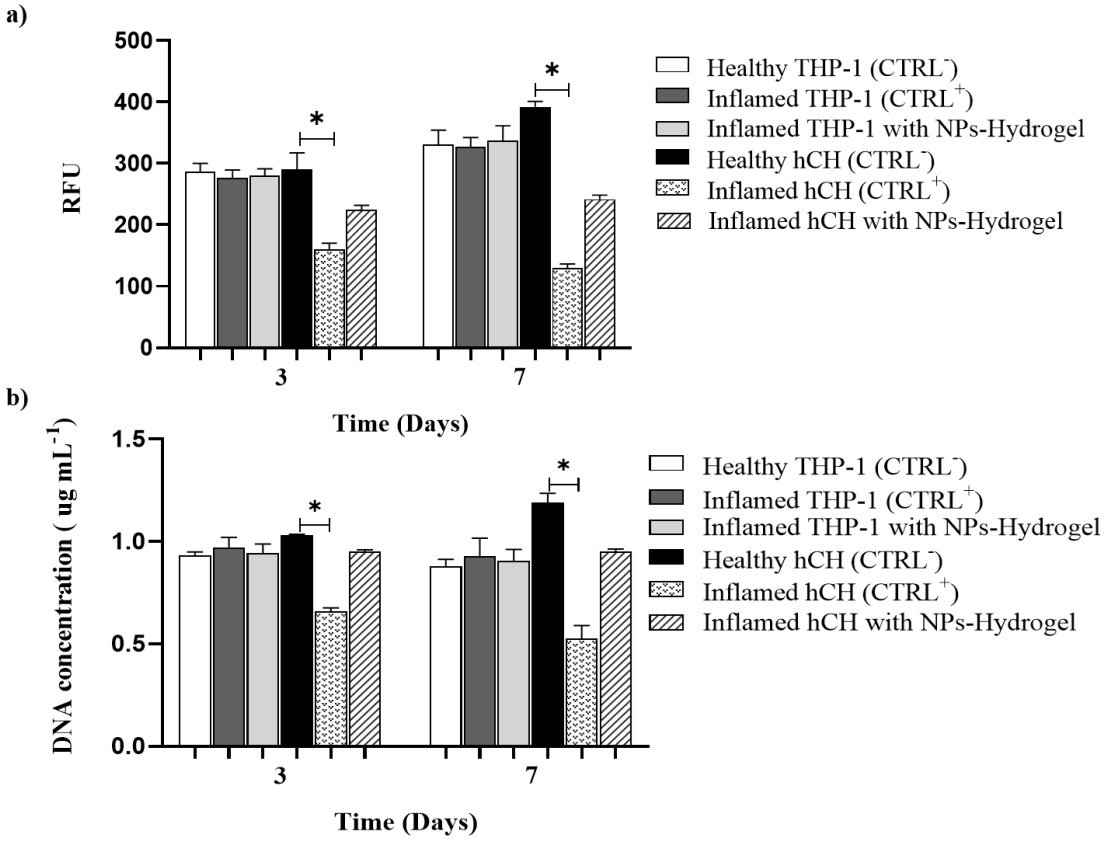

Figure IX-2 - Evaluation of metabolic activity and proliferation of THP-1 and hCH cells. a) Metabolic activity assessed within the three conditions: Healthy THP-1 (CTRL-) cultured with hCH, Inflamed THP-1 (CTRL+) cultured with hCH, and Inflamed THP-1 cultured with hCH, and with NPs-Hydrogel treatment for 3 and 7 days. b) Cell proliferation assessed by DNA quantification within the three conditions: Healthy THP-1 (CTRL-) cultured with hCH, Inflamed THP-1 (CTRL+) cultured with hCH, and Inflamed THP-1 cultured with hCH, and with NPs-Hydrogel treatment for 3 and 7 days. Data shown as Mean ± SD. * denotes statistical significant difference $p<0.05$.

After quantitatively assessing cell viability and proliferation after 3 and 7 days, cell viability was qualitatively assessed. At each time point, live (green) and dead (red) THP-1 and hCH cells were stained by adding Calcein/ EthD and the chips were observed under fluorescence microscopy (**Figure IX-3**). As observed in Figure 3a, at day 3, all the conditions tested showed that THP-1 cells (differentiated THP-1, inflamed THP-1, and inflamed THP-1 with NPs-Hydrogel) remained viable (all green cells) and no dead cells (red) were found. So, it was possible to verify that inflamed THP-1 cells remain viable, as seen in other studies [33], [34] and that NPs-Hydrogels have no cytotoxic effects on cells.

Furthermore, the healthy THP-1 cells did not affect the viability of hCH with no cell death detected. However, hCH cells in the presence of inflamed THP-1 cells showed cell death, corroborating previous proliferation and metabolic activity results. The same pattern was seen in inflamed THP-1 with NPs-Hydrogel, but the incidence of dead chondrocytes appears to be lower. On the seventh day (Figure 3 b), all the THP-1 conditions maintained a high incidence of cell viability. In addition, it was possible to observe a higher chondrocytes adhesion through the observation of the cytoplasmic membrane and a higher incidence of dead chondrocytes was verified in the inflamed THP-1 condition, corroborating the Alamar blue and DNA proliferation results as seen on Figure 2. As expected, the healthy THP-1 cells did not affect the viability of hCH cells over time. Furthermore, inflamed THP-1 cells subjected to the presence of NPs-Hydrogel also did not affect the cell viability. Moreover, in an inflammatory environment, it allowed to reduce the cell death of chondrocytes, showing the possible therapeutic efficacy of the approach under study. However, inflamed THP-1 cells induced hCH cell death. Thus, these results are in agreement with other studies [29],[30]. In fact, inflammatory environment induces chondrocytes cell death, as seen in patients with RA [29],[30].

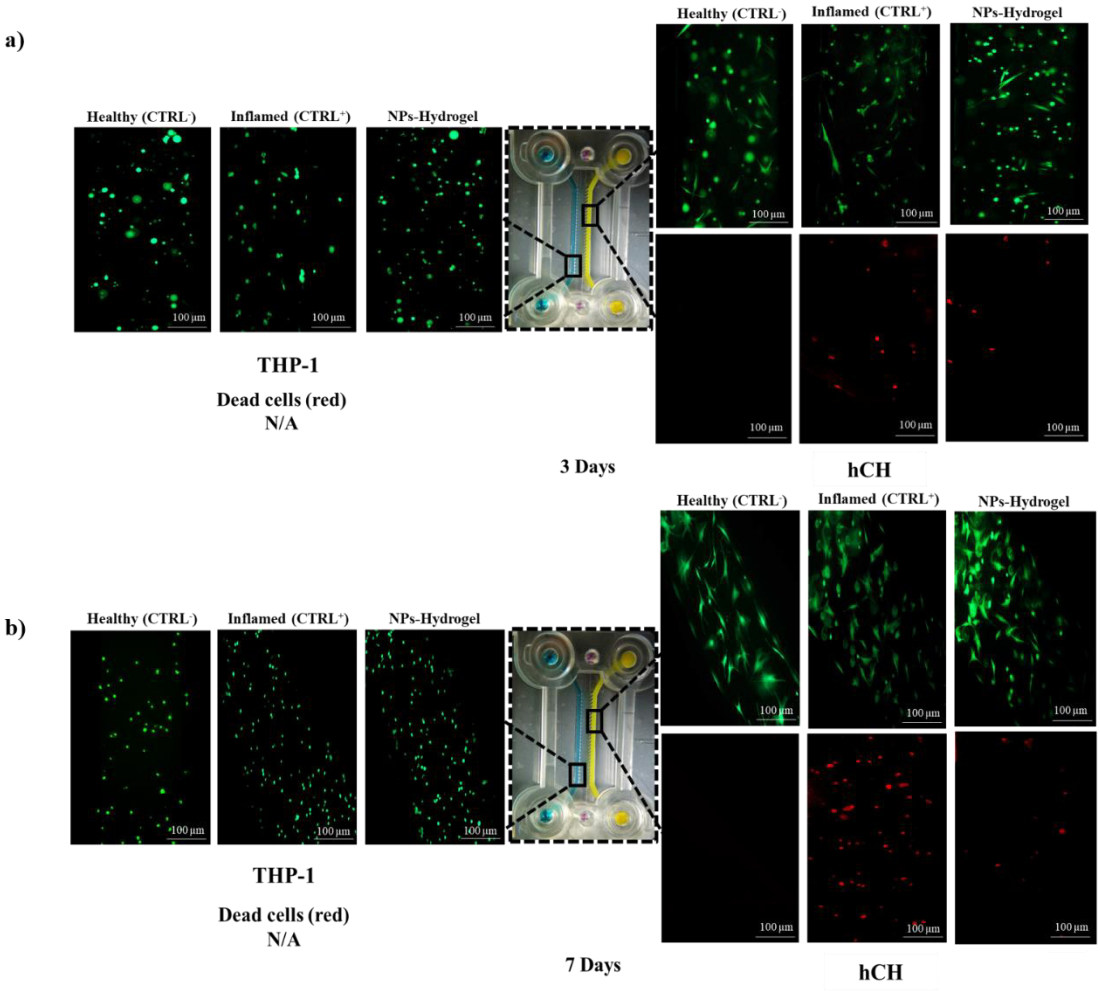

Figure IX-3 - Live/dead assay of THP-1 and hCH cells. Healthy CTRL⁻ (THP-1 differentiated with PMA cultured with hCH); Inflamed CTRL⁺ (THP-1 stimulated with LPS cultured with hCH); and NPs-Hydrogel (inflamed THP-1 cultured with hCH with NPs-Hydrogel treatment) for 3 (a) and 7 days (b).

IX-4.1.3. Hydrogel-based Anti-TNFα dendrimer NPs to modulate the inflammatory environment

In our previous work, NPs-Hydrogel was developed. This system demonstrated a good anti-inflammatory activity over time, allowing the retention of a high percentage of TNFα present within the inflammatory environment. For more reliable testing of the effectiveness of this approach in a more physiologically-relevant microenvironment, the microfluidic device was used as a preclinical model for drug screening.

In order to assess the therapeutic efficacy of NPs-Hydrogel in inflamed THP-1 and hCH cells, the levels of free TNFα in the medium of 7 days of culture were quantified using ELISA KIT (**Figure IX-4**).

THP-1 cells differentiated with PMA (healthy cells) were used as the negative control, and THP-1 stimulated with LPS were used as the positive control (inflamed cells). On day 3, the results demonstrated that the induction of inflammation was successful, with a low TNFα amount present in healthy THP-1 cells and high TNFα amount in inflamed THP-1 cells, with significant differences between the conditions. Furthermore, in the inflamed THP-1 cells with NPs-Hydrogel condition, there was a decrease in the free TNFα in the medium when compared with inflamed cells. However, there was no significant differences as compared with healthy cells. hCH cells in a healthy THP-1 environment also showed low amounts of TNF α present in the medium but in contrast, hCH in an inflamed THP-1 environment demonstrated high levels of free TNFα, with significant differences between the conditions. This means that the mimicry of the inflammatory environment in the cartilage was successful. In the inflamed THP-1 environment with NPs-Hydrogel, a low amount of TNFα in hCH cells was found in the culture medium when compared to the inflamed and untreated environment. On day 7, in the condition with inflamed THP-1 cells and NPs-Hydrogel, the amount of free TNFα present in the medium decreased significantly when compared to the inflamed THP-1 condition without treatment. Furthermore, the same behavior was found in chondrogenic cells with NPs-Hydrogel, where the amount of free TNFα in the medium decreased substantially when compared to the inflamed hCH condition. So, these results show that the inflamed THP-1 cells induced the production of an inflammatory environment in chondrocytes, indicating that the production of the inflammatory cartilage model was successfully achieved. In addition, this preclinical model allowed to reveal the possible therapeutic effect of NPs-Hydrogel in terms of protecting the chondrocytes from inflammation, corroborating the results obtained in other studies [35],[36]. In fact, anti-tumor necrosis factor (TNF) therapies have been successfully used in the treatment of RA [35],[36]. Importantly, it was shown that even linked to dendrimer NPs and encapsulated in the hydrogel, they maintain therapeutic efficacy over time.

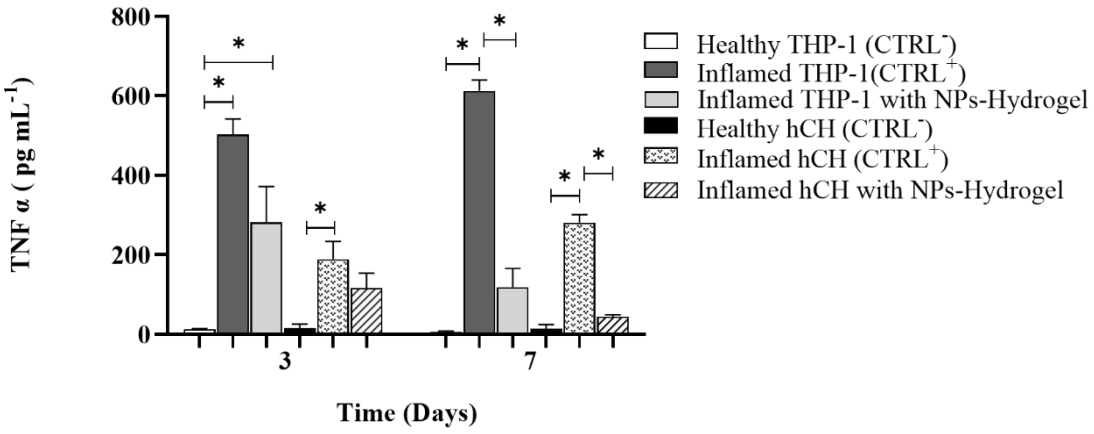

Figure IX-4 - Quantification of free TNF α in the culture medium. Amount of free TNF α within the three conditions: Healthy THP-1 (CTRL-) cultured with hCH; Inflamed THP-1 (CTRL+) cultured with hCH; and Inflamed THP-1 cultured with hCH, and with NPs-Hydrogel treatment for 3 and 7 days. Data shown as Mean ± SD. * denotes statistical significant difference $p < 0.05$.

IX-4.1.4. Collagen type II as a marker of chondrocyte functionality

To mimic Articular cartilage is composed of chondrocytes surrounded by a specialized matrix constituted predominantly of Coll type II and proteoglycan[37],[38]. Rheumatoid Arthritis is a chronic inflammatory disease characterized by joint inflammation that induces cartilage destruction[39],[40]. As Coll type II degradation may indicate cartilage destruction in the joints of RA patients, it is an important parameter to evaluate since it can be useful as a disease-specific biomarker[41],[42].

In this sense, the immunofluorescence staining was performed to qualitatively evaluate the presence of Coll type II in the chondrogenic cells matrix, under the three conditions: healthy THP-1 cells cultured with hCH, inflamed THP-1 cultured with hCH, and inflamed THP-1 cultured with hCH, and with NPs-Hydrogel treatment after 7 days of culture **(Figure IX-5)**. The results demonstrated that the state of THP-1 cells can influence the Coll type II marker in the hCH, being highly expressed in conditions where hCH were in contact with healthy THP-1 cells and with inflamed THP-1 cells with NPs-Hydrogel. However, in an inflammatory environment without NPs-Hydrogel, the incidence of Coll type II was very low, being in agreement with what was previously mentioned: the inflammation process induces Coll type II degradation[41],[42]. These results can suggest that the possible therapeutic efficacy of NPs-Hydrogel in this approach.

Despite the promising results, these assays were performed in normoxia conditions. However, hypoxia is the predominant microenvironment characteristic in inflamed cartilage [43],[44]. The increased oxygen consumption by inflamed cells and the infiltration of the immune cells with an interrupted blood supply caused by vascular dysfunction leads to tissue hypoxia in RA [45, 46]. In this sense would be interesting, and will be the focus of future works, to evaluate this preclinical model in a hypoxic scenario assess whether it would influence the results, and to mimic more precisely the cartilage inflammation environment.

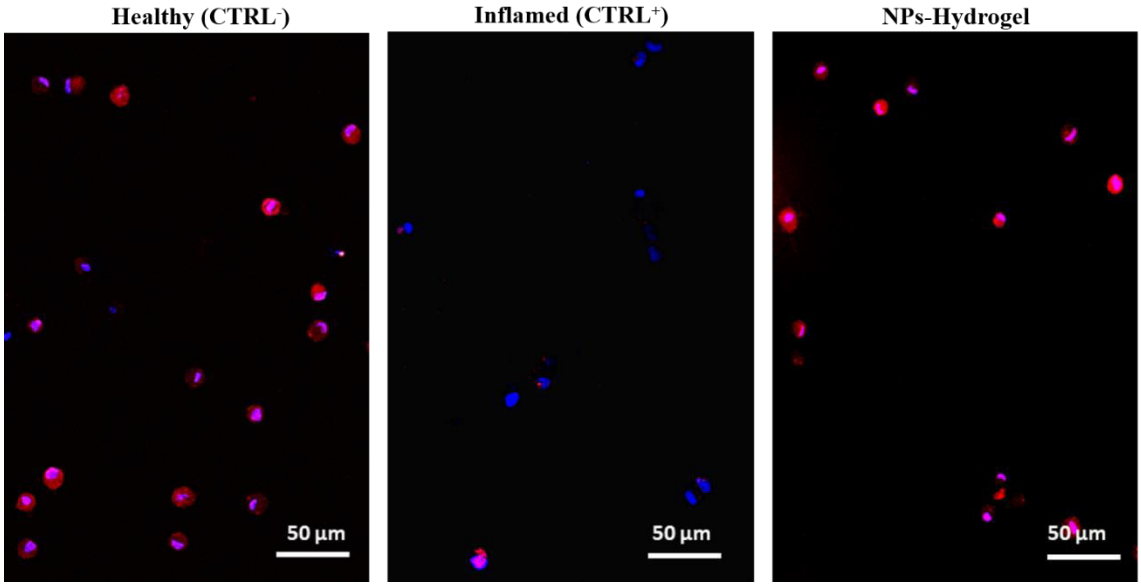

Figure IX-5 - Immunofluorescence staining of Coll type II in the chondrogenic cells matrix. Coll type II expression was assessed in hCH cultured within the three conditions: Healthy (CTRL-) that corresponds to healthy THP-1 cultured with hCH, Inflamed (CTRL+) that corresponds to inflamed THP-1 cultured with hCH, and NPs-Hydrogel that corresponds to inflamed THP-1 cultured with hCH, and with NPs-Hydrogel treatment for 7 days. Coll type II stained in red; Nucleus stained in blue. Scale bar = 50 µm.

IX-5. CONCLUSION

In this work, an *in vitro* human 3D inflammatory cartilage model on-a-chip was developed, which was used to evaluate the therapeutic efficacy of NPs-Hydrogel as an anti-inflammatory treatment, aiming to be used in RA therapy. The results showed that THP-1 and hCH cells encapsulation in Matrigel® and the establishment of the inflammatory environment by co-culturing them on-chip was successful. The THP-1 and hCH cells cultured with NPs-Hydrogel were metabolic active and proliferative along the study time. Furthermore, Live/Dead assays corroborated these results and showed that cell

death was lower in hCH cell-based inflammation system cultured with NPs-Hydrogel when compared to the inflamed environment without NPs-hydrogel treatment. In addition, the THP-1 and hCH cell-based inflammation model cultured with the therapeutic approach presented an increased anti-inflammatory capacity over time.

It was also possible to observe that Coll type II is highly expressed in hCH cell-based inflammation system cultured with NPs-Hydrogel, while its expression was not observed in a pro-inflammatory environment, indicating that in addition to modulating the inflammatory environment, the hCH maintain biological functionally. These important data supported the results obtained in the previous works on the effectiveness of this system regarding inflammation treatment. So, the preclinical model developed allows us to obtain more robust data on the potential therapeutic of NPs-Hydrogel in an *in vivo*-like inflammation environment, namely, to be used in the treatment of RA. Altogether, this work provided valuable information on the delivery of hydrogel-based drug carriers to better understand their clinical potentials prior to the resource intensive animal and clinical studies.

IX-6. ACKNOWLEDGMENTS

The authors thank the financial support under the Norte2020 project (NORTE-08-5369-FSE000044). M.R.C. acknowledges TERM RES Hub Ref. Norte-01-0145-FEDER-02219015 working contract. D.C.F. acknowledges Portuguese Foundation for Science and Technology (FCT) for his phD scholarship (PD/BD/143081/2018) and F.R.M. for her contract under the Transitional Rule DL 57/2016 (CTTI-57/18-I3BS(5)). C.M.A., D.C.V. and S.C.K. thank the support of FCT (PTDC/BTM-ORG/28070/2017). D.C.V acknowledges the CEEC individual contract (CEECIND/00352/2017). The FCT distinction attributed to J.M.O. under the Investigator FCT program (number IF/01285/2015) is also greatly acknowledged.

IX-7. REFERENCES

1. Guo, Q., et al., *Rheumatoid arthritis: pathological mechanisms and modern pharmacologic therapies.* Bone research, 2018. **6**: p. 15-15.
2. Lin, Y.-J., M. Anzaghe, and S. Schülke, *Update on the Pathomechanism, Diagnosis, and Treatment Options for Rheumatoid Arthritis.* Cells, 2020. **9**(4): p. 880.

3. Bullock, J., et al., *Rheumatoid Arthritis: A Brief Overview of the Treatment.* Medical principles and practice : international journal of the Kuwait University, Health Science Centre, 2018. **27**(6): p. 501-507.
4. Quan, L.-D., et al., *The Development of Novel Therapies for Rheumatoid Arthritis.* Expert opinion on therapeutic patents, 2008. **18**(7): p. 723-738.
5. Canadas, R.F., et al., *Biochemical Gradients to Generate 3D Heterotypic ‐ Like Tissues with Isotropic and Anisotropic Architectures.* Advanced Functional Materials, 2018. **28**(48): p. 1804148.
6. Liu, D., et al., *Can rheumatoid arthritis ever cease to exist: a review of various therapeutic modalities to maintain drug-free remission?* American journal of translational research, 2017. **9**(8): p. 3758-3775.
7. Kuyinu, E.L., et al., *Animal models of osteoarthritis: classification, update, and measurement of outcomes.* Journal of orthopaedic surgery and research, 2016. **11**: p. 19-19.
8. Lewis, B.J.B. and D.R. Branch, *Mouse Models of Rheumatoid Arthritis for Studies on Immunopathogenesis and Preclinical Testing of Fc Receptor-Targeting Biologics.* Pharmacology, 2020. **105**(11-12): p. 618-629.
9. Hawkins, P., et al., *Applying refinement to the use of mice and rats in rheumatoid arthritis research.* Inflammopharmacology, 2015. **23**(4): p. 131-150.
10. Fischer, B.D., et al., *Animal models of rheumatoid pain: experimental systems and insights.* Arthritis Research & Therapy, 2017. **19**(1): p. 146.
11. Schinnerling, K., et al., *Humanized Mouse Models of Rheumatoid Arthritis for Studies on Immunopathogenesis and Preclinical Testing of Cell-Based Therapies.* Frontiers in immunology, 2019. **10**: p. 203-203.
12. Moran, C.J., et al., *The benefits and limitations of animal models for translational research in cartilage repair.* Journal of experimental orthopaedics, 2016. **3**(1): p. 1-1.
13. Festing, S. and R. Wilkinson, *The ethics of animal research: talking point on the use of animals in scientific research.* EMBO reports, 2007. **8**(6): p. 526-530.
14. Fogel, D.B., *Factors associated with clinical trials that fail and opportunities for improving the likelihood of success: A review.* Contemporary clinical trials communications, 2018. **11**: p. 156-164.
15. Damerau, A. and T. Gaber, *Modeling Rheumatoid Arthritis In Vitro: From Experimental Feasibility to Physiological Proximity.* International Journal of Molecular Sciences, 2020. **21**(21): p. 7916.
16. ANDERSEN, M.L. and L.M.F. WINTER, *Animal models in biological and biomedical research - experimental and ethical concerns.* Anais da Academia Brasileira de Ciências, 2019. **91**.
17. Occhetta, P., et al., *Hyperphysiological compression of articular cartilage induces an osteoarthritic phenotype in a cartilage-on-a-chip model.* Nat Biomed Eng, 2019. **3**(7): p. 545-557.
18. Jodat, Y.A., et al., *Human-Derived Organ-on-a-Chip for Personalized Drug Development.* Current pharmaceutical design, 2018. **24**(45): p. 5471-5486.
19. Esch, E.W., A. Bahinski, and D. Huh, *Organs-on-chips at the frontiers of drug discovery.* Nature reviews. Drug discovery, 2015. **14**(4): p. 248-260.
20. Wu, Q., et al., *Organ-on-a-chip: recent breakthroughs and future prospects.* BioMedical Engineering OnLine, 2020. **19**(1): p. 9.

21. Rothbauer, M., et al., *Monitoring tissue-level remodelling during inflammatory arthritis using a three-dimensional synovium-on-a-chip with non-invasive light scattering biosensing.* Lab Chip, 2020. **20**(8): p. 1461-1471.
22. Cui, P. and S. Wang, *Application of microfluidic chip technology in pharmaceutical analysis: A review.* Journal of pharmaceutical analysis, 2019. **9**(4): p. 238-247.
23. Collison, J., *Cartilage-on-a-chip to aid OA drug development.* Nature Reviews Rheumatology, 2019. **15**(9): p. 511-511.
24. Oliveira, I.M., et al., *PAMAM dendrimers functionalised with an anti-TNF α antibody and chondroitin sulphate for treatment of rheumatoid arthritis.* Materials Science and Engineering: C, 2021. **121**: p. 111845.
25. Correia, S.I., et al., *Posterior talar process as a suitable cell source for treatment of cartilage and osteochondral defects of the talus.* J Tissue Eng Regen Med, 2017. **11**(7): p. 1949-1962.
26. Oliveira, I.M., et al., *PAMAM Dendrimers Functionalised with an Anti-TNF α Antibody and Chondroitin Sulphate for Treatment of Rheumatoid Arthritis.* Materials Science and Engineering: C, 1920: p. 111845.
27. Oliveira, I.M., et al., *Enzymatically crosslinked tyramine-gellan gum hydrogels as drug delivery system for rheumatoid arthritis treatment.* Drug Delivery and Translational Research, 2020: p. 1-13.
28. Wang, H.-F., et al., *Tumor-Microenvironment-on-a-Chip for Evaluating Nanoparticle-Loaded Macrophages for Drug Delivery.* ACS Biomaterials Science & Engineering, 2020. **6**(9): p. 5040-5050.
29. Goldring, M.B. and M. Otero, *Inflammation in osteoarthritis.* Current opinion in rheumatology, 2011. **23**(5): p. 471-478.
30. Tateiwa, D., H. Yoshikawa, and T. Kaito, *Cartilage and Bone Destruction in Arthritis: Pathogenesis and Treatment Strategy: A Literature Review.* Cells, 2019. **8**(8): p. 818.
31. Spano, A., S. Barni, and L. Sciola, *PMA withdrawal in PMA-treated monocytic THP-1 cells and subsequent retinoic acid stimulation, modulate induction of apoptosis and appearance of dendritic cells.* Cell Prolif, 2013. **46**(3): p. 328-47.
32. Richter, E., et al., *Induction of Macrophage Function in Human THP-1 Cells Is Associated with Rewiring of MAPK Signaling and Activation of MAP3K7 (TAK1) Protein Kinase.* Front Cell Dev Biol, 2016. **4**: p. 21.
33. Widdrington, J.D., et al., *Exposure of monocytic cells to lipopolysaccharide induces coordinated endotoxin tolerance, mitochondrial biogenesis, mitophagy, and antioxidant defenses.* Frontiers in immunology, 2018. **9**: p. 2217.
34. Liu, X., et al., *LPS-induced proinflammatory cytokine expression in human airway epithelial cells and macrophages via NF-κB, STAT3 or AP-1 activation.* Mol Med Rep, 2018. **17**(4): p. 5484-5491.
35. Geiler, J., M. Buch, and M.F. McDermott, *Anti-TNF treatment in rheumatoid arthritis.* Curr Pharm Des, 2011. **17**(29): p. 3141-54.
36. Ma, X. and S. Xu, *TNF inhibitor therapy for rheumatoid arthritis.* Biomedical reports, 2013. **1**(2): p. 177-184.
37. Boyan, B.D., et al., *Chapter 24 - Cartilage*, in *Vitamin D (Fourth Edition)*, D. Feldman, Editor. 2018, Academic Press. p. 405-417.
38. Sophia Fox, A.J., A. Bedi, and S.A. Rodeo, *The basic science of articular cartilage: structure, composition, and function.* Sports health, 2009. **1**(6): p. 461-468.

39. Tanaka, Y., *Rheumatoid arthritis.* Inflammation and Regeneration, 2020. **40**(1): p. 20.
40. Macfarlane, E., M.J. Seibel, and H. Zhou, *Arthritis and the role of endogenous glucocorticoids.* Bone Research, 2020. **8**(1): p. 33.
41. Landewé, R.B.M., et al., *Arthritis instantaneously causes collagen type I and type II degradation in patients with early rheumatoid arthritis: a longitudinal analysis.* Annals of the rheumatic diseases, 2006. **65**(1): p. 40-44.
42. Poole, A., et al., *Type II collagen degradation and its regulation in articular cartilage in osteoarthritis.* Annals of the rheumatic diseases, 2002. **61**(suppl 2): p. ii78-ii81.
43. Guo, X. and G. Chen, *Hypoxia-Inducible Factor Is Critical for Pathogenesis and Regulation of Immune Cell Functions in Rheumatoid Arthritis.* Frontiers in immunology, 2020. **11**: p. 1668-1668.
44. Cummins, E.P., et al., *The role of HIF in immunity and inflammation.* Mol Aspects Med, 2016. **47-48**: p. 24-34.
45. Taylor, C.T. and S.P. Colgan, *Regulation of immunity and inflammation by hypoxia in immunological niches.* Nature reviews. Immunology, 2017. **17**(12): p. 774-785.
46. Bodamyali, T., et al., *Influence of hypoxia in inflammatory synovitis.* Annals of the rheumatic diseases, 1998. **57**(12): p. 703-710.

SECTION 4

Conclusions and Future Perspectives

Chapter X

Conclusions and Future Perspectives

Chapter X

Conclusions and Future perspectives

X-1. GENERAL CONCLUSIONS

Rheumatoid Arthritis is a disease characterized by progressive incapacity, premature death, and socioeconomic problems. Despite recent advances in medical therapeutics, traditional drugs frequently involve high dosage or repeated administration in order to have a therapeutic effect. This can result in a decrease in overall efficacy and patient compliance, inducing several undesired side effects. In order to overcome these limitations, it is important to develop and validate new drug delivery strategies.

The main goal of the work developed under the scope of this thesis was to develop new strategies based on nanoparticles and biomaterials to improve the handicaps of the current therapies while the therapeutic effect from the drugs is maximized, aiming to be used in RA treatment.

In this sense, the development of dendrimer nanoparticles linked to antibodies, drug-loaded hydrogels, nanocomposite hydrogels, and 3D inflammatory cartilage-on-a-chip as a drug screening platform, seem to be promising approaches leading to a successful outcome. The smart delivery of biomaterials intends to overcome the main disadvantages observed in the currently available treatments by using innovative and personalized strategies.

In **Chapter V**, the work focused on the development of poly(amidoamine) dendrimers NPs, functionalized with chondroitin sulfate and covalently linked to anti-TNF α to allow a more targeted and effective anti-inflammatory activity for the treatment of inflammatory diseases, including RA. The anti-TNF α chondroitin sulfate/ poly(amidoamine) dendrimers NPs were successfully produced, exhibiting high TNF α capture capacity and suitable mechanical properties. That system did not negatively affect the metabolic activity of ATDC5, THP-1 and Jurkat cell lines and showing a high percentage of internalization by target cells (chondrocytes), good cytocompatibility and hemocompatibility. Furthermore, anti-TNF α chondroitin sulfate/poly(amidoamine) dendrimer NPs exhibited superior therapeutic efficacy as compared with the anti-TNF α alone, up to 7 days of culture. Thus, the results suggested that the anti-TNF α chondroitin sulfate/ poly(amidoamine) dendrimers NPs can be useful for controlled and sustained drug delivery, making it appealing for new immunotherapies in RA patients.

In order to develop new personalized strategies, in **Chapter VI**, an essential collaboration was established between 3Bs Research Group and the Department of Polymer Nanoscience and Polymer BIN Research Centre (Chonbuk National University, South Korea). The aim was to develop Tyramine-modified Gellan gum hydrogels via enzymatic crosslinking, as a new drug delivery system, loaded with Betamethasone in order to improve the therapeutic efficacy and safety in RA treatment. The developed approach demonstrated good mechanical properties and controlled Betamethasone release profile over time, suggesting that the properties of Gellan gum were improved with the chemical modification. Furthermore, Tyramine-Gellan gum hydrogels did not exhibit cytotoxicity effects on chondrogenic primary cells and showed a higher therapeutic effect over time as compared to the administration of Betamethasone. Therefore, it was possible to conclude that developed Tyramine-Gellan gum hydrogels can represent a promising drug delivery system and a viable alternative to overcome the limitations of traditional treatment used in patients with RA.

Since natural polymers have less stable mechanical properties and a higher degree of degradation when compared to synthetic polymers, natural and synthetic materials can be combined to achieve better performances. In this sense, the Tyramine–Gellan gum was used to increase the mechanical stability of silk fibroin and further improve the therapeutic effect as a drug delivery system **(Chapter VII)**. The Tyramine–Gellan gum/silk fibroin hydrogels showed a more stable structure and faster gelation time as compared to Silk Fibroin alone. Furthermore, the Tyramine–Gellan gum/silk fibroin hydrogels demonstrated stable mechanical properties, a suitable injectability profile, and a Betamethasone-controlled release profile over time. Hence, these hydrogels possessed the intended physicochemical characteristics for the final application. The Tyramine-Gellan gum/silk fibroin hydrogels with encapsulated Betamethasone also exhibited a higher therapeutic efficacy as compared to Betamethasone administration alone. Therefore, the synergetic combination of these two natural polymers provided advantageous features as a drug delivery system, allowing an improvement in therapeutic efficacy through controlled drug delivery. Thus, Tyramine–Gellan gum/silk fibroin hydrogel is an appealing alternative to overcome the handicaps of current strategies for treating RA.

In **Chapter VIII**, to explore the combined effect of the previously mentioned approaches **(Chapter V, VI,** and **VII)** anti-TNF α chondroitin sulfate/ poly(amidoamine) dendrimer NPs were encapsulated into Tyramine-Gellan gum hydrogels and Tyramine-Gellan gum/Silk Fibroin hydrogels. The therapeutic efficacy was evaluated using an inflammation in vitro model under standard static and dynamic conditions. At an early stage, in vitro models under static conditions showed that anti-TNF α chondroitin

sulfate/ poly(amidoamine) dendrimer NPs captured higher amounts of TNF α as compared to dendrimer NPs encapsulated into hydrogels. However, at 14 days, in anti-TNF α chondroitin sulfate/ poly(amidoamine) dendrimer NPs, the levels of free TNF α abruptly increased whereas with anti-TNF α chondroitin sulfate/ poly(amidoamine) dendrimer NPs loaded within Tyramine-Gellan gum and Tyramine-Gellan gum/silk fibroin hydrogels, the level of free TNF α decreased. Therefore, in a real scenario of disease on humans, frequent administration of anti-TNF α chondroitin sulfate/poly(amidoamine) dendrimer NPs is needed to successfully decrease inflammation. On the other hand, the presence of the hydrogel in the drug delivery system makes it possible for the administration to be less frequent.

Furthermore, in dynamic conditions, anti-TNF α chondroitin sulfate/poly(amidoamine) dendrimer NPs loaded within Tyramine-Gellan gum and Tyramine-Gellan gum/silk fibroin hydrogels presented higher anti-inflammatory activity over time, as compared to static conditions. Thus, these outcomes suggest that drug loaded hydrogels display higher therapeutic potential in an *in vivo* scenario.

In **Chapter IX**, it was aimed to validate the anti-TNF α chondroitin sulfate/ poly(amidoamine) dendrimer NPs loaded within Tyramine-Gellan gum hydrogel in a physiologically-relevant microenvironment. An *in vitro* 3D inflammatory human cartilage on-a-chip model was used. In this sense, an inflammatory environment was established by exposing human chondrogenic primary cells to inflamed THP-1 cells to evaluate with more efficiency the therapeutic effect of the anti-TNF α chondroitin sulfate/ poly(amidoamine) dendrimer NPs loaded within Tyramine-Gellan gum hydrogel in the inflammation treatment. Human chondrocyte primary cell-based inflammation system cultured with anti-TNF α chondroitin sulfate/ poly(amidoamine) dendrimer NPs loaded within Tyramine-Gellan gum hydrogel showed lower cell death as compared to an inflamed environment without treatment. The inflamed chondrogenic cells cultured with the therapeutic approach presented an increased anti-inflammatory capacity over time. Furthermore, Collagen type II, which is present in articular cartilage, was highly produced by human chondrocyte primary cell-based inflammation system cultured with anti-TNF α chondroitin sulfate/ poly(amidoamine) dendrimer NPs loaded within Tyramine-Gellan gum hydrogel. These important data showed that the therapeutic approach in addition to modulating the inflammatory environment also can maintain the chondrocytes biologically functional. Thus, the developed preclinical approach allowed the acquisition of more robust data regarding the potential effectiveness of anti-TNF α chondroitin sulfate/poly(amidoamine) dendrimer NPs loaded within

Tyramine-Gellan gum hydrogel in an in vivo inflammatory environment, namely to be used in the treatment of RA.

In brief, it is possible to conclude that the smart delivery biomaterials can fill the current limitations of traditional therapies to the treatment of Rheumatoid Arthritis. These therapeutic approaches can provide a more targeted and effective treatment while allowing less frequent administration and potentially decreasing the undesirable side effects caused by drug overdosing.

X-2. FUTURE PERSPECTIVES

In this section, the future perspectives in the field of cartilage inflammation treatment will be discussed and perspective studies related to the work developed in this thesis are suggested.

Despite the important scientific progress achieved in the treatment of Rheumatoid Arthritis, there is no ideal system that can assurance future success in clinical trials and that may certainly treat Rheumatoid Arthritis. To develop new therapeutic approaches, it is important to consider the progress in knowledge of the pathophysiology of the disease, the main biomarkers, and the emerged advances in drug delivery systems based on the use of nanoparticles and 3D biomaterial. The development of new strategies based on drug delivery systems can improve the drug absorption rate by the body, maintain a controlled therapeutic release over time and decrease side effects, overcoming the existing treatment limitations. Furthermore, one of the reasons that delay the development and approval of new RA therapies is the lack of preclinical models that can provide a reliable artificial testing system that fully mimics the human body, helping improve our knowledge about the treatment of Rheumatoid Arthritis.

This thesis aimed at combining several fields of research in order to improve the current knowledge on the treatment of inflammation, specifically in Rheumatoid Arthritis research. In this sense, nanotechnology and material science were combined with dynamic and microfluidic models. In this sense, the different smart delivery biomaterials developed under the scope of this thesis showed promising characteristics to be used as alternatives to current treatments. The dendrimers NPs and hydrogels developed in **Chapters V**, **VI**, and **VII** presented safety and a great ability to neutralize the target agent over time, showing great potential to be used as a specific and sustained treatment of inflammation. So, further studies using Rheumatoid Arthritis models are required to clarify its real effectiveness. The dendrimers NPs loaded hydrogels in **Chapter VIII** presented a synergetic effect with a

great drug release profile and simultaneously more effective over time, even in static and dynamic conditions. Further studies to evaluate the prolonged effect of the dendrimers NPs loaded hydrogels in the treatment of inflammation using arthritic cells would be extremely useful. Thus, it allows to verify the possibility of a less frequent administration of the therapy and decrease the side effects caused by overdosing of drugs, which is one of the limitations of current treatments for rheumatoid arthritis. In **Chapter IX**, the evaluation of dendrimers NPs loaded hydrogels using a 3D inflammatory cartilage on-a-chip model allowed to obtain more robust data about the potential effectiveness of this approach in an in vivo inflammation scenario. Preclinical models based on cells derived from patients` cartilage diagnosed with Rheumatoid Arthritis will allow the development of drug screening platforms that can better mimic the disease and more reliably evaluate the therapeutic efficacy. Further studies using arthritic cells-on-a-chip, in a hypoxia environment, and using dynamic perfusion systems, to mimic the human body conditions would be interesting to guarantee the effectiveness of the developed approaches in Rheumatoid Arthritis treatment.

The next step in this work would be the application of these advanced drug delivery systems in rheumatoid arthritis animal models. These models include the induced arthritis models such as Collagen Induced Arthritis (CIA), Collagen-Antibody-Induced Arthritis (CAIA) and Antigen Induced Arthritis (AIA). On the other hand, genetically manipulated or spontaneous arthritis models such as the TNF α transgenic mice, K/BxN mice, and the SKG mice can be also used. They are the many experimental models developed for human arthritic diseases. The use of animal models to assess the safety and efficacy of novel treatment continue to be extremely necessary before being evaluated in clinal studies.

The work developed on the scope of this thesis evidences the extreme advantages of using nanoparticles and biomaterials as a drug delivery system. The smart biomaterial systems showed potential to be used as personalized medicine to obtain better therapeutic outcomes and decreased adverse effects. Thus, in near future, it is expected that the knowledge acquired in the Tissue engineering field can be an important tool in the development of clinical medicine.

As general conclusion, although significant steps have been taken towards the study of nanoparticles and biomaterials as targeted drug delivery systems to treat the inflammation process, deeper studies using arthritic models still have to be performed to corroborate the data obtained in this

thesis. So, with the knowledge obtained with this work, it is expected that smart delivery biomaterials may have a significant impact on the Rheumatoid Arthritis treatment scope.